Ubiquitin E3 ligase mediated regulation of HMG-CoA reductase

Sam Menzies

Cambridge Institute of Medical Research

Pembroke College

University of Cambridge

October 2017

This dissertation is submitted for the degree of Doctor of Philosophy

Preface

This dissertation is the result of my own work and includes nothing which is the outcome of work done in collaboration with others, except as declared in the Acknowledgements and specified in the text.

It is not substantially the same as any that I have submitted, or, is being concurrently submitted for a degree or diploma or other qualification at the University of Cambridge or any other University or similar institution except as declared in the Preface and specified in the text. I further state that no substantial part of my dissertation has already been submitted, or, is being concurrently submitted for any such degree, diploma or other qualification at the University of Cambridge or any other University or similar institution except as declared in the Preface and specified in the text.

This dissertation contains less than 60,000 words.

The work described in this dissertation has resulted in the following publication:

Timms RT*, Menzies SA*, Tchasovnikarova IA*, Christensen LC*, Williamson JC, Antrobus R, Dougan G, Eligaard L, Lehner PJ (2016) Genetic dissection of mammalian ERAD through comparative haploid and CRISPR forward genetic screens. *Nat Commun.* 10;7:11786

(*equal contribution)

Sam Menzies

October 2017

Summary

Loss-of-function genetic screens are a powerful approach to identify the genes involved in biological processes. For nearly a century, forward genetic screens in model organisms have provided enormous insight into many cellular processes. However, the difficulty in generating and recovering bi-allelic mutations in diploid cells severely hindered the performance of forward genetic screens in mammalian cells. The development of a retroviral gene-trap vector to mutagenise the human near-haploid KBM7 cell line transformed forward genetic screens in human cells. The re-purposing of the microbial CRISPR/Cas9 system now offers an effective method to generate gene knockouts in diploid cells. Here, I performed a head-to-head comparison of retroviral gene-trap mutagenesis screens and genome-wide CRISPR knockout screens in KBM7 cells. The two screening approaches were equally effective at identifying genes required for the endoplasmic reticulum (ER)-associated degradation of MHC class I molecules.

The ER-resident enzyme HMG-CoA reductase (HMGCR) catalyses the rate-limiting step in the cholesterol biosynthesis pathway and is targeted therapeutically by statins. To maintain cholesterol homeostasis, the expression of HMGCR is tightly regulated by sterols transcriptionally and post-translationally. Sterols induce the association of HMGCR with Insig proteins, which recruit E3 ubiquitin ligase complexes to mediate degradation of HMGCR by the ubiquitin proteasome system. However, the identity of the E3 ligase(s) responsible for HMGCR ubiquitination is controversial. Here, I use a series of genome-wide CRISPR knockout screens using a fluorescently-tagged HMGCR exogenous reporter and an endogenous HMGCR knock-in as an unbiased approach to identify the E3 ligases and any additional components required for HMGCR degradation. The CRISPR screens identified a role for the poorly characterised ERAD E3 ligase RNF145. I found RNF145 to be functionally redundant with gp78, an E3 ligase previously implicated in HMGCR degradation, and the loss of both E3 ligases was required to significantly inhibit the sterol-induced degradation and ubiquitination of HMGCR. A focused E3 ligase CRISPR screen revealed that the combined loss of gp78, RNF145 and Hrd1 was required to completely block the sterol-induced degradation of HMGCR. I present a model to account for this apparent complexity.

Abbreviations

ACAT2	acyl-CoA:cholesterol acyltransferase 2
ApoB	apolipoprotein B100
ATP	adenosine triphosphate
AUP1	ancient ubiquitous protein 1
B2M	β2-microglobulin
BAG6	BCL2 associated athanogene 6
BiP	Immunoglobulin heavy chain binding protein
B&W	bind and wash
Cas9	CRISPR-associated system 9
Cdc48p	cell division cycle 48
CFTR	cystic fibrosis transmembrane conductance regulator
CHIP	C-terminus of HSP70-interacting protein
CoA	co-enzyme A
COPII	coat protein complex II
CRISPR	clustered regularly interspaced palindromic repeats
CUE	coupling of ubiquitin to ER degradation
Der1p	degradation in the ER 1
Derlin	Der1-like protein
DGAT2	diacylglycerol acyltransferase 2
DMEM	Dulbecco's modified eagle medium
Doa10p	degradation of Matα2-10 protein
dsRNA	double-stranded RNA
DUOX1	dual oxidase 1
ECL	enhanced chemiluminescence substrate
EDEM	ER degradation enhancer mannosidase α-like protein
EMC	ER membrane complex
ER	endoplasmic reticulum

ERAD	ER-associated degradation
ERManI	ER α1,2-mannosidase I
ERLIN	ER lipid raft associated
FACS	fluorescence-activated cell sorting
FCS	fetal calf serum
GALNT11	polypeptide N-acetylgalctosaminyltransferase 11
GFP	green fluorescent protein
Gp78	glycoprotein 78
gRNA	guide RNA
HCMV	human cytomegalovirus
HECT	homologous to E6 associated protein C-terminus
Herp	homocysteine/ER stress-inducible protein
HLA	human leukocyte antigen
HMG-CoA	3-hydroxy-3-methyl-glutaryl-CoA
HMGCR	HMG-CoA reductase
HO-1	heme oxygenase-1
Hrd1	HMG-CoA degradation 1
HRP	horseradish peroxidase
IAA	iodoacetamide
IDOL	inducible degrader of LDLR
IMDM	Iscove's Modified Dulbecco's Medium
Insig	insulin induced gene
Kar2p	karyogamie 2
LC-MS	liquid chromatography-mass spectrometry
LDL	low density lipoprotein
LDLR	LDL receptor
LXR	liver-X receptor
MARCH6	membrane-associated RING-CH protein 6
MEF	mouse embryonic fibroblast
MHC-I	major histocompatibility complex class I
mRNA	messenger RNA

NHEJ	non-homologous end joining
NK	natural killer
NPC	Niemann-Pick type C
OS9	osteosarcoma amplified 9
OST	oligosaccharide transferase
p97/VCP	97 kDa protein/valosin-containing protein
PAGE	polyacrylamide gel electrophoresis
PBS	phosphate buffered saline
PCSK9	proprotein convertase substilisin/kexin type 9
PCR	polymerase chain reaction
PDI	protein disulphide isomerase
PMSF	phenylmethanesulphonylfluoride
PVDF	polyvinylidene fluoride
Rad	radiation mutant
RFP2	RING-finger protein 2
RING	really interesting new gene
RISC	RNA-induced silencing complex
RNAi	RNA interference
RNF	RING finger protein
ROS	reactive oxygen species
Rpn	regulatory particle non-ATPase
SCAP	SREBP cleavage-activating protein
SCF	Skp-cullin 1-F box
SDS	sodium dodecyl sulphate
Sec24	secretory 24
Sec61	secretory 61
SEL1L	suppressor of lin-12, C. elegans (sel-1)-like
SFFV	spleen focus-forming virus
shRNA	small hairpin RNA
siRNA	small interfering RNA
SPP	signal peptide peptidase

SREBP	sterol regulatory binding element protein
SSD	sterol sensing domain
TBS	Tris-buffered saline
TCRα	T-cell receptor chain alpha
TECR	trans-2,3-enoyl CoA reductase
TMEM	transmembrane protein
TRC8	translocated in renal carcinoma, chromosome 8
TRIM	tripartite motif containing protein
Trx	thioredoxin-like domain
Ub	ubiquitin
UBA	ubiquitin-association domain
UBAC2	UBA containing protein 2
UBC	ubiquitin-conjugating
UBE2	ubiquitin-conjugating enzyme
UBL	ubiquitin like
UBX	ubiquitin-regulatory X domain
UBXD	UBX domain containing protein
Ufd	ubiquitin fusion degradation
UGT1	UDP glucose: glucose glucosyl-transferase 1
UIM	ubiquitin-interaction motif
UPS	ubiquitin proteasome system
UROD	uroporphyrinogen decarboxylase
US2	HCMV protein unique short region 2
US11	HCMV protein unique short region 11
VIM	VCP-intracting motif
VIMP	VCP interacting membrane protein
WT	wild-type
w/v	weight per volume
XTP3-B	XTP3-transactivated protein B
Yos9p	yeast OS9 homologous protein

Table of Contents

Chapter 1: Introduction

In the introduction, I will first describe endoplasmic reticulum-associated degradation (ERAD). I will then describe how cellular cholesterol homeostasis is regulated via transcriptional, post-translational and endocytic mechanisms, with emphasis on the post-translational regulation of HMG-CoA Reductase by ERAD, which will be the major focus of this thesis. I will conclude by describing how forward genetic screens are used as a powerful tool to determine gene function.

1.1 The Ubiquitin System

Ubiquitin is a highly conserved 76-amino acid polypeptide. Proteins are post-translationally modified by ubiquitin conjugation (ubiquitination) to mediate a range of cellular processes (Hershko and Ciechanover 1998). The ubiquitin modification is detected by proteins that contain ubiquitin-binding motifs, such as the coupling of ubiquitin to ER degradation (CUE), ubiquitin-interaction motif (UIM) and ubiquitin-association domain (UBA) (Hicke, Schubert, and Hill 2005). This thesis will focus on the ubiquitin proteasome system (UPS) in which ubiquitination targets a protein for degradation by the 26S proteasome (Nandi et al. 2006). However, ubiquitination is also critical for a range of nonproteolytic cellular functions including cell cycle progression, DNA repair, apoptosis and receptor mediated endocytosis (Komander and Rape 2012).

The ubiquitination process requires the sequential action of three enzymes. First, ubiquitin is activated by an E1 activating enzyme in an ATP-dependent reaction by forming a thioester bond between ubiquitin and the E1's active cysteine residue (Ciechanover et al. 1981, Haas and Rose 1982). The activated ubiquitin molecule is then transferred onto a cysteine residue on an E2 ubiquitin conjugating enzyme. A E3 ubiquitin ligase catalyses the transfer of ubiquitin from the E2 conjugating enzyme onto the substrate. The C-terminal glycine of ubiquitin typically forms an isopeptide bond with a substrate lysine residue (Pickart 2001). Some ubiquitin ligating enzymes act as E4 ligases to elongate a polyubiquitin chain (Koegl et al. 1999).

The ubiquitin modification can be added onto proteins to create a diverse range of ubiquitin structures. Monoubiquitination describes the attachment of a single ubiquitin molecule, however a protein can be monoubiquitinated on multiple residues. As ubiquitin contains seven lysine residues (residues 6, 11, 27, 29, 33, 48 and 63), ubiquitin molecules can be added onto other ubiquitin molecules to form a polyubiquitin chain (Kirisako et al. 2006). Polyubiquitin chains can be constructed entirely from the same linkage, i.e. all ubiquitin molecules are added onto the same lysine residue. Complex ubiquitin chains can be constructed that contain different linkages or ubiquitin-like molecules to create a diverse array of structures to mediate cell signalling (Boname et al. 2010, Kravtsova-Ivantsiv and Ciechanover 2012). A polyubiquitin chain of at least four Lysine-48 (K48) linked ubiquitin molecules is the canonical signal for proteasomal degradation (Thrower et al. 2000).

Most ubiquitin modifications involve the conjugation of ubiquitin onto a lysine residue. However, serine, threonine and cysteine residues can also be ubiquitinated to mediate proteasomal degradation or other cellular functions (Cadwell and Coscoy 2005, Carvalho et al. 2007, Tait et al. 2007, Wang et al. 2007, Wang, Bian, et al. 2017).

1.1.1 E2 ubiquitin conjugating enzymes

E2 conjugating enzymes have an active role in defining the features of ubiquitination, such as chain length and linkage type. E2s have a core ubiquitin-conjugating (UBC) domain containing the active cysteine residue that accepts activated ubiquitin from the E1 (Ye and Rape 2009). E2s have overlapping binding sites for E1s and E3s, therefore E2s cannot be recharged with ubiquitin while bound to an E3 ligase (Eletr et al. 2005). The interaction between E2s and E3s is typically weak, so some E3s have additional E2 binding sites to increase the affinity of the E2-E3 interaction (Chen et al. 2006). The localisation and activity of E2 conjugating enzymes can be influenced by cofactors (Biederer, Volkwein, and Sommer 1997, VanDemark et al. 2001, Kostova et al. 2009, Jo, Hartman, and DeBose-Boyd 2013).

As there are significantly more E3s (830) than E2s (45), a single E2 can interact with multiple E3s to mediate substrate ubiquitination. Specific E2-E3 pairings ubiquitinate a limited set of substrates, however some E2 conjugating enzymes are by definition much more promiscuous (Ye and Rape 2009).

1.1.2 HECT and RING E3 ubiquitin ligases

In eukaryotes, E3 ubiquitin ligases can be split into two groups by the presence of a HECT (homologous to E6 associated protein C-terminus) or RING (really interesting new gene) domain. RING E3 ligases can be further divided into groups based on the arrangement of cysteine and histidine residues in the RING domain (Deshaies and Joazeiro 2009). The cysteine and histidine residues coordinate two zinc ions to create a 'cross-brace' structure. For RING E3 ligases, the E2 conjugating enzyme interacts directly with the RING domain and the substrate is recruited via a separate binding site. RING E3 ligases are scaffold proteins; the ubiquitin molecule is transferred directly from a ubiquitin-charged E2 onto the substrate (Deshaies and Joazeiro 2009). In contrast, HECT E3 ligases have a catalytic cysteine residue that forms a ligase-ubiquitin intermediate before transferring ubiquitin onto the substrate (Metzger, Hristova, and Weissman 2012).

1.1.3 ER-associated degradation (ERAD)

The endoplasmic reticulum (ER) is a membrane-bound organelle that extends throughout the cytoplasm. The ER is the site of several metabolic pathways that are critical for lipid homeostasis as well as the entry point of the secretory pathway, where approximately one third of the eukaryotic proteome must fold correctly (Kanapin et al. 2003). The ER has developed a complex quality control system to monitor protein folding. However, protein folding is a complex process that can involve several intermediate states. Mutant polypeptides can arise from DNA mutations or errors in transcription and translation. Protein complexes require the correct stoichiometry of constituent polypeptides and the accumulation of unassembled polypeptides must be prevented. ERAD targets incorrectly-folded, mutant and unassembled polypeptides for proteasomal degradation (Vembar and Brodsky 2008). ERAD is also responsible for regulating the expression of correctly folded proteins in the ER to maintain lipid homeostasis (Hampton and Garza 2009).

Surprisingly, there are no E1 activating enzymes, E2 conjugating enzymes or proteasomes in the ER lumen. Therefore, ERAD substrates must be ubiquitinated on the cytosolic side of the

ER membrane and degraded in the cytosol (Hegde and Ploegh 2010, Christianson and Ye 2014). The use of the yeast *S. cerevisiae* as a model organism gave significant insights into the ERAD pathway (Sommer and Jentsch 1993, Hampton, Gardner, and Rine 1996, Hiller et al. 1996). Many underlying principles and components of ERAD are highly conserved from *S. cerevisiae* to mammalian cells. However, mammals have developed a more complex ERAD network, probably to accommodate a more diverse range of substrates (Christianson et al. 2012).

1.1.4 *S. cerevisiae* ERAD E3 ligase complexes

The ERAD machinery is organised in multi-protein complexes around an integral membrane E3 ligase to coordinate the ERAD process. The yeast genome encodes 80 E3 ubiquitin ligases, two of these are ERAD E3 ligases, Hrd1p (HMG-CoA degradation 1) and Doa10p (degradation of Matα2-10 protein). It is generally thought that substrates recognised in the ER lumen (ERAD-L) or ER membrane (ERAD-M) are ubiquitinated by Hrd1p. Whereas Doa10p targets substrates on the cytosolic side of the ER membrane (ERAD-C) (Taxis et al. 2003, Vashist and Ng 2004, Huyer et al. 2004, Carvalho, Goder, and Rapoport 2006). However, this division of substrates is probably an over-simplification and complete stabilisation is not observed in the absence of either Hrd1p or Doa10p (Gnann, Riordan, and Wolf 2004, Nakatsukasa et al. 2008, Goeckeler and Brodsky 2010).

S. cerevisiae Hrd1 complex

A genetic screen to identify genes required for the degradation of HMG-CoA Reductase identified the HRD genes, Hrd1p (a polytopic RING E3 ligase), Hrd2p (a proteasome component) and Hrd3p (Hampton, Gardner, and Rine 1996). Hrd3p is a type I transmembrane domain with a large ER-luminal domain that interacts with Hrd1p and stabilises Hrd1p (Gardner et al. 2000). The E2 conjugating enzyme Ubc7p is recruited to Hrd1p by Cue1p (Biederer, Volkwein, and Sommer 1997, Bagola et al. 2013). The Cdc48p/Npl4p/Ufd1p complex is recruited to Hrd1p by Ubx2p (Schuberth and Buchberger 2005, Neuber et al. 2005). Hrd1p-mediated degradation of ERAD-L substrates also requires Der1p, which is recruited by Usa1p (Carvalho, Goder, and Rapoport 2006). The ER-luminal domain of Hrd3p associates

with Yos9p and Kar2p to assist substrate recognition (Gardner et al. 2000, Denic, Quan, and Weissman 2006, Gauss et al. 2006).

***S. cerevisiae* Doa10 complex**

Doa10p is also a poytopic RING E3 ligase (Swanson, Locher, and Hochstrasser 2001). Like for Hrd1p, Ubx2 recruits Cdc58p/Npl4p/Ufd1p to Doa10p (Neuber et al. 2005, Schuberth and Buchberger 2005). It has been suggested that the E2 conjugating enzyme Ubc6p mediates monoubiquitination and that Ubc7p mediates ubiquitin chain extension (Weber et al. 2016).

1.1.5 Mammalian ERAD E3 ligase complexes

Many factors in the *S. cerevisiae* ERAD network are highly conserved, however the mammalian ERAD network is far more elaborate. The human genome is estimated to encode over 800 E3 ligases with at least 37 putative ERAD E3 ligases (Kaneko et al. 2016). There are two mammalian homologues of Hrd1p, Hrd1 and gp78, and only one mammalian Doa10 homologue, MARCH6 (also called TEB4).

Mammalian Hrd1 complex

Human Hrd1 (also called synoviolin) shares 26% sequence identity with *S. cerevisiae* Hrd1p, but shares similar topology with a N-terminal transmembrane domain and C-terminal cytosolic RING-H2 domain (Nadav et al. 2003, Kikkert et al. 2004). The Hrd3p homologue SEL1L associates with Hrd1 and recruits factors required for substrate recognition to its ER-luminal domain such as Yos9p homologues OS9 and XTP3B (Christianson et al. 2008, Hosokawa et al. 2008, Bernasconi et al. 2008), the mannosidases EDEM1 (ER-degradation enhancing α-mannosidase-like protein) and EDEM3 (Cormier et al. 2009, Saeed et al. 2011), the disulphide reductase ERDJ5 (Williams et al. 2013) and the chaperone BiP (Hosokawa et al. 2008). Other components of the Hrd1 complex include the Derlin proteins, Derlin-1, -2 and -3 (Der1p homologues), Herp (Usa1p homologue), UBXD8, UBE2J1 (Ubc6p) homologue, UBE2G2 (Ubc7p homologue) and AUP1 (Cue1p homologue) (Schulze et al. 2005, Hwang, Walczak, et al. 2017, Christianson et al. 2012). The Hrd1 complex associates with the p97/Npl4/Ufd1 complex, however it is not clear whether the p97 complex binds directly to Hrd1 or is recruited by the Derlin proteins, UBXD8 or VIMP (VCP interacting membrane

protein) (Ye et al. 2004, Ye et al. 2005, Lilley and Ploegh 2005, Yeung et al. 2008, Greenblatt, Olzmann, and Kopito 2011, Suzuki et al. 2012).

The ERAD of HMG-CoA Reductase will be discussed in more detail (see **1.2.2.3**), but Hrd1 has not yet been shown to be involved in the ERAD of human HMG-CoA Reductase (Kikkert et al. 2004). However, HMG-CoA Reductase was identified as a high confidence interaction partner of Hrd1 by mass spectrometry, suggesting that Hrd1 could influence HMG-CoA Reductase in an unknown manner (Christianson et al. 2012). A range of Hrd1 substrates have been reported including unassembled T cell receptor alpha chain (Kikkert et al. 2004), unassembled CD147 (Tyler et al. 2012), CD3-δ (Kikkert et al. 2004), immunoglobulin κ light chain (Shimizu, Okuda-Shimizu, and Hendershot 2010), p53 (Yamasaki et al. 2007), amyloid precursor protein (Kaneko et al. 2010), the Z variant of alpha 1-antitrypsin (Wang, Li, et al. 2011), gp78 (Shmueli et al. 2009), CD95/Fas (Kong et al. 2016), as well as both folded and unassembled major histocompatibility complex-I (MHC-I) heavy chain (Burr et al. 2011, Burr et al. 2013).

Mammalian gp78 complex

Gp78 (also called autocrine mobility factor receptor, AMFR) shares 15% sequence identity with *S. cerevisiae* Hrd1p (Fang et al. 2001). Gp78 contains a N-terminal transmembrane domain, a RING-H2 domain, a UBE2G2-binding region (G2BR), a Cue1p-like domain and a VCP-interaction motif (VIM) (Chen et al. 2006, Ballar et al. 2006). The G2BR and Cue1p-like domains are essential for gp78 E3 ligase activity (Chen et al. 2006). Like Hrd1, gp78 also interacts with the Derlin proteins and UBXD8 (Christianson et al. 2012). Whilst gp78 can recruit the p97 (VCP) complex directly, the VIM is dispensable for gp78-mediated ERAD (Ballar et al. 2006). UBA-domain containing protein 2 (UBAC2) recruits UBXD8 to gp78, UBXD8 can then recruit the p97/Npl4/Ufd1 complex to gp78 (Christianson et al. 2012).

Several proteins involved in cholesterol and lipid metabolism are gp78 substrates, making gp78 an important regulator of lipid homeostasis (see **1.2.2**). (Lee, Song, et al. 2006, Fisher, Khanna, and McLeod 2011, Liu et al. 2012, Choi et al. 2014).

MARCH6 (TEB4)

MACH6 belongs to the membrane-associated RING-CH (MARCH) family of E3 ubiquitin ligases. MARCH6 is the likely homologue of *S. cerevisiae* Doa10p (Kreft, Wang, and Hochstrasser

2006). MARCH6 has a N-terminal RING-CH domain and either 13 or 14 transmembrane helices (Kreft, Wang, and Hochstrasser 2006). The molecular mechanisms underlying MARCH6 function are far less characterised than Hrd1 and gp78. Like gp78, MARCH6 regulates cholesterol homeostasis (see **1.2.2.7**) (Zelcer et al. 2014, Loregger et al. 2015).

TRC8 (RNF139)

TRC8 is a polytopic, ER-resident RING-H2 ligase (Stagg et al. 2009). Human cytomegalovirus (HCMV) hijacks TRC8 to downregulate MHC-I as a part of HCMV's immune-evasion strategy. The virally encoded protein US2 recruits TRC8 to MHC-I in the ER resulting in the rapid proteasomal degradation of MHC-I (Stagg et al. 2009). It was later found that CMV encoded US2 also recruits other cell surface proteins, including 6 integrin α-chains, the anti-coagulation factor thrombomodulin, IL-12 receptor β1 chain and the NK cell ligand CD112, to TRC8 (Hsu et al. 2015).

TRC8 associates with the intramembrane cleaving aspartyl protease, signal peptide peptidase (SPP) (Boname et al. 2014). Tail anchor proteins are a class of type II orientated integral membrane proteins that are attached to the membrane by a single embedded C-terminal helix (Borgese, Colombo, and Pedrazzini 2003). SPP cleaves the signal sequence from tail anchored proteins, such as heme oxygenase-1 (HO-1), allowing the TRC8-dependent proteasomal degradation of HO-1 (Boname et al. 2014). In the absence of SPP, TRC8 targets the hepatitis C virus immature core protein for degradation (Aizawa et al. 2016).

TRC8's N-terminal transmembrane domain contains a sterol sensing domain (SSD) (Lee et al. 2010). Sterol sensing domains are found in several proteins involved in cholesterol metabolism, such as HMG-CoA Reductase, Niemann-Pick type C1 and SREBP cleavage-activating protein (SCAP) (Hua et al. 1996, Martín et al. 2001, Millard et al. 2005). A sterol sensing domain is a series of five transmembrane helices that can bind to sterol molecules (Kuwabara and Labouesse 2002). The role of TRC8 in cholesterol homeostasis is controversial and is discussed in **1.2.2.6**.

Other ERAD E3 ligases

TMEM129 is an ER-resident E3 ligase consisting of the N-terminal transmembrane helices and a C-terminal atypical RING domain (van den Boomen et al. 2014). TMEM129 is recruited to

the HCMV protein US11 by Derlin-1 to target MHC-I for ubiquitination and proteasomal degradation (van den Boomen et al. 2014). Unusually, two E2 conjugating enzymes, UBE2J2 and UBE2K, mediate the US11-induced downregulation of MHC-I (Flierman et al. 2006, van den Boomen et al. 2014).

RNF5 (RMA1) and RNF185 are homologous E3 ligases with 70% shared sequence identity. Both RNF5 and RNF185 have a N-terminal RING domain and two transmembrane helices. These homologous E3 ligases demonstrate functional redundancy for the ubiquitination of the cystic fibrosis transmembrane regulator (CFTR) (El Khouri et al. 2013). RNF170 is a polytopic RING E3 ligase that ubiquitinates inositol 1,4,5-triphosphate receptor (Lu et al. 2011, Wright et al. 2015). RFP2/TRIM13 and Nixin/ZNRF4 are single transmembrane helix RING E3 ligases that ubiquitinate L-type calcium channel components and calnexin respectively (Lerner et al. 2007, Altier et al. 2011, Neutzner et al. 2011).

Several cytosolic E3 ligases can also ubiquitinate ERAD substrates, including CHIP (Meacham et al. 2001), Nrdp1 (Fry et al. 2011), Parkin (Imai et al. 2002), Skp1-Cullin1-Fbx2-Roc1 (SCF(Fbx2)) (Yoshida et al. 2002), SCF(Fbx6) (Yoshida et al. 2003), Smurf1 (Guo et al. 2011). These E3 ligases must cooperate with integral ER membrane factors to ubiquitinate ER-localised substrates.

1.1.6 ERAD substrate recognition

To ensure protein homeostasis, ERAD must be able to target an enormous number of structurally diverse substrates.

1.1.6.1 Glycan dependent recognition

Most proteins that are co-translated into the ER are subject to the carbohydrate modification N-linked glycosylation. A glycan moiety is co-translationally attached onto asparagine residues in the consensus sequence N-X-T/S by the ER oligosaccharide transferase (OST) complex (Mohorko, Glockshuber, and Aebi 2011). The glycan moiety is modified extensively through the ER and Golgi to create a wide range of structures that influence protein structure and activity (Bieberich 2014).

The glycan structure is rapidly trimmed in the ER and binds to the chaperones calnexin and calreticulin (Hebert, Garman, and Molinari 2005). Cleavage of the final glucose residue in the glycan moiety by Glucosidase II releases the protein from calnexin or calreticulin. If the protein has not achieved its native folded state, the glycan is glucosylated by UDP glucose:glucose glucosyl-transferase 1 (UGT1). The reglucosylated protein can now re-associate with calnexin or calreticulin (Hebert, Foellmer, and Helenius 1995, Sousa and Parodi 1995). Proteins that are unable to exit the calnexin-calreticulin cycle are likely to be terminally misfolded and must therefore be targeted for ERAD. During each round of the calnexin-calreticulin cycle, the glycan moiety is trimmed by ER α1,2-mannosidase I (ERManI) and ER degradation-enhancing 1,2-mannosidase-like proteins -1, -2 and -3 (EDEM1, EDEM2 and EDEM3) (Oda et al. 2003, Hirao et al. 2006, Olivari and Molinari 2007).

The ER-resident lectins, OS9 and XPT3-B, recognise trimmed glycan structures with exposed mannose α1,6-linkages (Quan et al. 2008, Hosokawa et al. 2009, Yamaguchi et al. 2010). The functional relationship between OS9 and XPT3-B is unclear. Some studies show functional redundancy between OS9 and XPT3-B (Bernasconi et al. 2010, Burr et al. 2013). Whereas, other studies show that the loss of either OS9 or XPT3-B is sufficient to impair ERAD (Chen et al. 2011). SEL1L interacts with OS9, XPT3-B and the EDEM proteins and acts as a 'gate-keeper' to facilitate the transfer of substrates to Hrd1 (Denic, Quan, and Weissman 2006, Christianson et al. 2008).

1.1.6.2 Recognition of non-glycosylated substrates

Misfolded non-glycosylated proteins are also efficiently targeted by ERAD (Okuda-Shimizu and Hendershot 2007, Sekijima, Kelly, and Ikeda 2008). Chaperones, such as BiP, recognise features of unfolded proteins, such as hydrophobic amino acid residues that are normally sequestered within a protein's core (Otero, Lizák, and Hendershot 2010).

1.1.6.3 Specialised scaffold proteins

The ERAD of specific correctly-folded proteins can be induced by recruiting E3 ubiquitin ligase complexes to substrates by using a scaffold protein. HMCV uses two virally encoded proteins,

US2 and US11, to recruit MHC-I to E3 ubiquitin ligases to downregulated MHC-I (Stagg et al. 2009, van den Boomen et al. 2014). The ERAD of HMG-CoA Reductase is induced by the sterol-dependent interaction with the Insig proteins, which recruit an E3 ligase complex (Sever, Song, et al. 2003).

1.1.7 Oxidoreductases

Disulphide bonds formed by the oxidation of two thiol groups in cysteine residues help stabilise the structure of many proteins. The ER contains a large family of protein disulphide isomerase (PDI) enzymes that catalyse disulphide bond oxidation and reduction (Appenzeller-Herzog and Ellgaard 2008). The oxidoreductases of the ER must ensure the stability of folded proteins but also reduce disulphide bonds in misfolded proteins to allow extraction from the ER and proteasomal degradation. Erdj5, a PDI family member, interacts with EDEM1 and BiP and is required for the ERAD of glycosylated and non-glycosylated substrates (Ushioda et al. 2008, Dong et al. 2008, Hagiwara et al. 2011).

1.1.8 Retrotranslocation and membrane extraction

For ERAD substrates in the ER lumen to be ubiquitinated they must first be, at least partially, translocated across the ER membrane before they can be ubiquitinated and then released into the cytoplasm for degradation. This process is referred to as dislocation or retrotranslocation (Wiertz et al. 1996). For integral membrane ERAD substrates to be degraded by the cytosolic proteasome, they must be extracted from the ER membrane.

1.1.8.1 The dislocon

It is most likely that proteins are retronslocated across the ER through a protein channel, however the identity of this channel has yet to be conclusively determined. A candidate for the dislocon is the Sec61 complex, which facilitates the translocation of proteins into the ER (Johnson and van Waes 1999). However, the degradation of several ERAD ER-luminal substrates was independent of Sec61 (Sato and Hampton 2006, Wahlman et al. 2007, Garza, Sato, and Hampton 2009). A nascent polypeptide chain can fit through the Sec61 channel, however most glycosylated polypeptides are probably too bulky to fit through the pore

(Hebert, Bernasconi, and Molinari 2010). The Sec61 complex is therefore unlikely to provide the sole route for ER exit.

The Derlin proteins (Derlin-1, -2 and -3) are the *S. cerevisiae* Der1p homologues. The Derlin proteins are small, polytopic, non-catalytic rhomboid-like proteins that can oligomerise in the ER membrane (Lilley and Ploegh 2005, Lemberg 2013). Whilst several reports have shown a requirement for the Derlin proteins for retrotranslocation, it is not yet clear whether the Derlin proteins form part of a protein-conducting channel or enable retrotranslocation via another mechanism (Ye et al. 2004, Lilley and Ploegh 2005, Greenblatt, Olzmann, and Kopito 2011).

The ERAD E3 ligase Hrd1 has also been proposed to form an important component of the protein-conducting channel (Carvalho, Stanley, and Rapoport 2010, Stanley, Carvalho, and Rapoport 2011, Baldridge and Rapoport 2016). A recent structure of *S. cerevisiae* Hrd1p in complex with Hrd3p revealed that five of Hrd1p's eight transmembrane helices create an aqueous pore that through the ER membrane (Schoebel et al. 2017). Hrd1p forms a dimer in the ER membrane and a lateral seal for the potential Hrd1p channel is provided by the other Hrd1 molecule (Schoebel et al. 2017). Whilst these studies provide evidence for Hrd1's involvement in retrotranslocation, the transmembrane domain of *S. cerevisiae* Hrd1 has also been shown to be dispensable for retrotanslocation (Garza, Sato, and Hampton 2009).

The conflicting requirements for retrotranslocation and the failure to identify a universal protein-conducting channel most likely means that there is not a single route for ER extraction. The mechanism of retrotranslocation is probably substrate dependent and a single substrate might be able to follow multiple ER exit routes.

1.1.8.2 The VCP (p97) AAA-ATPase

The AAA-ATPase p97 (also called VCP, Cdc48p in *S. cerevisiae*) is essential for membrane extraction and retrotranslocation of ERAD substrates (Ye, Meyer, and Rapoport 2001, Rabinovich et al. 2002). Each p97 monomer contains two ATPase domains. P97 hexamers are organised as two stacked rings (D1 and D2) with a central pore (Zhang et al. 2000). The Npl4-Ufd1 heterodimer interacts with the p97 hexamer to form a complex that can engage with

ERAD substrates. The association of p97 with Ufd1 and polyubiquitinated substrates activates p97's ATPase activity (Bays et al. 2001, Jarosch et al. 2002, Meyer, Wang, and Warren 2002, Ye, Meyer, and Rapoport 2003, Flierman et al. 2003). ATP hydrolysis by p97 could drive the extraction process either by directly pulling on the ubiquitinated substrate or by perturbing the transmembrane component of the dislocon (Nakatsukasa and Brodsky 2008, Brodsky 2012).

1.1.9 Degradation by the proteasome

Retrotranslocated or membrane-extracted ERAD substrates must be delivered to the proteasome for degradation rapidly to prevent the aggregation of exposed hydrophobic regions. Degradation is tightly coupled to retrotranslocation by a poorly defined mechanism. The p97 complex does not form stable interactions with the proteasome (Isakov and Stanhill 2011, Verma et al. 2000). In *S. cerevisiae*, the UBL-UBA proteins Rad23p and Dskp promote the delivery of retrotranslocated ERAD substrates to the proteasome (Medicherla et al. 2004). In mammalian cells, the Bag6 complex and ubiuqilin have been implicated as chaperones for ubiquitinated retrotranslocated substrates (Ko et al. 2004, Lee and Ye 2013).

The 26S proteasome consists of a 20S cylindrical core, in which proteolysis occurs, and two 19S regulatory caps. Polyubiquitinated substrates bind to high affinity ubiquitin receptors, Rpn10 and Rpn13, in the 19S complex (Peth, Uchiki, and Goldberg 2010, Schreiner et al. 2008, Husnjak et al. 2008). The bound substrate is deubiquitinated by the 26S-associated deubiquitinating enzymes (DUBs), Usp14, Uch37 or Rpn11, unfolded and translocated into the 20S core (Smith et al. 2007, Finley 2009, Peth, Besche, and Goldberg 2009, Smith et al. 2011).

1.2 Cholesterol Homeostasis

Cholesterol and other lipids are critical molecules for cells and are essential for life. However, at very high concentrations, cholesterol is toxic to cells. Intricate regulatory mechanisms therefore maintain intracellular cholesterol homeostasis. This requires balancing the uptake of exogenous cholesterol and the endogenous production of cholesterol. The cholesterol biosynthesis pathway is tightly regulated at the level of transcription and degradation. I will emphasise the sterol-dependent regulation of HMG-CoA Reductase as the sterol-induced degradation of HMG-CoA Reductase will be a major topic of this thesis.

1.2.1 Transcriptional control of cholesterol homeostasis

1.2.1.1 The SREBP pathway

Mammalian cells encode three closely related sterol regulatory binding element protein (SREBP), called SREBP-1a, SREBP-1c and SREBP2 (Brown and Goldstein 1997). SREBP-1a and SREBP-1c are encoded by the same gene, but are the products of different promoters and alternative splicing. SREBP-2 is the predominant SREBP isoform in the liver and induces the expression of cholesterogenic proteins, such as HMG-CoA Reductase and the LDL Receptor. SREBP-1c induces the expression of fatty acid biosynthesis pathway enzymes, whereas, SREBP-1a regulates both the cholesterol and fatty acid biosynthesis pathways (Goldstein, Rawson, and Brown 2002).

All three SREBP proteins are synthesised as integral membrane proteins into the ER membrane, resulting in a hairpin orientation with the N-terminal transcription factor domain and C-terminal regulatory domain positioned in the cytosol (**Figure 1.1**). The C-terminal regulatory domain of all three SREBPs constitutively associates with SREBP cleavage-activating protein (SCAP) (Sakai et al. 1997).

SCAP has an N-terminal transmembrane domain, with eight transmembrane helices, and C-terminal WD repeats, which interact with the SREBPs (Nohturfft, Brown, and Goldstein 1998b). Transmembrane helices two-to-six constitute a sterol sensing domain (SSD) (Hua et al. 1996, Nohturfft, Brown, and Goldstein 1998a). At low cholesterol levels, SCAP is recruited by the COPII coat component Sec24 (Sun et al. 2005). The SCAP-SREBP heterodimer is

therefore transported to the Golgi (Sun et al. 2007). The mature SREBP transcription factor is liberated by sequential proteolytic cleavage in the Golgi. Firstly, Site-1 protease cleaves SREBP within the luminal loop (Duncan et al. 1997, Sakai et al. 1998). The Site-2 protease then cleaves within the transmembrane helix to release the N-terminal domain of SREBP (Duncan et al. 1998). The mature SREBP transcription factor can now migrate to the nucleus to interact with sterol response elements and induce target gene expression.

When the ER membrane cholesterol content exceeds 5% of ER membrane lipids, cholesterol binds to SCAP's SSD and SCAP now binds to the Insig proteins (Adams, Goldstein, and Brown 2003, Adams et al. 2004). SCAP can no longer be recruited to the COPII coat when it is bound to an Insig protein. Therefore, the SCAP-SREBP heterodimer is retained in the ER (Sun et al. 2005). The Brown and Goldstein laboratories identified three mutations in SCAPS's SSD (D443N, Y298C and L315F) that rendered SCAP unable to associate with Insig and therefore unable to prevent SREBP processing despite high levels of cholesterol (Hua et al. 1996, Nohturfft, Brown, and Goldstein 1998a, Yabe et al. 2002, Yang et al. 2002, Adams, Goldstein, and Brown 2003). The over-expression of either Insig protein lowered the cholesterol concentration required to induce conformational changes in SCAP's SSD (Adams, Goldstein, and Brown 2003). This allows the expression level of Insigs to regulate SREBP processing and therefore SREBP-target gene expression.

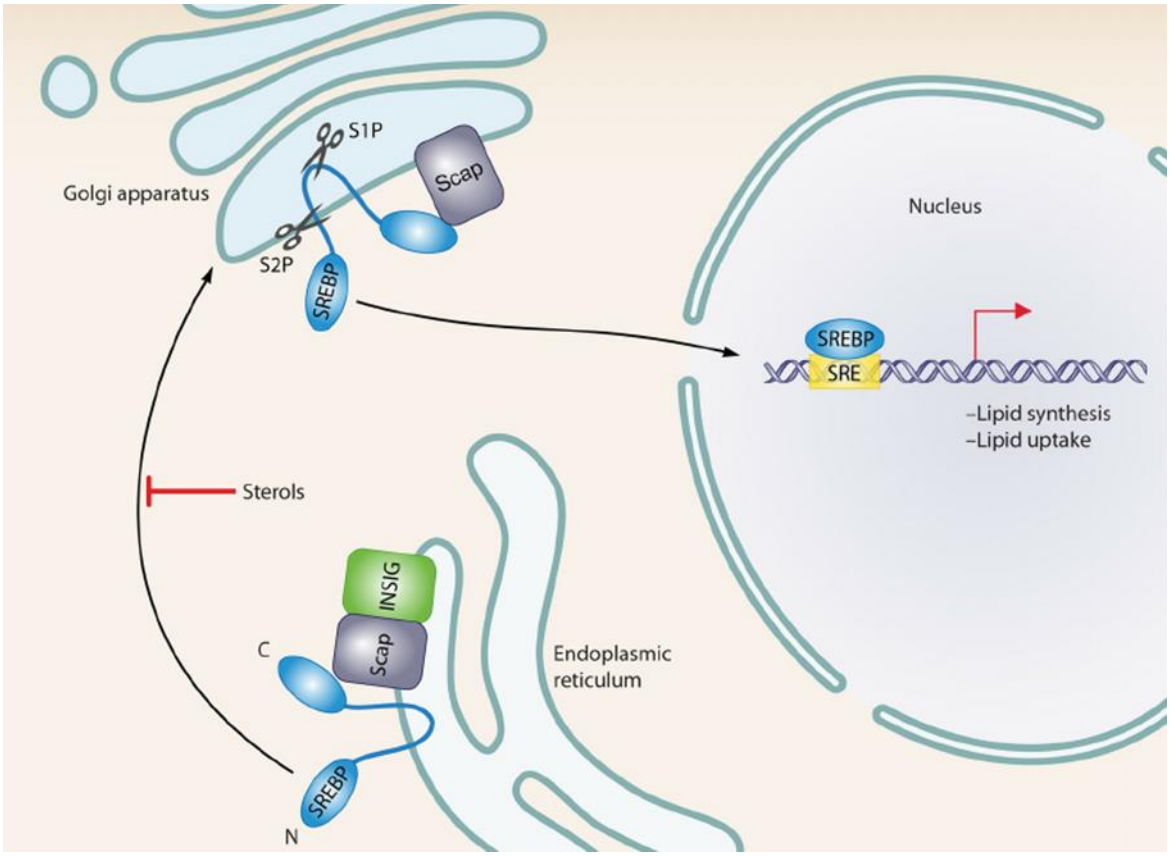

Figure 1.1 Mammalian SREBP pathway. At high cholesterol/sterol levels, immature SREBP-SCAP dimer is retained in the ER by Insig. At low cholesterol/sterol levels, SCAP is recruited by the COPII coat complex and the immature SREBP-SCAP complex is transported to the Golgi. Proteolytic cleavage of immature SREBP by Site-1 protease (S1P) and Site-2 protease (S2P) releases the mature SREBP transcription factor, which migrates to the nucleus to upregulate target gene expression. From (Bien 2010)

1.2.1.2 The Insig proteins

The human genome encodes two Insig isoforms, Insig1 and Insig2. Both Insig proteins are ER-resident glycoproteins containing six transmembrane helices (Feramisco, Goldstein, and Brown 2004). The two Insigs share 59% sequence identity. The main differences between the Insigs are in the hydrophilic N- and C-terminal regions as the transmembrane domains share 85% sequence identity (Goldstein, DeBose-Boyd, and Brown 2006). The Insigs are not predicted to contain a sterol sensing domain, however the Insig proteins can bind oxysterols such as 25-hydroxycholesterol (Radhakrishnan et al. 2007).

There is a significant overlap in the function of Insig1 and Insig2, for example both Insigs can retain SCAP-SREBP in the ER (Yang et al. 2002, Yabe, Brown, and Goldstein 2002). However, the Insigs are subject to differential regulation. Insig1 is a SREBP target gene, whereas Insig2 expression is independent of the SREBP pathway (Janowski 2002, Horton, Goldstein, and Brown 2002). The hypoxia-inducible factor 1α upregulates Insig2 during oxygen deprivation to limit cholesterol synthesis, an oxygen-demanding process (Hwang, Nguyen, et al. 2017).

The liver expresses an organ-specific Insig2 isoform, named Insig2a (Yabe et al. 2003). The Insig2a transcript is transcribed from an upstream promoter and contains an extra non-coding 5' exon that is removed by splicing. Therefore, Insig2a and Insig2b encode the same protein but are differentially regulated. Insulin strongly suppresses Insig2a expression, which is otherwise very highly expressed in the liver. Whereas Insig2b is expressed at a low level (Yabe et al. 2003).

1.2.1.3 Liver-X receptors

Liver-X receptors (LXRs) are a second family of cholesterol-regulating transcription factors. Unlike SREBPs, LXRs are activated at high cellular sterol levels and induce a suite of genes to reduce cellular cholesterol (Zelcer and Tontonoz 2006). LXRs are activated by binding ligands such as cholesterol biosynthesis intermediates and oxysterols (Janowski et al. 1996, Yang et al. 2006, Spann et al. 2012). LXR target genes aim to reduce the cellular cholesterol level through several mechanisms, such as promoting cholesterol efflux (Venkateswaran et al. 2000, Chawla et al. 2001, Kennedy et al. 2001), limiting cholesterol uptake (Zelcer et al. 2009) and reducing cholesterol biosynthesis (Sallam et al. 2016).

1.2.2 Regulation of cholesterol homeostasis by ERAD

ERAD is responsible for the regulated turnover of correctly folded enzymes in the ER, as well as being a critical component of ER protein quality control. The sterol-regulated degradation of key enzymes in the cholesterol biosynthesis pathway ensures that cholesterol production can be rapidly and significantly decreased.

1.2.2.1 HMG-CoA Reductase (HMGCR)

HMGCR is an 888 amino acid ER-resident protein that catalyses the major rate-limiting step of the cholesterol biosynthesis pathway, the reduction of HMG-CoA to mevalonate (**Figure 1.2**) (Goldstein and Brown 1990). Statins therapeutically target HMGCR to lower plasma cholesterol levels and reduce the risk of atherosclerosis by competitive inhibition of HMGCR's catalytic domain (Steinberg 2006). Mevalonate is also a precursor for many non-sterol isoprenoid molecules such as ubiquinone and haem A (**Figure 1.2**).

HMGCR has an N-terminal transmembrane domain containing eight helices, with helices two-to-six constituting a sterol sensing domain. The C-terminal cytoplasmic domain mediates HMGCR's catalytic activity (Roitelman et al. 1992, Liscum et al. 1985). As HMG-CoA and mevalonate are both water soluble molecules, membrane attachment is to enable regulation of HMGCR abundance. HMGCR expression is regulated by sterols at the transcriptional level as a SREBP-2 target gene. HMGCR protein is also rapidly degraded at high cellular sterol levels by ERAD (Gil et al. 1985).

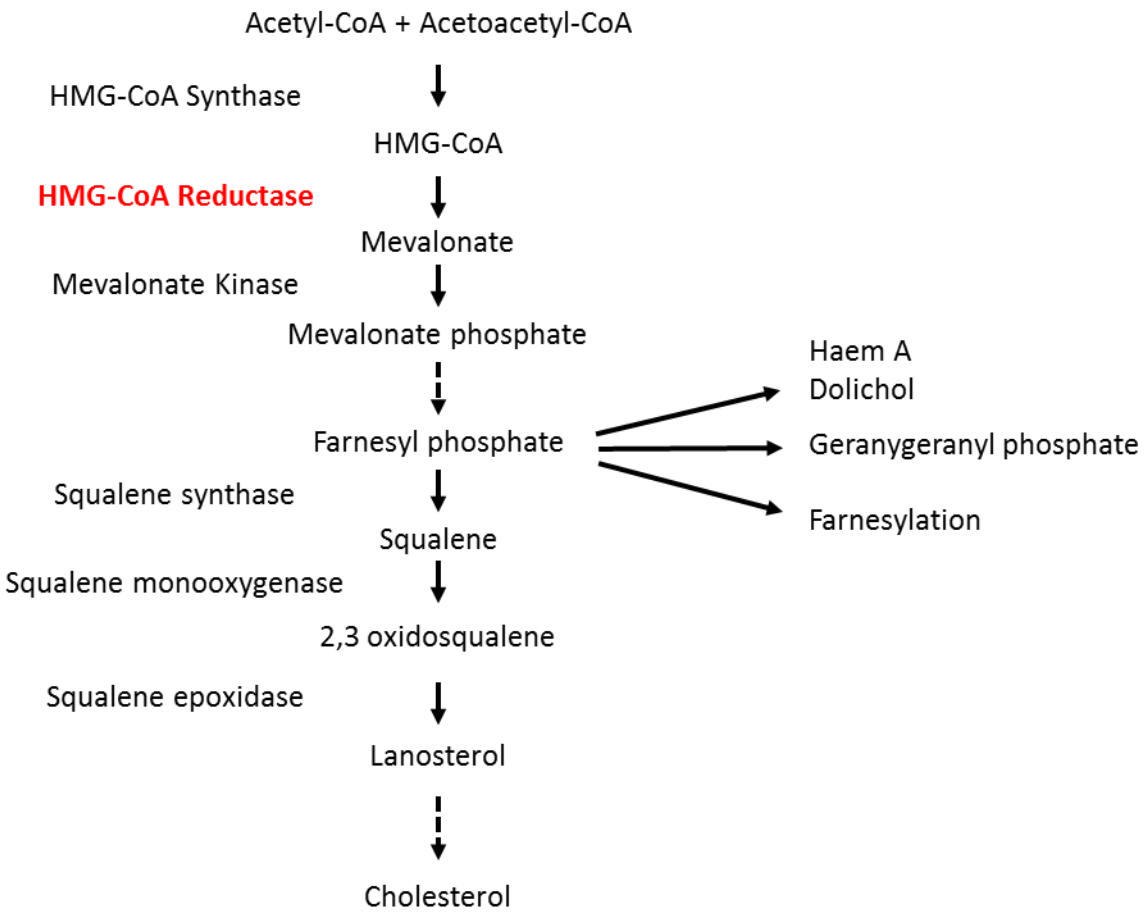

Figure 1.2 Mammalian cholesterol biosynthesis pathway. A series of cytosolic and integral ER membrane enzymes catalyse the biosynthesis of cholesterol from acetyl-CoA and acetoacetyl-CoA. HMG-CoA reductase (red) catalyses the major rate-limiting step of the cholesterol biosynthesis pathway, the conversion of HMG-CoA to mevalonate. Non-sterol isoprenoid products are derived from farnesyl pyrophosphate.

1.2.2.2 HMG2p degradation in *S. cerevisiae*

S. cerevisiae encodes two HMGCR orthologs, Hmg1p and Hmg2p. Whilst Hmg1p is a stable protein, Hmg2p is rapidly degraded in response to non-sterol isoprenoids by ERAD mediated by the Hrd1p E3 ubiquitin ligase (Hampton, Gardner, and Rine 1996, Gardner and Hampton 1999, Garza, Tran, and Hampton 2009). Farnesyl pyrophosphate binding to the SSD domain of Hmg2p altered the tryptic digest of Hmg2p and caused a greater tendency for aggregation (Shearer and Hampton 2005). Shearer and Hampton concluded that farnesyl pyrophosphate

binding induces a reversible conformational change in the SSD to a less ordered state and that this partially misfolded state is recognised by the HRD quality control pathway.

Lanosterol induces Nsg1p, the Insig ortholog, to associate with Hmg2p's transmembrane domain. The interaction with Nsg1p prevents the Hrd1p-mediated degradation of Hmg2p even in the presence of non-sterol isoprenoids (Flury et al. 2005, Theesfeld and Hampton 2013).

1.2.2.3 Sterol-induced degradation of HMGCR in mammalian cells

The ubiquitin proteasome system is responsible for the rapid sterol-dependent degradation of mammalian HMGCR. Treating cells with proteasome inhibitors stabilised HMGCR and resulted in an accumulation of ubiquitinated HMGCR (Ravid et al. 2000). The N-terminal transmembrane domain of HMGCR is entirely responsible for the sterol-induced degradation of HMGCR (Gil et al. 1985). At low cholesterol/sterol levels, HMGCR is a stable protein. However, the degradation of HMGCR can be rapidly induced by cholesterol and mevalonate-derived metabolites (Faust et al. 1982, Edwards, Lan, and Fogelman 1983, Nakanishi, Goldstein, and Brown 1988, Song, Javitt, and DeBose-Boyd 2005).

The presence of sterols induces the association of Insig1 and Insig2 with the SSD in HMGCR's transmembrane domain (**Figure 1.3**) (Sever, Yang, et al. 2003, Sever, Song, et al. 2003). The sterol-induced binding of Insigs to HMGCR is dependent on a YIYF motif in HMGCR's SSD (Sever, Song, et al. 2003). The first tyrosine in the YIYF motif is equivalent to Y286 in SCAP, which is required for the sterol-dependent interaction between Insigs and SCAP (Nohturfft, Brown, and Goldstein 1998a, Adams, Goldstein, and Brown 2003). In stark contrast to *S. cerevisiae*, it is thought that the Insig proteins act as scaffolds to recruit E3 ubiquitin ligase complexes to HMGCR (Jo and Debose-Boyd 2010, Jo et al. 2011). Ubiquitinated HMGCR is extracted from the ER membrane by the p97 complex and degraded by the 26S proteasome (Cao et al. 2007, Morris et al. 2014).

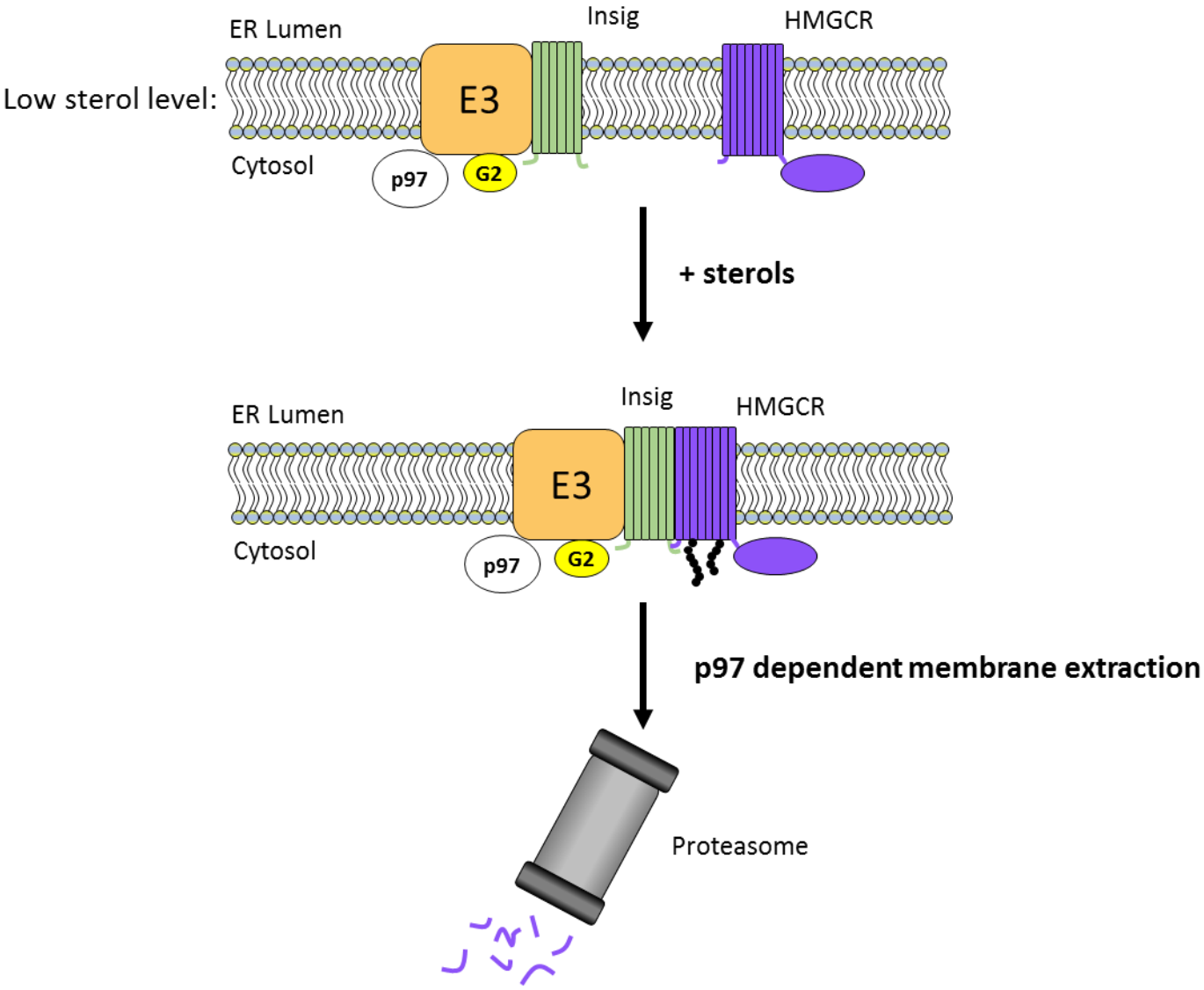

Figure 1.3 Sterol-induced degradation of HMGCR. High sterol levels induce the recruitment of the Insig proteins to HMGCR's transmembrane domain. The Insig proteins recruit ubiquitin E3 ligase complexes containing the E2 conjugating enzyme UBE2G2 (G2) and the p97 complex. HMGCR is ubiquitinated, extracted from the membrane and degraded by the proteasome.

1.2.2.4 The identity of the ubiquitin E3 ligase for HMGCR is controversial

The ubiquitin E2 conjugating enzyme UBE2G2 mediates the sterol-induced ubiquitination of HMGCR (Miao et al. 2010). However, the identity of the E3 ubiquitin ligase responsible for HMGCR ubiquitination is controversial. The *S. cerevisiae* Hrd1p E3 ligase has two mammalian orthologues, Hrd1 and gp78. Whilst, the loss of Hrd1 caused an increased steady-state expression level of HMGCR, a role for Hrd1 in sterol-induced HMGCR degradation was quickly dismissed (Kikkert et al. 2004).

The Debose Boyd laboratory suggested that gp78 was responsible for the sterol-induced degradation of HMGCR based on several observations (Song, Sever, and DeBose-Boyd 2005). They found gp78 to associate with Insig1 in the presence or absence of sterols and that Insig1 mediates a sterol-dependent gp78 and HMGCR interaction. The over-expression of the gp78's transmembrane domain had a dominant negative effect on HMGCR degradation. Depletion of gp78 by siRNA resulted in decreased sterol-induced degradation and ubiquitination of HMGCR (Song, Sever, and DeBose-Boyd 2005).

A few years later, the Debose Boyd laboratory suggested that the sterol-induced degradation of HMGCR was mediated by two partially redundant E3 ligases, gp78 and TRC8 (Jo et al. 2011). The depletion of either gp78 or TRC8 in the human fibroblast cell line SV-589 resulted in a partial decrease in sterol-induced HMGCR degradation. The simultaneous depletion of gp78 and TRC8 appeared to cause a nearly complete block in sterol-induced HMGCR degradation (Jo et al. 2011). Furthermore, hepatocytes from a liver-specific gp78-knockout mouse had an elevated level of steady state HMGR and a significant decrease in sterol-induced HMGCR degradation and ubiquitination (Liu et al. 2012).

In an independent study by Allan Weissman's laboratory, who first identified gp78 as an ERAD E3 ligase (Fang et al. 2001), mouse embryonic fibroblasts (MEFs) derived from gp78-knockout embryos showed no evidence of a role for gp78 in the sterol-induced degradation of HMGCR (Tsai et al. 2012). The Weissman laboratory addressed this discrepancy by depleting gp78 and TRC8 in the human fibroblast cell line (SV-589) used by the Debose Boyd laboratory (Song, Sever, and DeBose-Boyd 2005, Jo et al. 2011). These experiments showed no effect of the loss of gp78 and TRC8 on HMGCR degradation. The Weissman laboratory used a total siRNA concentration of 20 nM to deplete gp78 and TRC8, whereas the Debose Boyd laboratory used

a total siRNA concentration of 200 nM. When the Weissman laboratory repeated the experiment using 200 nM siRNA they observed a significant reduction in the sterol-induced degradation of HMGCR. However, the expression of an siRNA-resistant gp78 transgene could not restore HMGCR degradation (Tsai et al. 2012). Critically, the re-expression of gp78 could restore the expression of another gp78 substrate, CD82/KAI11 (Tsai et al. 2007). This strongly suggests that the phenotype observed by the Debose Boyd laboratory is the result of 'off-target' effects.

The identity of the E3 ubiquitin ligase responsible for the sterol-induced ubiquitination and degradation of HMGCR is therefore controversial. A major aim of this thesis will be to identify this ligase.

In *S. cerevisiae*, geranylgeranyl pyrophosphate induces the Hrd1-mediated ubiquitination of Hmg2 (Garza, Tran, and Hampton 2009). In mammalian cells, geranylgeraniol, the alcohol derivative of geranylgeranyl pyrophosphate, enhances the sterol-induced degradation of HMGCR by promoting the membrane extraction and dislocation of ubiquitinated HMGCR (Sever, Song, et al. 2003, Schumacher et al. 2015).

1.2.2.4 Cholesterol-regulated ERAD of the Insig proteins

Whilst the ability for gp78 to ubiquitinate HMGCR is controversial, independent laboratories have observed the sterol-regulated ubiquitination of Insig1 by gp78 (Lee, Song, et al. 2006, Tsai et al. 2012). In sterol depleted cells, Insig1 is ubiquitinated by gp78 and has a half-life of less than 30 minutes. In the presence of cholesterol, Insig1 interacts with SCAP and is protected from gp78-mediated ubiquitination. In the absence of SCAP, the addition of cholesterol does not stabilise Insig1 (Lee, Song, et al. 2006).

Insig1 is differentially regulated by sterols at the level of transcription and degradation. At low cholesterol levels, the Insig proteins dissociate from SCAP and so the SCAP-SREBP complex is transported to the Golgi for SREBP maturation. This results in SREBP-mediated upregulation of Insig1 transcription (Janowski 2002, Horton, Goldstein, and Brown 2002). Newly synthesised Insig1 will be degraded following gp78-mediated ubiquitination until the cholesterol level has increased sufficiently to induce the conformational change in SCAP to

allow Insig1 binding (Lee, Song, et al. 2006). At higher cholesterol levels, the Insig1-SCAP interaction retains SREBP in the ER, thereby inhibiting SREBP processing and Insig1 transcription, as well as stabilising the Insig1 protein (Gong et al. 2006).

Following ubiquitination, Insig1 must be extracted from the ER membrane before it can be degraded by cytosolic 26S proteasomes. UBXD8 recruits the p97 complex to gp78 to enable the membrane extraction of ubiquitinated Insig1. Unsaturated fatty acids block Insig1 ERAD by preventing the recruitment of the p97 complex to gp78 by UBXD8 (Lee et al. 2008).

In cultured cell lines, Insig2 is significantly more stable than Insig1 and is not degraded in a sterol-dependent manner (Lee and Ye 2004, Lee, Song, et al. 2006). Surprisingly, gp78-knockout murine primary hepatocytes had a dramatic increase in Insig2 expression and only a modest increase in Insig1 (Liu et al. 2012). Furthermore, a cycloheximide chase experiment also showed a significant decrease in Insig2 turnover in the gp78-knockout murine primary hepatocytes. This suggests that Insig2 might only be a gp78 substrate in hepatic cells (Liu et al. 2012).

1.2.2.5 Other gp78 substrates

Acyl-CoA:cholesterol acyltransferase 2 (ACAT2) catalyses the conversion of cholesterol and fatty acids to cholesteryl esters (Chang, Chang, and Cheng 1997). ACAT2 is ubiquitinated on cysteine 277 by gp78 in an Insig dependent manner (Wang, Bian, et al. 2017). High cellular cholesterol and lipid levels leads to the generation of reactive oxygen species (ROS) (Boden 2011). Cysteine 277 is oxidised by ROS, preventing ubiquitination and degradation (Wang, Bian, et al. 2017). ACAT2 is therefore stabilised at high cholesterol levels to increase the conversion of cholesterol to cholesteryl esters to reduce cellular lipid overload.

Diacylglycerol acyltransferase 2 (DGAT2) is one of the enzymes that catalyses the final step in triacylglycerol biosynthesis (McFie et al. 2011). Triacylglycerol is the dominant form of lipid storage in eukaryotes and so the regulation of DGAT2 is critical for lipid metabolism. Gp78 has been suggested to mediate the ubiquitination of DGAT2, however the stimulus and requirements for DGAT2 ERAD are yet to be defined (Choi et al. 2014)

Apolipoprotein B-100 (ApoB) is an essential member of the very low density lipoprotein (VLDL) and LDL complexes and is therefore required for plasma cholesterol transport (Fisher and Ginsberg 2002). When the lipids transported by the VLDL and LDL complexes are limited, ApoB is ubiquitinated by gp78, dislocated by the p97 complex and degraded by the 26S proteasome (Liang et al. 2003, Fisher, Khanna, and McLeod 2011).

1.2.2.6 TRC8 and cholesterol homeostasis

TRC8 is an ER resident, polytopic, RING-H2 E3 ligase that mediates the HCMV US2-induced degradation of cell surface receptors such as MHC-I and SPP-dependent degradation of tail-anchor proteins (Stagg et al. 2009, Boname et al. 2014, Hsu et al. 2015). TRC8 is the second E3 ubiquitin ligase implicated in HMGCR ERAD by the Debose Boyd laboratory but dismissed by the Weissman laboratory (Jo et al. 2011, Tsai et al. 2012). Both the Debose Boyd and Gemmill laboratories observed the co-precipitation of Insig1 and Insig2 with exogenous TRC8 (Lee et al. 2010, Jo et al. 2011). TRC8 has been reported to inhibit SREBP-2 processing by hindering the recruitment of SCAP to Sec24 (Irisawa et al. 2009). The transmembrane domain of TRC8 contains a sterol sensing domain (Irisawa et al. 2009). These observations suggest that TRC8 could contribute to the regulation of cholesterol homeostasis.

1.2.2.7 MARCH6 and cholesterol homeostasis

Squalene monooxygenase catalyses the oxygenation of squalene into monooxidosqualene and is considered a key, frequently over-looked, rate-limiting step down-stream of HMGCR in cholesterol biosynthesis (Sharpe and Brown 2013). Squalene monooxygenase is after the isoprenoid (farnesyl pyrophosphate) branch of the mevalonate pathway and so committed to cholesterol production. Two independent studies reported the cholesterol-dependent degradation of squalene monooxygenase by the ER-resident E3 membrane-associated RING Finger 6, MARCH6 (Foresti et al. 2013, Zelcer et al. 2014). Zelcer *et al*. noticed that MARCH6 influenced HMGCR expression. They observed an increase in the basal level of HMGCR when MARCH6 was depleted by siRNA, but could not see a definitive effect of MARCH6 depletion on the sterol-induced degradation of HMGCR (Zelcer et al. 2014).

The Zelcer laboratory published a later paper showing that MARCH6 acts as a negative regulator of SREBP-2 in hepatic cells, although no difference in SREBP-2 abundance or processing was detected (Loregger et al. 2015). The loss of MARCH6 also increased expression of the E3 ligase inducible degrader of LDLR (IDOL) in a wide range cell lines (Loregger et al. 2015). IDOL is the E3 ubiquitin ligase that targets LDLR for degradation (Zelcer et al. 2009). There is therefore a significant decrease in LDLR protein abundance and LDL uptake following MARCH6 depletion (Loregger et al. 2015).

1.2.3 Cholesterol Uptake

To maintain cholesterol homeostasis, cells must balance the uptake of exogenous cholesterol as well as the endogenous production of cholesterol. Cholesterol is transported in low density lipoprotein (LDL) particles as cholesterol esters. LDL particles bind to the LDLR, which is internalised by clathrin-mediated endocytosis (Brown and Goldstein 1986). LDL particles dissociate from the LDLR as the pH of endosomes decreases. The LDLR is recycled back to the plasma membrane, whereas the LDL particles continue through the endosomal pathway to lysosomes (Brown, Anderson, and Goldstein 1983). Lysosomal acid hydrolases hydrolyse the LDL bound cholesteryl esters to release cholesterol from LDL particles (Sugii et al. 2003). The Niemann-Pick type C (NPC) proteins then facilitate cholesterol exit from lysosomes. Unesterified cholesterol first binds to NPC2, a small lysosomal protein. NPC2 bound cholesterol is transferred to NPC1, a large membrane spanning protein, and inserted into the membrane (Infante et al. 2008, Kwon et al. 2009, Wang et al. 2010). Cholesterol can then be transported to other cellular membranes (Chang et al. 2006, Urano et al. 2008). Loss-of-function mutations in the NPC genes cause a dramatic accumulation of cholesterol in lysosomes, particularly in the liver, brain, and lungs, leading to death during childhood (Vanier and Millat 2003).

The expression of the LDLR is tightly regulated transcriptionally and post-transcriptionally to control cholesterol uptake. The LDLR is a SREBP target gene (Horton, Goldstein, and Brown 2002). Therefore, at low cellular cholesterol levels, LDLR expression is upregulated to increase cholesterol uptake.

Two distinct mechanisms target the LDLR for degradation. Proprotein convertase subtilisin/kexin type 9 (PCSK9) is a secreted protein that binds to the LDLR. In the presence of the autosomal recessive hypercholesterolaemia (ARH) adapter, the PCSK9/LDLR complex is internalised (Lagace et al. 2006). Whilst the lower pH in endosomes promotes the dissociation of LDL from the LDLR, PCSK9 has a higher affinity for the LDLR in the more acidic environment. The PCSK9-bound LDLR cannot be recycled back to the plasma membrane, instead the complex is degraded in lysosomes (Horton, Cohen, and Hobbs 2007).

Activation of the transcription factor LXR by ligands, such as oxysterols, upregulates the expression of the ubiquitin E3 ligase IDOL. IDOL contains a C-terminal RING domain that mediates the ubiquitination of the LDLR, targeting the LDLR for lysosomal, rather than proteasomal, degradation (Zelcer et al. 2009).

1.3 Forward genetic screens

The genomic era, in which we now have a detailed description of an organism's genetic content, has been enabled by next generation sequencing. The task is now to understand the function of the sequence of nucleotides. In 2007, it was estimated that two-fifths of the human genome remained uncharacterised (Reichardt 2007). Forward genetic screens are used to determine gene function, are a powerful tool in providing insight into the cellular pathways genes are involved in and can be used to implicate genes in pathological processes.

Forward genetic screens can be performed in a remarkable range of cell types or model organisms using a variety of techniques. All forward genetic screens share the same underlying concept: select a process of interest, predict the phenotype that mutants unable to carry out this process will present, select the mutants with that phenotype and determine the sites of mutations to identify the affected genes (Forsburg 2001).

1.3.1 Forward genetic screens in model organisms

Hermann Müller pioneered the concept of forward genetic screens by studying the effect of X-ray induced mutations in *Drosophila melanogaster* (Muller 1927). Since this early work a

diverse repertoire of techniques has made *D. melanogaster* one of the most tractable organisms for geneticists (Rubin and Lewis 2000, Venken and Bellen 2014). *D. melanogaster* forward genetic screens have provided significant insight into fundamental biological processes (Nüsslein-Volhard and Wieschaus 1980, St Johnston 2002, Housden et al. 2017).

The budding yeast *S. cerevisiae* has been used extensively as a model organism to study a diverse range of biochemical processes (Hartwell, Culotti, and Reid 1970, Novick, Field, and Schekman 1980, Hampton, Gardner, and Rine 1996). The ability to maintain *S. cerevisiae* in a haploid state is extremely useful for geneticists (Nasmyth and Shore 1987). A haploid genome enables forward genetic screens, because the disruption of a gene cannot be compensated for by a second allele and so results in the loss of gene expression.

In *S. cerevisiae* based screens, chemical or insertional mutagenesis is typically used to generate a population of mutants. Chemical mutagenesis involves treating cells with a chemical mutagen to create point and frame-shift mutations. Whereas, insertional mutagenesis involves the integration of a construct into a gene. Whilst chemical mutagenesis can induce a wider range of mutations, insertional mutagenesis is generally favoured as it is considerably easier to identify insertion sites than to identify chemically induced mutations.

While the results from model organisms are insightful, the phylogenetic distance from mammals often renders the extrapolation of results into mammalian cell biology inappropriate (Grimm 2004). It is therefore important to interrogate mammalian biological processes using genetic screens in mammalian cells.

1.3.2 Forward genetic screens in human cells

1.3.3.1 Gene silencing by RNA interference

The application of forward genetic screens in mammalian systems was hindered by the difficulty of generating and recovering bi-allelic mutations in diploid cells. Initial efforts to perform genome-wide loss of function screens used RNA-interference (RNAi) to silence gene expression by targeting mRNA.

RNA interference refers to a gene silencing mechanism that was discovered in *C. elegans* (Fire et al. 1998). Long double-strand RNAs (dsRNAs) are processed by a Dicer ribonuclease to

create ~21 nucleotide dsRNAs (Bernstein et al. 2001). The processed dsRNAs are loaded into the RNA-induced silencing complex (RISC), which is then targeted to and degrades the cognate mRNA (Song et al. 2004). This mechanism can be exploited by transfecting cells with small interfering RNA (siRNA) duplexes that can be loaded onto RISC and therefore silence a gene of interest. Alternatively, short hairpin RNAs (shRNAs) can be stably expressed to mediate gene silencing. The RNaseIII enzyme Drosha initially processes shRNAs in the nucleus before further processing by Dicer in the cytosol to generate dsRNAs that can be loaded onto the RISC complex (Hutvágner et al. 2001, Lee et al. 2003).

1.3.3.2 Genome-wide RNAi screens

By targeting mRNA to silence a gene, RNAi circumvents the problem presented by multiple alleles. Genome-wide siRNA screens can be performed by transfecting cells with siRNAs targeting every gene in the genome. This method has successfully identified genes involved in lipid droplet formation (Guo et al. 2008), influenza virus replication (Karlas et al. 2010) and embryonic stem cell identity (Chia et al. 2010). However, RNAi usually only results in a partial knockdown of gene expression, which is not always sufficient to induce a phenotype. Off-target effects of siRNAs are also a major problem, where siRNAs target a non-cognate mRNA (Jackson et al. 2003, Jackson et al. 2006, Sudbery et al. 2010). Another significant drawback of genome-wide siRNA screens is that they are very labour-intensive and expensive. Each gene is individually targeted in a separate pool of cells, therefore analysing approximately 20,000 genes with multiple independent siRNAs for each gene requires an extraordinary number of individual experiments.

An alternative approach to siRNA libraries was to use shRNA libraries, which offered several advantages (Bernards, Brummelkamp, and Beijersbergen 2006, Chang, Elledge, and Hannon 2006, Moffat et al. 2006, Root et al. 2006, Bassik et al. 2009). As shRNAs can be stably expressed from a viral vector, they provide a longer period for gene knockdown to occur. A shRNA screen can be performed as a pooled experiment, instead of thousands of individual knockdowns. The shRNAs in the selected cells can be identified by amplifying and barcode from the shRNA vector by a conventional PCR reaction and deep sequencing (Bernards, Brummelkamp, and Beijersbergen 2006). Whilst genome-wide shRNA screens have provided useful insights, partial knockdown of gene expression and off-target effects still hamper shRNA screens.

1.3.4 Retroviral gene-trap mutagenesis screens in near-haploid human cells

The Brummelkamp laboratory reported a major breakthrough using the near-haploid human KBM7 cell line (**Figure 1.4**) (Carette et al. 2009). The KBM7 cell line was derived from a patient with chronic myeloid leukaemia and has a haploid karyotype except for chromosome 8 and the sex chromosomes (Andersson et al. 1987, Kotecki, Reddy, and Cochran 1999). Carette et al. developed a retroviral gene-trap vector to randomly mutate a population of KBM7 cells (Carette et al. 2009). The gene-trap vector contains a strong adenoviral splice acceptor site upstream of a promoterless reporter gene (mCherry in this thesis) and an SV40 polyadenylation signal. Following integration into the sense-strand of a gene, the strong splice acceptor site will accept splicing from the upstream exon, thereby producing a mCherry-fusion transcript terminating at the polyadenylation signal. As KBM7 cells only have a single allele of most genes, insertion of the retroviral gene-trap vector into a gene results in its inactivation. Carette et al. demonstrated that the retroviral gene-trap vector integrates into 98% of all expressed genes, 90% of marginally expressed genes and 65% of non-expressed genes (Carette, Guimaraes, et al. 2011). Brummelkamp and collaborators have used this forward genetic screen system to identify host genes required for the toxic effects of the cytolethal distending toxins (Carette, Guimaraes, et al. 2011), the binary actin-ADP ribosylating toxin *Clostridium difficile* transferase (Papatheodorou et al. 2011), tunicamycin (Reiling et al. 2011), cholera toxin (Guimaraes et al. 2011), Ebola virus (Carette, Raaben, et al. 2011), *Chlamydia trachomatis* (Rosmarin et al. 2012), 3-bromopyruvate (3-BrPA) (Birsoy et al. 2013), Lassa virus (Jae et al. 2013), Andes virus (Kleinfelter et al. 2015) and Rift Valley fever virus (Riblett et al. 2015). This approach has proven to be extremely powerful and successful when screening for resistance to a lethal phenotype.

The Lehner laboratory has developed this technique to use a fluorescence-based phenotypic selection. This allows the investigation of a diverse range of cellular processes as we are no longer restricted to a lethal phenotype (Duncan et al. 2012, Timms et al. 2013, van den Boomen et al. 2014, Tchasovnikarova et al. 2015). At the start of my thesis, retroviral gene-trap mutagenesis screens in near-haploid cells represented the gold standard for forward genetic screens in human cells.

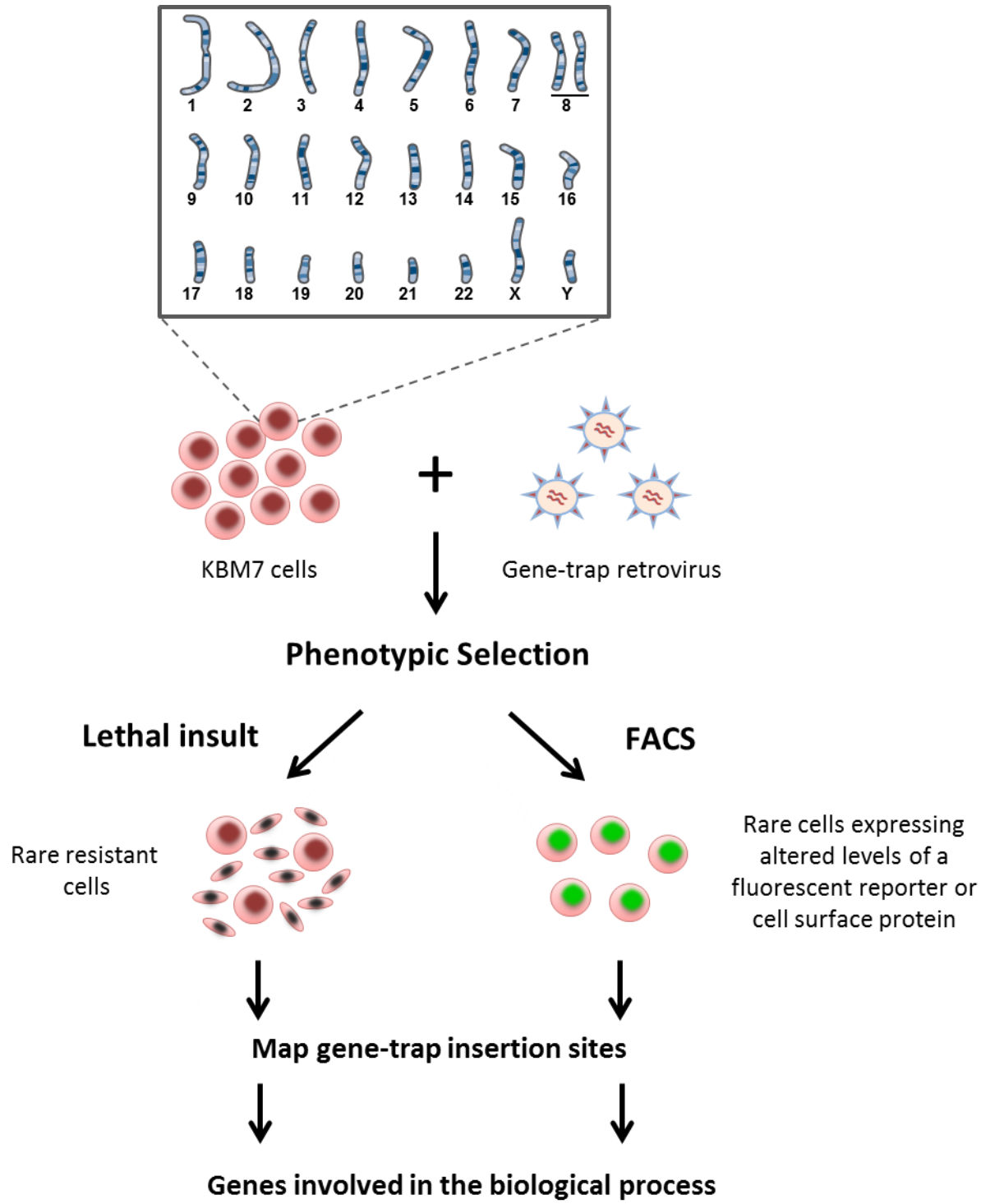

Figure 1.4 Retroviral gene-trap mutagenesis screens in the near-haploid KBM7 cell line. The KBM7 cell line has a haploid karyotype except for chromosome 8 and the sex chromosomes. Mutagenesis of the KBM7 cell line using the gene-trap retrovirus creates a library of knockout cells. A selection can be performed to identify knockouts that display a phenotype of interest. Mapping the integration sites of the gene-trap retrovirus in the selected cells reveals the identity of the disrupted genes whose loss resulted in the phenotype of interest.

1.3.5 Genome-wide CRISPR/Cas9 knockout screens

Precise genome editing using programmable nucleases are a transformative technology for cell biology research. Custom nucleases that can be designed to target a specific locus have been used for several years, including zinc-finger nucleases (ZFNs) (Carroll 2011) and transcription activator-like effector nucleases (TALENs) (Joung and Sander 2013). However, the microbial Type-II Clustered Regularly Interspaced Palindromic Repeats (CRISPR)/ associated (Cas9) system is an exciting advance with a wide range of applications (Hsu, Lander, and Zhang 2014). A short guide RNA (gRNA), typically 20 bp, targets the Cas9 nuclease to a specific locus where the two nuclease domains of Cas9, HNH and RuvC, create a double strand break (DSB) in the DNA (**Figure 1.5A**) (Nishimasu et al. 2014, Sternberg et al. 2014). In most cases, the DSB will be repaired by the non-homologous end joining (NHEJ), an error-prone process that frequently results in small insertions or deletions (Chiruvella, Liang, and Wilson 2013). If the inserted or deleted sequence disrupts the coding sequence that allele will be knocked-out (**Figure 1.5B**). Alternatively, if a donor template is provided, the double strand break can be repaired precisely by homologous recombination (HR). Sequences can be introduced to endogenous loci by inserting the desired sequence into the donor template (**Figure 1.5B**). The simplicity of the CRISPR/Cas9 system enables cheap and rapid genome editing.

By using a large library of gRNAs to target the Cas9 nuclease to all annotated genes, CRISPR/Cas9 can be used to perform genome-wide forward genetic screens. At the start of my thesis project, four independent laboratories had reported proof-of-principle genome-wide CRISPR knockout screens (Shalem et al. 2014, Wang et al. 2014, Zhou et al. 2014, Koike-Yusa et al. 2014). These studies opened the exciting potential of performing genome-wide CRISPR/Cas9 screens in any cell type, as the CRISPR/Cas9 system is not restricted to a haploid karyotype.

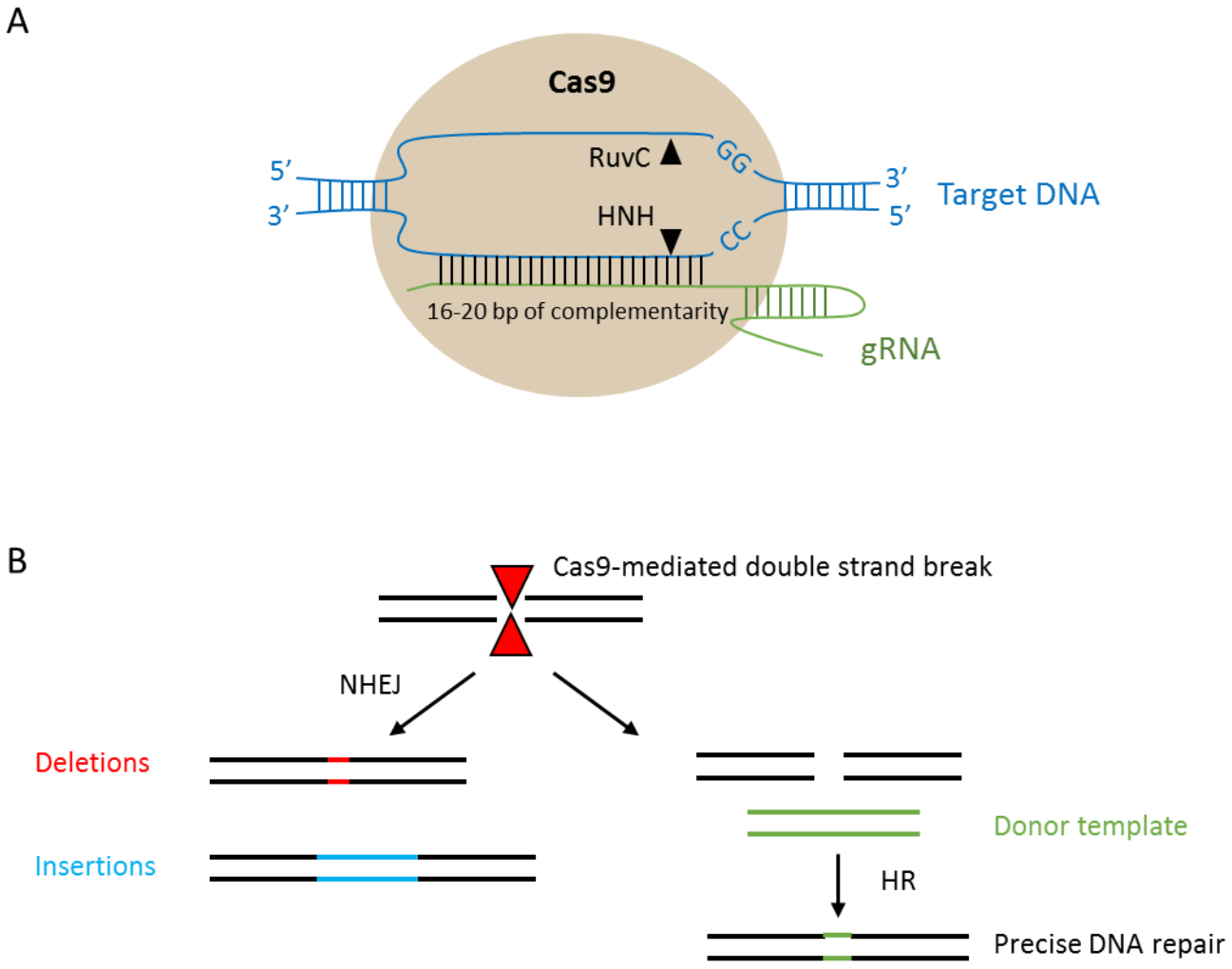

Figure 1.5 The CRISPR/Cas9 system (A) Schematic view of CRISPR/Cas9-mediated DNA cleavage. A gRNA targets the Cas9 nuclease to its complementary sequence. The HNH and RuvC nuclease domains cleave the DNA resulting in a double strand break. **(B)** A CRISPR/Cas9-mediated double strand break can be repaired by non-homologous end joining (NHEJ) or homologous recombination (HR). NHEJ is an error-prone process that results in small insertions or deletions. HR uses a template to precisely repair a double strand break.

1.4 Aims of this thesis

1. Forward genetic screens are a powerful tool to elucidate gene function. At the beginning of my thesis project, the gold standard in forward genetic screens in cultured human cells were retroviral gene-trap mutagenesis screens in the near-haploid KBM7 cell line. The advent of CRISPR/Cas9 technology offers a method to generate bi-allelic mutations and therefore gene knockouts. The first proof-of-principle studies demonstrated that large gRNA libraries could be used to target the Cas9 nuclease to all annotated genes and thereby perform genome-wide CRISPR knockout screens. The major aim of the first part of my thesis project was to compare gene-trap mutagenesis haploid screens to CRISPR screens to determine which technology is more effective. This is described in Chapter 4.

2. The sterol-induced degradation of HMGCR, the enzyme that catalyses the rate-limiting step in cholesterol biosynthesis, is a critical mechanism used by cells to regulate cholesterol homeostasis. At high cholesterol/sterol levels, HMGCR is rapidly degraded by the ubiquitin proteasome system. The Debose-Boyd laboratory has reported that gp78 and TRC8 are responsible for the sterol-induced ubiquitination of HMGCR (Song, Sever, and DeBose-Boyd 2005, Jo et al. 2011). However, an independent study by the Weissman laboratory did not observe a requirement for gp78 or TRC8 in HMGCR degradation (Tsai et al. 2012). I therefore wanted to use forward genetic screens as an unbiased approach to identify the E3 ubiquitin ligase(s) responsible for HMGCR ubiquitination. I would then aim to biochemically characterise the E3 ubiquitin ligases identified by the forward genetic screens. These data are described in Chapters 5, 6 and 7.

Chapter 2: Materials and Methods

2.1 Materials

2.1.1 Buffers

Phosphate-buffered saline (PBS): 137 mM NaCl, 2.7 mM KCL, 10 mM Na_2NPO_4, 2 mM KH_2PO_4, pH 7.4

TRIS-buffered saline (TBS): 10 mM Tris, 150 mM NaCl, pH 7.4

Luria-Bertani (LB) medium: 1% (w/V) Bacto-trptone, 0.5% (w/v) Bacto-yeast extract, 1% (w/v) NaCl, 0.1% (w/v) glucose

SOC medium: 2% tryptone, 0.5% w/v yeast abstract, 10 mM NaCl, 2.5 mM KCl, 10 mM $MgCl_2$, 10 mM $MgSO_4$ and 20 mM glucose

6X SDS Loading Buffer: 60% glycerol, 300 mM Tris pH 6.8, 6% (w/v) SDS, 9% (w/v) DTT, 0.03% (w/v) bromophenol blue

Bind and wash (B&W) buffer: 5 mM Tris-HCl pH 7.5, 0.5 mM EDTA, 1 M NaCl

2.1.2 Enzymes, Reagents and Inhibitors

Enzymes for manipulation of DNA were purchased from New England Biolabs (NEB). Reagents and inhibitors were purchased from Sigma unless otherwise stated.

2.1.3 Antibodies

Primary antibodies used were as follows: mAb W6/32 (recognises conformational MHC-I), rabbit α-TXNDC11 (Abcam, ab188329), rabbit α-FLAG (Sigma-Aldrich, F7425), mouse M1 α-FLAG (Sigma-Aldrich, F3040), mouse α-B-Actin (Sigma-Aldrich, A5316), rabbit α-GANAB (GeneTex, GTX102237), rabbit α-EDEM2 (Sigma-Aldrich, E1728), rabbit α-EDEM3 (Sigma-Aldrich E0409), rabbit α-PDI (Cell Signaling, #2446), SEL1L (Santa Cruz, sc-48080), GLU2B, mouse α-calnexin (AF8, a kind gift from M. Brenner, Harvard Medical School), Calreticulin,

mouse α-HMGCR (Santa Cruz, sc-27195), rabbit α-HMGCR (Abcam, ab174830), rabbit α-gp78 (ProteinTech, 16675-1-AP), rabbit α-RNF145 (ProteinTech, 24524-I-AP), mouse α-V5 (Abcam, ab27671), mouse VU-1 α-ubiquitin (Life Sensors, VU101), rabbit α-myc (Cell Signalling, 2278), mouse α-UBE2G2 (Santa Cruz, sc-100613), mouse α-mCherry (Novus Biologicals, NBP1-96752), rabbit α-UROD (Novus Biologicals, NBP2-20818).

HRP-conjugated goat α-mouse and goat α-rabbit (Jackson). Alexa Fluor 647-conjugated α-mouse (Life Technologies).

2.2 Molecular biology

2.2.1 Polymerase chain reaction

Oligonucleotide primers were purchased from Sigma-Aldrich. For DNA template, typically used 10 ng of plasmid DNA, 60 ng of cDNA library or 100 ng of genomic DNA in a total volume of 50 µl using Phusion DNA polymerase (NEB). Standard conditions were:

10 µl	5x Phusion-HF Buffer (NEB)
X ng	DNA template
1 µl	10 mM dNTP mix
0.25 µl	Primer 1 (100 µM)
0.25 µl	Primer 2 (100 µM)
0.5 µl	Phusion polymerase
To 50 µl	ddH_2O

Typical cycling parameters were:

95°C	30 s	
95°C	10 s	x 30 cycles
55-68°C	20 s	
72°C	20 s per kb	
72°C	5 min	

2.2.2 Fluorescent PCR to identify CRISPR-induced frame-shift mutations

Genomic DNA was extracted from wild type HeLa cells and RNF145 CRISPR clones using the Quick-gDNA MicroPrep kit (Zymo Research). Oligonucleotides were ordered from Sigma-Aldrich. To ensure a clean product, a nested PCR was performed. One of each primer pair for the second PCR was modified with 6FAM at its 5' end. For gRNA #5 PCR1_Forward: *GATTACAGGCGTGAGCCACCG*, PCR1_Reverse: *GTCTTTCTCCAGGAGCTTGTG*, PCR2_Forward: *CATAACCTGCCATCTAACTCC* and PCR2_Reverse: *GAAACACTTCCGTGCTGTAAGC*. For gRNA #8 PCR1_Forward: *CAGAATGCTCACTAGAAGATTAG*, PCR1_Reverse: *GTAGTATACGTTCTCACATAG*, PCR2_Forward: *GTGATGTAGACACTCACCTAC* and PCR2_Reverse *GTGACAACCTATTAGATTCGTG*. The size of the PCR product from the genomic DNA from wild type HeLa cells and each RNF145 CRISPR clone was resolved using an ABI 3730xl DNA Analyser.

2.2.3 DNA Cloning

2.2.3.1 Gibson assembly

Recombinant DNA plasmids were constructed using standard ligation or the Gibson assembly method (Gibson et al. 2009). Plasmid vectors were digested for 4 h with restriction enzymes at the appropriate temperature, typically 37^{o}C, and then run out on an agarose gel. Bands were excised and purifired using the QIAquick gel extraction kit (Qiagen). PCR was used to amplify inserts with 20-30 bp overhangs with the desired vector. PCR products were also run out on an agarose gel and purified using the QIAquick gel extraction kit. The DNA concentration of inserts and vectors were measured using a NanoDrop spectrophotometer. Typically, 50 ng of vector and a 2-3 fold molar excess of inserts were mixed with and equal volume of 2x Gibson Assembly Maser Mix (NEB) and incubated for 1 h at 50^{o}C. Two microliters of the mix was used to transform 5-alpha Competent *E. coli* (NEB) which were then spread on agar plates, containing ampicillin or kanamycin, and incubated overnight at 37oC. Individual colonies were picked into 3 ml LB medium containing ampicillin or kanamycin and cultured at 37oC for 16 h with shaking.

The *E. coli* were pelleted by centrifugation and plasmid DNA was isolated using the QIAprep Spin miniprep kit (Qiagen). A sample of the plasmid DNA from each colony was digested and resolved on an agarose gel to ensure the insert was the correct size. Constructs were verified by Sanger sequencing (SourceBioscience).

2.2.3.2 DNA ligation cloning

Plasmid vectors were digested for 4 hr with restriction enzymes, run out on a gel and the desired bands were purified using the QIAquick gel extraction kit. Inserts were cut from plasmid DNA or amplified by PCR. PCR products were digested with restriction enzymes for at least 6 h, run out on a gel and purified using the QIAquick gel extraction kit. The DNA concentration of digested vectors and inserts was measured using a NanoDrop spectrophotometer. The vector and insert were mixed in a 1:4 molar ratio with T4 DNA Ligase (NEB) and incubated at room temperature for 1 h. Two microliters of the ligation mix were used to transform DH5α *E. coli* (Bioline) which were spread on selective agar plates and incubated overnight at 37^{o}C. Individual colonies were selected into 3ml of LB medium containing ampicillin or kanamycin and cultured at 37^{o}C for 16 h with shaking. Plasmid DNA was then isolated using the QIAprep spin miniprep kit. Constructs were verified by Sanger sequencing (SourceBioscience).

2.2.3.3 gRNA cloning

For CRISPR-mediated gene disruption, gRNAs were cloned as recommended by the Zhang laboratory (Ran et al. 2013). Oligonucleotides were ordered from Sigma-Aldrich, annealed, and cloned into the dual Cas9 and gRNA expression vector pSpCas9(BB)-2A-Puro (Addgene #48139, deposited by Dr. Feng Zhang) or the lentiviral gRNA expression vector pKLV-U6gRNA(BbSI)-PGKpuro2ABFP (Addgene #50946, deposited by Dr. Kosuke Yusa).

2.3 Constructs

2.3.1 Lentiviral vectors

The pHRSIN lentiviral system was used for the expression of exogenous genes (Demaison et al. 2002). These vectors contain the cis-acting HIV1 viral elements, the long terminal repeats (LTRs), the ψ packaging signal, the rev response element (RRE) and the central polypurine

tract (cPPT), with an internal spleen-focus forming virus (SFFV) promoter to drive expression of the gene of interest, followed by the woodchuck hepatitis virus post-transcriptional regulatory element (WPRE) to increase the stability of the transcribed mRNA. A downstream promoter drives the expression either a fluorescent protein or a selectable marker.

2.3.2 Lentiviral expression of exogenous genes

The lentiviral vectors pHRSIN-P_{SFFV}-GFP-P_{PGK}-Blasticidin^R, pHRSIN-P_{SFFV}-GFP-P_{PGK}-Hygromycin^R and pHRSIN-P_{SFFV}-GFP-P_{PGK}-Puromycin^R were used for exogenous expression, with the gene of interest cloned in place of GFP.

pHRSIN GFP-HLA-A2 was a kind gift from Dr. Louise Boyle. TXNDC11 coding sequence was ordered as a series of gBlocks (IDT) and assembled using the Gibson Assembly method by Richard Timms. TXNDC11 mutants were cloned by Richard Timms using site directed mutagenesis.

The transmembrane domain of HMGCR and mCherry encoding sequences were amplified by PCR from plasmid vectors (HMGCR construct was a kind gift from Dr Joseph Roitelman) and assembled into pHRSIN using the Gibson Assembly method.

RNF145 and Insig1 IMAGE clones were purchased from Geneservice by Dick van den Boomen. The open reading frames were amplified by PCR and cloned into pHRSIN vectors. RING and sterol sensing domain mutations were created by amplifying the RNF145 coding sequence by PCR in fragments so that mutations could be introduced in the primers. The PCR fragments were assembled into pHRSIN using the Gibson Assembly method. The coding sequence for Insig2 was amplified from HeLa cDNA and cloned into pHRSIN using the Gibson Assembly method. The nuclease Cas9 was cloned from the lenti-Blast vector (Addgene #49535, kindly deposited by Feng Zhang) into pHRSIN using BamHI and NotI.

2.3.3 Donor template vector for CRISPR-mediated knock-in

A donor template for creating a HMGCR-Clover knock-in was created by modifying the pDonor loxP Ub-Puro vector (a generous gift from Prof Ron Kopito). Homology arms of approximately

1 kb were amplified from HeLa genomic DNA by PCR, and assembled with the loxP-Ub-Puro cassette from pDonor loxP Ub-Puro and the backbone from pMAX-GFP (Amaxa) digested with NsiI and PciI using the Gibson Assembly method.

2.3.4 Lentiviral expression of shRNAs

For expression of shRNAs, the pHR-SIREN vector was used. Oligonucleotides were ordered from Sigma-Aldrich, annealed, cloned into the pHR-SIREN vector using BamHI and EcoRI, and sequence verified. Hairpins were designed using Clontech's RNAi target sequence selector. Oligonucleotide sequences in Appendix 1.

2.4 Cell culture

2.4.1 Tissue culture

KBM7 cells were maintained in IMDM supplemented with 10% fetal calf serum and penicillin/streptomycin. HeLa and 293T cells were maintained in DMEM supplemented with 10% fetal calf serum and penicillin/streptomycin. Single cell HeLa cells were seeded into flat-bottomed 96-well plates.

2.4.2 Sterol depletion

HeLa cells were seeded prior to sterol depletion. Attached, approximately 50% confluent, HeLa cells were washed five times with PBS. Washed cells were then cultured overnight in DMEM supplemented with 10% lipoprotein-depleted fetal calf serum (a kind gift from Prof David Savage then purchased from Biosera) plus 10 µM Mevastatin (Source Bioscience) and penicillin/streptomycin. Final concentrations of 2 µg/ml 25-hydroxycholesterol (Sigma-Aldrich) and 20 µg/ml cholesterol (Sigma-Aldrich) were added to sterol depleted cultures to analyse sterol-induced protein degradation.

2.4.3 Transfection of HeLa cells

HeLa cells were transfected using the TransIT-HeLaMONSTER kit (Mirus) according to the manufacturer's instructions. Cells were seeded at a confluency of 20-30% in 12-well plates and transfected with 1 µg DNA, 3 µl TransIT-HeLa reagent and 2 µl MONSTER reagent in OptiMEM (Gibco). When HeLa cells were transfected with pools of gRNAs, the 1 µg was split evenly between the individual gRNA-expressing constructs.

2.4.4 Transfection of siRNAs

HeLa cells were transfected at 20-30% confluency in 6-well plates. 10 µl of Oligofectamine (Invitrogen) as mixed with 20 µl of OptiMEM (Gibco) and incubated at room temperature for 5 min. In a separate tube, siRNA was diluted in OptiMEM (total volume 170 µl), combined with the oligofectamine/OptiMEM mixture and incubated at room temperature for a further 20 min. The medium was removed from the cells and replaced with antibiotic-free DMEM supplemented with 20% FCS. The siRNA/oligofectamine mixture was diluted further with 800 µl of OptiMEM before being added to the cells. Control samples were transfected MISSION siRNA Universal Negative Control (Sigma-Aldrich). Gene-targeting siRNA sequences are in Appendix 1.

2.4.5 Lentivirus production

Lentivirus was generated by triple transfection of HEK 293T cells with the pHRSIN lentiviral vector plus the packaging vectors pCMVΔR8.91 and pMD.G. For a standard transection in a 6-well plate, HEK 293T cells seeded at 70% confluency in antibiotic free medium were transfected with 2 µg total DNA (comprising 1 µg pHRSIN vector, 0.7 µg pCMVΔR8.91 and 0.3 µg pMD.G) using TransIT-293 (Mirus) as recommended by the manufacturer. After 48 h the supernatant was harvested, filtered through a 0.45 µm filter and added to target cells, which were then centrifuged at 1800 rpm for 45 min. Transgene expression was typically assessed 48 h post-transduction. Drug selection typically started 24 h post-transduction.

2.4.6 Flow cytometry

Cells were washed with PBS and resuspended in cold PBS. Samples were analysed using a FACSCalibur (BD) or a LSRFortessa (BD). Flow cytometry data was analysed using FlowJo software.

2.4.7 Fluorescence-activated cell sorting (FACS)

Cells were harvested, washed with PBS, resuspended in sort solution (PBS containing 10 mM HEPES and 2% FCS) and filtered through a 50 µm filter. Samples were sorted on an Influx machine (BD).

2.5 Haploid Genetic Screen

2.5.1 Retroviral gene-trap mutagenesis

Gene-trap retrovirus was produced by triple transfection of HEK 293T cells with the gene-trap retrpviral vector plus the packaging vectors pMD.GagPol and pMD.G in a ratio of 10:7:3. Gene-trap retrovirus was produced in 14 cm plates. The viral supernatant was harvested 48 h post-transfection and directly applied to KBM7 cells for a screen to ensure maximise the viral titer.

Transduction of 100 million KBM7 cells was performed in 24-well plates with 500 µl of viral supernatant added to $1x10^6$ KBM7 cells per well with 10 µg/ml polybrene. The plates were spun for at 1800 rpm for 1 h. Three hours later, the cells were pooled, spun down and resuspended in fresh IMDM. The transduction efficiency was determined 48 h post-transduction by assessing mCherry (marker on the retrovirus) by flow cytometry.

2.5.2 Iterative FACS selection

Mutagenised KBM7 cells were cultured for eight days before being sorted by FACS. Typically, the highest 0.6% of GFP-expressing cells are selected in the first round of FACS. The selected cells were expanded in culture before a second round of FACS was performed to purify the GFP^{high} population.

2.5.3 Mapping retroviral integration sites

Genome DNA was isolated from 5 million selected KBM7 cells and 5 million unselected mutagenised KBM7 cells using the Gentra Puregene kit (Qiagen). The genomic DNA was digested overnight with either NlaIII or MseI. The digested DNA was then purified using the Qiagen PCR purification kit. Annealed adaptors (sequences in Appendix 2) were ligated onto the genomic DNA fragments using T4 DNA Ligase (NEB) overnight at 4^{o}C. Another column clean-up was performed using the Qiagen PCR purification kit followed by a further clean up with 0.75x Ampure XP beads (Agencourt). The adapter annealed-DNA was then used as the template for a linear PCR (Accuprime Taq HiFi, Invitrogen; 250 cycles) with a biotinylated primer binding just upstream of the 5'LTR of the integrated retrovirus. The product was then annealed to 5 µl streptavidin dynabeads (M-280 Invitrogen, blocked for 20 min with 0.5% BSA) for 2 h at room temperature in binding and wash (B&W) buffer plus 0.1% Tween-20 with orbital shaking at 1100 rpm. After washing, the beads were used as the template for an exponentrial PCR (18 cycles) with a P5-adapted primer binding to the viral 5' LTR and a barcoded and P7-adapted primer binding the 3' adaptor. After a final column clean-up the PCR product was sequenced using the Illumina HiSeq platform using a custom primer binding to the extreme end of the viral 5' LTR.

2.5.4 Analysis of sequencing data to identify retroviral integration sites

Illumina HiSeq data as analysed through a custom analysis pipeline developed by Richard Timms. Using the fastx toolkit (http://hannonlab.cshl.edu/fastx_toolkit/) the raw cram files were converted into fastq files and bases with low quality scores and adaptor sequence were trimmed from the 3' end of the reads. Reads less than 20 bp long were then discarded, and identical sequences amoung the remaining reased were collapsed into a single fasta file. These reads were then mapped to the human genome (hg19) using Bowtie (Langmead et al. 2009). Reads that mapped uniquely to the human genome were imported into SeqMonk (http://www.bioinformatics.babraham.ac.uk/projects/seqmonk/), converted into a set of inique integration sites and quantified using the gene-trap analysis pipeline. For the bubble plot presented in **Figure 3.2C**, the degree of enrichment of each gene in the selected population compared to the unselected cells was calculated using a Bonferroni-corrected one-sided Fisher's exact test. All genes found to contain gene-trap integrations are listed

alphabetically on the x-axis; bubble size is proportional to the number of gene-trap integrations predicted to inactivate gene expression (in parentheses).

2.6 CRISPR knockout screens

2.6.1 gRNA libraries

For the genome-wide CRISPR knockout screens in **Figure 3.3D**, **Figure 4.2E** and **Figure 4.6E**, the Genome-Scale CRISPR Knock-out (GeCKO v2) library was used (addgene #1000000049, deposited by Feng Zhang) (Sanjana, Shalem, and Zhang 2014). For the genome-wide CRISPR knockout screens in **Figure 5.3D** and **Figure 5.5E** the Bassik gRNA library was used (a kind gift from Dr Michael Bassik, Stanford). The ubiquitome gRNA library used in **Figure 7.3B** and **Figure 7.6** is the product of a collaboration between the Lehner and Nathan laboratories.

2.6.2 gRNA library lentivirus

Lentivirus was produced using the standard protocol in 14 cm plates of HEK 293T cells by the triple transfection of the gRNA library plasmid pool and the packaging vectors pCMVΔR8.91 and pMD.G in a ratio of 10:7:3. The viral supernatant was harvested 48 h post-transfection, filtered through a 45 µm filter and immediately frozen in aliquots of 5 ml and 1 ml to be stored at -80^{o}C.

To determine the viral titer of the gRNA library viral supernatant, a 1ml aliquot of the frozen supernatant was thawed and a range of volumes were added wells containing 1 million cells to be used in the screen. Plates were spun at 1800 rpm for 1 h. The transduction efficiency was determined 48 h post transduction. For the GeCKO v2 library, the percentage of puromycin resistant cells was determined. For the Bassik and ubiquitiome gRNA libraries, transduction efficiency was measured by assessing the percentage of cells expressing the mCherry and BFP markers respectively. The volume of viral supernatant required to achieve a multiplicity of infection (m.o.i.) of approximately 0.3 was noted for use in forward genetic screens.

2.6.3 Fluorescence based CRISPR screens

For the CRISPR screen with the GeCKO library in **Figure 3.2** $1x10^8$ KBM7 cells were transduced at an m.o.i. of 0.3. For the CRISPR screens with the GeCKO library in **Figure 4.2** and **Figure 4.6** 5×10^7 HeLa cells were transduced at an m.o.i. of 0.3. For the CRISPR screens with the Bassik library in **Figure 5.3** and **Figure 5.5** 1×10^8 HeLa cells were transduced at an m.o.i of 0.3. For the ubiquitome library screens in **Figure 7.3** and **Figure 7.6** 1×10^7 HeLa cells were transduced at an m.o.i. of 0.3.

The cell line chosen to use in a CRISPR screen was transduced with pHRSIN-P_{SFFV}-Cas9-P_{PGK}-Hygromycin^R. Transduced cells were selected with hygromycin treatment. To confirm Cas9 activity in the screen cell line, the Cas9-expressing cells were transduced the pKLV vector encoding a β-2-microglobulin (B2M)-targeting gRNA. Transduced cells were selected with puromycin. MHC-I surface expression was assessed five days post-transduction by flow cytometry. B2M knockout results in the loss of MHC-I surface expression. The B2M gRNA typically results in >90% population with low MHC-I surface expression, although there is some variation between cell types.

For KBM7 cells, transductions were performed in 24-well plates with $1x10^6$ cells per well. For HeLa cells, transductions were performed in 6-well plates with $1x10^6$ cells per well. All plates were spun for 1 h at 1800 rpm. Transduced cells were selected with 1 μg/ml puromycin 24 hours post-transduction. The puromycin concentration was increased to 2 μg/ml 48 hours post-transduction. Puromycin treatment was maintained until the first FACS selection as recommended by the Zhang laboratory (Shalem et al. 2014)

A first FACS selection was performed on day 8 post-transduction to select gene knockouts with altered expression of the fluorescent reporter. Typically, $1x10^8$ cells were processed by the FACS machine to select the top 0.6% reporter-expressing cells. For the ubiquitome screens in **Figure 7.3** and **Figure 7.6** $2x10^5$ selected cells were pelleted and genomic DNA extracted immediately after sorting, using the Quick-gDNA MicroPrep kit (Zymo Research). For the genome-wide screens, the selected cells were expanded in culture, typically for eight days, before a second FACS selection was performed to purify the population of mutants. The cells selected in the second sort were expanded in culture until $5x10^6$ cells could be harvested for genomic DNA extraction using the Gentra Puregene kit (Qiagen).

2.6.4 DNA preparation and sequencing

To amplify the gRNA sequences from extracted genomic DNA, two PCR steps were performed. The first PCR amplified the gRNAs using 50 separate 100 µl reactions with 4 µg genomic DNA in each reaction using Q5 High-Fidelity DNA Polymerase (NEB). Primer sequences in appendix 2. For each sample, the PCR products were pooled. A tenth was taken and purified by QIAquick PCR Purification (Qiagen). A second PCR was performed to attach Illumina adaptors to barcode the samples. This was done with a single 100 µl reaction for each sample using 1 ng of prodct from PCR 1. Amplification was carried out using 12, 16 or 20 cycles. The products from PCR 2 were purified using Ampure XP beads (Agencourt). The sample with the smallest, clearly defined peak on a Agilent Bioanalyser DNA1000 Chip (Agilent) was selected for sequencing. Samples from genome-wide CRISPR screens were sequenced on the Illumina HiSeq platform; samples from the ubiquitome CRISPR screens were sequenced on the Illumina MiniSeq platform.

2.6.5 CRISPR screen data analysis

Illumina HiSeq data as analysed through a custom analysis pipeline developed by Richard Timms. Using the fastx toolkit (http://hannonlab.cshl.edu/fastx_toolkit/) the raw cram files were converted into fastq files. The 3' end of the resulting reads were trimmed to the leave the gRNA sequences, and then mapped to an index of the gRNA sequences in the relevant gRNA library using Bowtie 2 (Langmead et al. 2009). The resulting gRNA counts were analysed using the RSA algorithm using the default settings (König et al. 2007).

2.7 Biochemistry

2.7.1 Cell Lysis

For α-UBE2G2 and α-UROD immunoblots, cells were lysed in 1% SDS plus 1:100 Benzonase (Sigma-Aldrich) in TBS for 30 min at room temperature. The lysates were then heated to 70^{o}C in SDS sample buffer for 10 min.

For all other immunoblots and immunoprecipitations, cells were lysed in 1% digitonin plus 10 mM iodoacetate (IAA), 0.5 mM phenylmethylsulfonyl fluoride (PMSF) and Roche complete protease inhibitor, as well as 10 mM N-ethylmaleimide for ubiquitination assays, for 30 min

at 4°C. Lysates were spun for 10 min at 13000 xg to remove insoluble material. The supernantant was then processed for immunoblot or immunoprecipitation.

2.7.2 Immunoprecipitation

Post-nuclear supernatants where made up to 1 ml with 0.5% digitonin and then precleared with IgG Sepharose for 1 h on a rotator at 4°C. HMGCR was immunoprecipitated using rabbit α-HMGCR (Abcam, ab174830) and protein A-sepharose overnight at 4°C on a rotator. RNF145-V5 was immunoprecipitated using mouse α-V5 (Abcam, ab27671) and protein A-sepharose overnight at 4°C on a rotator. Endogenous RNF145 was immunoprecipitated using rabbit α-RNF145 (ProteinTech, 24524-I-AP) and protein A-sepharose for 4 h at 4°C on a rotator.

After one wash with 0.5% digitonin and at least five washes with 0.1% digitonin, samples were eluted by heating in 2x SDS sample buffer. HMGCR and RNF145 immuno-precipitations were eluted by heating at 50°C for 15 min, whereas RNF145-V5 immunoprecipitations were eluted by heating at 65°C for 15 min.

2.7.3 SDS-PAGE

Lysates and immunoprecipitates were separated by SDS-PAGE. Tris-glycine acrylamide gels were made using the following recipe:

Resolving gel	**Stacking gel**
0.375 mM Tris-HCl pH 8.8	0.125 mM Tris-HCl pH 6.8
0.1% SDS	0.1% SDS
0.1% APS	0.1% APS
6-12% acrylamide	1.8% acrylamide

2.7.4 Immunoblotting

Polyvinylidene fluoride (PVDF) membranes (Millipore) were incubated in methanol before soaking in transfer buffer. Proteins separated by SDS-PAGE were transferred onto PVDF membrane at 20V for 1 h using a Bio-Rad Semi-Drey Transfer Cell. Membranes were blocked with 5% milk in PBS-T (PBS plus 0.2% Tween-20) for 1 h at room temperature and probed with primary antibody in 5% milk in PBS-T overnight at 4°C. After three washes of 5 min in PBS-T,

membranes were probed with secondary goat anti-mouse or anti-rabbit horseradish peroxidase (HRP) secondary antibody (Jackson) in 5% milk in PBS-T for 1 h at room temperature. Membranes were washed at least 5 times for 5 min with PBS-T before visualising reactive bands with ECL, West Pico or West Dura (Thermo Fisher Scientific).

To visualise ubiquitinated HMGCR with VU-1 antibody, after protein transfer onto a PVDF membrane, the PVDF membrane is treated with 0.5% glutaraldehyde/PBS for 20 min, washed with PBS and then blocked in 5% mile in 0.1% Tween-20 in PBS.

2.8 Mass spectrometry

2.8.1 Gel-based sample preparation

Eluates from RNF145-V5 immunoprecipitations (**Table 6.1**) were run approximately 1 cm into a polyacrylamide gel (NuPage, Invitrogen). Subsequently the gel pieces containing samples were excised and cut into small pieces. Gel pieces were washed by dehydration in 100% ACN and rehydration with 50 mM TEAB 3x. To reduce and alkylate, gel pieces were rehydrated in 10 mM TCEP and 20 mM IAA and incubated at room temperature in the dark for 30 min, followed by an additional wash. Gel pieces were finally dehydrated in 100% ACN followed by a short additional drying step in a vacuum centrifuge before rehydration in a solution of 50 mM TEAB and 10 ng/µl Trypsin and incubation on ice for 30 min. Excess trypsin solution was removed and replaced with 50 mM TEAB before digestion overnight at 37^{o}C.

2.8.2 Bead-based sample preparation

To 100 µl eluates from endogenous RNF145 immunoprecipitation (**Figure 6.9**) 10 µl "SP3 beads" were added and the samples were processed similarly to Hughes et al (PMID: 25358341) with minor modification. First, eluate were reduced and alkylated by adding TCEP/IAA (Tris(2-carboxyethyl)phosphine hydrochloride / Iodoacetamide) to a final concentration of 10 mM and 20 mM respectively and incubated at RT in the dark for 30 min shaking at 1000 rpm. Following alkylation 10 µl formic acid (FA) and 110 µl Acetonitrile (ACN) were added and incubated at RT for 10 min. Then after standing on a magnetic rack for 2mins supernatant was removed and the beads washed vigorously with the following solvents, waiting for beads to collect on the magnet after each wash: 180 µl ACN, 70% EtOH X2, ACN.

The final acetonitrile wash was removed and the tubes briefly centrifuged and the replaced on the magnetic rack, the final few microliters of ACN were then removed. SP3 beads were then suspended in 30 µl of 50mM HEPES pH 8.5/0.1% Sodium Deoxycholate (SDC) containing 250 ng of trypsin. Beads were then incubated for 16 h at 37^{o}C in a Thermomixer with a heated lid, shaking at 1200 rpm. Digests were then made up to 100uL with 50mM HEPES and acidified with 3 ul 10% TFA to precipitate SDC. SDC precipitates were removed by two phase partitioning by adding 500 µL Ethyl Acetate, thorough vortexing, centrifugation (15'000 g, 5 min) and removal of the lower phase. Cleaned up samples were dried in a vacuum centrifuge and resuspended in 10 µl 5% DMSO/1% TFA for LC-MS analysis.

2.8.3 LC-MS/Data Analysis

LC-MS analysis was performed by a revered phase nano-chromatography system interfaced via an electrospray ionization source with an Orbitrap Fusion spectrometer in a 1 h analysis per sample. Raw data were searched against the Uniprot Human reference proteome by an implementation of MASCOT within Proteome Discover ver 2.1 (PD). A peptide and protein FDR threshold of <0.01 was set and peptides were grouped into protein according to the minimum parsimony principle. Proteins were quantified using the PD node "precursor ions quantifier" which is an implementation of the Hi3 method of label free quantification.

Unless otherwise stated, experiments were performed once.

3.0 Results summary

The layout of my thesis is described below:

Chapter 3, I demonstrate that gene-trap mutagenesis and genome-wide CRISPR knockout screens are equally effective at identifying factors required for MHC-I ERAD in KBM7 cells. The parallel forward genetic screens both identify a requirement for TXNDC11 in glycoprotein ERAD. To complete the story, I include work performed by collaborators who found TXNDC11 to be an ER-localised disulphide reductase that acts on a component of the ERAD machinery.

Chapters 4 and 5, I performed a series of genome-wide CRISPR screens using a fluorescently-tagged exogenous HMG-CoA Reductase (HMGCR) reporter and then an endogenous HMGCR-Clover knock-in to identify the E3 ubiquitin ligase for HMGCR. These screens identified the poorly characterised ERAD E3 ligase RNF145. The loss of RNF145 resulted in a partial loss of HMGCR reporter degradation, however I did not detect a difference in the degradation of endogenous, untagged HMGCR.

Chapter 6, I show that the E3 ligases gp78 and RNF145 are functionally redundant in HMGCR degradation. The combined loss of gp78 and RNF145 results in a pronounced block in the sterol-induced degradation and ubiquitination of HMGCR. However, the presence of either E3 ligase is sufficient for efficient HMGCR degradation. I demonstrate that RNF145 interacts with both Insig proteins independent of the sterol environment and I observed an interaction between RNF145 and HMGCR by mass spectrometry that is enhanced by sterols and proteasome inhibition.

Chapter 7, I use a focused E3 ligase CRISPR screen to identify a role for Hrd1 in HMGCR degradation. The combined loss of all three ligases (gp78, RNF145 and Hrd1) is required to completely block the sterol-induced degradation of HMGCR. However, the loss of Hrd1 alone or in combination with either gp78 or RNF145 does not inhibit the sterol-induced degradation of HMGCR.

I present a model for the sterol-induced degradation of HMGCR in which gp78 and RNF145 are partially redundant, primary E3 ubiquitin ligases for HMGCR that are recruited to HMGCR

by the Insig proteins at high sterol levels. In the absence of both gp78 and RNF145, Hrd1 acts as a secondary E3 ubiquitin ligase to mediate HMGCR degradation.

Chapter 3: A genetic dissection of mammalian ERAD through comparative haploid and CRISPR forward genetic screens

3.1 Introduction

Forward genetic screens in human cells have been significantly hindered by the difficulty in recovering bi-allelic knockouts. A major advance by the laboratory of Thijn Brummelkamp used a retroviral gene-trap vector in the near-haploid KBM7 cell line (Carette et al. 2009). The Lehner laboratory has adapted this technology to perform fluorescence-based forward genetic screens to investigate a range of cellular processes (Duncan et al. 2012, Timms et al. 2013, van den Boomen et al. 2014, Tchasovnikarova et al. 2015). At the start of my PhD project, gene-trap mutagenesis screens in the near-haploid KBM7 cell line were the gold standard in forward genetic screens in human cells.

Precise genome editing using programmable nucleases is a transformative technology for cell biology research (Kim and Kim 2014). CRISPR/Cas9 technology is a major advance with a wide range of applications (Hsu, Lander, and Zhang 2014). The CRISPR/Cas9 system offers a rapid and efficient method to generate bi-allelic mutations and therefore gene knockouts. By using a large library of gRNAs to target the Cas9 nuclease to all annotated genes, CRISPR/Cas9 technology can be used to perform genome-wide forward genetic screens (Shalem et al. 2014, Wang et al. 2014, Koike-Yusa et al. 2014).

A major aim of the first part of my thesis project was to directly compare the effectiveness of genome-wide CRISPR knockout screens against retroviral gene-trap mutagenesis screens.

Previous work in the Lehner laboratory has shown that the MHC-I allele HLA-A2 is degraded by ERAD via the canonical glycoprotein control pathway (Burr et al. 2011, Burr et al. 2013). I chose to perform my forward genetic screens on MHC-I ERAD because I wanted to use a

system that was familiar to the Lehner laboratory with multiple known components to act as positive controls in my screens.

3.2 Results 1

3.2.1 A fluorescent reporter system to monitor MHC-I ERAD

I first set out to perform a gene-trap mutagenesis screen to identify factors required for the ERAD of MHC-1. To enable a fluorescence-based phenotypic selection, KBM7 cells were transduced with a lentiviral construct encoding a green fluorescent protein (GFP)-tagged MHC-I allele (HLA-A2) (**Figure 3.1A**). The transduced population was single cell cloned and a clone was identified with low GFP-HLA-A2 expression. Depletion of SEL1L, a known component required for MHC-1 ERAD, by RNA interference showed a significant increase in GFP fluorescence, demonstrating that GFP-HLA-A2 was being degraded by ERAD in this clone (**Figure 3.1B**).

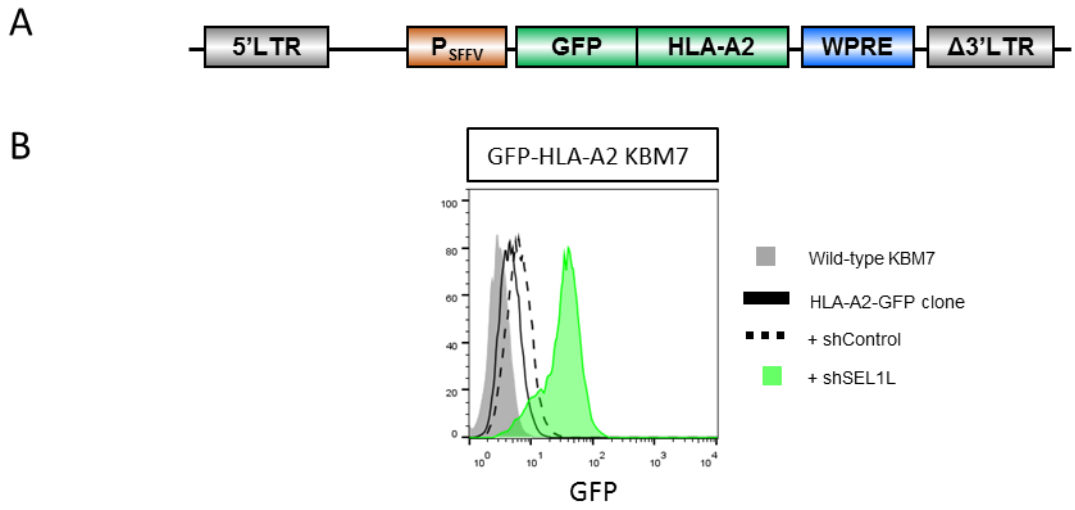

Figure 3.1 Establishing a fluorescent reporter for MHC-I ERAD. (A) A Schematic of the lentiviral construct encoding the GFP-HLA-A2 fusion protein. Expression is driven by the powerful spleen focus-forming virus (SFFV) promoter. (LTR, long-terminal repeat; WPRE, Woodchuck hepatitis virus posttranscriptional regulatory element). **(B)** Identifying a KBM7 clone expressing GFP-HLA-A2 that is degraded by ERAD. The KBM7 clone was transduced with a lentiviral construct expressing a non-targeting or SEL1L-targeting shRNA. Transduced cells were selected with puromycin treatment and GFP fluorescence was measured by flow cytometry.

3.2.2 A haploid gene-trap mutagenesis screen for MHC-I ERAD

To perform the gene-trap mutagenesis screen, 10^8 GFP-HLA-A2 KBM7 cells were transduced with a gene-trap retrovirus carrying a mCherry marker. I cultured the library to allow the generation of gene knockouts. A minimum of 10^8 cells were kept in culture to ensure that representation of the library was maintained. After 8 days, I performed a first round of selection by FACS to isolate $mCherry^{positive}$ (retroviral gene-trap transduced) GFP^{high} cells. The frequency of gene knockouts that results in the loss of MHC-I ERAD is very low in a library of KBM7 cells mutagenised by a retroviral gene-trap vector. It is extremely difficult to see a distinct population of cells with the desired phenotype during a first sort and so the 0.6-0.8% of cells with highest GFP expression are typically selected. The selected cells were expanded for 7 days before a second round of FACS. The resultant population contained a significant enrichment for GFP^{high} cells (**Figure 3.2B**).

Genomic DNA was extracted from the selected GFP^{high} cells and a library of the original mutagenised cells that had not been selected and had grown for the same amount of time. The retroviral integration sites in each population were identified by linear amplification-mediated PCR (LAM-PCR) and sequencing on the Illumina HiSeq platform. Retroviral gene-trap integration sites were analysed for their ability to inactivate the gene into which they had integrated. Analysing the enrichment of inactivating insertions in the FACS selected cells compared to the unselected library identified a suite of candidate genes (**Figure 3.2C**).

The screen was very successful in identifying many hits that could be grouped into several functional classes. The largest group contains genes previously shown to be required for ERAD, including the mannosidases *EDEM1* and *EDEM2*, the E3 ubiquitin ligase Hrd1 (gene name is *SYVN1*), the Hrd1 binding partners *SEL1L* and *DERLIN2*, and the E2 conjugating enzymes *UBE2J1* and *UBE2G2* (**Figure 3.2C**) (Burr et al. 2011, Burr et al. 2013). The second functional group of candidate genes contained factors required for N-glycosylation. This group included all three members of the dolichol-phosphate-mannose (DPM) synthase complex (*DPM1, DPM2* and *DPM3*), the complex required to generate mannosyl donors (Maeda et al. 2000). The mannosyltransferase enzymes, *ALG3* and *ALG9* were also identified. The ERAD of glycoproteins is initiated by the trimming of mannose residues on N-glycans (Ninagawa et al. 2014). The loss of the mannosyltransferases identified in the gene-trap

mutagenesis screen will result in a glycan moiety that does not enter the mannose-trimming cycle and so preventing the recognition of GFP-HLA-A2 as a glycoprotein ERAD substrate. The third class of candidate genes consists of known components of the non-sense mediated decay pathway (**Figure 3.2C**). The identification of these genes suggests that the GFP-HLA-A2 mRNA is also being targeted for degradation.

The screen also identified two uncharacterised genes, *PRR7-AS1* and *TXNDC11*. TXNDC11 is an uncharacterised protein disulphide isomerase (PDI) family member, also known as EFP1, and was originally identified as a binding partner of dual oxidase 1 (DUOX1), a hydrogen peroxide-generating enzyme (Wang et al. 2005). Richard Timms later validated TXNDC11 and a selection of other hits using CRISPR-mediated gene disruption (**Figure 3.2D**). For each gene, a population of GFP^{high} cells could be seen by flow cytometry following CRISPR-mediated gene-disruption (**Figure 3.2D**). The use of a single gRNA against a gene results in a mixed population of knockouts cells and cells expressing a functional protein because in some cases non-homologous end joining will result in an insertion or deletion that does not result in a frameshift mutation.

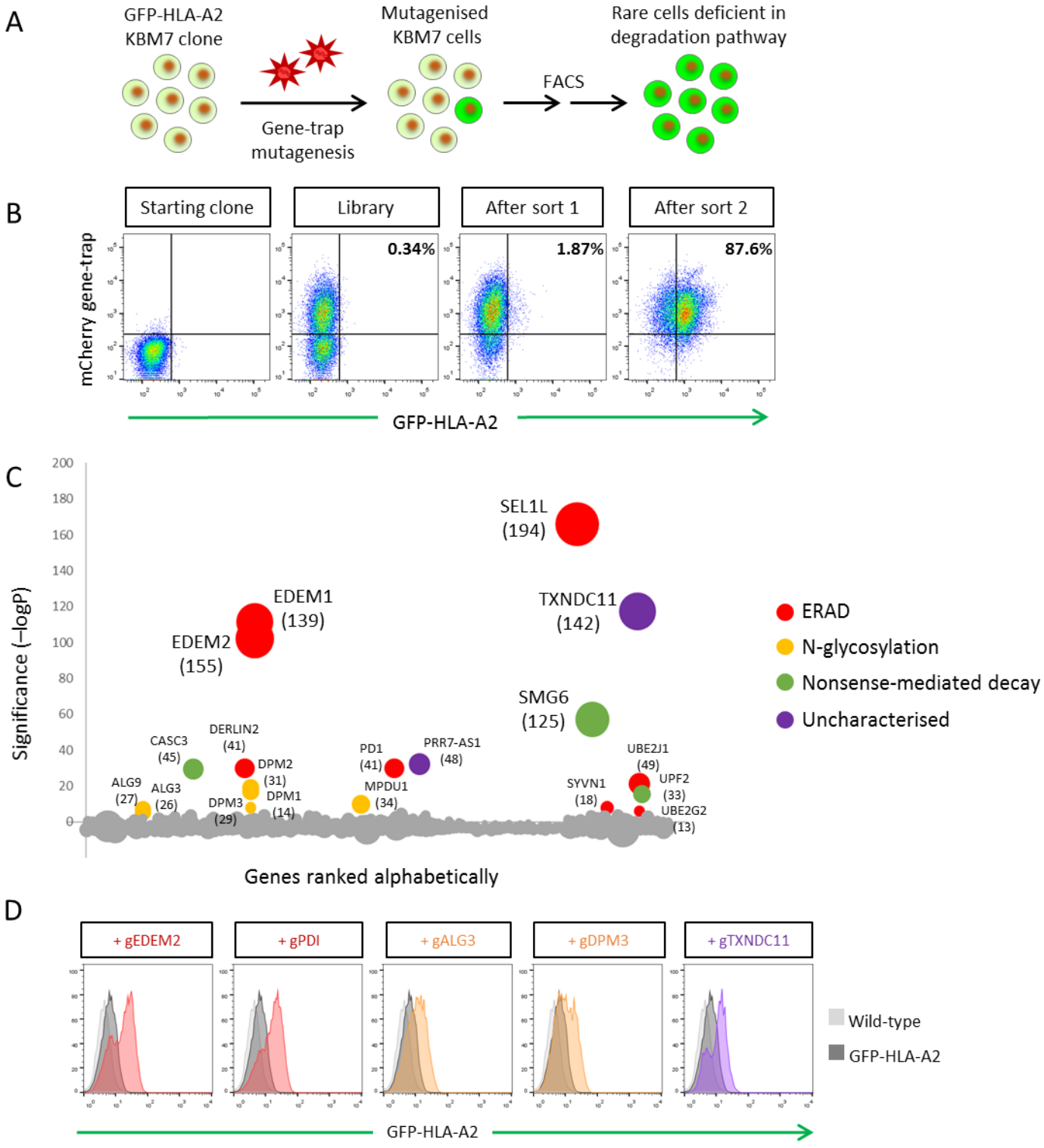

Figure 3.2 A haploid gene-trap mutagenesis forward genetic screen identifies genes required for glycoprotein ERAD. (A) A schematic overview of the gene-trap mutagenesis screen. **(B)** GFP-HLA-A2 KBM7 cells were transduced with a retroviral gene-trap vector carrying a mCherry marker, GFP^{high} cells were isolated by two rounds of FACS. **(C)** Bubble plot illustrating hits from the screen. Bubble size is proportional to the number of independent inactivating gene-trap integrations (number in parentheses). **(D)** CRISPR knockout validation of candidate genes. GFP-HLA-A2 cells were transduced with Cas9 and gRNA targeting a candidate gene. Increased GFP-HLA-A2 was detected by flow cytometry (Richard Timms).

3.2.3 A parallel genome-wide CRISPR knockout screen for MHC-I ERAD

The GFP-HLA-A2 KBM7 clone identified in Figure 3.2A had proven to be an extremely powerful tool. I identified many candidate genes when I used this clone in a gene-trap mutagenesis screen, providing a benchmark against which I could compare a genome-wide CRISPR knockout screen. I transduced the GFP-HLA-A2 clone with a lentiviral reporter encoding the nuclease Cas9 and selected transduced cells. Before performing the screen, I wanted to ensure that the Cas9 expressed in the clone could efficiently generate gene knockouts. A gRNA targeting β2-microglobulin (B2M) was transduced into the Cas9-expressing GFP-HLA-A2 KBM7 cells. Cell surface MHC-I expression was analysed 5 days post-transduction by flow cytometry, demonstrating efficient CRISPR-mediated gene disruption of B2M.

The GeCKO v2 library, from Feng Zhang's laboratory, was one of the first genome-wide CRISPR libraries made available via Addgene (Sanjana, Shalem, and Zhang 2014). The GeCKO v2 library contains 123,411 gRNAs targeting 19,050 genes. Each gene is targeted by 6 gRNAs and the library also includes non-targeting controls (Sanjana, Shalem, and Zhang 2014). Lentivirus was produced by transfecting HEK293T cells with the pooled gRNA plasmids and standard lentivirus packaging vectors. The viral supernatant was titrated onto GFP-HLA-A2 Cas9 cells to determine the volume of supernatant required to infect 30% of the cells. The gRNA expression plasmid encodes a puromycin resistance gene enabling the multiplicity of infection (M.O.I.) to be determined by calculating the percentage of cells that survive puromycin treatment. A M.O.I. of 0.3 is desirable to ensure that each cell only receives a single gRNA.

To perform the genome-wide CRISPR knockout screen, 10^8 GFP-HLA-A2 cells were transduced at a M.O.I. of 0.3. This means that $3x10^7$ cells were transduced with gRNA library virus. As the library contains 123,411 gRNAs, the coverage of the screen was 243 cells/gRNA. The library was treated with puromycin to select transduced cells. Puromycin selection was maintained until the first sort (on day 8) following the advice of the Zhang laboratory (Shalem et al. 2014). I enriched mutant GFP^{high} cells using two sequential rounds of FACS as described for the gene-trap mutagenesis screen. A significantly greater enrichment was observed after the first sort in the CRISPR screen compared to the gene-trap mutagenesis screen and a highly enriched population of GFP^{high} cells was obtained from the second sort (**Figure 3.3C**).

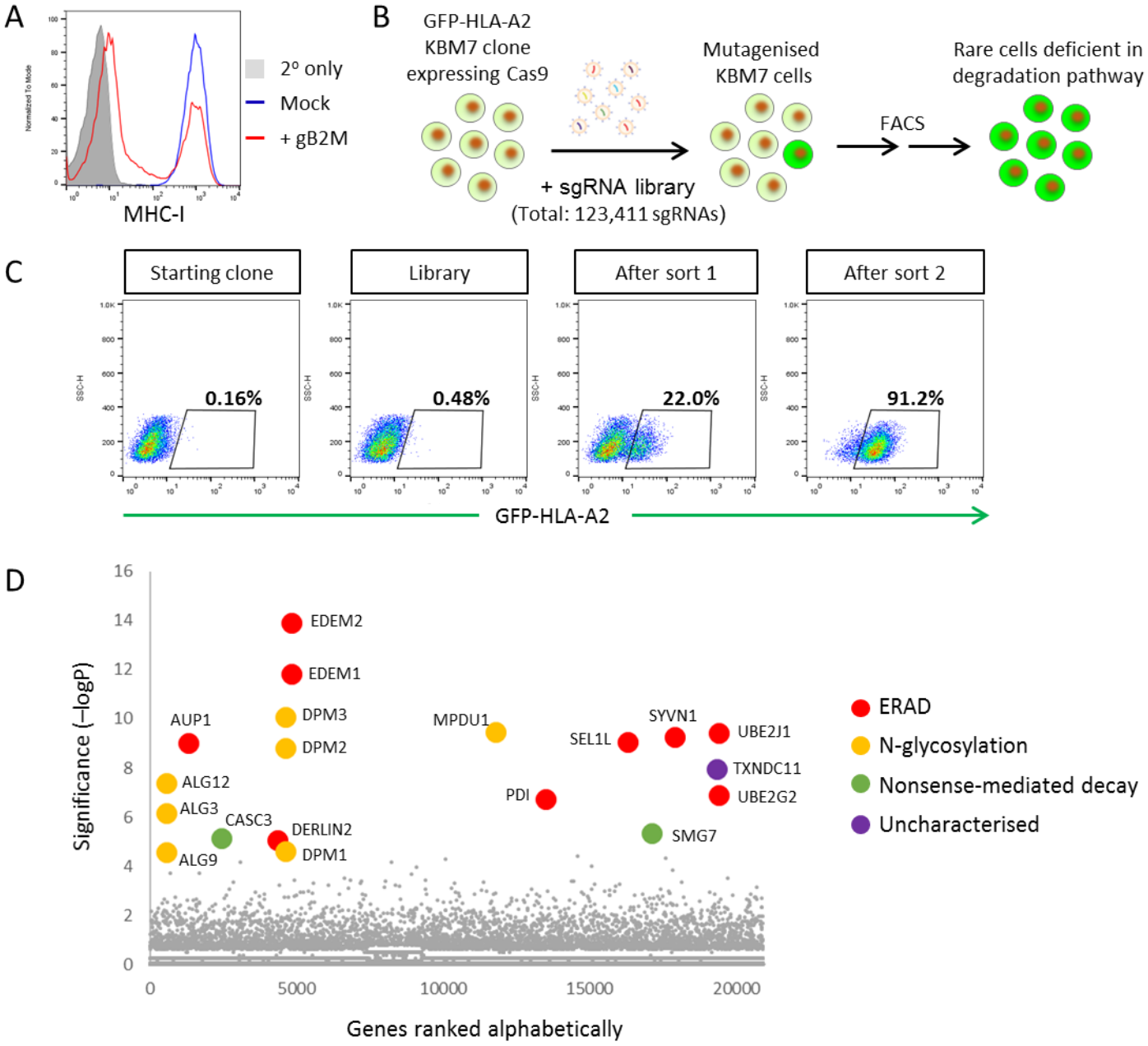

Figure 3.3 A parallel genome wide CRISPR knockout screen identifies genes required for glycoprotein ERAD. (A) Cas9-expressing GFP-HLA-A2 KMB7 cells were transduced with a B2M-targetting gRNA to confirm Cas9 activity. B2M knockout efficiency was determined by measuring MHC-I cell surface expression by flow cytometry five days post-transduction. B2M gRNA lentiviral construct also expressed BFP to allow selection of transduced cells. **(B)** Schematic overview of the CRISPR screen. **(C)** Cas9-expressing GFP-HLA-A2 KBM7 cells were transduced with the GeCKO v2 gRNA library. GFP^{high} cells were selected by two sequential rounds of FACS. **(D)** The RSA algorithm identified candidate genes that were significantly enriched in the selected cells.

Genomic DNA was extracted from the selected GFP^{high} population together with the library of unselected mutagenised cells grown over the same time period. The gRNA sequences in each population were amplified by PCR using primers that bind to the integrated lentiviral construct. The abundance of the gRNAs in each population was determined by deep sequencing using the Illumina HiSeq platform. The RSA algorithm was then used to identify candidate genes (**Figure 3.3D**) (König et al. 2007). This revealed that the CRISPR screen was successful at identifying candidate genes that were grouped into the same functional classifications as the hits in the gene-trap screen.

To determine whether a gene is a hit in this CRISPR screen, the degree of enrichment of each of the 6 gRNAs targeting that gene must be considered. The RSA algorithm first assigns each gRNA with an activity score based on the enrichment of the normalised count of the gRNA in the selected cells compared to the unselected library (**Table 3.1**). The activity scores for all gRNAs targeting a gene are then used to determine a p-value for the probability that the enrichment is statistically significant. Three example genes are given in Table 3.1. Three gRNAs targeting DPM3 are very highly enriched, their normalised count increased by two orders of magnitude following the two sorts, so these are assigned a high activity score (greater than 2). Two of the other gRNAs targeting DPM3 are modestly enriched, their normalised count increased by an order of magnitude, so these are assigned a high activity score (between 1 and 2). The last gRNA targeting DPM3 is only slightly enriched and so this is assigned a low activity score (less than 1). Therefore, there are 3 very active, 2 active and 1 weakly active gRNAs targeting DPM3 and so DPM3 was assigned a very low p-value. In contrast, there are 2 very active, 2 weakly active and 2 inactive gRNAs targeting Derlin-2, which was therefore assigned a moderate p-value. If I consider the gRNAs targeting HMG-CoA Reductase, there is a single gRNA that is reasonably enriched, one diluted and the remaining four gRNAs are not detected in the selected cells. The inactivity of the other 5 gRNAs strongly suggests that an off-target effect is responsible for the enrichment of gRNA #21680 against HMG-CoA Reductase. HMG-CoA Reductase was therefore assigned a high, insignificant p-value.

Gene	gRNA_ID	Normalised count		Activity	Signifiicance (-logP)
		Library	Sort		
DPM3	HGLibA_13862	1.29	7.44	0.76	10.065
	HGLibA_13863	4.94	508.21	2.01	
	HGLibA_13864	1.45	39.63	1.44	
	HGLibB_13841	1.97	449.04	2.36	
	HGLibB_13842	3.72	576.94	2.19	
	HGLibB_13843	2.62	90.43	1.54	
DERL2	HGLibA_12997	24.21	4952.74	2.31	5.047
	HGLibA_12998	2.04	0.00	0.00	
	HGLibA_12999	3.51	11.87	0.53	
	HGLibB_12979	7.12	1591.89	2.35	
	HGLibB_12980	8.97	27.53	0.49	
	HGLibB_12981	0.12	0.00	0.00	
HMGCR	HGLibA_21707	1.26	0.00	0.00	1.3
	HGLibA_21708	9.53	0.34	-1.45	
	HGLibA_21709	9.37	0.00	0.00	
	HGLibB_21679	2.18	0.00	0.00	
	HGLibB_21680	15.50	366.62	1.37	
	HGLibB_21681	1.83	0.00	0.00	

Table 3.1 CRISPR screen analysis. Break down of gRNA normalised count, RSA activity score and RSA p-value for *DPM3, DERL2* and *HMGCR* from screen in **Figure 3.3**.

3.2.4. Gene-trap mutagenesis and genome-wide CRISPR knockout screens yield comparable results in KBM7 cells

Both genome-wide screening methods identified 19 candidate genes, with 16 (>70%) shared hits and 3 hits unique to each (**Figure 3.4A**). This high concordance rate demonstrates that the two technologies are comparable and both are very effective at identifying candidate genes.

CRISPR-mediated gene disruption was used to knockout four of the genes identified by a single screen. The loss of each component resulted in an increase in GFP-HLA-A2 expression (**Figure 3.4B**). This shows that SMG6 and UPF2 are false negatives in the CRISPR screen. All 6 gRNAs against each gene were detected in the library, however they failed to be enriched by the iterative sorting process (**Figure 3.4C**). This strongly suggests that gRNAs in the library targeting SMG6 and UPF2 are inefficient at generating gene knockouts. At the same time, ALG12 and SMG7 are false negatives in the gene-trap mutagenesis screen. Inactivating gene-trap integrations were not enriched in SMG7. There appears to be a small enrichment in inactivating gene-trap integrations in ALG12, however ALG12 falls below the cut-off for statistical significance (**Figure 3.4D**). The low number of total integrations into ALG12 suggests that ALG12 might lie in a relative 'cold-spot' for retroviral integration. Neither SMG7 or ALG12 are located in a section of diploid chromosome in KBM7 cells.

A

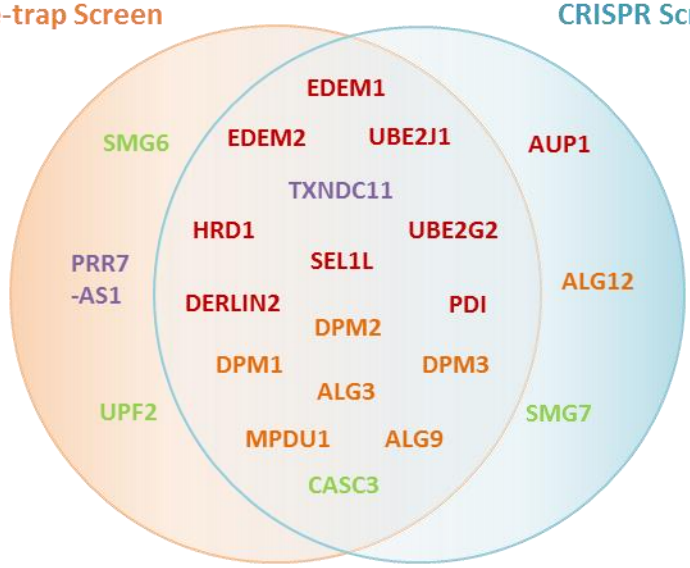

B

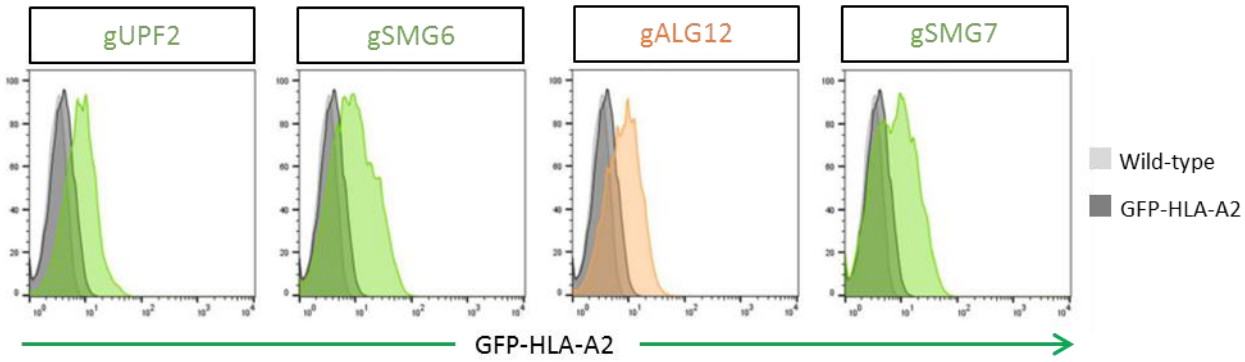

C

Gene	sgRNA_ID	Normalised count	
		Library	Sort 2
UPF2	HGLibA_60346	2.53	0.00
	HGLibA_60347	10.04	0.00
	HGLibA_60348	10.37	0.00
	HGLibB_52993	1.80	68.34
	HGLibB_52994	3.91	0.34
	HGLibB_52995	7.84	7.35
SMG6	HGLibA_52991	2.51	7.18
	HGLibA_52992	1.69	0.22
	HGLibA_52993	2.04	0.00
	HGLibB_45648	0.96	0.00
	HGLibB_45649	0.33	0.31
	HGLibB_45650	4.21	0.00

D

Gene	Bonferoni p-value	Unique integration sites			
		Sort 2 cells		Unselected library	
		Inactivating	Total	Inactivating	Total
ALG12	0.011	9	10	3	7
SMG7	727.2	8	9	25	49

Figure 3.4 Gene-trap mutagenesis and genome-wide CRISPR knockout screens yield comparable results in KBM7 cells. (A) Overlap of the screen hits from the gene-trap mutagenesis and CRISPR screens. **(B)** CRISPR validation of genes only identified in one screen. Cas9-expressing GFP-HLA-A2 cells were transduced with a lentiviral construct expressing a candidate gene targeting gRNA. GFP expression was determined by flow cytometry (Richard Timms). **(C)** Illumina sequencing data from the CRISPR screen relating to *UPF2* and *SMG6* shows all gRNAs were detected in the library but only one gRNA was enriched for each gene in the selected cells. **(D)** Illumina sequencing data from the gene-trap mutagenesis screen relating to *ALG12* and *SMG7*.

Despite yielding very similar results the mutagenic coverage of the two technologies was remarkably different (**Figure 3.5**). The CRISPR screen was limited to the 19,050 protein coding genes targeted by the gRNA, whereas the gene-trap mutagenesis screen could target 32,000 open reading frames. The mutagenic coverage of the CRISPR screen appears to be much more even than the gene-trap screen. However, Figure 3.5 shows gRNA count and does not reveal any information regarding a gRNA's effectiveness at generating a gene knockout and the integration of the retrovirus is biased towards actively expressed genes (Carette, Guimaraes, et al. 2011).

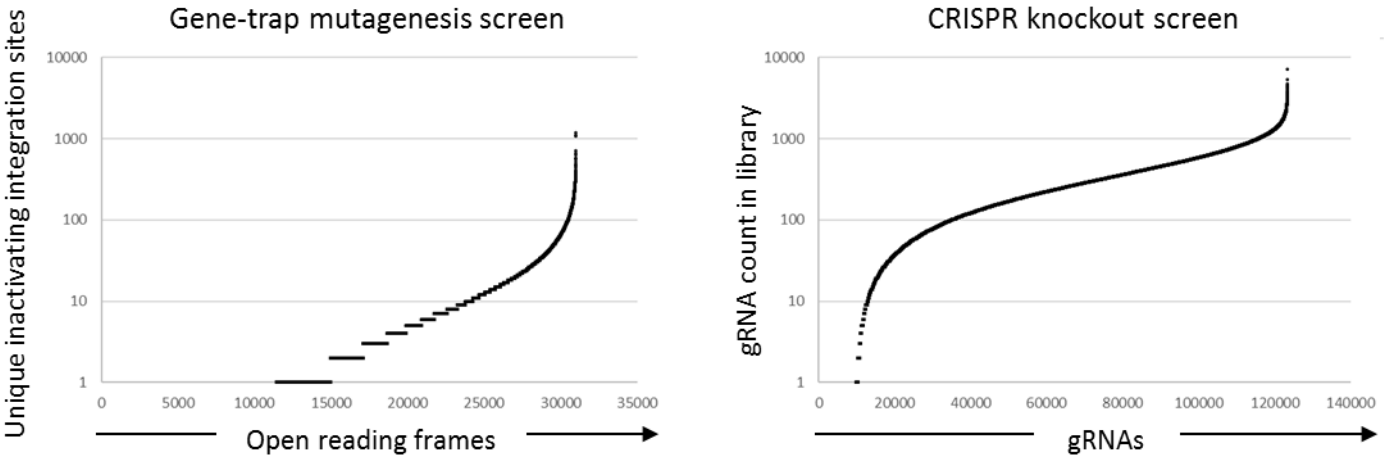

Figure 3.5 GeCKO v2 RNA library provides more even mutagenic coverage than retroviral gene-trap mutagenesis. The number of unique inactivating integration sites in each open reading frame and the number of times each gRNA was detected by Ilumina sequencing.

3.3 Results 2

The work presented in the section **3.3** is not my own work and is included to complete the TXNDC11 story. This section is from a collaboration between Richard Timms and Iva Tchasovnikarova from Paul Lehner's laboratory and Lea Christensen from Lars Ellgaard's laboratory at the University of Copenhagen, Denmark.

3.3.1 TXNDC11 is an ER-resident thioredoxin domain protein

TXNDC11, an uncharacterised PDI family member, was identified by both the gene-trap mutagenesis and CRISPR screens. TXNDC11 had been previously identified in a yeast two-hybrid screen for dual oxidase 1 (DUOX1) binding partners (Wang et al. 2005). However, nothing was known about the function of TXNDC11.

TXNDC11 is predicted to contain a single transmembrane domain, five thioredoxin-like (Trx) domains and a coiled-coil region (**Figure 3.6A and 3.6B**) (Webb and Sali 2014, Yang et al. 2015, Kelley et al. 2015). PDI-family proteins use two catalytic cysteine residues in a CXXC motif to catalyse the oxidation or reduction of disulphide bonds (Chivers, Laboissière, and Raines 1996). Only Trx5 of TXNDC11 contains a CXXC ($C_{GF}C$) motif, whereas Trx1 contains a CXXS ($C_{GQ}S$) motif and the remaining three Trx domains do not contain any active site cysteine residues.

The localisation of TXNDC11 was investigated by immunofluorescence (**Figure 3.6C**). Co-localisation of epitope-tagged TXNDC11 with the ER-resident protein Calnexin suggested an ER localisation for TXNDC11. This was supported by the sensitivity of endogenous TXNDC11 to Endoglycosidase H (Endo H) digestion (**Figure 3.6D**).

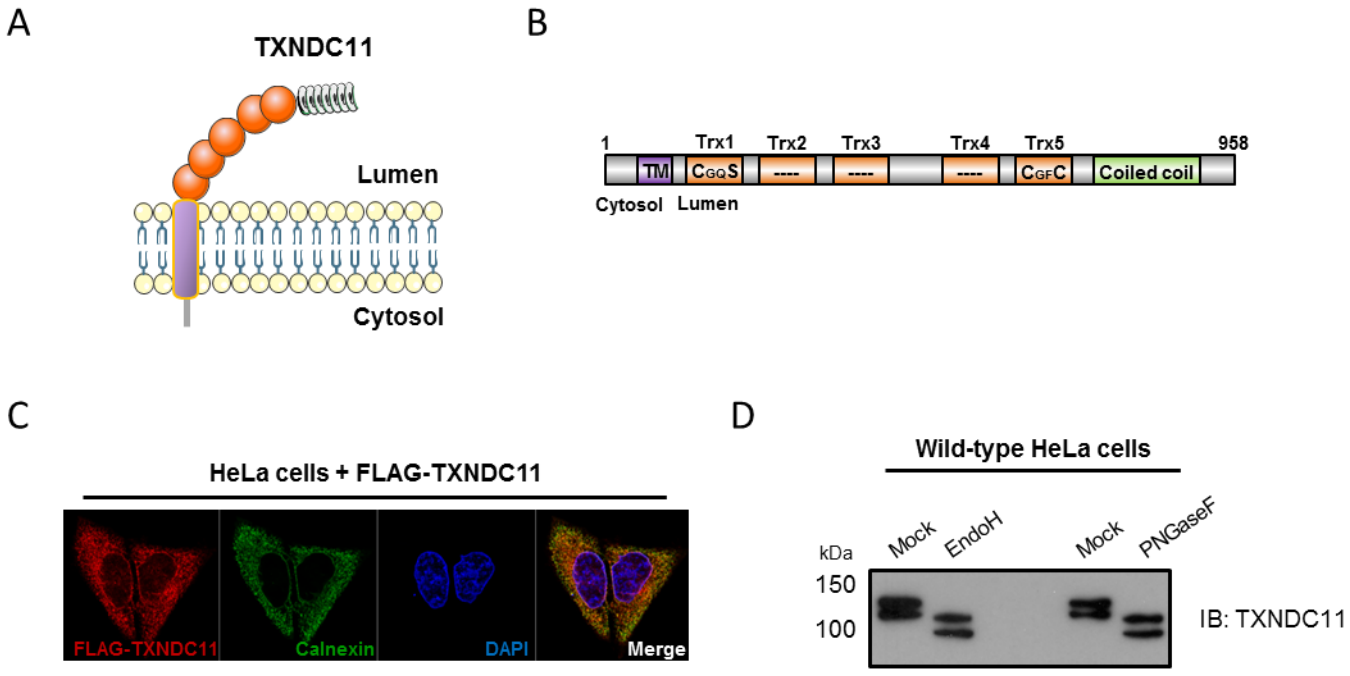

Figure 3.6 TXNDC11 localises to the ER (A) Schematic of predicted TXNDC11 protein architecture. **(B)** Schematic depicting predicted domains of TXNDC11. **(C)** FLAG-tagged exogenous TXNDC11 co-localises with calnexin (ER) as assessed by immunofluorescence. **(D)** Endogenous TXNDC11 is sensitive to EndoH digestion confirming ER localisation.

3.3.2 Redox activity of TXNDC11 is required for GFP-HLA-A2 degradation

TXNDC11 knockout clones were derived from the GFP-HLA-A2 KBM7 clone using CRISPR-mediated gene disruption (**Figure 3.7A**). As expected, each TXNDC11 knockout clone had an elevated level of GFP-HLA-A2 expression (**Figure 3.7B**). Re-expression of wild type TXNDC11 rescued GFP-HLA-A2 degradation (**Figure 3.7C**). To determine whether a redox function of TXNDC11 was required for GFP-HLA-A2 degradation, a TXNDC11 mutant was cloned in which Trx5's catalytic cysteines were mutated to alanine (AXXA). The Trx5 AXXA TXNDC11 mutant was unable to rescue GFP-HLA-A2 degradation (**Figure 3.7C**). Expression of Trx5 AXXA TXNDC11 was confirmed by immunoblot, therefore implicating a redox function for TXNDC11 (**Figure 3.7D**). A Trx1 AXXA TXNDC11 mutant could rescue GFP-HLA-A2 degradation, confirming that Trx1 is not an active thioredoxin domain (**Figure 3.7C**).

3.3.3 TXNDC11 is a disulphide reductase

We next sought to determine whether TXNDC11 catalyses the oxidation or reduction of disulphide bonds. The Trx5 domain was expressed in *E. coli* and purified by Lea Christensen (**Figure 3.8B**). An AMS shift assay estimated a reduction potential of between -234 mV and -242 mV for the Trx5 domain. Comparing this value to the reduction potential of other PDI-family members indicates that TXNDC11 is a disulphide reductase (Frickel et al. 2004, Chambers et al. 2010, Hagiwara et al. 2011).

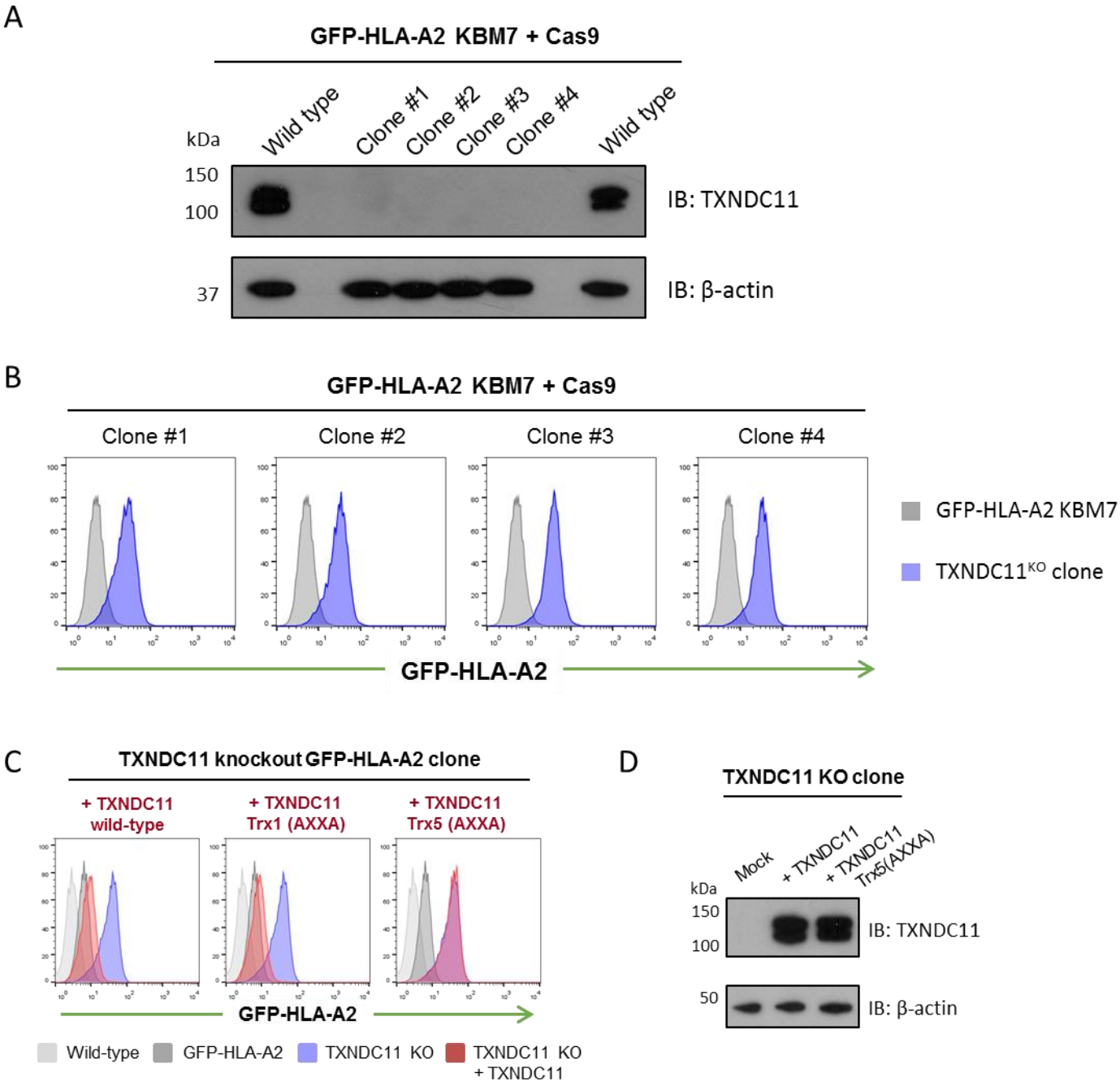

Figure 3.7 TXNDC11 redox activity is required for efficient ERAD (A) TXNDC11 knockout clones from GFP-HLA-A2 KBM7 cells transduced with Cas9 and TXNDC11-targeting gRNA. Absence of TXNDC11 protein was confirmed by immunoblot **(B)** GFP-HLA-A2 expression in TXNDC11 knockout clones was assessed by flow cytometry. **(C)** Re-expression of TXNDC11 in TXNDC11 knockout cells. TXNDC11 knockout cells were transduced with a lentiviral construct encoding wild type, Trx1 (AXXA) or Trx5 (AXXA) TXNDC11. GFP-HLA-A2 expression was measured by flow cytometry. **(D)** Immunoblot analysis confirmed expression of Trx5 (AXXA) mutant TXNDX11.

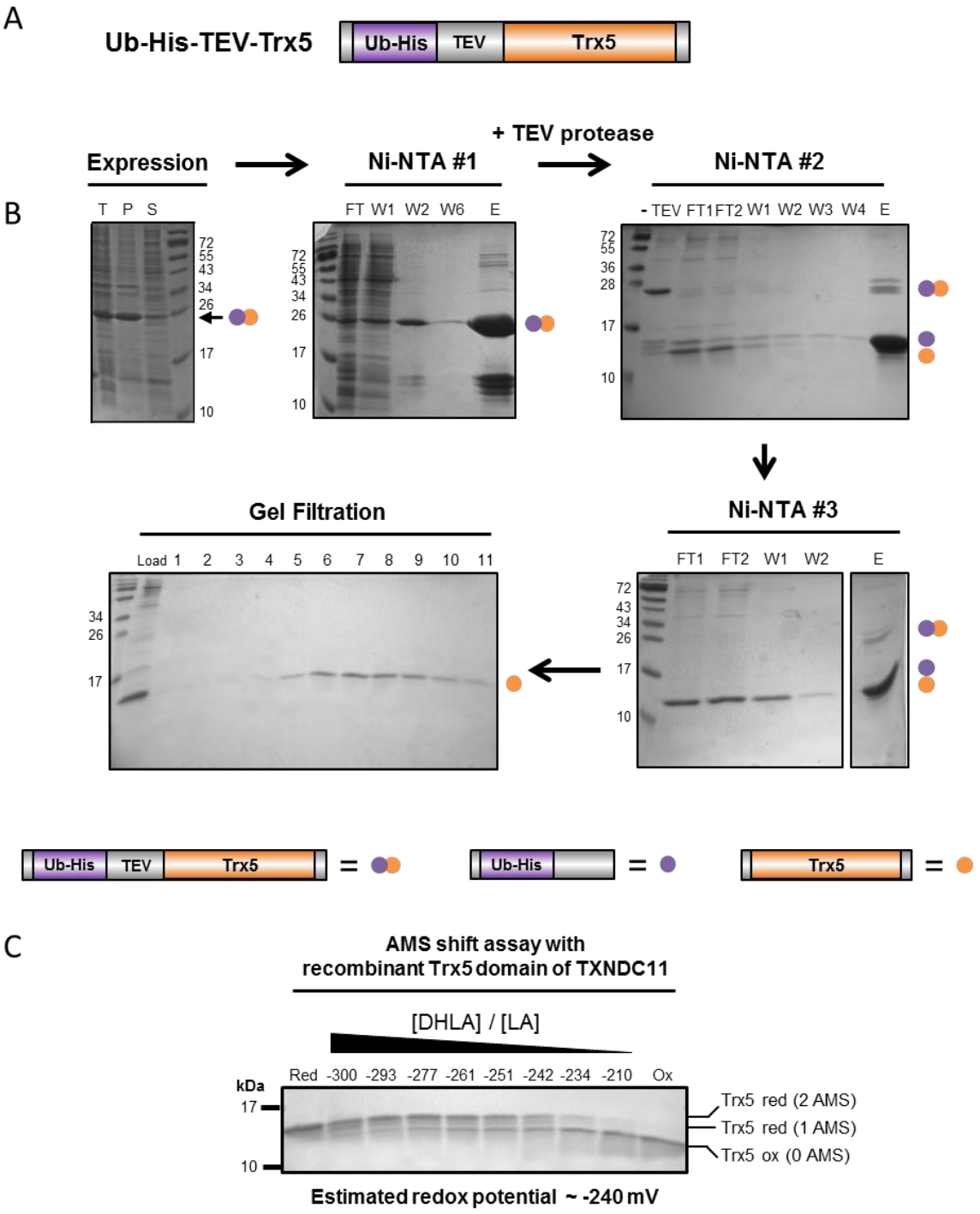

Figure 3.8 TXNDC11 is a disulphide reductase. (A) A Ubiquitin (Ub)-HIS-Trx5 domain of TXNDC11 fusion protein was expressed in *E. coli*. A non-active site cysteine was mutated (C743S) to prevent disulphide-mediated oligomerisation. **(B)** Trx5 domain was purified by Ni-NTA affinity chromatography, TEV protease cleavage and gel filtration (T, total protein after expression; P, pellet after lysis; S, supernatant after lysis; FT, flow-through; W, wash; E, elution. Numbers indicate different fractions). **(C)** Redox titration of Trx5 (C743) domain with lipoic acid (DHLA/LA). The alkylating agent 4-acetamido-4'maleimidylstilbene-2,2'-disulfonic acid (AMS) reacts with free thiol groups, adding 490 Da per thiol. The oxidised and reduced forms of Trx5 can therefore be resolved on a polyacrylamide gel. Lipoic acid (DHLA/LA; reduction potential -290 mV) was used to titrate reducing conditions (Lees and Whitesides 1993)

3.3.4 TXNDC11 is required for the degradation of other ERAD substrates

A selection of ERAD substrates were selected to determine whether TXNDC11 was required for the ERAD of proteins other than HLA-GFP-A2. Depletion of TXNDC11 by shRNA rescued expression of unassembled CD3 delta chain (CD3δ), unassembled T cell receptor alpha chain (TCRα) and the Null-Hong Kong (NHK) variant of alpha 1-antitrypsin, implicating a requirement for TXNDC11 in the ERAD of a range of substrates (**Figure 3.9A**).

To determine whether the reductase activity of TXNDC11 acts on the ERAD substrate itself or a component of the ERAD machinery, two NHK mutants were cloned. In the first mutant, NHK (QQQ), all N-gylcosylation sites were removed (asparagine to glutamine). In the second mutant, NHK (C/S), the single cysteine residue in NHK was mutated to serine to prevent disulphide-bonded dimer formation (Ushioda et al. 2008). TXNDC11 depletion had little effect on NHK (QQQ), providing more evidence to place TXNDC11 in glycoprotein-ERAD (**Figure 3.9B**). However, TXNDC11 depletion impaired the degradation of cysteine-free NHK (C/S) (**Figure 3.9B**). This suggests that TXNDC11 acts on a component of the ERAD machinery rather than the ERAD substrate.

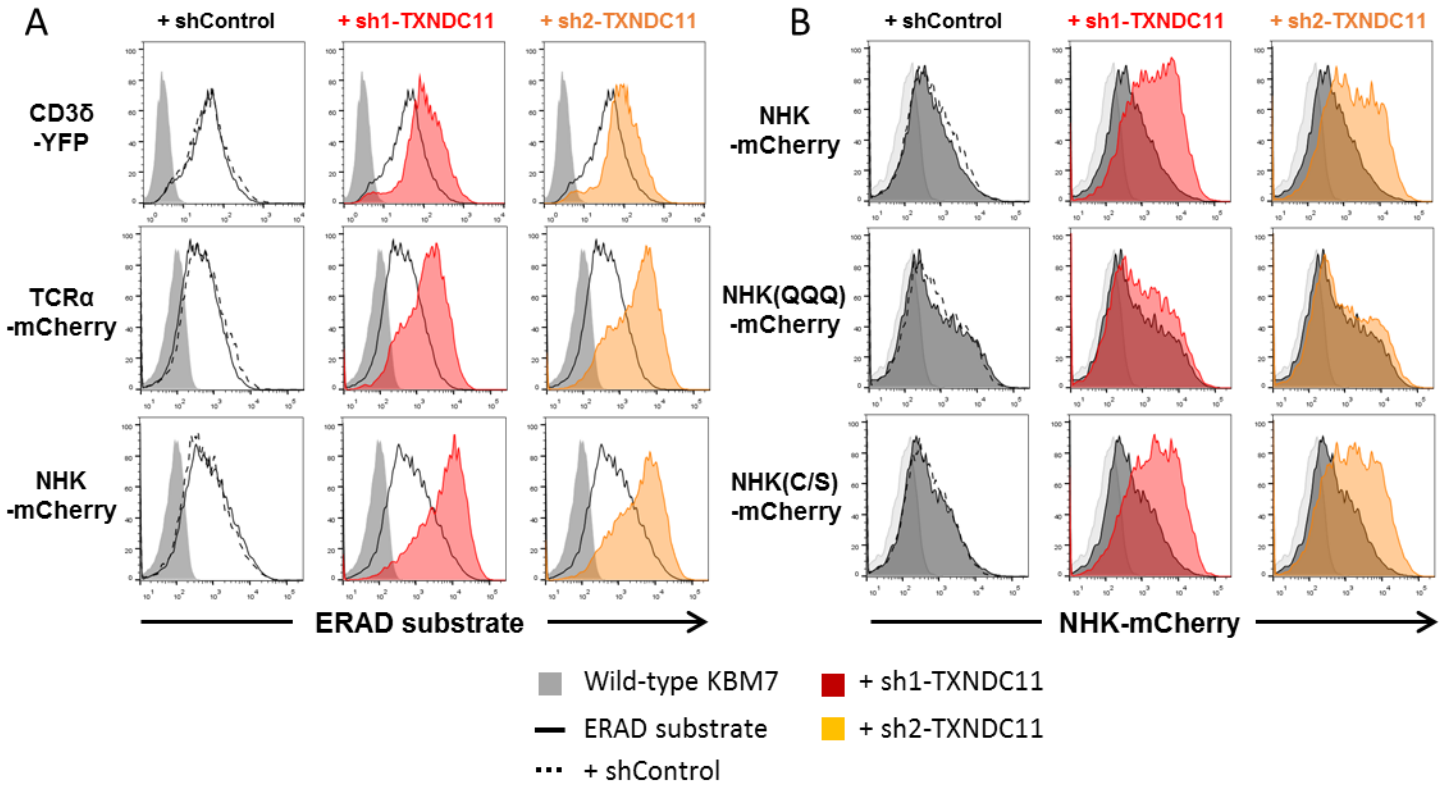

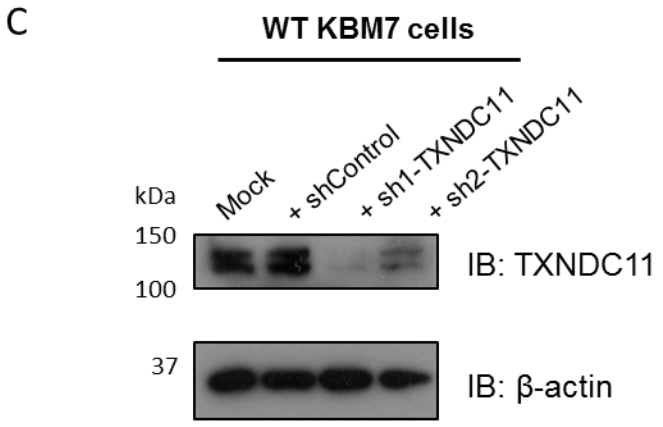

Figure 3.9 TXNDC11 depletion inhibits the degradation of other ERAD substrates. (A) KBM7 cell lines stably-expressing mCherry-tagged CD3δ, TCRα or NHK were transduced with a lentiviral construct encoding a TXNDC11-targeting or control shRNA. ERAD substrate expression was measured by flow cytometry. **(B)** KBM7 cell lines stably-expressing fluorescently-tagged wild type, non-glycosylated (QQQ) or cysteine-free (C/S) NHK were transduced with a lentiviral construct encoding a TXNDC11-targeting or control shRNA. NHK-mCherry expression was measured by flow cytometry. **(C)** Efficient depletion of TXNDC11 by shRNA was confirmed by immunoblot.

3.3.5 TXNDC11 interacts with glycoprotein ERAD machinery

We next sought to identify TXNDC11 interaction partners to further elucidate its function. Immunoprecipitation of endogenous TXNDC11 was performed followed by mass spectrometry analysis, with an immunoprecipitation from a TXNDC11 knockout clone to control for non-specific binding to TXNDC11 antibody and Protein A Sepharose. This identified six TXNDC11 binding partners (**Figure 3.10A**): the mannosidases EDEM2 and EDEM3, the oxidoreductase PDI, TXNDC5 and both subunits of the alpha-glucosidase complex (GANAB and GLU2B) (D'Alessio, Caramelo, and Parodi 2010). The co-immunoprecipitation of TXNDC11 with GANAB, EDEM2, EDEM3 and PDI was confirmed by immunoblot (**Figure 3.10B**). We also observed an increase in EDEM2 and EDEM3 protein abundance in the absence of TXNDC11 (**Figure 3.11**). EDEM2 and PDI were hits in both forward genetic screens, indicating that the interactions between TXNDC11 and EDEM2 and PDI are crucial for glycoprotein ERAD.

A

Identified Proteins	# peptides	
	Wild-type	**TXNDC11 KO**
PDI	22	1
EDEM2	20	0
GANAB	19	0
TXNDC11	19	0
EDEM3	15	0
GLU2B	13	0
TXNDC5	10	0

B

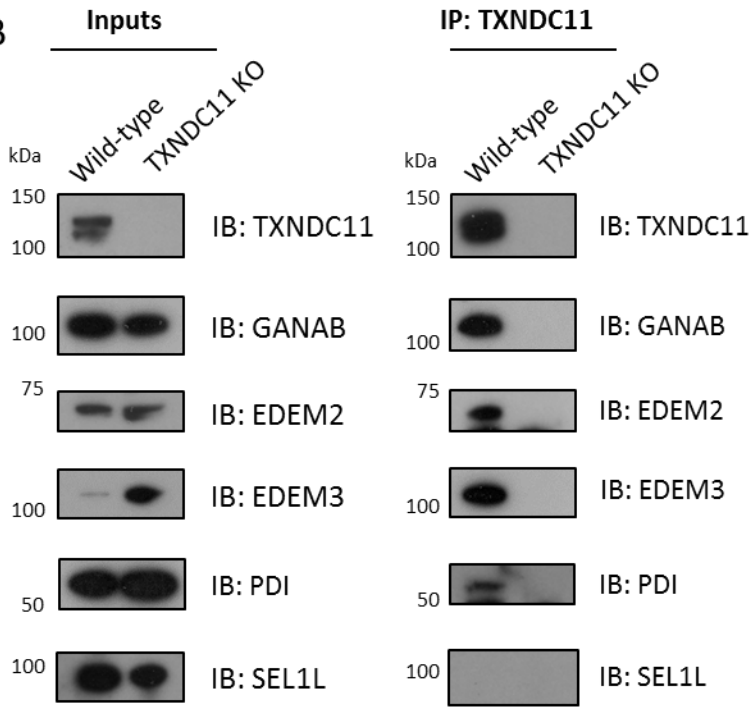

Figure 3.10 TXNDC11 interacts with glycoprotein ERAD machinery. (A) TXNDC11-interacting partners were identified by mass spectrometry analysis following an immunoprecipitation of endogenous TXNDC11. **(B)** TXNDC11-interacting partners were validated by immunoblot.

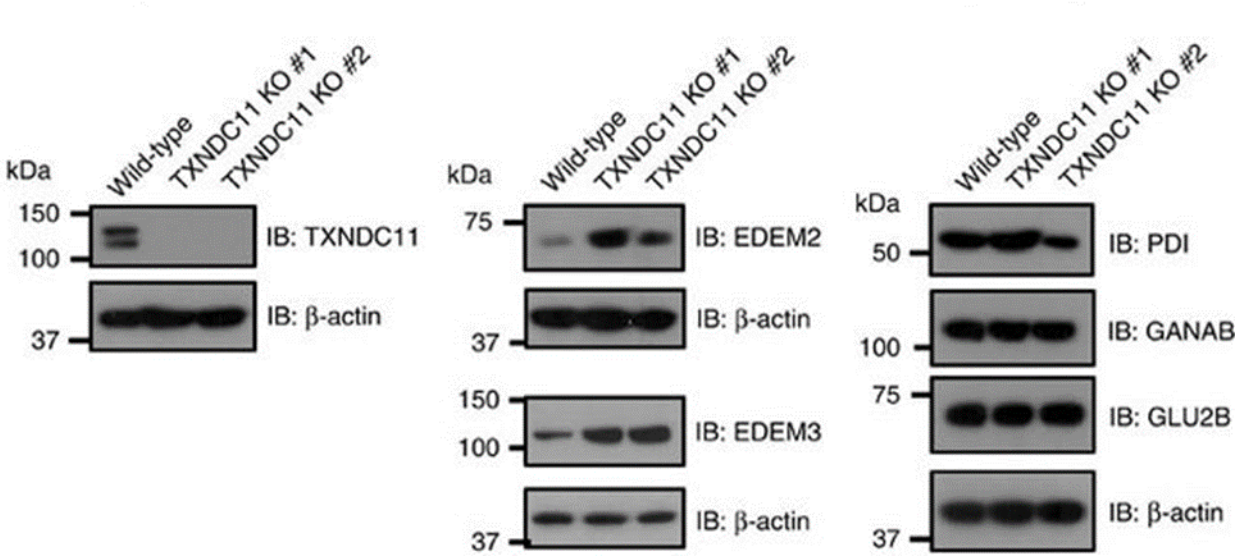

3.11 Loss of TXNDC11 increases EDEM2 and EDEM3 expression. Immunoblot analysis of TXNDC11-interacting partners in TXNDC11 knockout clones.

3.4 Discussion

The first part of my thesis project has demonstrated that genome-wide CRISPR knockout screens are as effective at identifying candidate genes in KBM7 cells as the previous gold-standard in human forward genetic screens. David Sabatini's laboratory have also reported a strong similarity in results from gene-trap mutagenesis and genome-wide CRISPR knockout screens (Wang et al. 2015). However, they did not identify any hits from chromosome eight in the gene-trap screen (as this chromosome is diploid) whilst the CRISPR screen did.

It was not surprising when two groups demonstrated that CRISPR knockout screens were more effective than shRNA screens, as RNA interference screens were not the previous gold standard screening method (Morgens et al. 2016, Evers et al. 2016).

3.4.1 Mutagenic potential of retroviral gene-trap versus genome-wide CRISPR library

A major advantage of the retroviral gene-trap vector is the ability to target all accessible chromatin, although there is a bias towards actively expressed genes (Carette, Guimaraes, et al. 2011). In contrast, a genome-wide CRISPR knockout screen is limited to the pre-determined genes targeted by the gRNAs that make up the library. Although not pursued as a part of this project, the gene-trap mutagenesis screen identified the antisense RNA encoded by *PRR7-AS1*, which is not targeted by the GeCKO v2 library. The gene-trap mutagenesis method also has the potential to disrupt regulatory elements in promoter regions of genes.

A genome-wide CRISPR knockout screen is immediately limited by the gRNA library. The GeCKO v2 library contains six gRNAs per gene and gRNAs were designed on the basis of minimising gRNA off-target effects (Sanjana, Shalem, and Zhang 2014). Other gRNA libraries contain more gRNAs per gene and place more emphasis on gRNA efficacy. The Bassik library, which is used later in this thesis, and Sabatini's activity-optimised library contain 10 gRNAs per gene (Wang et al. 2015, Morgens et al. 2017). The presence of more gRNAs for each gene means that genes that have a couple of ineffective gRNAs are more likely to be identified by the screen. The later gRNA libraries were designed using algorithms that prioritise gRNA efficacy, but exclude gRNAs with high off-target predictions (Wang et al. 2015, Morgens et al.

2017). It is likely that gRNA libraries will evolve to be increasingly effective as our understanding of CRISPR-mediated gene disruption develops.

3.4.2 Practical considerations of gene-trap mutagenesis versus CRISPR screens

The most significant advantage offered by CRISPR screens is the potential to perform forward genetic screens in human non-haploid cells, such as poly-ploid cancer cell lines and primary cells. The genome-wide CRISPR knockout screen presented in this Chapter was carried out in a haploid KBM7 clone. From this data, I cannot comment on whether the effectiveness of a CRISPR screen will diminish in diploid cells.

The mutagenesis is more straightforward in a haploid gene-trap screen as a CRISPR screen requires the construction and propagation of a genome-wide gRNA library. However, the amplification of gRNA sequences in a CRISPR screen is significantly easier than the large-scale mapping of retroviral integration sites using LAM-PCR in a gene-trap mutagenesis screen.

I chose to use genome-wide CRISPR knockout screens for the next section of my thesis project because of the significant practical advantage in preparing a CRISPR screen for sequencing.

3.5 Summary

In this Chapter, I used complementary forward genetic screens to identify factors required for MHC-I ERAD. There was a significant overlap between the results from the gene-trap mutagenesis and genome-wide CRISPR knockout screens, demonstrating that CRISPR screens are as effective as the previous gold-standard genome-wide screening method. Both screens identified a novel requirement for TXNDC11 in MHC-I ERAD. My collaborators went on to show that TXNDC11 is an ER-localised disulphide reductase that acts on another component of the ERAD machinery.

Chapter 4: A series of genome-wide CRISPR knockout screens to identify the E3 ubiquitin ligase(s) for HMG-CoA Reductase

4.1 Introduction

The expression level of HMGCR is tightly regulated by the intracellular sterol environment at the level of transcription and post-translation. At low sterol levels, SCAP does not associate with the ER-resident Insig proteins and so the SCAP-SREBP heterodimer can traffic to the Golgi (**Figure 1.1**) (Yabe, Brown, and Goldstein 2002, Yang et al. 2002). SREBP is cleaved in the Golgi to release the active form of SREBP, which migrates to the nucleus and up-regulates the expression of its target genes, including HMGCR (Goldstein, DeBose-Boyd, and Brown 2006). The loss of the cholesterol-dependent interaction with SCAP results in the degradation of Insig1 by gp78 (Lee, Song, et al. 2006). Additionally, at low sterol levels, the Insig proteins do not associate with HMGCR and so HMGCR is not targeted for ERAD (**Figure 1.3**) (Sever, Song, et al. 2003, Sever, Yang, et al. 2003).

At high sterol levels, the Insig proteins bind to SCAP to retain the SCAP-SREBP complex in the ER, thereby decreasing SREBP target gene expression (**Figure 1.1**) (Yabe, Brown, and Goldstein 2002, Yang et al. 2002). The Insig proteins also associate with the transmembrane domain of HMGCR and act as a sterol-sensitive scaffold to recruit an E3 ubiquitin ligase complexes to HMGCR (**Figure 1.3**) (Sever, Song, et al. 2003, Sever, Yang, et al. 2003). Cholesterol protects Insig1 form gp78-mediated degradation (Lee, Song, et al. 2006). Whilst the role of Insigs as a sterol-sensitive scaffold is widely accepted, the identity of the E3 ubiquitin ligase responsible for the sterol-induced degradation of HMGCR is controversial (Jo et al. 2011, Tsai et al. 2012). This controversy is described in **1.2.2.4** on page 39.

In the first section of my thesis project, I successfully used genome-wide forward genetic screens to identify many ERAD components, including the E3 ubiquitin ligase required for the degradation of MHC-I (Chapter 3). Other members of the Lehner laboratory have also used forward genetic screens to identify ERAD E3 ligases (Stagg et al. 2009, van den Boomen et al. 2014). Therefore genome-wide CRISPR knockout screens seemed a useful and unbiased approach to identify the E3 ubiquitin ligase for HMGCR.

4.2 Results

4.2.1 Establishing a fluorescent HMGCR reporter in HeLa cells

I needed to establish a fluorescent reporter for HMGCR expression as the basis for my fluorescence-based phenotypic selection. My first approach was to use a fluorescently-tagged HMGCR exogenous transgene. The post-translational sterol-dependent regulation of HMGCR only requires the transmembrane domain of HMGCR (Gil et al. 1985). By replacing the catalytic domain of HMGCR with mCherry I generated a fluorescent reporter for HMGCR expression without disrupting the cellular cholesterol homeostasis by over-expressing the catalytic domain of HMGCR (**Figure 4.1A**). Transcription of the HMG-mCherry fusion protein was driven by the powerful SFFV promoter and is therefore independent of the SREBP pathway (**Figure 4.1B**). This ensures that the HMG-mCherry fusion protein will only be subject to post-translational sterol-dependent regulation.

HeLa cells were transduced with a lentiviral construct encoding the HMG-mCherry fusion-protein and a single cell clone was obtained (**Figure 4.1C**). HMG-mCherry was stabilised following a 16-hour treatment with Bortezomib, a proteasome inhibitor, demonstrating that the HMG-mCherry fusion protein was constitutively degraded by the proteasome under normal, sterol-replete tissue culture conditions (**Figure 4.1D**).

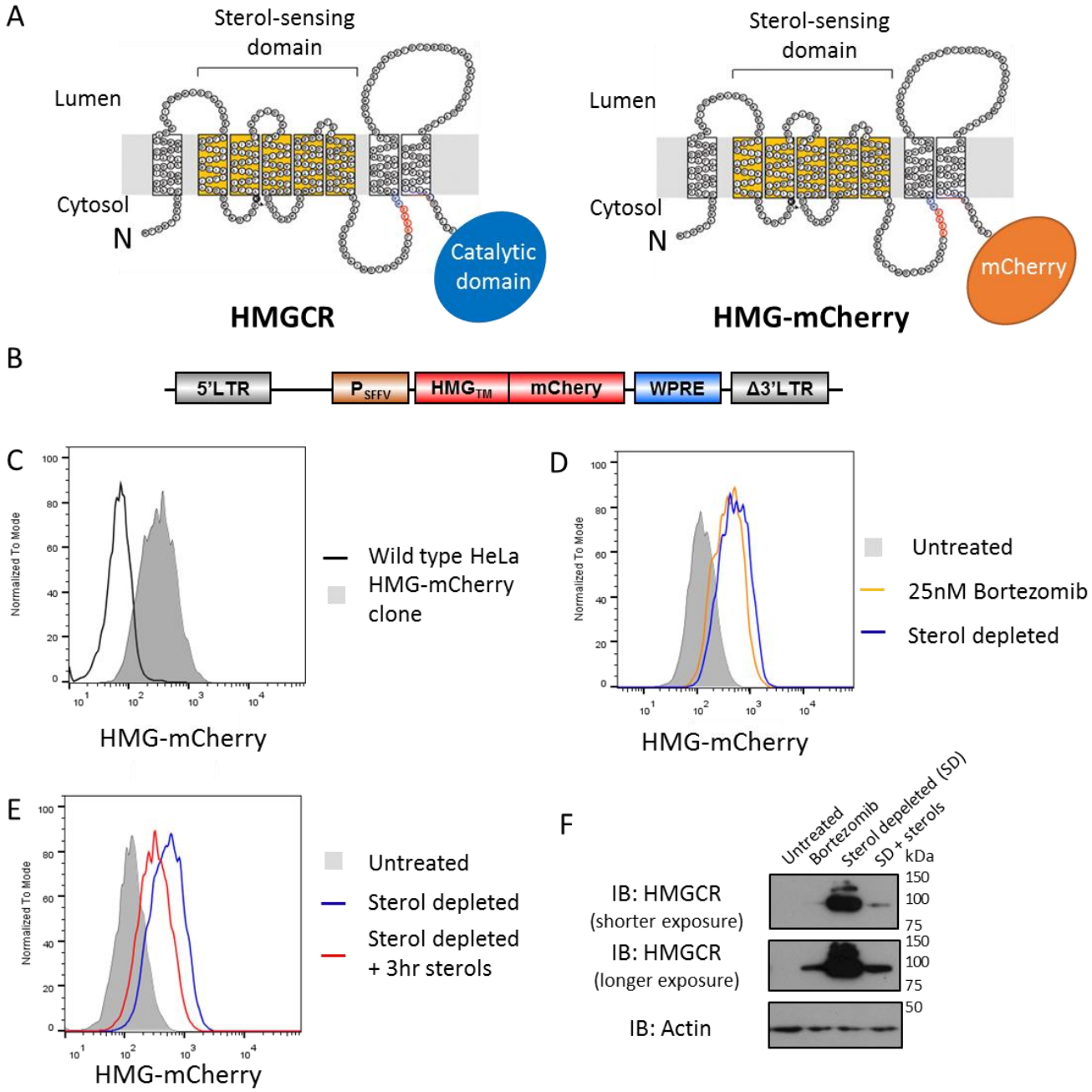

Figure 4.1 Establishing a fluorescent HMGCR reporter in HeLa cells. (A) A schematic of HMGCR illustrating the transmembrane domain, containing a sterol sensing domain, and the cytosolic catalytic domain. The catalytic domain is replaced by mCherry in the HMG-mCherry construct. **(B)** A Schematic of the lentiviral construct encoding the HMG-mCherry fusion protein. Expression is driven by the powerful spleen focus-forming virus (SFFV) promoter. (LTR, long-terminal repeat; WPRE, Woodchuck hepatitis virus posttranscriptional regulatory element). **(C)** A single cell clone stably expressing HMG-mCherrry was isolated. Steady state expression of HMG-mCherry was measured by flow cytometry. **(D)** The HMG-mCherry expressing clone was sterol depleted by culture in LPDS containing medium with 10μM mevastatin overnight or treated with 25nM Bortezomib for 16 hours. **(E)** The HMG-mCherry clone was sterol depleted overnight then cultured for a further 3 hours in the presence or absence of sterols (2 μg/ml 25-hydroxycholesterol plus 20 μg/ml cholesterol) to demonstrate correct sterol dependent degradation of the reporter. **(F)** Wild type HeLa cells were treated with 25nM Bortezomib for 16 hours or sterol depleted overnight then cultured for 3 hours in the presence or absence of sterols. The cells were lysed and immunoblotted for endogenous HMGCR.

Cells can be sterol depleted by overnight culture in medium containing lipoprotein-depleted serum and 10μM mevastatin. Sterol depletion increases endogenous HMGCR expression by upregulating SREBP-dependent transcription and stabilises HMGCR protein by reducing sterol-dependent degradation. As HMG-mCherry transcription is independent of the SREBP pathway, the increase in HMG-mCherry following overnight sterol depletion is caused by decreased sterol-induced degradation (**Figure 4.1D**). The increase in HMG-mCherry expression was similar following proteasome inhibition and sterol depletion, suggesting that HMG-mCherry is predominantly degraded in a sterol-dependent manner. The degradation of HMG-mCherry could be induced by adding sterols (2 μg/ml 25-hydroxycholesterol plus 20 μg/ml cholesterol) into the sterol-depleted culture (**Figure 4.1E**). This shows that HMG-mCherry is subject to sterol-induced degradation and is therefore an appropriate tool to use in a forward genetic screen to identify the E3 ubiquitin ligase responsible for the sterol-induced ubiquitination and degradation of HMGCR.

Blocking the degradation of HMGCR in wild type HeLa cells with Bortezomib rescued HMGCR (**Figure 4.1F**). However, blocking the degradation of HMGCR and inducing SREBP-dependent transcription by overnight sterol depletion resulted in significantly higher expression of HMGCR. The addition of sterols induces the rapid degradation of HMGCR, as well as stopping SREBP-driven transcription. There is a marked difference in the effect of Bortezomib treatment and sterol depletion on HMG-mCherry and endogenous HMGCR, which highlights the pronounced effect that SREBP-dependent transcription has on HMGCR expression (**Figure 4.1D** and **Figure 4.1F**). Therefore, a forward genetic screen for increased HMG-mCherry expression will focus on the post-translational regulation of HMGCR rather than SREBP-dependent transcription.

4.2.2 A genome-wide CRISPR knockout screen to identify the E3 ubiquitin ligase of HMGCR

I hypothesised that the loss of the E3 ubiquitin ligase responsible for targeting HMG-mCherry for degradation would result in the stabilisation of HMG-mCherry. I would then be able to enrich this HMG-mCherry^{high} phenotype by FACS.

I performed a genome-wide CRISPR knockout screen using the GeCKO v2 library as described in Chapter 3. Briefly, the HMG-mCherry clone was transduced with the Cas9 nuclease and Cas9 function was confirmed using the control B2M gRNA. The Cas9-expressing HMG-mCherry clone was transduced with the GeCKO v2 library at a M.O.I. of 0.35 and HMG-mCherry^{high} cells were selected by two sequential rounds of FACS (**Figure 4.2A**). The resultant population had a modest enrichment of 30% mCherry^{high} cells. However, when the selected cells were compared to the starting clone on a histogram plot, the majority of the population showed a notably higher level of HMG-mCherry expression.

The selected cells and starting clone were then analysed for their ability to degrade HMG-mCherry in response to sterols (**Figure 4.2B**). HMG-mCherry was still stabilised by sterol depletion and degraded in response to sterols in the selected population, indicating that I had not enriched a population of mutants with impaired sterol-induced HMG-mCherry degradation, despite the rescue at steady state. Immunoblot analysis of these cells showed a significant rescue of endogenous HMGCR in the selected cells at steady state compared to the starting clone (**Figure 4.2C**). This demonstrates that the rescue of HMG-mCherry in the selected cells was not an artefact of over-expression. However, there was no difference in the sterol-induced degradation of endogenous HMGCR.

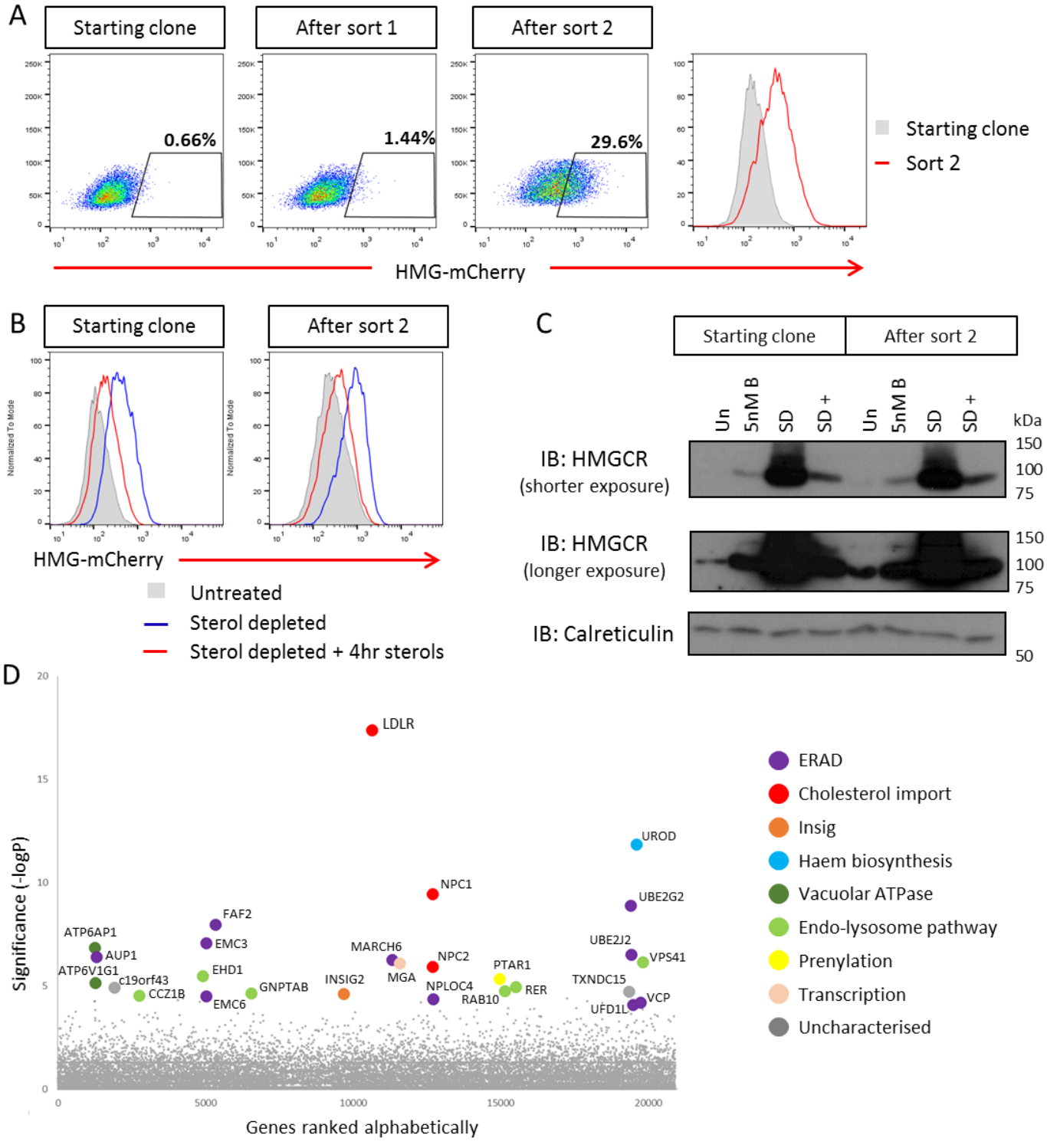

Figure 4.2 A genome wide CRISPR knock-out screen to identify the E3 ubiquitin ligase for HMGCR identifies MARCH6 (A) The level of HMG-mCherry was determined by flow cytometry in the starting clone and the population from each round of FACS to measure the enrichment in HMG-mCherry^{high} cells. **(B)** The un-mutagenised HMG-mCherry clone and the selected cells were sterol depleted overnight followed by a four-hour culture in the presence or absence of sterols to determine the enrichment of mutants unable to degrade HMG-mCherry in response to sterols **(C)** Cells from (C) were lysed and immunoblotted for endogenous HMGCR. (Un, untreated; 5nM B, treated with 5nM Bortezomib for 16 hours; SD, overnight sterol depletion; SD +, overnight sterol depletion plus 4 hours with sterols). **(D)** Identification of candidate genes using the RSA algorithm (König et al. 2007).

The gRNA abundance was quantified in the selected cells and an unselected library that had been grown for the same amount of time. The RSA algorithm was used to identify candidate genes (**Figure 4.2D**). The screen was successful in identifying multiple hits that could be readily grouped into several functional classifications listed below.

ERAD and UPS

The largest group contains genes involved in ERAD and the UPS, including the E3 ubiquitin ligase *MARCH6* (see 4.2.3). Two E2 conjugating enzymes, *UBE2G2* and *UBE2J2*, were also identified. UBE2G2 is already known to be critical for the sterol-induced ubiquitination of HMGCR (Miao et al. 2010). Ancient Ubiquitous Protein 1 (*AUP1*) is an ERAD associated protein that recruits the soluble E2 conjugating enzyme UBE2G2 to membrane-bound E3 ubiquitin ligases and has been implicated in the sterol-dependent degradation of HMGCR (Jo, Hartman, and DeBose-Boyd 2013, Klemm, Spooner, and Ploegh 2011). The screen identified multiple components of the VCP/p97 ATPase complex, UBXD8 (*FAF2*), Npl4 (*NPLOC4*), *UFD1L* and p97 (*VCP*) itself. The p97 complex is required to extract HMGCR from the ER membrane so that HMGCR can be degraded by the proteasome in the cytosol (Morris et al. 2014). The screen also identified components of the poorly characterised ER membrane complex (EMC), *EMC3* and *EMC6*, suggesting a role for the EMC in the ERAD of HMGCR (Christianson et al. 2012).

Insig

The Insig proteins act as scaffolds to recruit the E3 ubiquitin ligase to HMGCR in a sterol-dependent manner (Jo and Debose-Boyd 2010). This screen identified *Insig2* but not *Insig1* suggesting that the screen was not saturating.

Cholesterol import and the endocytic pathway

The low-density lipoprotein receptor (*LDLR*) and Niemann-Pick proteins (*NPC1* and *NPC2*) are required for the import of cholesterol from the extracellular space (Brown and Goldstein 1986, Infante et al. 2008, Kwon et al. 2009). The screen also identified components of the vacuolar ATPase (*ATP6AP1* and *ATP6V1G1*) and endo-lysosome pathway (light green in **Figure 4.2D**), which are required for the endocytosis and recycling of the LDLR (Brown and Goldstein 1986). The loss of these genes will block the uptake of exogenous cholesterol and sterol deplete the cell leading to the stabilisation of HMG-mCherry.

Haem biosynthesis and protein prenylation

Unexpectedly, the screen identified uroporphyrinogen decarboxylase (*UROD*) as a candidate gene. UROD catalyses the decarboxylation of four acetate side chains of iroporphyrinogen in the haem biosynthetic pathway (Whitby et al. 1998). Haem A contains an isoprenoid side chain that is derived from farnesyl pyrophosphate, an intermediate in the cholesterol biosynthetic pathway downstream of HMGCR (Dhar, Koul, and Kaul 2013). The identification of UROD in the forward genetic screen raises the possibility that a feedback loop exists to increase mevalonate production (i.e. stabilise HMGCR) when haem biosynthesis is blocked. Farnesyl pyrophosphate derivatives are covalently attached to proteins in a process referred to as protein prenylation (Dhar, Koul, and Kaul 2013). The identification of protein prenyltransferase alpha subunit repeat-containing protein 1 (*PTAR1*) suggests that inhibiting protein prenylation stabilises HMGCR. Alternatively, the activity of an enzyme required for the degradation of HMGCR might be dependent on prenylation.

Other

TXNDC15 is a poorly characterised PDI family member. *C19orf43* is an uncharacterised protein consisting of 176 amino acids. Secondary structure and protein domain prediction programs did not identify any features shared between c19orf43 and other proteins and so it was not pursued for validation or investigation. *MGA* encodes a transcription factor that is routinely detected in screens and is likely to be an artefact of expression from the lentiviral construct.

4.2.3 MARCH6 and the cholesterol biosynthesis pathway

The aim of the genome-wide CRISPR knockout screen was to identify the E3 ubiquitin ligase for HMGCR. The only candidate gene that encodes an E3 ubiquitin ligase is MARCH6. MARCH6 plays an important role in regulating cholesterol biosynthesis pathway by targeting squalene monooxygenase for degradation in a cholesterol-dependent manner (Gill et al. 2011, Foresti et al. 2013, Zelcer et al. 2014). Nolan Zelcer's paper describing the induction of IDOL and subsequent decrease in LDLR expression following MARCH6 depletion had not been published when I identified MARCH6 in the CRISPR screen (Loregger et al. 2015).

Zelcer *et al.* observed an increase in the basal level of HMCGR when MARCH6 was depleted by siRNA but did not see a definitive effect of MARCH6 depletion of the sterol-induced degradation of HMGCR (Zelcer et al. 2014). To address the effect of MARCH6 on HMGCR I used siRNA to deplete MARCH6 in the HMG-mCherry HeLa clone. I observed an accumulation of HMG-mCherry in cells transfected with MARCH6 siRNA compared to those transfected with a control siRNA, validating the CRISPR screen (**Figure 4.3A**). These cells were sterol depleted overnight and then cultured in the presence or absence of sterols for a further four hours. In the absence of sterols, control cells stabilised HMG-mCherry leading to a 4.8-fold increase in MFI (green to blue in Figure 4.3A), whereas cells depleted of MARCH6 stabilised HMG-mCherry by 3.9-fold. When sterols were added following sterol depletion, control cells decreased their MFI by 46% and MARCH6 knockdown cells decreased their MFI by 53% (blue to red in Figure 4.3A). This suggests that MARCH6 is not required for the sterol-induced degradation of HMG-mCherry. Immunoblot analysis of the cells in Figure 4.3A showed no rescue of endogenous HMGCR at steady state, in contrast to Zelcer *et al*., and no change in the sterol-induced degradation of HMGCR following MARCH6 depletion (**Figure 4.3B**) (Zelcer et al. 2014).

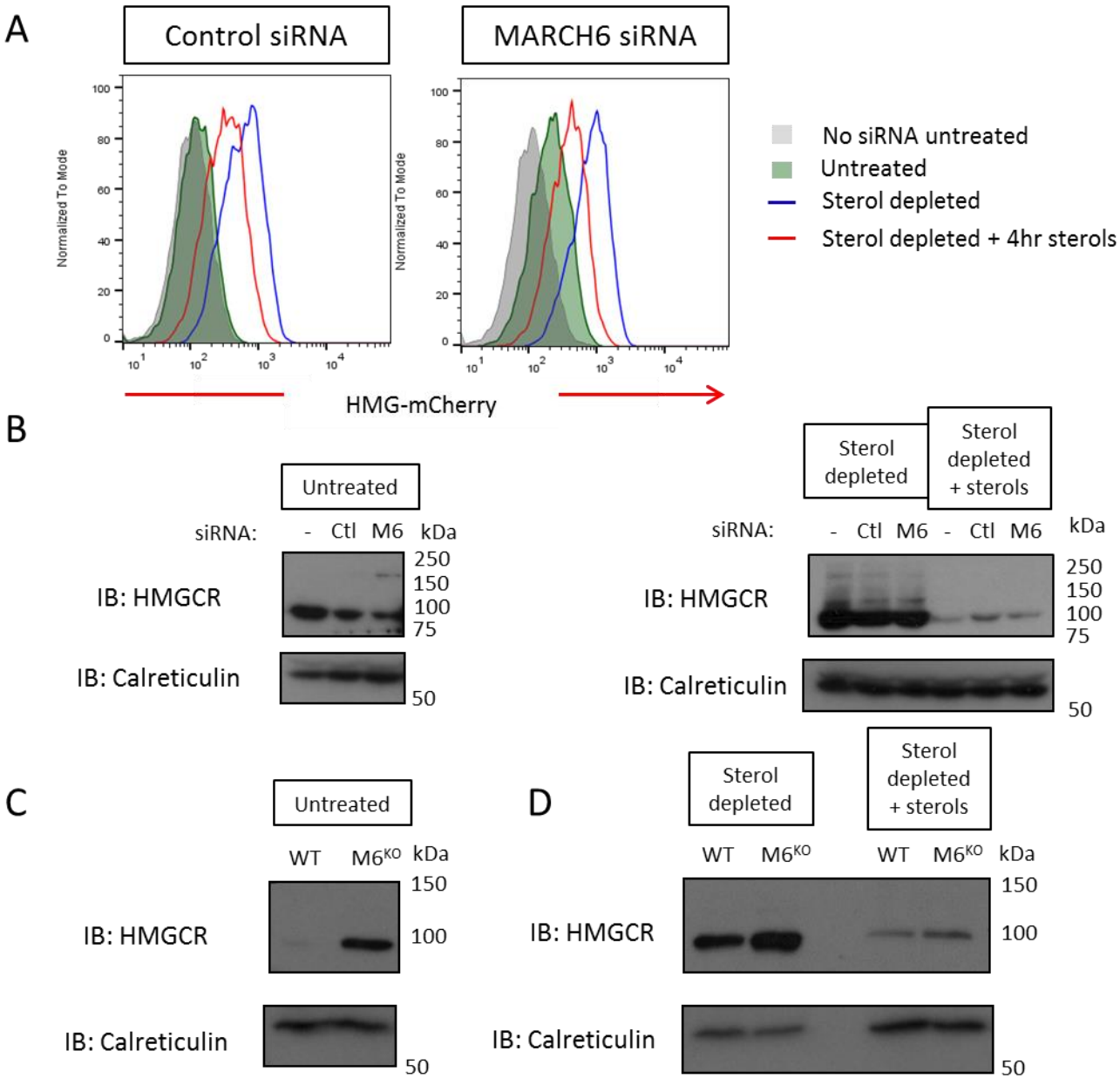

Figure 4.3 MARCH6 depletion does not inhibit the sterol-induced degradation of HMGCR. **(A)** The HMG-mCherry expressing HeLa clone was transfected with 90nM MARCH6 or control siRNA. Cells were sterol depleted 3 days post-transfection. On day 4 post-transfection, cells were cultured for a further 4 hours in the presence or absence of sterols. HMG-mCherry expression was determined by flow cytometry. **(B)** Cells from (A) were lysed and immunoblotted for endogenous HMGCR. **(C)** Immunoblot of untreated cells for HMGCR in wild type HeLa cells and a MARCH6 knockout HeLa clone. **(D)** Wild type HeLa cells and a MARCH6 knockout HeLa clone were sterol depleted overnight then in the presence or absence of sterols for a further 4 hours. Cells were lysed and immunoblotted for endogenous HMGCR.

I did not determine the extent of the depletion of MARCH6 but it is likely that there is an incomplete knockdown due to the absence of a rescue of HMGCR at steady state. A MARCH6 knockout HeLa clone (kindly provided by Sandra Stefanovic-Barrett (Nathan laboratory, Cambridge)), generated by CRISPR-mediated gene disruption, was employed to assess HMGCR degradation in a MARCH6 null background. The loss of MARCH6 had been confirmed by Sandra Stefanovic-Barrett by sequencing the locus targeted by the gRNA to confirm the presence of frameshift insertions or deletions in all alleles. The clone also exhibits a significant rescue of squalene monooxygenase, demonstrating a functional rescue due to the loss of MARCH6. Immunoblot analysis of the MARCH6 knockout clone and its parental HeLa line showed a significant increase in HMGCR at steady state (**Figure 4.3C**). Following sterol depletion more HMGCR was detected in the MARCH6 knockout clone than the parental HeLa cell line. Whilst there appears to be slightly more HMGCR in the MARCH6 knockout clone following the sterol-induced degradation of HMGCR, the higher starting point shows that there is no defect in HMGCR degradation in the absence of MARCH6 (**Figure 4.3C**).

4.2.4 HeLa cells are autofluorescent in the absence of UROD

UROD was an unexpected high-confidence hit in the screen and suggested a potential feedback loop from the haem biosynthesis pathway to the cholesterol biosynthesis pathway (**Figure 4.2E**). I observed an apparent increase in HMG-mCherry expression following CRISPR-mediated gene disruption of UROD (**Figure 4.4A**). However, the gMFI was increased in the channel (610nm) used to detect mCherry by flow cytometery from wild type HeLa cells (which do not express any exogenous transgene) following CRISPR-mediated gene disruption of UROD. Knockdown of UROD by shRNA in the HMG-mCherry HeLa clone also lead to an increase in fluorescence detected by the 610nm channel on the flow cytometer (**Figure 4.4B**). However, immunoblot analysis of these cells showed no increase in HMG-mCherry protein abundance (**Figure 4.4C**). Taken together these data show that the CRISPR screen correctly identified UROD as a gene whose loss leads to increased fluorescence detected by the 610nm channel. However, HMG-mCherry expressing HeLa cells become autofluorescent following UROD depletion, presumably due to the accumulation of a fluorescent intermediate in the haem biosynthesis pathway, not due to the stabilisation of HMGCR.

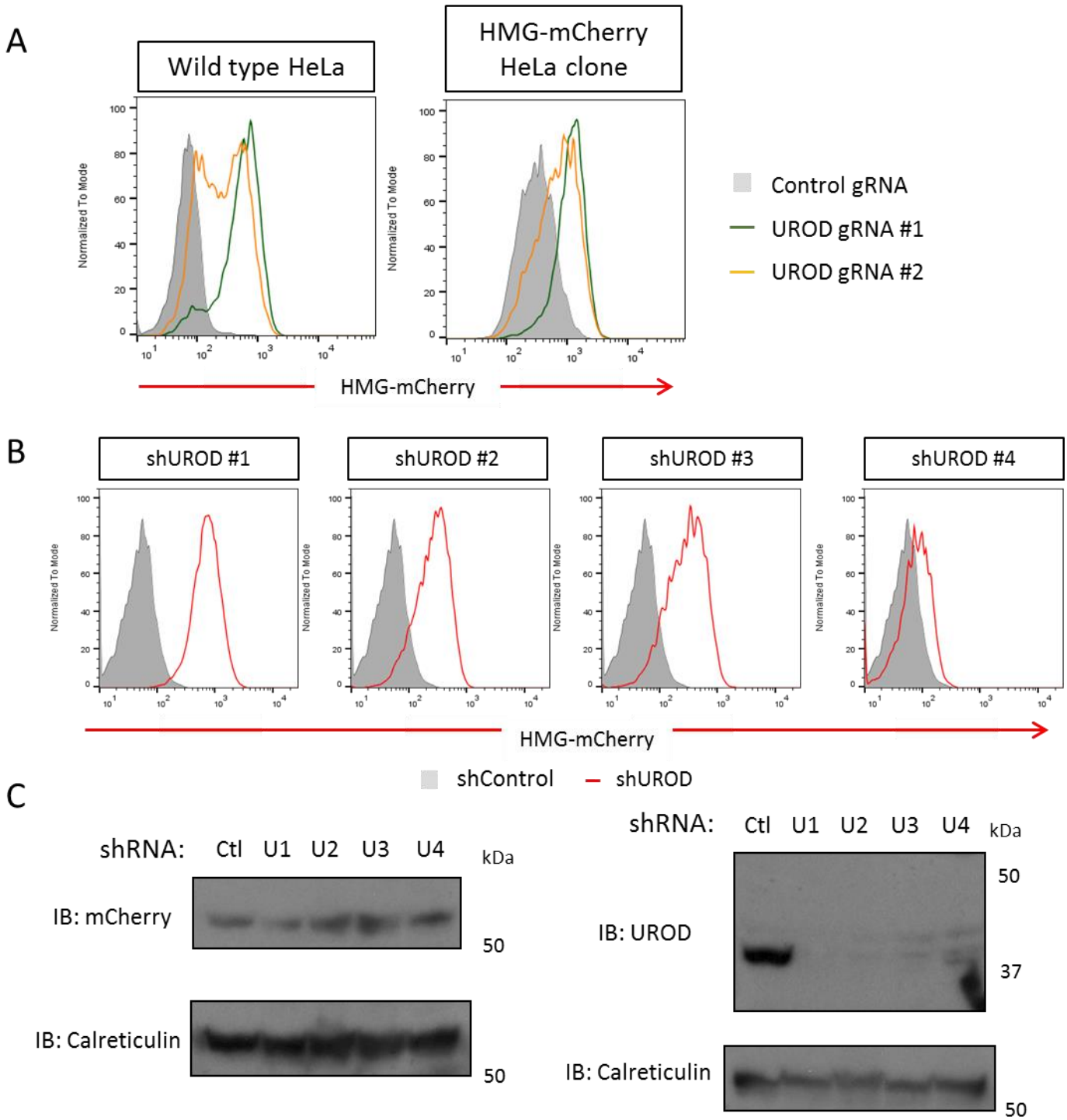

Figure 4.4 HeLa cells are autofluorescent following depletion of UROD. (A) Wild type HeLa cells and the HMG-mCherry expressing clone were transiently transfected with Cas9 and a control or UROD-targeting gRNA. Cells were analysed by flow cytometry 7 days post-transfection. **(B)** The HMG-mCherry HeLa clone was transduced with a control or UROD shRNA. Cells were analysed by flow cytometry 7 days post-transduction. **(C)** Cells from (B) were lysed and immunoblotted to determine HMG-mCherry expression and UROD depletion. (Ctl, control; U, UROD)

4.2.5 UBE2G2 is critical for the sterol-induced degradation of HMG-mCherry

Despite the success of the CRISPR screen in identifying many factors required for the regulation of HMGCR, the only E3 ligase identified was MARCH6. Whilst MACRH6 influences HMGCR expression, it does not target HMGCR (**Figure 4.3**). I next sought to examine the HMG-mCherry system further and identify a method for adapting the CRISPR screen to identify the E3 ubiquitin ligase for HMGCR.

UBE2G2 has been previously reported as an E2 conjugating enzyme required for the sterol-induced ubiquitination of HMGCR (Miao et al. 2010). I generated UBE2G2 knockout clones by transiently transfecting the HMG-mCherry clone with Cas9 and a UBE2G2-targeting gRNA, selecting transfected cells with puromycin treatment and single cell cloning by serial dilution. UBE2G2 knockout clones were identified by immunoblot (**Figure 4.5A**). HMG-mCherry was strongly rescued at steady state in the UBE2G2 knockout clones (comparing green and grey in **Figure 4.5B**), showing a defect in the degradation of HMG-mCherry and validating the identification of UBE2G2 in the CRISPR screen. A small stabilisation of HMG-mCherry was observed when the UBE2G2 knockout clones were sterol-depleted overnight, but there was no decrease in HMG-mCherry when sterols were added to the sterol-depleted culture for four hours (**Figure 4.5B**). UBE2G2 is therefore an essential component required for the sterol-induced degradation of HMG-mCherry. Immunoblot analysis confirmed a significant rescue of endogenous HMGCR at steady state and a significant block in the sterol-induced degradation of endogenous HMGCR in the UBE2G2 knockout clones (**Figure 4.5C**).

It is possible that more than one E3 ligase might use UBE2G2 to ubiquitinate HMGCR, in a manner similar to the previously suggested model by Russel Debose-Boyd (Jo et al. 2011). If one of the E3 ligases responsible for ubiquitinating HMG-mCherry is lost, the rate of sterol-induced HMG-mCherry degradation could be reduced and therefore selected by FACS in a screen.

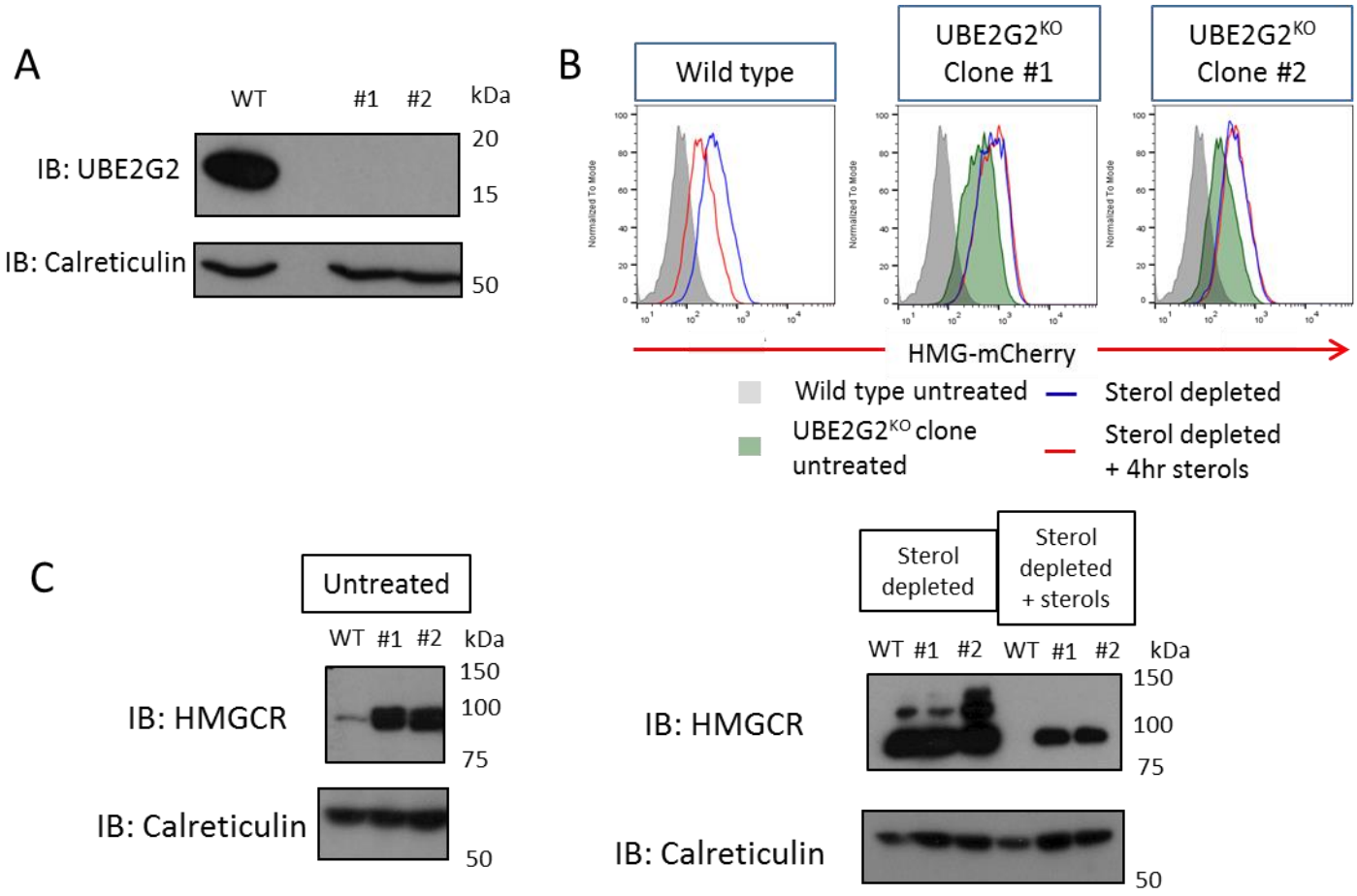

Figure 4.5 UBE2G2 is critical for the sterol-induced degradation of HMG-mCherry. (A) HMG-mCherry HeLa UBE2G2 knockout clones were identified by immunoblot. **(B)** The HMG-mCherry HeLa clone and the UBE2G2 knockout clones were sterol depleted overnight then cultured for a further four hours in the presence or absence of sterols. HMG-mCherry expression was analysed by flow cytometry. **(C)** Untreated HMG-mCherry expressing wild type cells and UBE2G2 knockout clones were lysed and immunoblotted for endogenous HMGCR. **(D)** Cells from (B) were lysed and immunoblotted for endogenous HMGCR. (WT, wild type)

4.2.6 A genome-wide CRISPR knockout screen using sterol depletion to identify the E3 ubiquitin ligase for HMGCR

I performed a second genome-wide CRISPR knockout screen in the HMG-mCherry HeLa clone to identify the E3 ubiquitin ligase(s) for HMGCR. I changed the FACS strategy to further focus the screen on the sterol-induced degradation of HMGCR. The day before sorting, the mutagenised library was sterol depleted overnight to stabilise HMG-mCherry. Sterols were added to the culture for five hours and HMG-mCherry^{high} cells were then selected by FACS (**Figure 4.6A**). A time course experiment showed the continuous degradation of HMG-mCherry in response to sterols over five hours (**Figure 4.6B**). A five-hour incubation was the longest practical culture possible in the screen. The aim of this FACS strategy was to select cells that could not degrade HMG-mCherry in response to sterols or had a slower rate of HMG-mCherry degradation.

The Cas9-expressing HMG-mCherry clone was transduced with the GeCKO v2 library at a M.O.I. of 0.3. I attempted to enrich mutants with a reduced rate of sterol-induced HMG-mCherry by sequential rounds of FACS using the strategy illustrated in Figure 4.6A. Whilst the resultant population had a significant rescue of HMG-mCherry at steady state, the sterol depletion assay showed that HMG-mCherry was still stabilised by sterol depletion and degraded in response to sterols (**Figure 4.6C**). Immunoblotting demonstrated that the selected cells also expressed more endogenous HMGCR at steady state than the starting clone. However, the selected cells only showed a slight decrease in the sterol-induced degradation of endogenous HMGCR (**Figure 4.6D**). Together the flow cytometry and immunoblot analysis of the selected cells show that there was very little enrichment for cells that had a reduced ability to degrade HMGCR in response to sterols.

Despite this, genomic DNA was extracted from the selected cells together with an unselected library that had grown for the same amount of time. The gRNA abundance was determined in the selected cells and the library by sequencing on the Illumina HiSeq platform. The RSA algorithm only identified a small number of candidate genes in this screen (**Figure 4.6E**) (König et al. 2007). It was reassuring to identify *UBE2G2* as a high-confidence hit, proving that the screen was technically successful. *UBE2J2* is also identified by the screen and is a common hit with the steady state HMG-mCherry screen (**Figure 4.2E**).

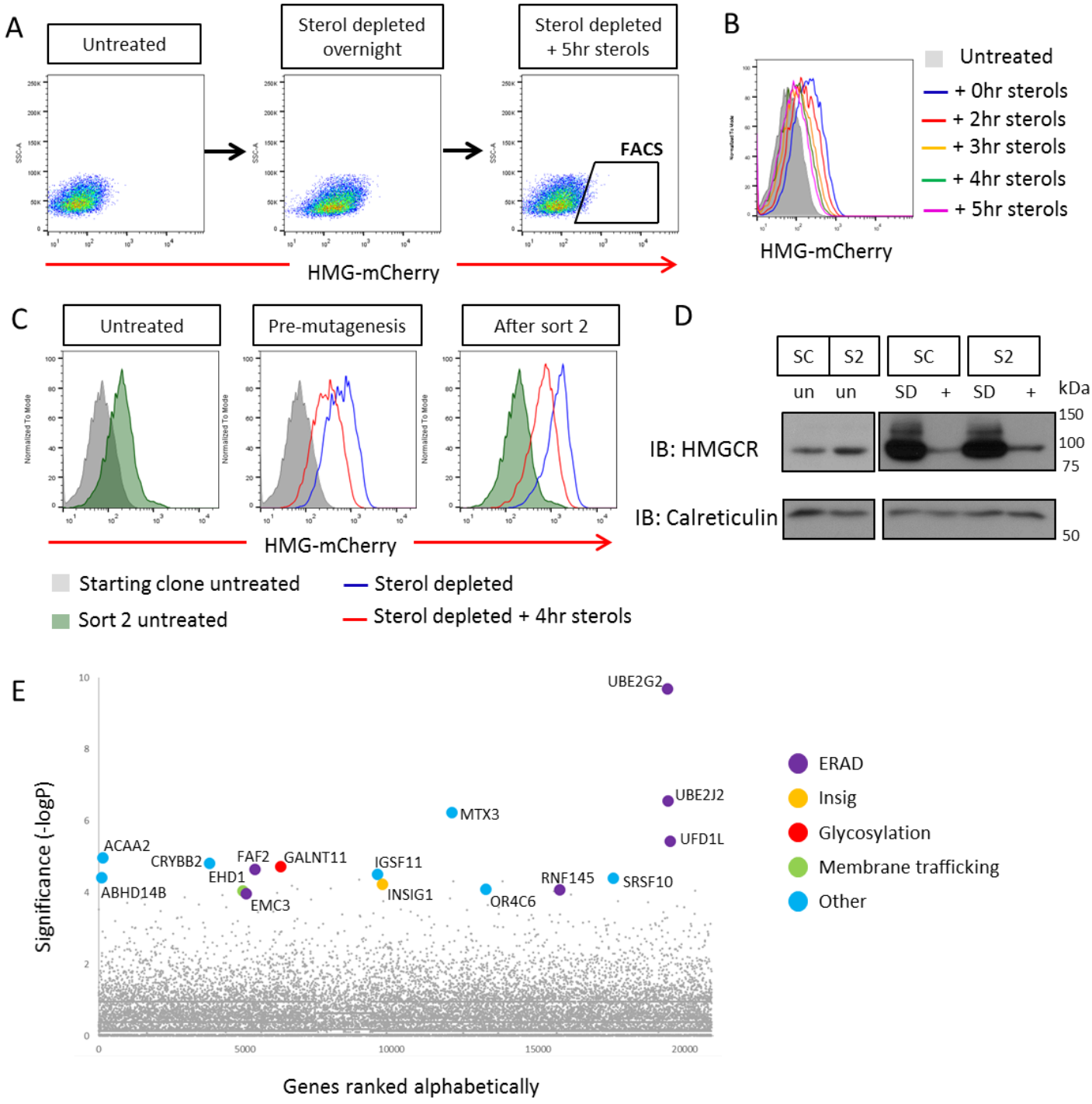

Figure 4.6 A genome wide CRISPR knockout screen using sterol depletion to identify the E3 ubiquitin ligase for HMGCR identifies RNF145. (A) The FACS strategy used in the CRISPR screen to identify factors required for the sterol induced degradation of HMG-mCherry. Cells with a reduced ability to degrade HMG-mCherry in response to sterols should be selected by FACS in the gate indicated. **(B)** The HMG-mCherry expressing HeLa clone was sterol depleted overnight and then cultured in the presence of sterols for the indicated time periods. **(C)** The HMG-mCherry expressing clone and selected cells were sterol depleted and cultured for a further four hours in the presence or absence of sterols. HMG-mCherry expression was measured by flow cytometry. **(D)** Cells from (C) were lysed and immunoblotted for endogenous HMGCR (SC, starting clone; S2, sort 2; un, untreated; SD, sterol depleted; +, sterol depleted plus four hours sterols). **(E)** Candidate genes were identified using the RSA algorithm (König et al. 2007).

Other factors known to be required for the sterol-induced degradation of HMGCR (*FAF2*, *INSIG1* and *UFD1L*) are identified as borderline hits (Sever, Yang, et al. 2003, Cao et al. 2007, Morris et al. 2014). The screen also identified the poorly characterised ERAD E3 ligase RNF145 as a borderline hit (Graham et al. 2015, Kaneko et al. 2016). RNF145 is a homolog of TRC8, one of the E3 ligases suggested to ubiquitinate HMGCR (Jo et al. 2011). Alignment coverage against TRC8 was 94%, with 47% similarity and 27% shared sequence identity. I also identified a YLYF motif near the N-terminus of RNF145. A YIYF in the sterol-sensing domain (SSD) of SCAP and HMGCR is required for these proteins to interact with the Insig proteins (Yang et al. 2002, Sever, Song, et al. 2003). The presence of the YLYF motif suggested that RNF145 might contain a SSD and interact with the Insig proteins. RNF145 is therefore a highly promising candidate gene from this CRISPR screen.

4.2.7 Loss of RNF145 partially inhibits the sterol-induced degradation of HMG-mCherry

I sought to validate a role for RNF145 in the sterol-induced degradation of HMGCR by CRISPR-mediated gene disruption using four independent gRNAs. In each case I observed an increase in HMG-mCherry expression at steady state, a decreased stabilisation of HMG-mCherry with sterol depletion (5-fold increase compared to 7.8-fold increase in control cells) and a slight decrease in the sterol-induced degradation of HMG-mCherry (49-51% decrease compared to 54.5% decrease in control cells) (**Figure 4.7A**). These three observations show that the loss of RNF145 inhibits the sterol-induced degradation of HMG-mCherry. However, this partial phenotype could be the result of an indirect effect or redundancy at the level of the E3 ligase.

When the cells from Figure 4.7A were immunoblotted for endogenous HMGCR, it was initially very promising to see an increase in HMGCR at steady state (**Figure 4.7B**). However, only RNF145 gRNA #4 appeared to show a slight decrease in the sterol-induced degradation of endogenous HMGCR. The consistent phenotype obtained with these four RNF145-targeting gRNAs was difficult to see against endogenous HMGCR. I therefore concluded that the loss of RNF145 alone did not result in a decrease in the sterol-induced degradation of endogenous HMGCR detectable by immunoblotting.

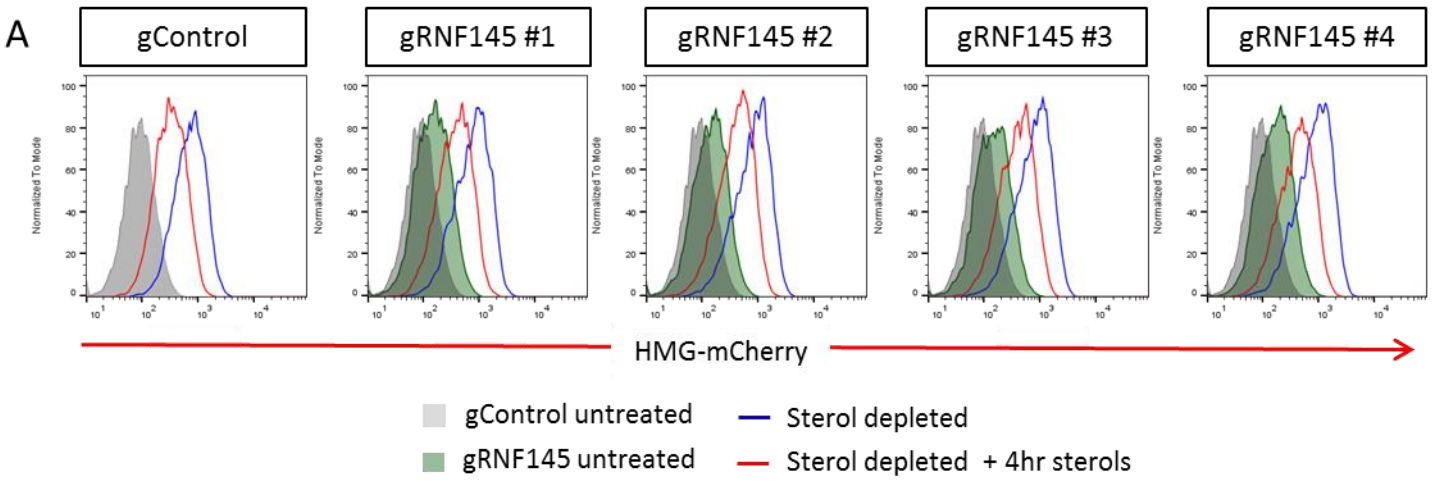

gRNA	Control	RNF145 #1	RNF145 #2	RNF145 #3	RNF145 #4
untreated gMFI	86.8	142	133	138	157
Sterol depleted (SD) gMFI	679	710	740	732	784
SD fold increase	**7.82**	**5.00**	**5.56**	**5.30**	**4.99**
SD + sterols gMFI	309	346	379	361	383
+ sterols % decrease	**54.5**	**51.3**	**48.8**	**50.7**	**51.1**

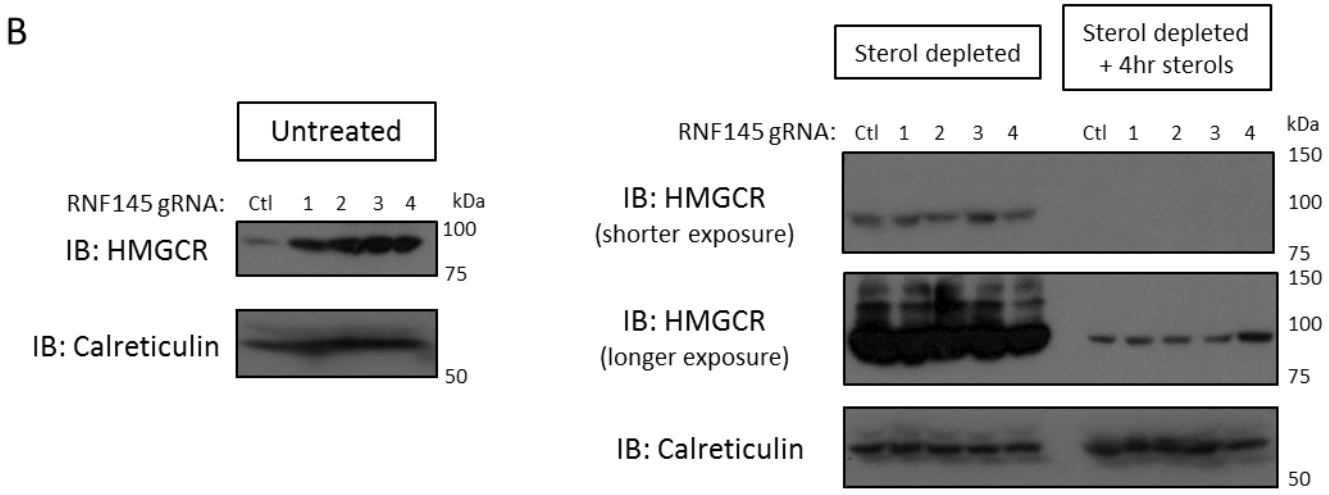

Figure 4.7 Loss of RNF145 partially inhibits the sterol-induced degradation of HMG-mCherry. (A) The HMG-mCherry expressing clone was transfected with Cas9 and a control or RNF145-targeting gRNA. Transfected cells were selected by treatment with puromycin. Cells were sterol depleted overnight seven days post-transfection then cultured for a further four hours on day eight post-transfection in the presence or absence of sterols. HMG-mCherry expression was measured by flow cytometry. The geometric mean fluorescence intensity (gMFI) for each sample is given in the table. Sterol depletion (SD) fold increase was calculated by dividing sterol depleted gMFI by the untreated gMFI. The percent decrease in gMFI with the addition of sterols following sterol depletion was calculated by dividing the difference between sterol depleted gMFI and sterol depleted plus sterols gMFI by the sterol depleted gMFI then multiplying by 100. **(B)** The cells from (A) were lysed and immunoblotted for endogenous HMGCR.

4.3 Discussion

4.3.1 Genome-wide CRISPR knockout screens in non-haploid cells

Previously, I have shown that gene-trap mutagenesis and CRISPR knockout screens generate comparable results in KBM7 cells (Chapter 3). However, it was unknown whether the efficiency of CRISPR-mediated gene disruption might be reduced by the presence of multiple alleles if a CRISPR screen was performed in a non-haploid cell line. The CRISPR screens presented in this chapter were performed in HeLa cells. I have not performed a direct comparison of CRISPR screens in KBM7 cells and HeLa cells, but the presence of multiple alleles does not appear to have hindered the efficacy of CRISPR screens as the screen for cells with increased HMG-mCherry at steady state identified a significant number of hits required to regulate HMGCR expression (**Figure 4.2E**).

It is striking that the steady state HMG-mCherry screen identified components of the p97 complex (**Figure 4.2E**) whereas neither the gene-trap mutagenesis nor CRISPR screen in KBM7 cells identified any p97 complex components (**Figure 3.2C** and **Figure 3.3D**). It is likely that the loss of the p97 complex is lethal to a cell within the timeframe the KBM7 forward genetic screens (21 days). A potential advantage of genome-wide CRISPR knockout screens in non-haploid cells could be the possibility of incomplete gene knockouts where a wild type allele of a gene remains. The single wild type allele might be able to express sufficient protein to maintain cell viability for the duration of the screen but the decreased protein abundance results in a phenotype that can be selected, i.e. haploinsufficiency.

4.3.2 MARCH6 affects HMGCR expression

The genome-wide CRISPR knockout screen for cells with increased HMG-mCherry expression identified the E3 ligase MARCH6 (**Figure 4.2**). At the time Zelcer *et al.* had already shown that MARCH6 depletion rescued HMGCR at steady state, although the role of MARCH6 in the sterol-induced degradation of HMGCR was unclear (Zelcer et al. 2014). My validation of MARCH6 in HMG-mCherry expressing HeLa cells using siRNA-mediated silencing and a MARCH6 knockout clone confirmed an increase in HMGCR expression at steady state in the absence of MARCH6 and I did not observe a requirement for MARCH6 in the sterol-induced

degradation of HMGCR (**Figure 4.3**). My results are consistent with those published by Zelcer et al and a personal communication from Pedro Carvalho (Zelcer et al. 2014).

The Zelcer laboratory later reported that IDOL expression is induced when MARCH6 is depleted in a range of cell types, including those of non-hepatic origin (Loregger et al. 2015). Increased IDOL expression causes a decrease in LDLR protein abundance which results in reduced LDL uptake, thereby lowering the intracellular cholesterol concentration. Therefore SREBP-dependent transcription will be upregulated and HMGCR will be stabilised in the absence of MARCH6, accounting for the steady state phenotype observed by myself and the Brown laboratory (**Figure 4.3**) (Zelcer et al. 2014).

4.3.3 UBE2G2 is essential for the sterol-induced degradation of HMG-mCherry

The ubiquitin E2 conjugating enzyme UBE2G2 has previously been shown to contribute to the sterol-induced ubiquitination of HMGCR (Miao et al. 2010). In this chapter, I used CRISPR-mediated gene disruption to generate UBE2G2 knockout clones from the HMG-mCherry expressing HeLa clonal cell line. I found that the loss of UBE2G2 completely blocked the sterol-induced degradation of HMG-mCherry (**Figure 4.5B**). The UBE2G2 clones had a significantly decreased rate of sterol-induced degradation of endogenous HMGCR, however there was a decrease in HMGCR abundance after a four-hour sterol treatment of sterol depleted cells (**Figure 4.5C**). This decrease could be the result of preventing SREBP-dependent transcription or ERAD mediated by another E2 conjugating enzyme that cannot lead to the sterol-induced degradation of HMG-mCherry.

If the loss of an E2 conjugating enzyme caused a complete block to the sterol-induced degradation of HMG-mCherry, there must be an E3 ligase or a combination of E3 ligases whose loss also causes this phenotype. For a gene to be identified as a hit in a forward genetic screen, the loss of a gene must not be lethal within the timeframe of the screen (typically 18-21 days). Functional redundancy is another barrier to gene identification in forward genetic screens. A gene cannot be identified if the loss of that gene is compensated for by another factor.

Several studies have shown the action of multiple E3 ligases on a single ERAD substrate (Zhang et al. 2015, Younger et al. 2006, Morito et al. 2008). However, none of these studies report a completely redundant system in which no phenotype is observed if only one ligase is depleted. If there are multiple E3 ligases responsible for ubiquitinating HMGCR, the loss of one ligase might not result in an increase in HMG-mCherry at steady state because the other ligase(s) can compensate and maintain low HMG-mCherry expression. I hypothesised that the loss of one of the E3 ligases responsible for the sterol-induced ubiquitination of HMG-mCherry would result in a decreased rate of HMG-mCherry degradation in response to sterols. To test this hypothesis, I performed a second genome-wide CRISPR knockout screen using sterol depletion to enrich mutants with a reduced rate of sterol-induced HMG-mCherry degradation. This second CRISPR screen identified the poorly characterised ERAD E3 ligase RNF145 as a borderline hit (**Figure 4.6**).

4.3.4 Is RNF145 the ubiquitin E3 ligase for HMGCR?

RNF145 was a poorly characterised E3 ligase at the time of its identification in the CRISPR screen. The Lehner laboratory was aware of RNF145 due to its strong homology with TRC8, an ERAD E3 ligase that the Lehner laboratory uncovered (Stagg et al. 2009). TRC8 is also one of the ERAD E3 ligases implicated in HMGCR ERAD by the Debose Boyd laboratory but has been dismissed by the Weissman laboratory (Jo et al. 2011, Tsai et al. 2012).

An shRNA screen had identified RNF145 as a negative regulator of phagocytic oxidative burst in macrophages and demonstrated an ER localisation for RNF145 (Graham et al. 2015). A more recent study profiled 37 potential ERAD E3 ubiquitin ligases, including RNF145 (Kaneko et al. 2016). This study identified RNF145 as a ubiquitously expressed, ER-localised E3 ligase with 12 transmembrane helices and a C-terminal RING domain.

A transcriptomics screen for LXR-regulated genes has recently identified RNF145 (Cook et al. 2017). This study used the Constrained Consensus TOPology prediction server to predict 14 transmembrane helices and a C-terminal cytoplasmic RING domain. It is also suggested that the first six transmembrane helices constitute a putative sterol sensing domain. They also reported the presence of the YLYF motif that I observed in the second predicted transmembrane helix, suggesting RNF145 could interact with the Insigs (Sever, Song, et al.

2003, Yang et al. 2002). An ER localisation for RNF145 was confirmed and E3 ligase activity was confirmed in an *in vitro* autoubiquitination assay (Cook et al. 2017). Taken together these studies provide evidence for RNF145 as an ERAD E3 ligase and make RNF145 a very promising candidate gene for the E3 ligase for HMGCR.

The validation experiment of RNF145 in the HMG-mCherry HeLa clone showed a decrease in the sterol-induced degradation of HMG-mCherry in the absence of RNF145 (**Figure 4.7A**). This partial phenotype supports the model in which multiple E3 ligases are involved in HMGCR ERAD. Although, an indirect effect cannot be ruled out at this stage, the absence of a notable difference in the sterol-induced degradation of endogenous HMGCR in cells depleted of RNF145 might be too small a difference to be resolved by immunoblot.

The genome-wide CRISPR knockout screen using sterol depletion did not identify many high-confidence hits. This is probably due to the low enrichment of mutants with a reduced rate of sterol-induced HMGCR degradation (**Figure 4.6C**). The failure to achieve a significant enrichment is likely the result of the small assay window as there is considerable overlap on a FACS plot between the HMG-mCherry clone after sterol depletion and after a five-hour culture with sterols. It is significantly easier to enrich a population in a fluorescence-based forward genetic screen if the desired mutants form a distinct population compared with the starting cell line (i.e. a wide dynamic range).

Consequently, the next aim of my thesis project was to create a more sensitive system with a wider dynamic range to perform a genome-wide CRISPR knockout screen to identify the ubiquitin E3 ligases responsible for the sterol-induced degradation of HMGCR.

4.4 Summary

Genome-wide CRISPR knockout screens are a powerful approach to identify genes required for HMGCR regulation. I performed two genome-wide CRISPR knockout screens using a fluorescently tagged HMGCR reporter. The first screen selected cells with an increase in HMG-mCherry expression at steady state whereas the second screen used sterol depletion to select cells with a reduced rate of sterol-induced HMG-mCherry degradation. The second CRISPR screen identified a poorly characterised ERAD E3 ubiquitin ligase, RNF145. I validated the involvement of RNF145 in the sterol-induced degradation of HMG-mCherry, however I could not detect a requirement for RNF145 in the sterol-induced degradation of endogenous HMGCR.

Chapter 5: Genome-wide CRISPR knockout screens using fluorescently-tagged endogenous HMGCR identify RNF145

5.1 Introduction

The aim of my thesis project is to identify the E3 ubiquitin ligase(s) responsible for HMGCR ERAD. The genome-wide CRISPR knockout screens described in Chapter 4 identified a role for RNF145, a poorly characterised E3 ligase, in the sterol-induced degradation of an ectopic, fluorescently-tagged HMGCR reporter.

The genome-wide CRISPR screens discussed in Chapter 4 showed two major limitations: firstly, the low enrichment of mutants with a reduced rate of sterol-induced HMG-mCherry degradation, most likely caused by a modest difference in fluorescence following sterol depletion. Secondly, the small difference in sterol-induced degradation of HMG-mCherry and endogenous HMGCR in the absence of UBE2G2 suggested that HMG-mCherry was not targeted for ERAD by all the ERAD machinery that endogenous HMGCR is.

In the previous chapters I have used CRISPR-mediated gene disruption to knockout genes to analyse a phenotype caused by their absence. CRISPR/Cas9 genome editing technology can also be used to insert desired sequences into the genome. If an oligonucleotide template is provided, the Cas9-mediated DNA double strand break can be repaired accurately by homologous recombination instead of NHEJ (Hsu, Lander, and Zhang 2014). Due to the aforementioned shortcomings of the screens based on HMG-mCHerry overexpression, I sought to create a knock-in cell line in which endogenous HMGCR was tagged with a fluorescent protein. I hypothesised that SREBP-dependent transcription would increase the fluorescent window between sterol depleted and sterol repleted cells, increasing the probability of enriching a population of mutants that cannot degrade HMGCR efficiently in response to sterols in a forward genetic screen. Analysing the endogenous protein expression

would also remove the concern that the HMG-mCherry protein was not targeted by all the ERAD machinery that mediate the ubiquitination of endogenous HMGCR.

5.2 Results

5.2.1 Using CRISPR/Cas9 technology to tag endogenous HMGCR

To create a HMGCR knock-in cell line, I transfected HeLa cells with Cas9, a gRNA targeting immediately downstream of the HMGCR stop codon and a donor template encoding Clover, an enhanced GFP variant (**Figure 5.1A**). The donor template consists of two arms that are homologous to the one kilobase genomic DNA sequence on either side of the HMGCR stop codon (**Figure 5.1B**). The sequence between the homologous arms will be incorporated into the genome when the template is used in homologous recombination to repair the CRISPR/Cas9-induced double strand break. The sequence to be inserted contained a myc-tag and Clover sequence that would form a HMGCR-myc-Clover endogenous fusion protein, as well as a drug resistance gene with an exogenous promoter flanked by loxP sites (**Figure 5.1B**). I simultaneously transfected HeLa cells with three different donor templates, each encoding a different drug resistance marker enabling selection of cells that had incorporated the template into multiple alleles. The resulting population of drug-resistant cells was then transfected with Cre-recombinase to remove the resistance cassette. The Cre-recombinase plasmid expressed mCherry so that I could select transfected cells by FACS. Single cell clones were isolated and the loss of the resistance cassette was confirmed by loss of cell viability when cultured in selection medium.

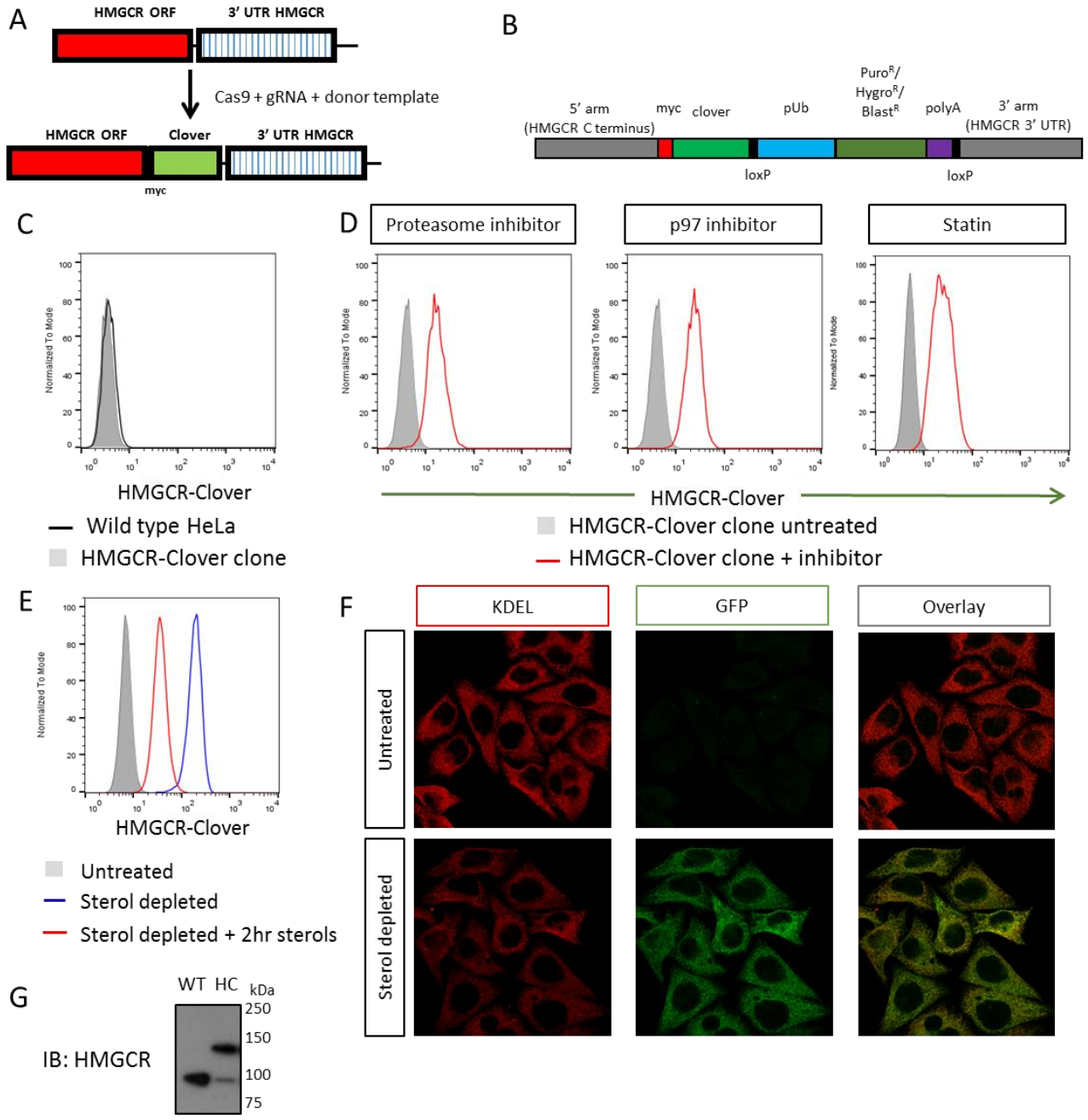

Figure 5.1 Using CRISPR/Cas9 to tag endogenous HMGCR with Clover. (A) Schematic illustrating the production of a knock-in. HeLa cells are transiently transfected with Cas9, a gRNA and a donor template. (ORF, open reading frame; UTR, untranslated region). **(B)** Schematic of the donor template used to create HMGCR-Clover knock-in. Three donor templates were used. Each encoded a resistance gene for puromycin, hygromycin or blasticidin. **(C)** HMG-Clover expression could not be detected in an untreated HMGCR-Clover clone by flow cytometry. **(D)** HMGCR-Clover HeLa cells were treated overnight with 25nM Bortezomib, overnight with 10µM mevastatin or for 8 hours with 10µM NMS-873 (a p97 inhibitor). **(E)** HMGCR-Clover HeLa cells were sterol depleted overnight then cultured for a further 2 hours in the presence or absence of sterols. HMG-Clover expression was measured by flow cytometry to show appropriate sterol dependent regulation of HMGCR-Clover. **(F)** HMGCR-Clover was induced by overnight sterol depletion. HMGCR-Clover co-localised with the KDEL marker in the ER as assessed by immunofluorescence (Dick van den Boomen). **(G)** Immunoblot analysis of sterol depleted wild type HeLa cells (WT) and the HMGCR-Clover (HC) clone shows the higher molecular weight HMGCR-Clover protein.

5.2.2 Chemical inhibitors and sterols correctly modulate HMGCR-Clover expression

A HMGCR-Clover single-cell clone was selected for characterisation. The HMGCR-Clover clone was indistinguishable from wild type HeLa cells by flow cytometry, demonstrating the low level of HMGCR expression at steady state when grown in tissue culture medium (**Figure 5.1C**). Chemical inhibitors were then used to show that HMGCR-Clover was constitutively degraded by the proteasome in a p97-dependent manner (**Figure 5.1D**). Inhibiting HMGCR, and therefore cholesterol biosynthesis, with overnight statin (mevastatin) treatment also lead to the stabilisation of HMGCR-Clover (**Figure 5.1D**). Treating wild type HeLa cells with these inhibitors did not cause any change in fluorescence.

It was critical to ensure that sterols correctly regulated HMGCR-Clover expression. A 25-fold increase in HMGCR-Clover was detected by flow cytometry after overnight sterol depletion (grey to red in **Figure 5.1E**) because of increased SREBP-induced transcription and decreased sterol-induced degradation. Adding sterols into the sterol depleted culture caused the rapid degradation of HMGCR-Clover (80% decrease in 2 hr), demonstrating appropriate sterol-dependent regulation of HMGCR-Clover (red to blue in **Figure 5.1E**). Immunofluorescence was used to confirm an ER-localisation for HMGCR-Clover to ensure that the addition of Clover to the C-terminus had not disrupted HMGCR localisation (**Figure 5.1F**). Immunoblot analysis of sterol depleted HMGCR-Clover cells and wild type HeLa cells showed a higher molecular weight band (below 150 kDa) corresponding to the HMGCR-Clover fusion protein (**Figure 5.1G**). The HMGCR-Clover cells also contained a (approximately 100 kDa) band corresponding to wild type HMGCR protein indicating that an allele remained untagged. This was fortunate as it allows me to determine whether an enrichment of HMGCR-Clover in a forward genetic screen reflected an enrichment of wild type HMGCR. The locus was also sequenced to confirm the correct DNA sequence of HMGCR-Clover and the integrity of the wild type allele.

5.2.3 Genetic validation of the HMGCR-Clover clone

To confirm that the HMGCR-Clover cell line was an appropriate tool to use in a forward genetic screen, I sought to validate the positive controls for the screen. UBE2G2 has previously been reported to be the E2 conjugating enzyme for the sterol-induced degradation of HMGCR (Miao et al. 2010). I first used three independent UBE2G2-targeting gRNAs to knockout UBE2G2 by CRISPR-mediated gene disruption. In each case, I observed a significant rescue of HMGCR at steady state (grey to green in **Figure 5.2A**) suggesting that the basal turnover of HMGCR was impaired. I also observed a significant block in the sterol-induced degradation of HMGCR-Clover (blue to red in **Figure 5.2A**). The loss of UBE2G2 did not result in a complete block in HMGCR-Clover degradation, which is addressed in Chapter 7.

Additionally, pools of four gRNAs were employed to knockout Insig1, Insig2 or both Insig1 and Insig2 by CRISPR-mediated gene disruption. Insig proteins retain the SCAP-SREBP complex in the ER in the presence of sterols and recruit an E3 ubiquitin ligase complex to HMGCR in response to sterols (Yabe, Brown, and Goldstein 2002, Yang et al. 2002, Sever, Song, et al. 2003). The loss of either Insig caused a small rescue of HMGCR-Clover at steady state (row 1 **Figure 5.2B**). However, the concomitant loss of both Insigs caused an almost complete rescue of HMGCR-Clover expression at steady state to the same level as seen following sterol depletion. The loss of both Insigs and sterol depletion show a similar phenotype as in both cases the SREBP-SCAP complex is not retained in the ER, leading to constitutive SREBP-mediated transcription of HMGCR-Clover irrespective of the sterol environment. The steady state phenotypes demonstrate the functional redundancy between the Insigs.

Adding sterols into a sterol-depleted culture in the absence of Insig1 revealed a significant defect in sterol-induced HMGCR-Clover degradation. In contrast, only a very small decrease in sterol-induced HMGCR-Clover degradation was observed in the absence of Insig2 (**Figure 5.2B**). Therefore, Insig1 is dominant over Insig2 in this system. These non-redundant phenotypes suggest the Insig proteins act in different pathways, for example with different components. Adding sterols to cells deficient of both Insigs did not decrease HMGCR-Clover expression because HMGCR-Clover could not be targeted for degradation.

HMGCR-Clover is regulated appropriately by UBE2G2 and the Insig proteins. The HMGCR-Clover cell line is therefore an appropriate tool to use in forward genetic screens.

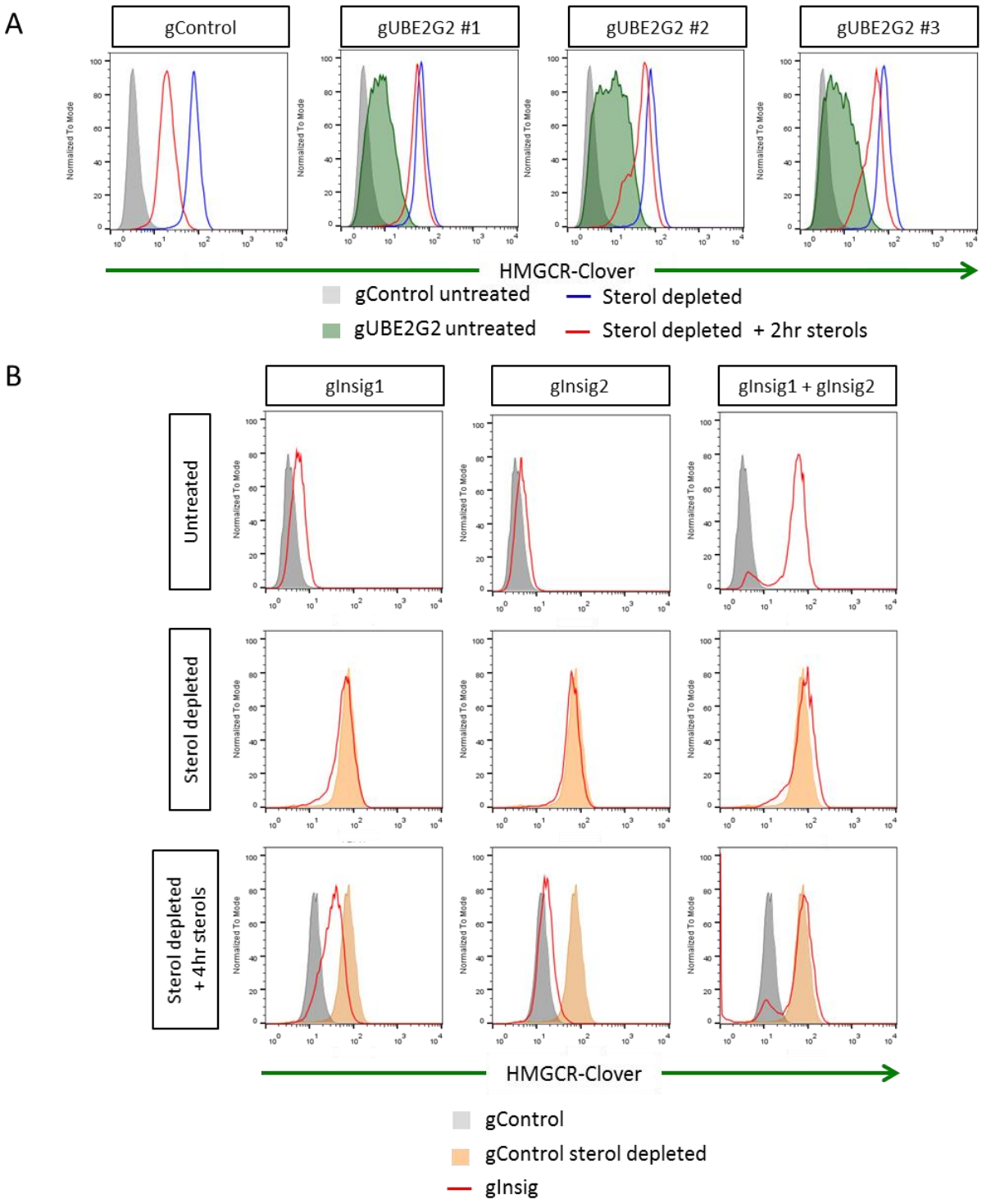

Figure 5.2 HMGCR-Clover expression is regulated correctly by UBE2G2 and Insigs. (A) The HMGCR-Clover HeLa clone was transiently transfected with Cas9 and a UBE2G2-targeting or a control gRNA. Transfected cells were selected by puromycin treatment. Sterol induced degradation of HMGCR-Clover was assessed ten days post-transfection by sterol depleting cells overnight followed by a two-hour culture in the presence or absence of sterols. **(B)** The HMGCR-Clover HeLa clone was transiently transfected with Cas9 and either a control gRNA, a pool of 4 gRNAs targeting Insig1, a pool of 4 gRNAs targeting Insig2, or a pool of 8 gRNAs with 4 gRNAs targeting each Insig. Transfected cells were selected with puromycin treatment. Sterol induced degradation of HMGCR-Clover was assessed 8 days post-transfection by sterol depletion followed by a further four-hour culture in the presence or absence of sterols. Representative of three independent experiments.

5.2.4 Genome-wide CRISPR knockout screen for increased HMGCR-Clover expression at steady state

The first genome-wide CRISPR knockout screen performed in the HMGCR-Clover clone selected cells with increased HMGCR-Clover expression at steady state. The HMGCR-Clover clone was transduced with Cas9 nuclease as described in previous chapters. The library used in this screen was a kind gift from Michael Bassik (Stanford University). This library contains a total of 211,695 gRNAs, with 10 gRNAs targeting 19,930 genes and 12,395 control gRNAs (Morgens et al. 2017).

The Cas9-expressing HMGCR-Clover clone was transduced with the Bassik library at an M.O.I of 0.3. HMGCR-Clover^{high} cells were selected by two sequential rounds of FACS. The resultant population contained a significant enrichment of HMGCR-Clover^{high} cells across a wide range of HMGCR-Clover expression levels, suggesting that multiple cellular pathways had been disrupted (**Figure 5.3A**). Despite the increased level of HMGCR-Clover expression at steady state, the majority of the enriched population did not appear to have a significant defect in the sterol-induced degradation of HMGCR-Clover (**Figure 5.3B**). Immunoblot analysis of the cells in Figure 5.3B showed that, at steady state, the expression of the wild type HMGCR allele (~100 kDa band in **Figure 5.3C**) in the enriched population was increased demonstrating that the enrichment of HMGCR-Clover was due to the loss of genes required to regulate HMGCR expression (**Figure 5.3C**). The wild type HMGCR allele in the enriched population did not demonstrate decreased sterol-induced degradation.

The abundance of gRNAs in the enriched population was compared to an unselected library as described in Chapter 3. The RSA algorithm showed that the screen successfully identified many candidate genes (**Figure 5.3D**). The screen identified the positive control *UBE2G2* but neither of the Insig proteins suggesting that, despite the large number of candidate genes identified, the screen was not saturating.

The significant hits (**Figure 5.3D**) can be separated into two functional groups:

Cholesterol biosynthesis

The screen identified many genes that encode enzymes in the cholesterol biosynthesis pathway (yellow in **Figure 5.3D**). The loss of these genes will block the production of

cholesterol (like statin treatment in Figure 5.1D) leading to a decrease in intracellular cholesterol and therefore increased SREBP-dependent transcription and the stabilisation of HMGCR.

Cholesterol import

The LDLR and the Niemann-Pick genes (*NPC1* and *NPC2*) are required for cholesterol import (Brown and Goldstein 1986, Infante et al. 2008, Kwon et al. 2009). A large suite of genes was also identified that encode proteins involved in the endo-lysosome pathway. The vacuolar ATPase (components *ATPV1B2* and *ATP6V1A* were identified) is required for endosomal acidification along the endo-lysosome pathway as well as the activity of lysosomal hydrolases (Maxson and Grinstein 2014). Acidification of endosomes is required for LDL release from LDLR (Rudenko et al. 2002). The *GNPTAB* gene encodes N-acetylglucosamine-1-phospotransferase subunits alpha and beta, an enzyme required for the formation of mannose 6-phosphate (M6P) on mannose glycans in the Golgi, the marker that targets lysosomal hydrolases to the lysosome (Braulke and Bonifacino 2009, Qian et al. 2010). Lysosomal hydrolases release cholesterol esters from LDL that has been imported via the LDLR pathway (Brown and Goldstein 1986). Therefore, the loss of GNPTAB will block cholesterol uptake by preventing the release of cholesterol esters from LDL particles. Other hits such as *ARF6* and members of the GARP complex (*VPS54, VPS52, VPs45, VPS53, VPS51*) are required for a functional endo-lysosomal pathway (Schweitzer, Sedgwick, and D'Souza-Schorey 2011, Fröhlich et al. 2015, Wei et al. 2017). The loss of a gene that inhibits cholesterol uptake via the LDLR and the endo-lysosomal pathway will lead to a decrease in intracellular cholesterol concentration that will in turn activate SREBP-dependent transcription and promote the stabilisation of HMGCR.

The screen also identified two uncharacterised genes (*c18orf8* and *c19ord25*). Secondary structure and domain prediction algorithms did not identify any features reminiscent of E3 ligases and so they were not pursued as a part of this thesis project.

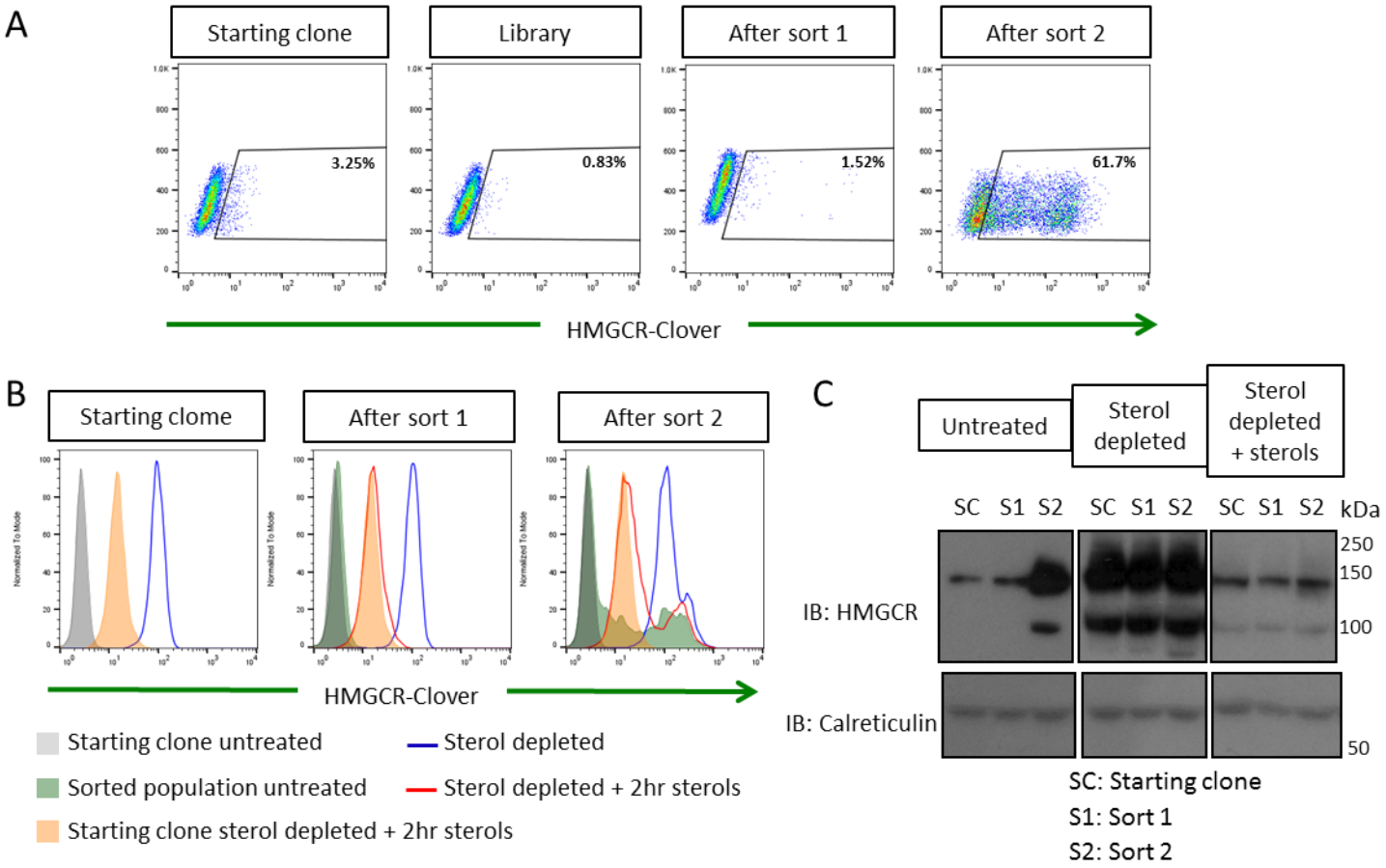

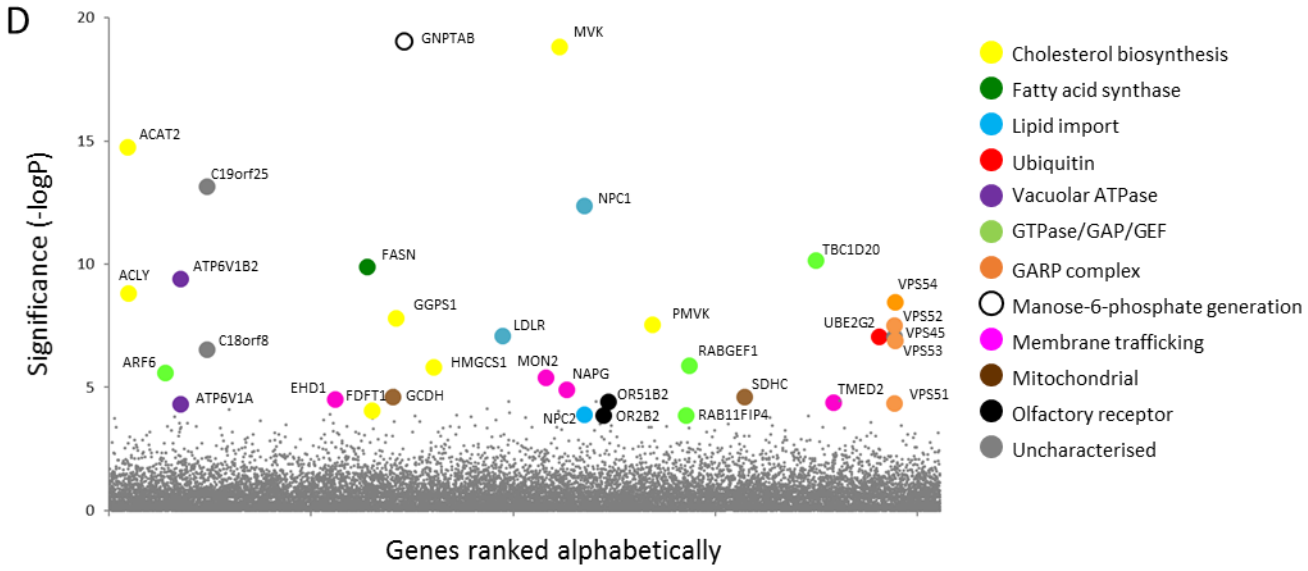

Figure 5.3 A genome-wide CRISPR knockout screen in the HMGCR-Clover knock-in clone to identify the E3 ubiquitin ligase for HMGCR. (A) The Cas9-expressing HMGCR-Clover clone was transduced with the Bassik gRNA library. HMGCR-Clover^{high} mutants were enriched by two rounds of FACS. **(B)** The sterol induced degradation of HMGCR-Clover was assessed in the selected cells by overnight sterol depletion followed by a two-hour culture in the presence or absence of sterols. **(C)** Cells from (B) were lysed and immunoblotted for HMGCR (SC, starting clone; S1, sort 1; S2, sort 2). **(D)** Candidate genes were identified using the RSA algorithm (König et al. 2007).

5.2.5 CRISPR validation of HMGCR-Clover steady state screen hits

I selected five hits from the HMGCR-Clover steady state screen for CRISPR validation alongside Insig1, a false-negative in the CRISPR screen. In each case, I observed an increase in HMGCR-Clover expression following CRISPR-mediated gene disruption (**Figure 5.4**). The increase in HMGCR-Clover expression seen here is small compared to the level of expression seen in the HMGCR-Clover^{high} cells enriched in the CRISPR screen (**Figure 5.3B**). It should be noted that the enriched cells in the screen were analysed by flow cytometry 20 days after gRNA library transduction, whereas the cells were analysed in the validation experiment (**Figure 5.**4) 7 days after gRNA transfection. It is possible that the level of HMGCR-Clover could increase if the validation experiment was continued beyond seven days. A higher HMGCR-Clover expression level might also be caused by the loss of a gene that was not selected for validation, i.e. a component of the cholesterol biosynthesis pathway.

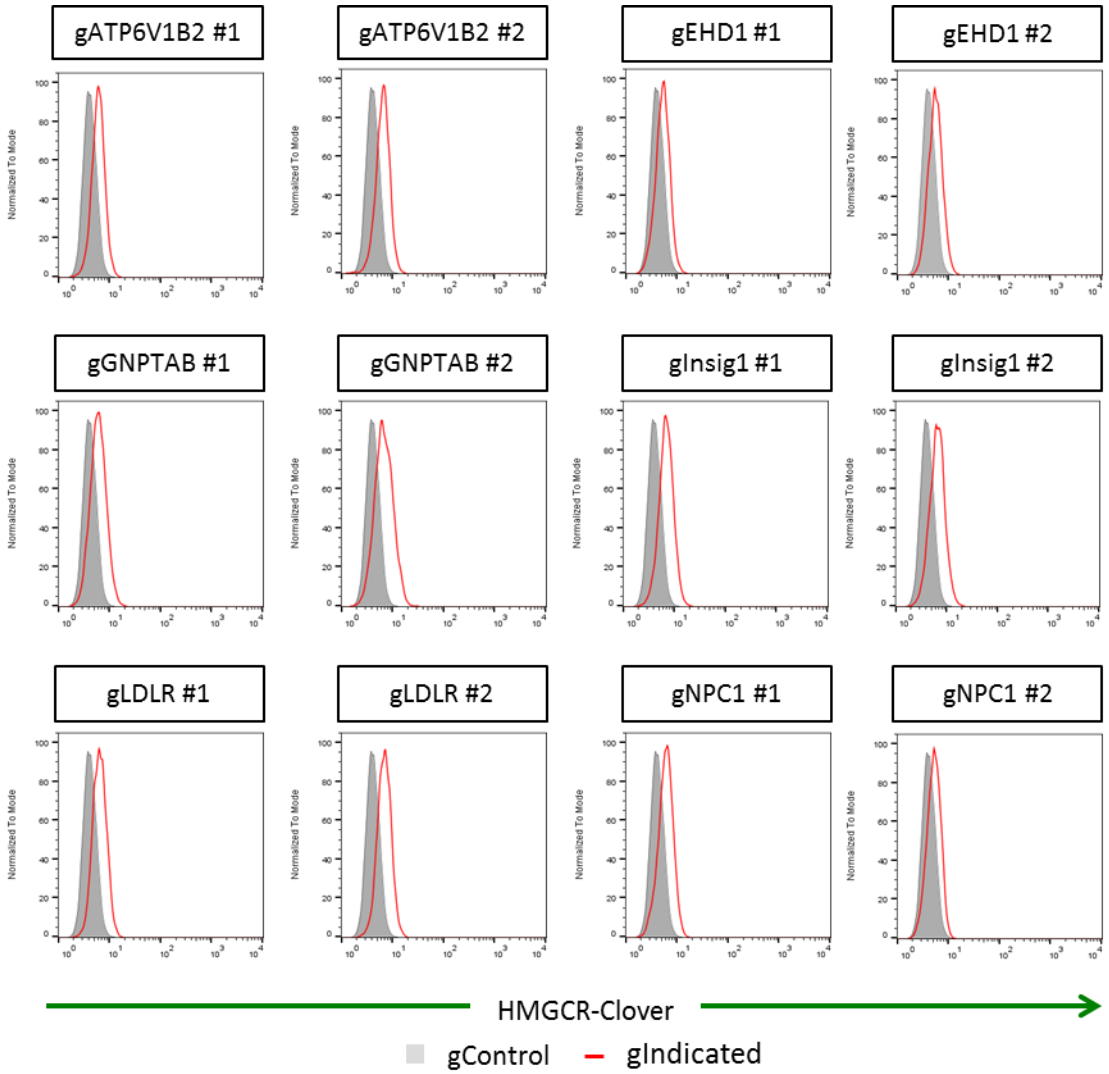

Figure 5.4 Validation of candidate genes identified in steady state HMGCR-Clover genome-wide CRISPR knockout screen. The HMGCR-Clover HeLa clone was transiently transfected with Cas9 and a candidate gene-targeting gRNA or control gRNA. Transfected cells were selected with puromycin treatment. HMGCR-Clover expression was measured by flow cytometry 7 days post-transfection.

5.2.6 A genome-wide CRISPR knockout screen using sterol depletion in the HMGCR-Clover clone identified RNF145

Despite identifying a large suite of genes in the steady state HMGCR-Clover screen, the only hit reported to be involved in ERAD was UBE2G2. To identify genes required for HMGCR degradation, I re-focussed my screen and performed a second genome-wide CRISPR knockout screen using the HMGCR-Clover cell line. In this second screen, I took advantage of the significant increase in HMGCR-Clover expression induced by sterol depletion due to SREBP driven transcription and stabilisation of HMGR-Clover protein. I then added sterols into the sterol depleted culture and selected cells by FACS with a decreased rate of HMGCR degradation (**Figure 5.5A**). I found that a five-hour incubation with sterols following overnight sterol depletion provided the maximum decrease in HMGCR-Clover (**Figure 5.5B**). The difference in HMGCR-Clover expression between sterol depleted and sterol replete incubation is significantly larger than that in the ectopic HMG-mCherry HeLa cell line used in Chapter 4. This should enable the enrichment of mutant cells that have a decreased rate of sterol-induced HMGCR degradation.

The Cas9-expressing HMGCR-Clover clone was transduced at a M.O.I. of 0.3 with the Bassik gRNA library. The mutagenised cells were sterol depleted overnight and sterols were added back into the culture for five hours the following day. Rare mutant cells with a reduced ability to degrade HMGCR-Clover were selected by two sequential rounds of FACS using the strategy illustrated in **Figure 5.5A**. The resultant population only contained a small population of cells with an increased steady state level of HMGCR-Clover expression (green in **Figure 5.5C**). However, when compared to the starting clone, the majority of the cells in the selected population had a reduced ability to degrade HMGCR-Clover in response to sterols following sterol depletion (comparing red to orange **Figure 5.5C**). The width of the red histogram in Figure 5.5C indicates that the enriched population contains a variety of mutants with different abilities to degrade HMGCR-Clover. Immunoblot analysis of cells shown in Figure 5.5C confirmed that the selected cells also had a decreased ability to degrade wild type HMGCR in response to sterols following sterol depletion (compare S2 to SC in right panel of **Figure 5.5D**). Together, the flow cytometry and immunoblot analysis demonstrate that I have now performed a forward genetic screen that has enriched a population of mutants showing significantly inhibited sterol-induced HMGCR degradation.

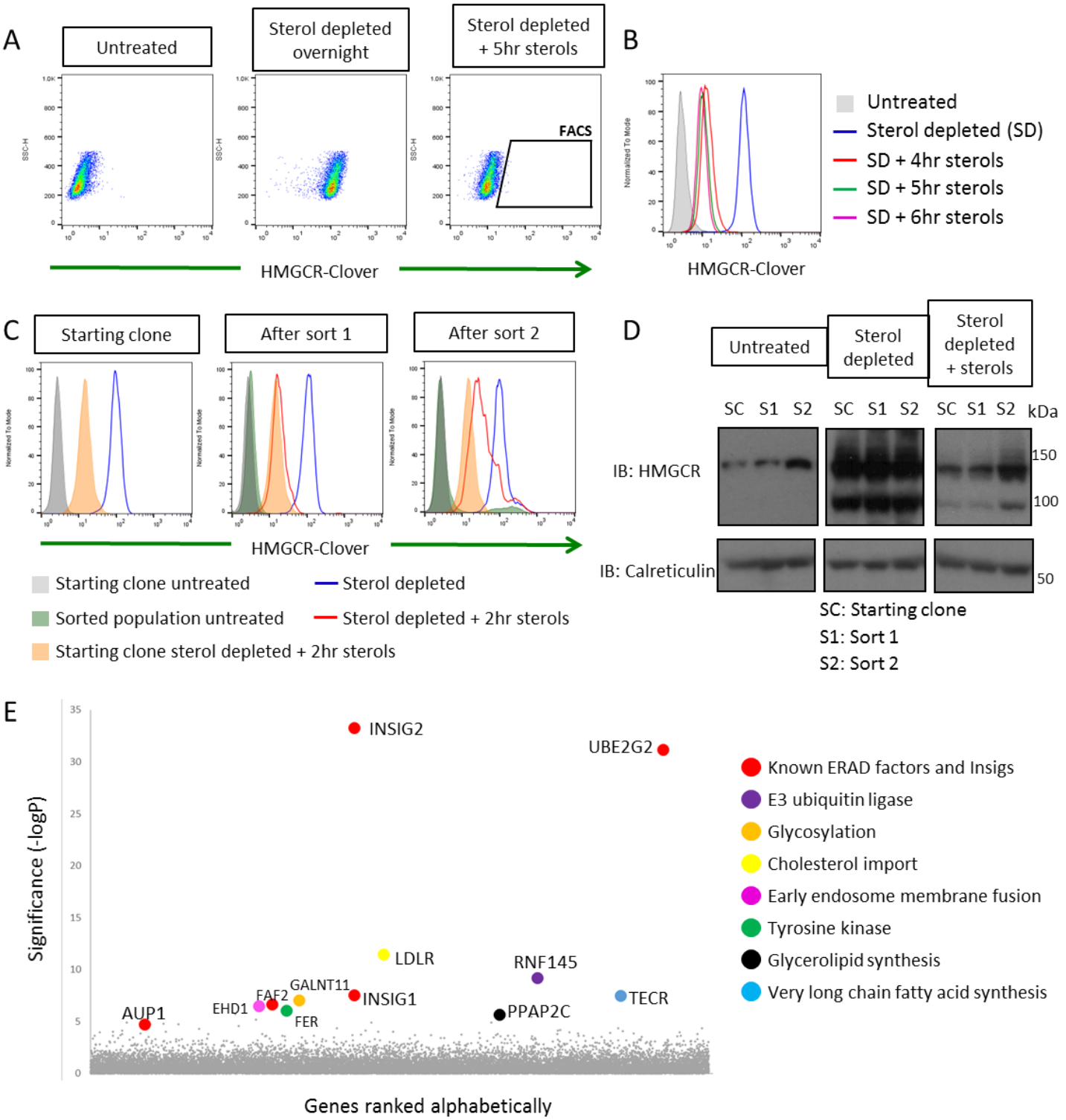

Figure 5.5 A genome-wide CRISPR knockout screen in the HMGCR-Clover knock-in clone using sterol depletion to identifies RNF145 (A) FACS strategy to select mutants with a decreased ability to degrade HMGCR-Clover in response to sterols. **(B)** A five-hour culture provides the maximum window for the sterol induced degradation of HMGCR-Clover. HMGCR-Clover cells were sterol depleted overnight followed by the presence or absence of sterols for the indicated time. **(C)** The selected cells from the screen showed a reduced rate of sterol induced HMGCR-Clover degradation. Cells were sterol depleted overnight then cultured in the presence or absence of sterols for a further two hours. **(D)** Cells from (C) were lysed and immunoblotted for HMGCR (SC: starting clone, S1: sort 1, S2: sort 2). **(E)** Candidate genes were identified using the RSA algorithm (König et al. 2007)

I quantified the gRNA abundance in the selected cells and an unselected library using the Illumina HiSeq platform. The RSA algorithm identified a focussed suite of genes required for the sterol-induced degradation of HMGCR (**Figure 5.5E**) (König et al. 2007). The screen identified *UBE2G2*, as well as its accessory factor *AUP1* which is thought to recruit UBE2G2 to membrane E3 ubiquitin ligases (Klemm, Spooner, and Ploegh 2011, Jo, Hartman, and DeBose-Boyd 2013). Both Insig proteins were also identified, which are known to be required for the sterol-induced degradation of HMGCR (as demonstrated in **Figure 5.2B**) (Yabe, Brown, and Goldstein 2002, Yang et al. 2002, Sever, Song, et al. 2003). Strikingly, the screen identified RNF145, the same E3 ubiquitin ligase identified in the sterol depletion ectopic HMG-mCherry screen (**Figure 4.6E**).

Trans-2,3-enoyl CoA reductase (TECR) catalyses the final steps in the synthesis of very long-chain fatty acids (Moon and Horton 2003). The accumulation of long-chain fatty acid intermediates in the absence of TECR could disrupt the signal inducing the degradation of HMGCR-Clover. Polypeptide N-acetylgalctosaminyltransferase 11 (*GALNT11*) is a hit in both CRISPR screens that used sterol depletion (**Figure 4.6E** and **Figure 5.5E**). GALNT11 initiates protein O-linked glycosylation, suggesting that a protein involved in the degradation of HMGCR requires O-linked glycosylation (Schwientek et al. 2002).

I was surprised to identify the LDLR in this screen. The medium used for sterol depletion contains serum that has been depleted of lipoprotein, so the cholesterol and 25-hydroxycholesterol added after sterol depletion should not be taken up via the LDLR pathway. EH domain-containing protein 1 (*EHD1*) is a hit in all four HMGCR CRISPR screens. EHD1 is required for the internalisation and recycling of several plasma membrane receptors, including the LDLR (Naslavsky et al. 2007, Naslavsky and Caplan 2011). No other genes required for cholesterol up-take or the LDLR pathway were identified by the screen.

5.2.7 The loss of RNF145 causes a small decrease in the sterol-induced degradation of HMGCR-Clover

CRISPR-mediated gene disruption was used to validate additional hits from the genome-wide CRISPR knockout screen that used sterol depletion. The loss of EHD1 and LDLR resulted in a small decrease in the sterol-induced degradation of HMGCR-Clover, suggesting that there is a small amount of residual lipoprotein in the medium (**Figure 5.6A**). However, the loss of NPC1, which was not a hit, did not affect the sterol-induced degradation of HMGCR-Clover, despite the rescue of HMGCR-Clover at steady state indicating the loss of NPC1. Taken together, this suggests that the LDLR can influence cholesterol homeostasis independent of the Niemann-Pick proteins.

The loss of TECR following CRISPR-mediated gene disruption resulted in an increase in HMGCR-Clover expression at steady state and inhibited the sterol-induced degradation of HMGCR-Clover (**Figure 5.6A**). I did not determine the efficiency of CRISPR-mediated gene disruption of GALNT11, I therefore cannot conclude from this data that GALNT11 is a false positive of the sterol depletion CRISPR screens.

Throughout my thesis project, I consistently observed a pronounced block in the sterol-induced degradation of HMGCR in the absence of UBE2G2. The phenotype at steady state in the absence of UBE2G2 is less consistent. The loss of UBE2G2 predominantly caused an increase in HMGCR-Clover expression, however Figure 5.6A shows an instance when this did not occur. This is most likely because transcription also controls the steady state expression of HMGCR-Clover.

I previously identified RNF145 in a genome-wide CRISPR screen for factors required for the sterol-induced degradation of a fluorescently-tagged ectopic HMGCR reporter (**Figure 4.6E**). CRISPR-mediated gene disruption of RNF145 caused a small decrease in the sterol-induced degradation of HMG-mCherry, but I did not detect a convincing effect on endogenous HMGCR (**Figure 4.7**). The only E3 ligase identified in my genome-wide CRISPR knockout screen using an endogenous HMGCR-Clover knock-in was RNF145 (**Figure 5.5E**). I therefore used CRISPR-mediated gene disruption to validate a requirement of RNF145 in the sterol-induced degradation of HMGCR-Clover. To knockout RNF145, four independent gRNAs targeting RNF145 were used individually or as a pool. In each case I observed no difference to control

cells at steady state or following sterol depletion (top and middle rows **Figure 5.6B**). However, there was a small but highly reproducible decrease in the sterol-induced degradation of HMGCR-Clover in the absence of RNF145 (bottom row **Figure 5.6B**). In comparison, the loss of Insig1 resulted in a significant decrease in the sterol-induced degradation of HMGCR-Clover (**Figure 5.6B**). Whilst it was encouraging to see a decrease in the sterol-induced degradation of endogenous HMGCR in the absence of RNF145, this difference might be too small to detect by immunoblot and explain why I did not detect a pronounced difference in the sterol-induced degradation of wild type HMGCR in Figure 4.7E.

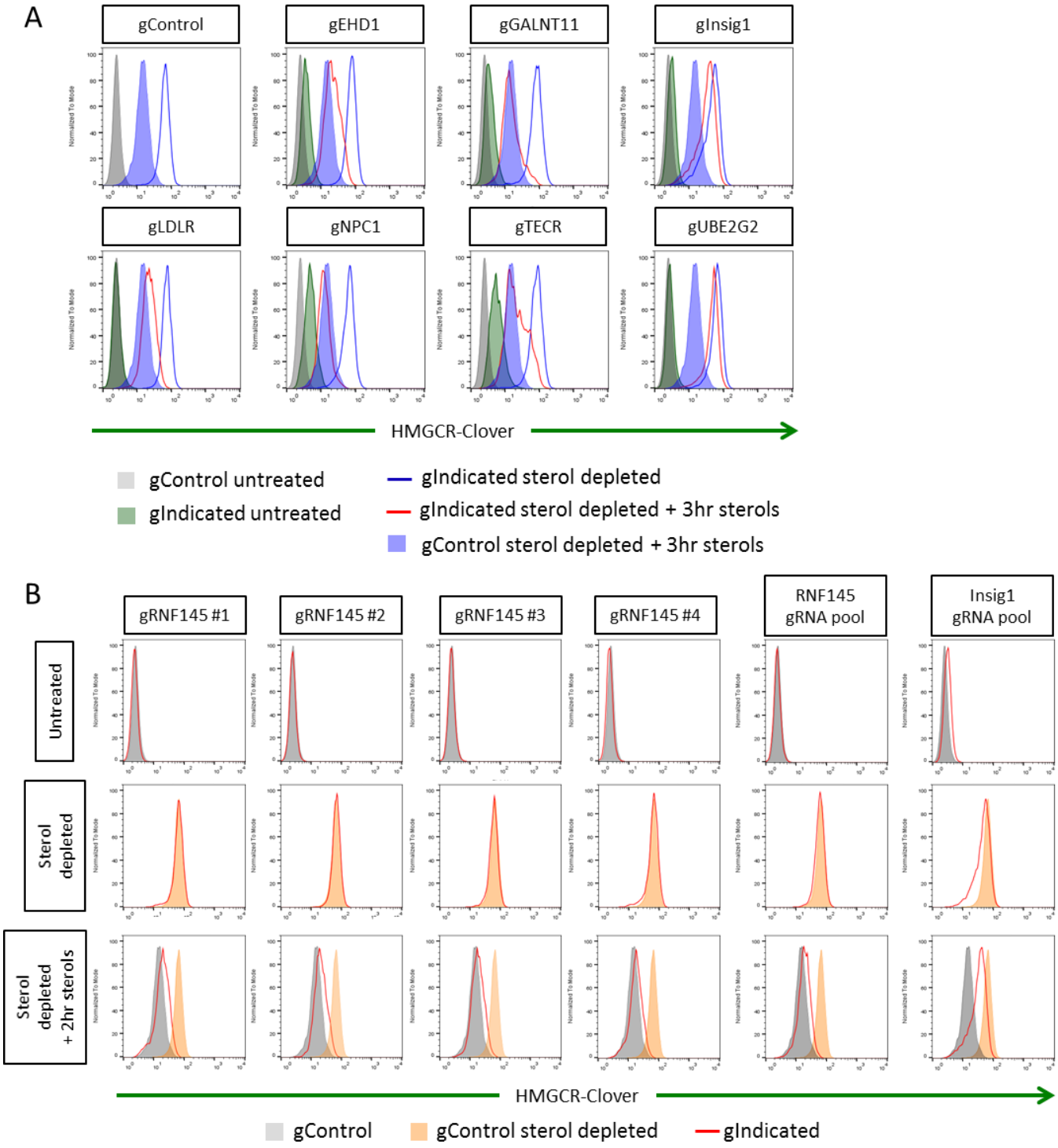

Figure 5.6 Loss of RNF145 causes a small decrease in the sterol-induced degradation of HMGCR-Clover. (A) HMGCR-Clover cells were transiently transfected with Cas9 and either a control gRNA or a pool of four gRNAs targeting the indicated gene. Transfected cells were selected with puromycin treatment. The sterol-induced degradation of HMGCR-Clover was assessed nine days post-transfection. Cells were sterol depleted overnight eight days post-transfection and cultured for a further two hours in the presence or absence of sterols on day nine post-transfection. **(B)** HMGCR-Clover cells were transiently transfected with Cas9 and a control gRNA, an RNF145-targeting gRNA, a pool of four RNF145-targeting gRNAs or a pool of four Insig1-targeting gRNAs. The sterol induced degradation of HMGCR-Clover was assess nine days post-transfection as described in (A). (B) is representative of more than three independent experiments.

5.2.8 RNF145 knockout HeLa clones do not exhibit decreased sterol-induced HMGCR degradation

I next generated RNF145 knockout clones derived from wild type HeLa cells to assess whether RNF145 influences the sterol-induced degradation of wild type endogenous HMGCR. Wild type HeLa cells were transfected with Cas9 and an RNF145-targetting gRNA, transfected cells were selected with puromycin and single cells isolated by serial dilution. At the time, antibodies against RNF145 were not commercially available. Therefore, clones were screened for CRISPR/Cas9-induced frameshift insertion or deletion mutations by genomic PCR across the gRNA target site using fluorescent primers. The size of the fluorescent PCR product was determined, to single base pair resolution, using an ABI 3730xl DNA Analyser (**Figure 5.7A**). The size of the PCR product across gRNA #8's target site was 325bp. Clones were identified that did not have insertions or deletions of multiples of three base pairs. A representative example is given in Figure 5.7A, clone #20 from the gRNA #8 transfection has a single peak on the fluorescent trace at 314bp indicating that all alleles in clone #20 have an 11bp deletion. The PCR products were TOPO-cloned and frameshift insertion or deletions were confirmed by Sanger DNA sequencing (**Figure 5.7A**). When, an antibody against RNF145 became available, the loss of RNF145 protein in the selected clones was confirmed by immunoblot (**Figure 5.7B**). The RNF145 band is indicated above 50 kDa, below the background band.

To further investigate the involvement of RNF145 in HMGCR degradation, I chose two RNF145 knockout clones derived from gRNA #5 (5_7 and 5_26) and two more derived from gRNA #8 (8_8 and 8_20). I observed no difference in the sterol-induced degradation of HMGCR in these RNF145 knockout clones with a four-hour sterol treatment following sterol depletion (**Figure 5.7C**). I also carried out a time-course experiment to see if the clones had a decreased rate of HMGCR degradation in response to sterols over a shorter period (**Figure 5.7D**). Clone 5_7 shows a small difference after a three-hour incubation with sterols, however no difference was observed between wild type HeLa cells and the RNF145 knockout clones at other time points, as was further confirmed by clone 8_20 (**Figure 5.7D**). These findings do not support a requirement for RNF145 in the sterol-induced degradation of wild type endogenous HMGCR. A possible explanation for this discrepancy could be that the minor effect seen on HMGCR-Clover was insufficient to be detected by immunoblot and is followed in Chapter 6.

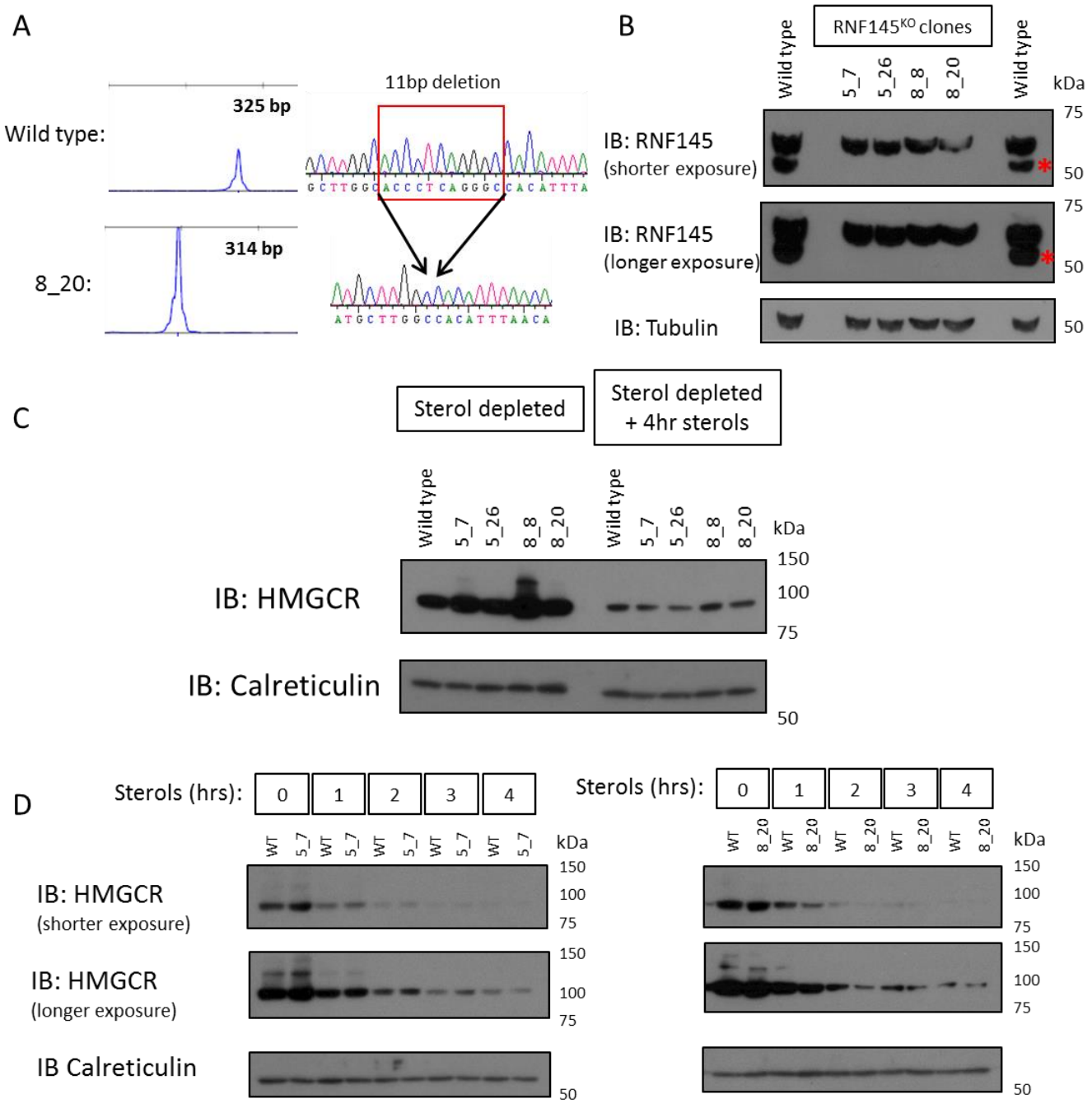

Figure 5.7 RNF145 knockout HeLa clones do not have a decreased rate of sterol-induced HMGCR degradation (A) RNF145 knockout clones were screened by genomic PCR using fluorescent primers across the gRNA target site locus. The size of the fluorescent PCR products was determined to single base pair resolution to identify frameshift insertion or deletion mutations. Fluorescent trace of PCR products from wild type HeLa cells and clone 20 from gRNA 8 (8_20) are shown. Sanger DNA sequencing confirmed the presence of frameshift insertions or deletions. **(B)** Immunoblot of lysates from selected RNF145 knockout clones to confirm loss of RNF145 protein. **(C)** Wild type HeLa cells and RNF145 knockout HeLa clones were sterol depleted overnight then cultured for four hours in the presence or absence of sterols. Cells were lysed and immunoblotted for HMGCR to assess the sterol induced degradation of HMGCR. **(D)** Wild type HeLa cells and two RNF145 knockout clones derived from independent gRNAs (5_7 and 8_20) were sterol depleted overnight then cultured with sterols for the time indicated. Cells were harvested, lysed and immunoblotted for HMGCR to assess the sterol induced degradation of HMGCR in the absence of RNF145 over a four-hour period.

5.3 Discussion

5.3.1 Tagging endogenous proteins using CRISPR/Cas9 genome editing technology

CRISPR/Cas9 technology is an incredibly powerful tool for cell biology research. Not only does CRISPR-mediated gene disruption allow the rapid generation of gene knockouts, it can be used to create knock-in cell lines, in which endogenous proteins are tagged with markers such as fluorescent proteins. The ability to perform a fluorescence-based forward genetic screen on the endogenous protein allowing me to monitor cellular changes in real time is a major advantage over the artefact-prone over-expression of an exogenous transgene. Before the advent of CRISPR/Cas9 technology, a fluorescence-based screen could only be performed on the expression of an endogenous protein if a good antibody was available against the protein of interest. Moreover, iterative sorts were not possible if an intracellular stain was required.

I started the search for the ubiquitin E3 ligase targeting HMGCR using a HMG-mCherry reporter. I originally thought that the use of an exogenous SREBP-independent promoter would focus the screen on the sterol-regulated degradation of HMGCR. However, both genome-wide CRISPR screens did not significantly enrich a population of mutants that showed significantly reduced sterol-induced HMGCR degradation. Tagging endogenous HMGCR with Clover using CRISPR/Cas9 genome editing technology allowed me to take advantage of the SREBP-dependent transcription to create a large window to screen for mutants with impaired sterol-induced HMGCR degradation. This approach enabled a significant enrichment of mutants that were unable to degrade HMGCR as efficiently as the starting clone in response to sterols. Consequently, the HMGCR-Clover screen using sterol depletion identified more candidate genes with higher confidence.

5.3.2 Differential effects of Insig proteins on the sterol-induced degradation of HMGCR

The human genome encodes two Insig isoforms, Insig1 and Insig2. Both proteins function as sterol-sensing domain (SSD) interacting proteins (Dong and Tang 2010). At high levels of cellular cholesterol, both Insigs can interact with SCAP's SSD and retain the SCAP-SREBP complex in the ER to inhibit SREBP-dependent transcription (Yabe, Brown, and Goldstein 2002, Yang et al. 2002). Both Insig proteins also enable the sterol-induced degradation of

HMGCR by associating with HMGCR's SSD in a sterol-dependent manner (Sever, Yang, et al. 2003, Sever, Song, et al. 2003).

As a part of the characterisation of the HMGCR-Clover cell line, I knocked out the Insig genes using CRISPR-mediated gene disruption (**Figure 5.2B**). In the absence of Insig1 I observed a significant block in the sterol-induced degradation of HMGCR-Clover, whereas in the absence of Insig2 there was only a small decrease in the sterol-induced degradation of HMGCR-Clover. These partially redundant phenotypes imply a more significant role for Insig1 in the sterol-induced degradation of HMGCR in this cell line. Insig2 might have a comparatively low expression level in HeLa cells and might not be able to efficiently mediate the sterol-induced degradation of HMGCR. There are no commercially available antibodies against the Insig proteins, so I cannot readily compare the protein abundance of an Insig in the absence of the other.

5.3.3 Statistical significance in a forward genetic screen does not correlate with the gene-knockout phenotype

As the loss of Insig2 alone only had a minor effect on the sterol-induced degradation of HMGCR-Clover (**Figure 5.2B**), it might be surprising that Insig2 is the most statistically significant gene in the CRISPR screen (**Figure 5.5E**). This example demonstrates the power of forward genetic screens to identify genes with small intermediate phenotypes. The statistical significance of a candidate gene is determined by the enrichment of the gRNAs that target that gene. The enrichment of a gRNA is not only dependent on the phenotype of the gene knockout, but also the efficiency of gene knockout and the growth disadvantage (or advantage) of the gene knockout. Therefore, the statistical significance of a gene as a candidate in a forward genetic screen does not provide insight into the strength of the phenotype caused by the loss of that gene, i.e. the phenotype caused by the loss of Insig1 is greater than that caused by the loss of Insig2 (**Figure 5.2B**).

5.3.4 RNF145 is required for the sterol-induced degradation of HMGCR-Clover

In Chapter 4 I validated the involvement of RNF145 in the sterol-induced degradation of HMG-mCherry, however I was unable to see a requirement for RNF145 on the sterol-induced degradation of endogenous HMGCR. In this chapter, I refined the forward genetic screen by using a knock-in cell line expressing Clover-tagged endogenous HMGCR. However, RNF145 was still the only E3 ligase identified. Using a flow cytometry-based assay, I could now see a small decrease in the sterol-induced degradation of endogenous HMGCR in the absence of RNF145 (**Figure 5.6A**). This finding could indicate an indirect effect on HMGCR degradation in the absence of RNF145 or functional redundancy amongst multiple ubiquitin E3 ligases able to ubiquitinate HMGCR in response to sterols. The next aim of my thesis project was therefore to identify other E3 ubiquitin ligases that ubiquitinate HMGCR alongside RNF145.

5.4 Summary

In this chapter, I generated a knock-in cell line, in which endogenous HMGCR is tagged with the fluorescent protein Clover. I demonstrated the correct regulation of HMGCR-Clover expression using chemical inhibitors, modulating sterol conditions, and using CRISPR-mediated gene disruption to knockout UBE2G2 and the Insigs. I went on to use the HMGCR-Clover cell line in two genome-wide CRISPR knockout screens. The first screen identified a large suite of genes required to maintain basal expression of HMGCR. The second screen focussed on the sterol-induced degradation of HMGCR and identified known components of the ERAD machinery alongside the ERAD E3 ligase RNF145, which I had previously identified in Chapter 4. CRISPR validation of RNF145 revealed a small decrease in sterol-induced degradation of HMGCR-Clover in the absence of RNF145.

Chapter 6: Gp78 and RNF145 are required for the sterol-induced degradation of HMGCR

6.1 Introduction

I have presented a series of genome wide CRISPR knockout screens to identify the ubiquitin E3 ligase for HMGCR. The poorly characterised E3 ligase RNF145 was identified by two screens that used sterol depletion to focus on the degradation of HMGCR. However, the CRISPR validation of RNF145 only revealed a small but reproducible decrease in the degradation of HMGCR-Clover and I could not detect an effect on wild type HMGCR by immunoblot. The two most likely possibilities for the small decrease in HMGCR-Clover degradation in the absence of RNF145 are that RNF145 regulates HMGCR degradation indirectly or that another ubiquitin E3 ligase compensates for the loss of RNF145 and can ubiquitinate HMGCR as well.

Several studies have previously found a requirement for multiple E3 ligases to efficiently target ERAD substrates for degradation (El Khouri et al. 2013, Zhang et al. 2015). The next aim of my thesis project was therefore to identify the E3 ligase that is functionally redundant with RNF145.

6.2 Results

6.2.1 Depletion of gp78 suggests functional redundancy with RNF145

I took a candidate gene approach to investigate whether RNF145 is redundant with other ubiquitin E3 ligases. As gp78 and TRC8 had previously been implicated in HMGCR ERAD, I started by testing the sterol-induced degradation of HMGCR-Clover following the depletion of gp78 and TRC8 in the presence and absence of RNF145 (**Figure 6.1**). I used CRISPR-mediated gene disruption to produce a RNF145 null background in the HMGCR-Clover HeLa cell line. The loss of RNF145 caused a small decrease in the sterol-induced degradation of HMGCR-Clover, as described in Chapter 5.

Depletion of gp78 in the gControl population resulted in a decrease in the sterol-induced degradation of HMGCR-Clover, implicating a role for gp78 in HMGCR degradation (**Figure 6.1**). When I depleted gp78 in the RNF145 null background, I observed a significant increase in HMGCR-Clover at steady state and a pronounced decrease in the sterol-induced degradation of HMGCR-Clover. This strongly suggests that there is redundancy between gp78 and RNF145 in the sterol-induced degradation of HMGCR.

There was no difference in sterol-induced HMGCR-Clover degradation between cells transfected with control siRNA or TRC8-targeting siRNA in the presence or absence of RNF145. I did not confirm TRC8 depletion by qPCR or immunoblot, however I used the laboratory protocol that results in the efficient depletion of TRC8 (Stagg et al. 2009).

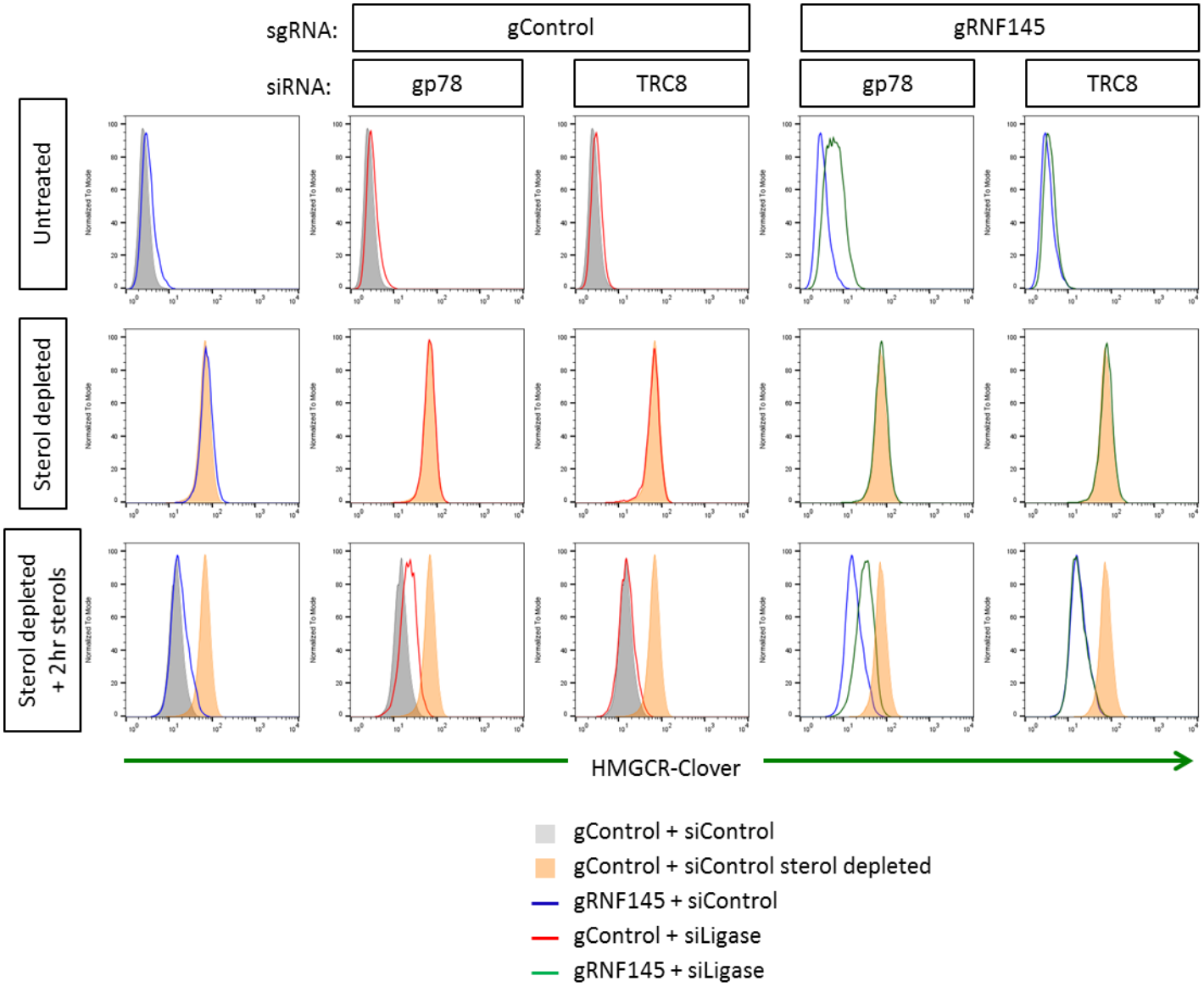

Figure 6.1 Gp78 and TRC8 siRNA-mediated knockdown in the presence and absence of RNF145 HMGCR-Clover HeLa cells were transfected with Cas9 and either a control gRNA or a pool of four RNF145-targeting gRNAs. Transfected cells were selected with puromycin treatment. Selected cells were transfected with 100nM control siRNA on day 5 post gRNA transfection, 100nM gp78 siRNA on day 5 post gRNA transfection or 50nM TRC8 siRNA day 6 post gRNA transfection. The cells were sterol depleted overnight eight days post gRNA transfection. On day 9 post gRNA transfection, cells were cultured for a further two hours in the presence or absence of sterols. HMGCR-Clover expression was assessed by flow cytometry. Representative of two independent experiments.

6.2.2 Gp78 and RNF145 are required for sterol-induced HMGCR-Clover degradation

I sought to determine whether the decreased sterol-induced HMGCR-Clover degradation in gp78 siRNA-treated cells was caused by the loss of gp78 or an siRNA off-target effect. I used a pool of four gRNAs to knockout gp78 by CRISPR-mediated gene disruption. Here, I saw no difference in sterol-induced HMGCR-Clover degradation between gGp78 and gControl HMGCR-Clover cells (**Figure 6.2A**). Targeting RNF145 with a pool of four gRNAs, once again, resulted in a small decrease in sterol-induced HMGCR-Clover degradation. When I simultaneously targeted gp78 and RNF145 with a pool of four gRNAs against each ligase, I saw a marked increase in HMGCR-Clover at steady state and a pronounced decrease in the sterol-induced degradation of HMGCR-Clover. The loss of both gp78 and RNF145 resulted in a phenotype reminiscent of the absence of UBE2G2. This provides strong evidence of the functional redundancy of gp78 and RNF145 and implies that both ligases are required for the sterol-induced degradation of HMGCR-Clover.

When TRC8 was targeted by CRISPR-mediated gene disruption using a single gRNA, I did not observe functional redundancy between RNF145 and TRC8 in the degradation of HMGCR (**Figure 6.2B**). I confirmed the efficient generation of TRC8 knockout cells by analysing the TRC8-dependent degradation of MHC-I by the human cytomegalovirus protein US2 (Stagg et al. 2009). Transducing control cells with US2 resulted in the down-regulation of MHC-I at the cell surface (red line in **Figure 6.2C**). However, less than 30% of the gTRC8 population displayed a low MHC-I cell surface phenotype following US2 transduction (cells gated on CFP marker for US2 expression), demonstrating the efficient generation of TRC8 knockouts by CRISPR-mediated gene disruption.

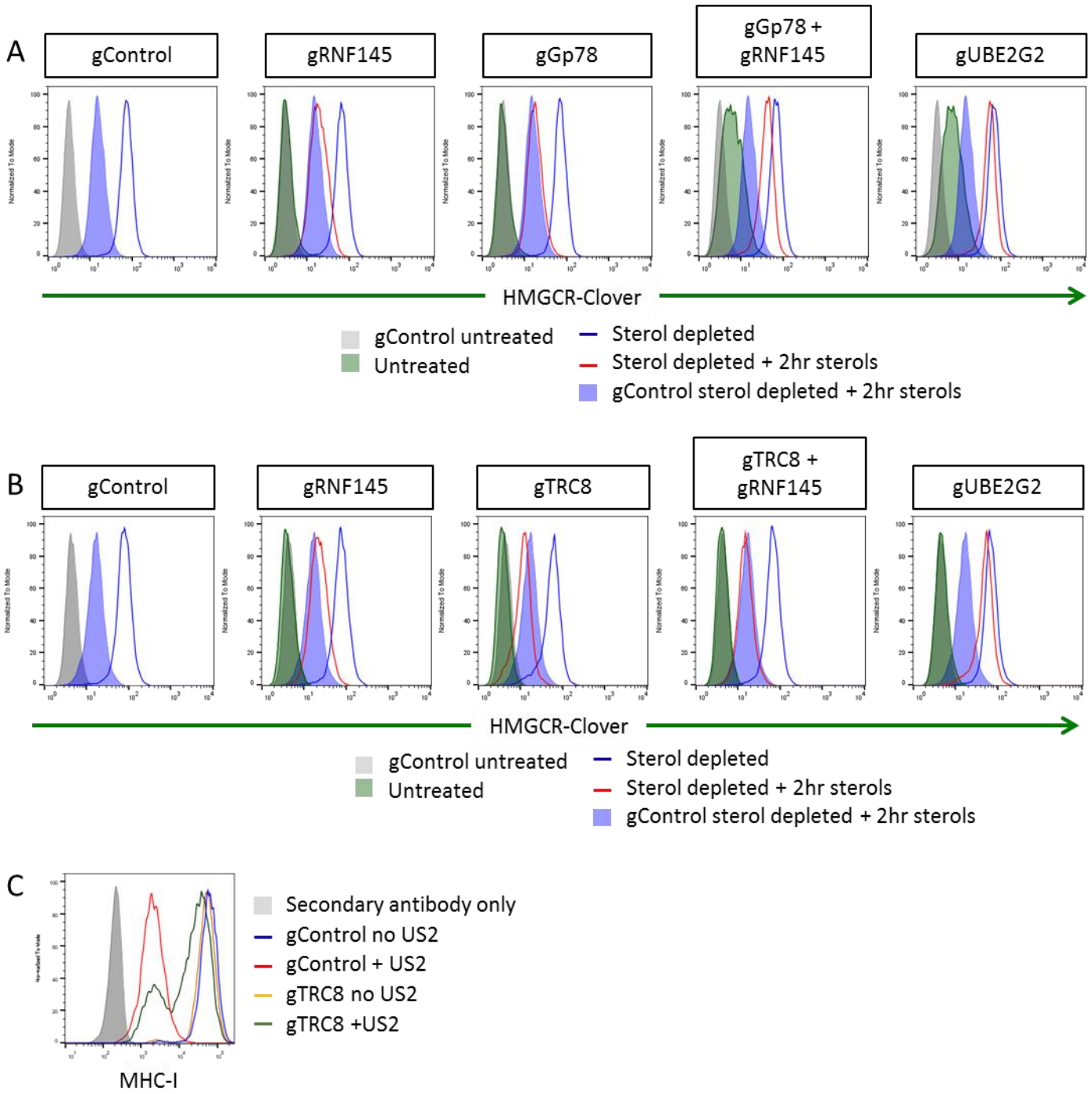

Figure 6.2 CRISPR-mediated gene disruption of both gp78 and RNF145 causes a significant decrease in sterol-induced HMGCR-Clover degradation. (A) HMGCR-Clover HeLa cells were transiently transfected with Cas9 and either a control gRNA, a pool of three gRNAs targeting UBE2G2, a pool of four gRNAs targeting gp78, a pool of four gRNAs targeting RNF145, or a pool of eight gRNAs in which four target gp78 and four target RNF145. Transfected cells were selected with puromycin. Cells were sterol depleted overnight seven days post-transfection and then cultured for a further two hours in the presence or absence of sterols. **(B)** As (A) but a single gRNA targeted TRC8 instead of a pool of four gRNAs targeting gp78. **(C)** US2-mediated downregulation of MHC-I to confirm TRC8 knockout. HeLa cells were transfected with Cas9 and either a control or TRC8-targeting gRNA. Transfected cells were selected by puromycin treatment. Selected cells were transduced with a lentiviral construct encoding US2 and a CFP marker on day 5 post-transfection. MHC-I cell surface expression was measured by flow cytometry on day 10 post-transfection. Representative of more than three independent experiments.

6.2.3 Gp78 and RNF145 are required for the sterol-induced degradation of wild type HMGCR

It was crucial to confirm that the loss of gp78 and RNF145 caused a significant decrease in the sterol-induced degradation of wild type HMGCR and that the Clover tag was not responsible for the double knockout phenotype. I generated gp78 and RNF145 double knockout HeLa clones by transfecting RNF145 knockout clones derived from gRNA #5 (5_7 and 5_26 from **Figure 5.7**) with gp78 gRNA #4 and by transfecting RNF145 knockout clone 8_20 (derived from gRNA #8) with gp78 gRNA #3. I used different combinations of gRNAs to minimise the risk of pursuing a gRNA off-target effect. The loss of gp78 in clones derived from RN145 knockout cells was confirmed by Immunoblot (**Figure 6.3A**).

Immunoblot analysis of the gp78 and RNF145 double knockout HeLa clones revealed a significant recue of HMGCR at steady state (**Figure 6.3B**). Whereas, the loss of RNF145 alone only caused a small increase in steady state HMGCR expression. The ability of the gp78 and RNF145 double knockout clones to degrade HMGCR in response to sterols was assessed by sterol depleting the clones overnight followed by a further four-hour culture in the presence or absence of sterols. Encouragingly in every case, the double knockout clones had a marked reduction in sterol-induced HMGCR degradation (**Figure 6.4**). In comparison, the RNF145 knockout clones were indistinguishable from wild type HeLa cells. Thereby demonstrating the requirement of both gp78 and RNF145 to efficiently degrade endogenous wild-type HMGCR in response to sterols.

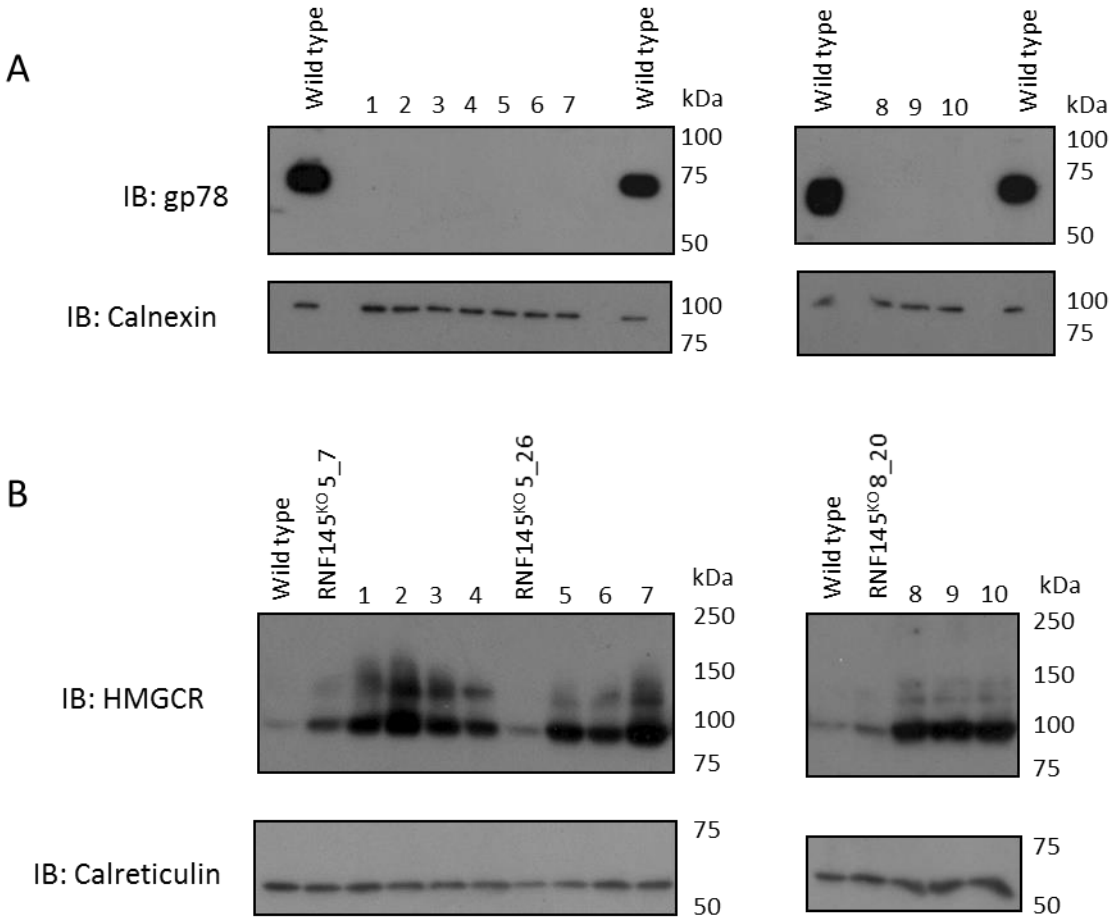

gp78 and RNF145 double knockout clones
1: RNF145^{KO} #5_7 + gp78 gRNA 4 clone 1
2. RNF145^{KO} #5_7 + gp78 gRNA 4 clone 3
3. RNF145^{KO} #5_7 + gp78 gRNA 4 clone 6
4. RNF145^{KO} #5_7 + gp78 gRNA 4 clone 7
5. RNF145^{KO} #5_26 + gp78 gRNA 4 clone 6
6. RNF145^{KO} #5_26 + gp78 gRNA 4 clone 19
7. RNF145^{KO} #5_26 + gp78 gRNA 4 clone 20
8. RNF145^{KO} #8_20 + gp78 gRNA 3 clone 5
9. RNF145^{KO} #8_20 + gp78 gRNA 3 clone 10
10. RNF145^{KO} #8_20 + gp78 gRNA 3 clone 12

Figure 6.3 Gp78 and RNF145 double knockout clones have increased HMGCR expression at steady state (A) Gp78 knockout clones were identified by immunoblot. Clones were derived using different combinations of gp78 and RNF145 gRNAs. **(B)** Steady state HMGCR expression was assessed by immunoblot in parental wild type HeLa cells, RNF145 knockout clones and gp78 and RNF145 double knockout clones.

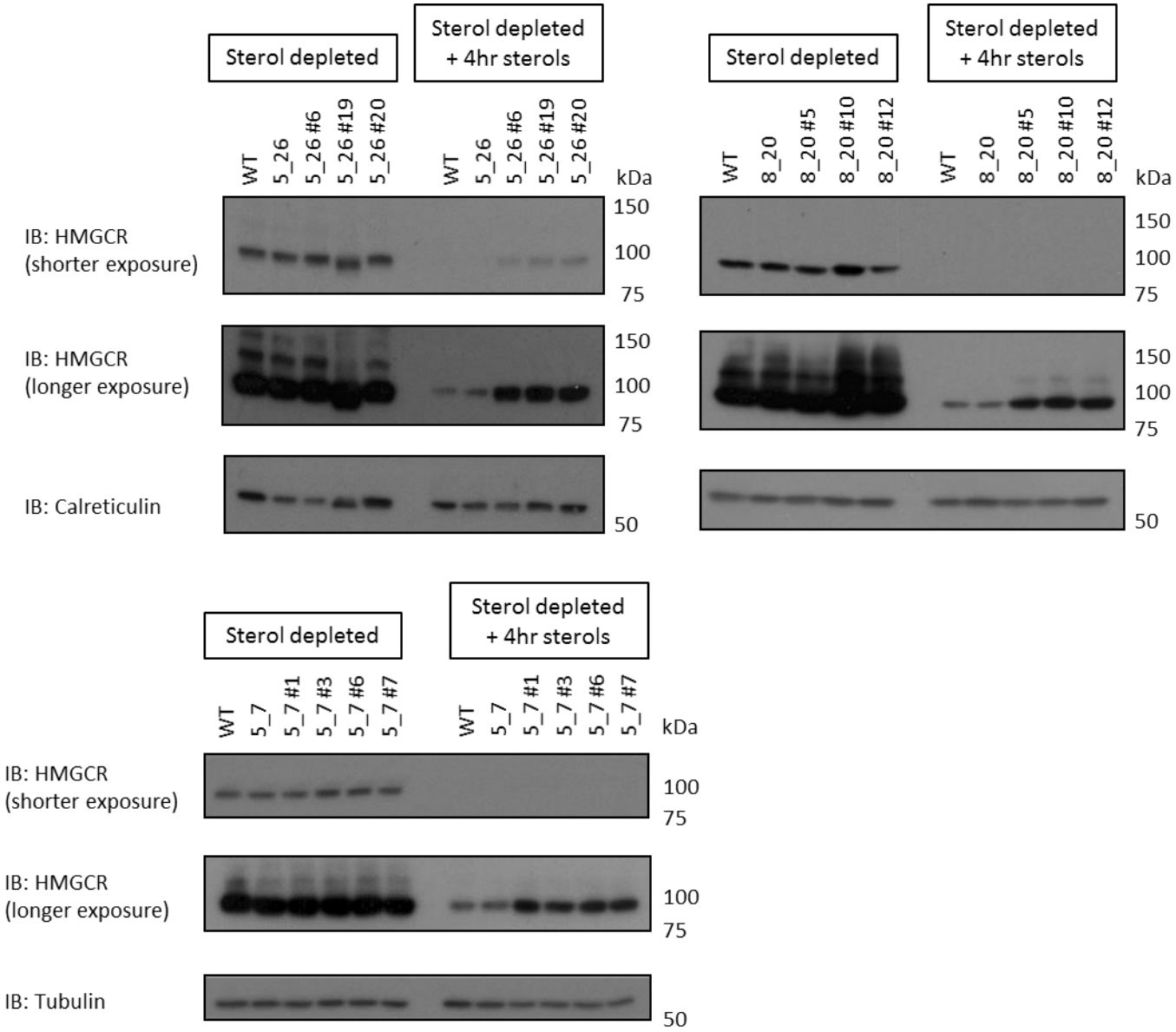

Figure 6.4 Gp78 and RNF145 double knockout clones cannot degrade HMGCR efficiently in response to sterols. Wild type HeLa cells or knockout clones were sterol depleted overnight, then cultured for a further four hours in the presence or absence of sterols. Cells were then lysed and immunoblotted for HMGCR (WT, wild type).

6.2.4 Generating a gp78 and RNF145 double knockout HMGCR-Clover HeLa cell line

I used FACS to generate a gp78 and RNF145 double knockout HMGCR-Clover cell line. To this end, HMGCR-Clover cells were transiently transfected with Cas9, gp78 gRNA #4 and RNF145 gRNA #8. Eight days after transfection and selection of puromycin-resistant cells, an overnight sterol depletion was performed. The following day, sterols were added to the sterol depleted culture for two hours. I then selected cells expressing high levels of HMGCR-Clover by FACS

(**Figure 6.5A**) and confirmed the successful enrichment of a population that had a significant block in the sterol-induced degradation of HMGCR-Clover. Immunoblot analysis of the selected population confirmed the absence of gp78 and RNF145 protein (**Figure 6.5B**).

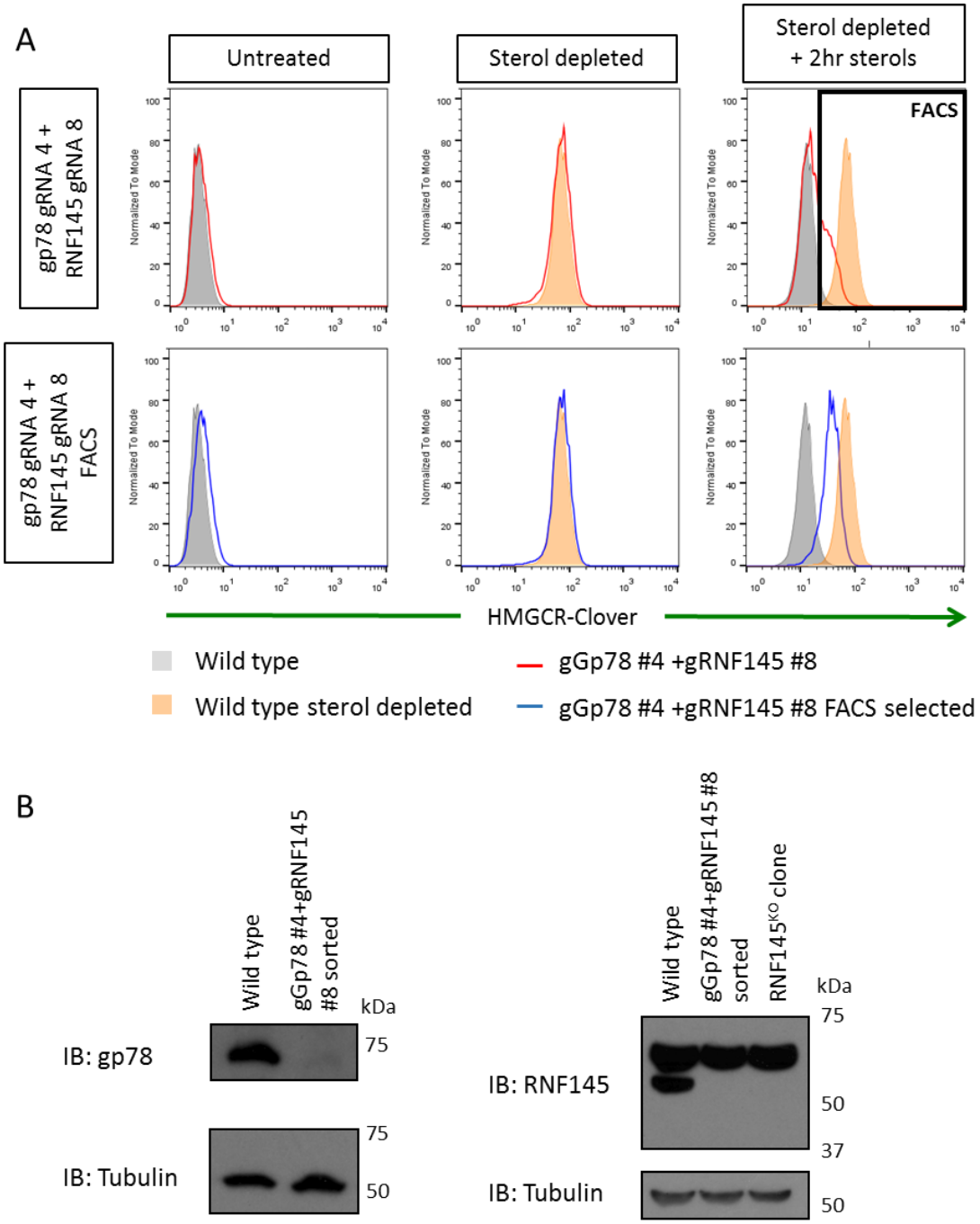

Figure 6.5 Generating a gp78 and RNF145 double knockout HMGCR-Clover HeLa cell line (A) HMGCR-Clover cells were transfected with gp78 gRNA #4 and gp78 gRNA #8. Transfected cells were selected with puromycin. Cells were sterol depleted overnight 8 days post transfection and then cultured for a further two hours in the presence or absence of sterols. HMGCR-Clover^{high} cells were selected by FACS. **(B)** Immunoblot to confirm loss of gp78 and RNF145 protein in the FACS selected population. RNF145 knockout clone 5_7 was used to confirm the RNF145 band.

6.2.5 Sterol-induced degradation of HMGCR requires E3 ligase activity of RNF145

To confirm a role for RNF145 in the sterol-induced degradation of HMGCR, I sought to restore HMGCR-Clover degradation in the gp78 and RNF145 double knockout line by genetic complementation. Wild type RNF145 cDNA expressed by lentiviral transduction in the gp78 and RNF145 double knockout HMGCR-Clover cell line resulted in a near-complete rescue of sterol-induced HMGCR-Clover degradation (**Figure 6.6A**). The expression of a RING-mutant (C552A H554A) RNF145 in the gp78 and RNF145 double knockout HMGCR-Clover cell line could not rescue sterol-induced HMGCR-Clover degradation showing that the E3 ligase activity of RNF145 is required for HMGCR degradation. Immunoblotting revealed that mutating the RING domain increased the expression of RNF145 (**Figure 6.6B**). This is a common observation for ubiquitin E3 ligases owing to their intrinsic auto-ubiquitination activity (Deshaies and Joazeiro 2009).

The first five transmembrane helices of RNF145 are predicted to constitute a sterol sensing domain (SSD) (Cook et al. 2017). The second helix contains a YLYF motif, which shares sequence homology with the YIYF motif in the SSDs of SCAP and HMGCR. Mutating the YIYF motif in SCAP prevents association with Insigs and therefore inhibits the retention of SREBP in the ER (Yang et al. 2002). Mutating the YIYF motif in HMGCR also prevents the association with Insigs and therefore blocks the sterol-induced degradation of HMGCR (Sever, Song, et al. 2003). To determine whether RNF145's YLYF motif is required for the sterol-induced degradation of HMGCR, I mutated the YLYF motif to ALAF and AAAA, the same mutations introduced to HMGCR by Sever *et al.* (Sever, Song, et al. 2003). Unfortunately, the ALAF and AAAA RNF145 mutants were poorly expressed (**Figure 6.6B**), barring a comparison of their ability to restore HMGCR degradation to wild type RNF145. A possible solution to this problem could be to mutate the tyrosine residues to another hydrophobic residue such as phenylalanine. This might disrupt Insig binding but maintain the structure of the helix in the ER membrane.

It was not until later in the project that a RNF145 antibody became available. The RNF145 cDNA constructs in Figure 6.4C and 6.4D were therefore tagged with V5 to allow detection by immunoblot. Once I had a RNF145 antibody I could compare the expression level of the exogenous to endogenous RNF145. This revealed that there was only a modest over-expression of exogenous RNF145 (**Figure 6.6C)**.

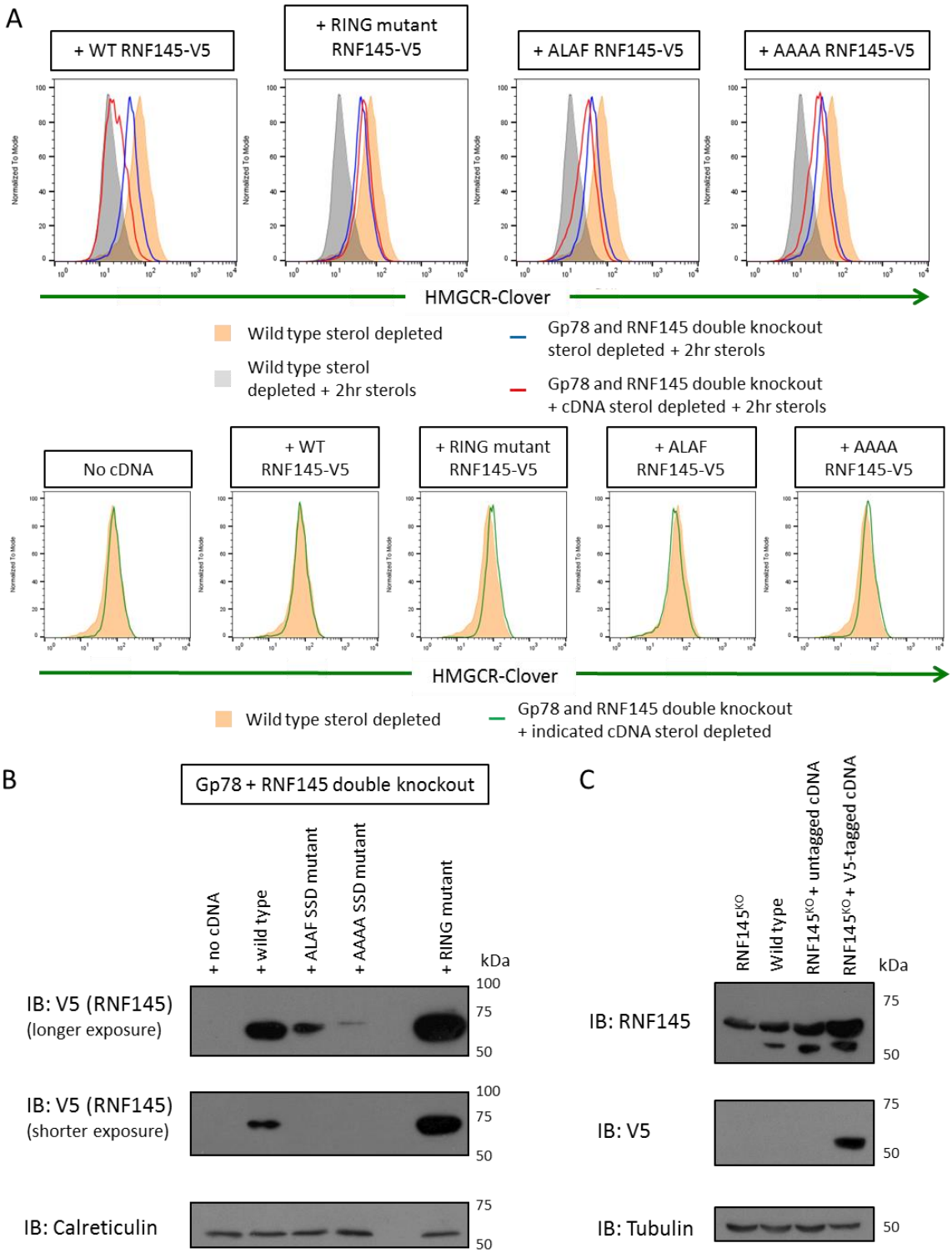

Figure 6.6 E3 ligase activity of RNF145 is required for HMGCR degradation (A) The gp78 and RNF145 double knockout HMGCR-Clover cell line was transduced with a lentiviral construct encoding an RNF145 cDNA (wild type, RING-mutant, ALAF (SSD mutant) or AAAA (SSD mutant). Transduced cells were selected by hygromycin selection. Sterol-induced degradation was assessed 6 days post transduction. **(B)** Immunoblot analysis of the cells from (A) revealed lower expression of SSD mutants and increased expression of RING-mutant compared to wild type RNF145 cDNA. **(C)** RNF145 knockout clone 5_7 was transduced with a lentiviral construct encoding either untagged or V5-tagged wild type RNF145. Transduced cells were selected by hygromycin selection, then lysed and immunoblotted to compare the expression level of endogenous and exogenous RNF145.

6.2.6 Gp78 knockout HeLa clones do not have impaired sterol-induced HMGCR degradation

To determine the effect that the loss of gp78 has on HMGCR ERAD and to create stable reagents for future assays, I generated gp78 knockout clones using CRISPR-mediated gene disruption. Gp78 knockout clones, derived from two independent gRNAs, were identified by immunoblot (**Figure 6.7A**).

I used Insig1, a known gp78 substrate, to demonstrate a functional consequence for the loss of gp78 (Lee, Song, et al. 2006). I transduced the parental wild type HeLa cells and gp78 knockout clones, at a low M.O.I., with a lentiviral construct encoding myc-tagged Insig1. Immunoblot analysis revealed a dramatically higher expression of Insig1 in the gp78 knockout clones than in wild type HeLa cells, demonstrating a functional consequence for the loss of gp78 (**Figure 6.7B**).

The fact that gp78 targets Insig1 for degradation complicates the effect that the loss of gp78 has on HMGCR. There are no human Insig antibodies available, so I could not determine the expression level of endogenous Insig1 in the gp78 knockout HeLa clones. Gp78 knockout mouse embryonic fibroblasts and hepatocytes exhibit increased Insig1 expression at steady state (Tsai et al. 2012, Liu et al. 2012). Increased Insig1 expression will promote SCAP-SREBP retention in the ER, decreasing transcription of SREBP target genes. The increase in Insig1 could also promote the degradation of HMGCR (Song, Sever, and DeBose-Boyd 2005).

Some of the gp78 knockout clones showed a minor increase in HMGCR expression at steady state (**Figure 6.7A**), potentially driven by the reduced metabolic flux through the cholesterol biosynthesis pathway as a result of increased Insig1 levels (Liu et al. 2012). Decreased cholesterol production will feedback to stabilise HMGCR.

The gp78 knockout HeLa clones could degrade HMGCR in response to sterols as efficiently as the parental wild type HeLa cells (**Figure 6.7C**). This is consistent with the observation that gp78 knockout MEFs can degrade HMGCR as efficiently as wild type MEFs (Tsai et al. 2012).

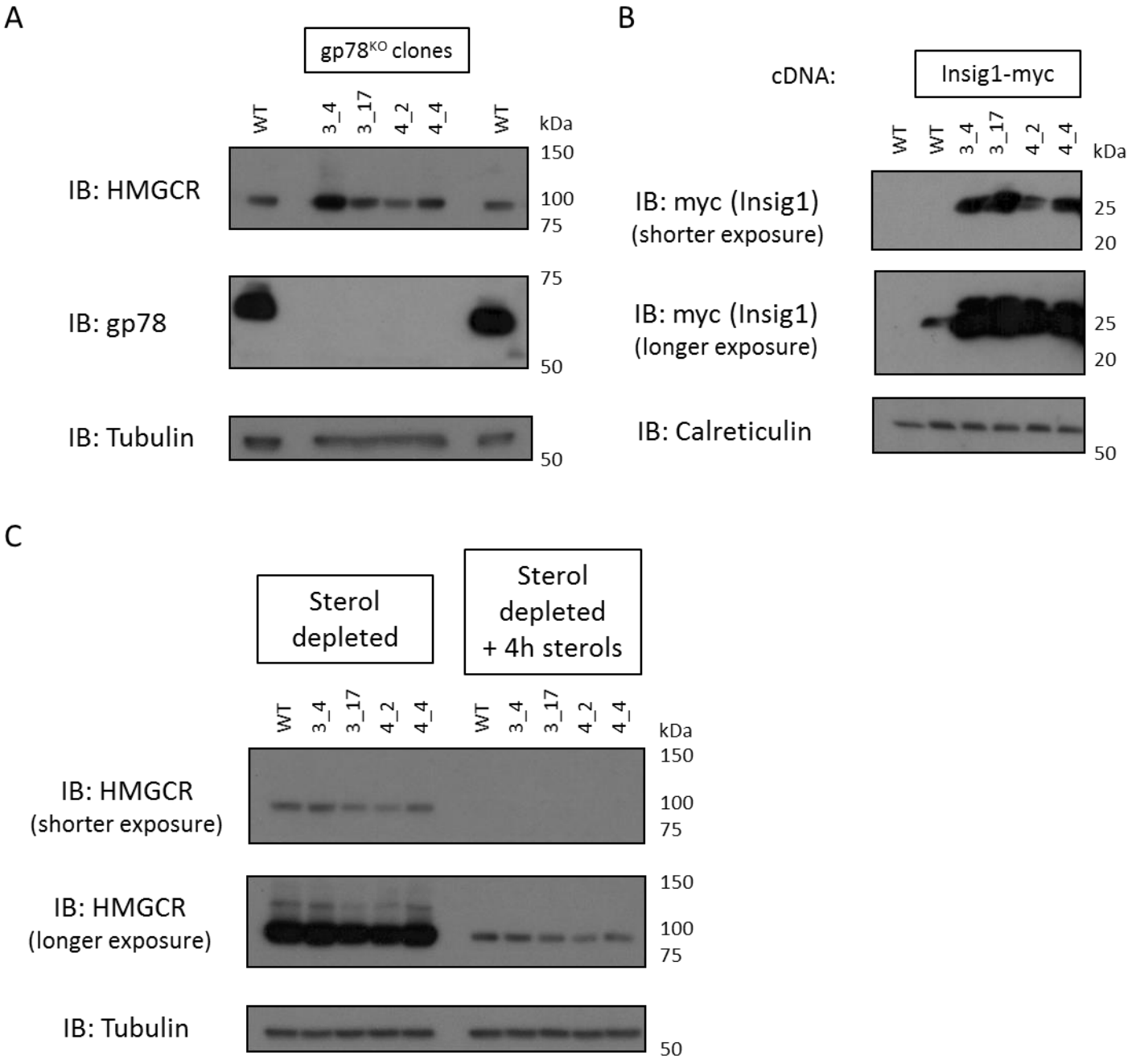

Figure 6.7 Gp78 knockout clones to analyse HMGCR degradation (A) Wild type HeLa cells were transfected with Cas9 and either gp78 gRNA #3 or #4. Transfected cells were selected by puromycin treatment then single cell cloned by serial dilution. Clones were screened by immunoblot. The absence of gp78 in two clones derived from each gRNA (3_4 and 3_17 from gRNA #3, 4_2 and 4_4 from gRNA #4) was confirmed (WT, wild type). **(B)** Wild type HeLa cells and gp78 knockout clones were transduced an M.O.I. of 0.1 with a lentiviral vector encoding myc-tagged Insig1. Transduced cells were selected with puromycin treatment. The selected cells were harvested, lysed and immunoblotted to assess Insig1-myc expression. **(C)** Parent wild-type HeLa cells and gp78 knockout HeLa clones were sterol depleted overnight followed by a further four-hour culture in the presence or absence of sterols. Cells were harvested, lysed and immunoblotted for HMGCR.

6.2.7 UBE2G2 is required for the sterol-induced degradation of HMGCR

Throughout this thesis project, I have used UBE2G2 as a positive control for a gene whose loss leads to a significant block in sterol-induced HMGCR degradation. Consequently, UBE2G2 knockout HeLa clones were generated as a positive control to assess HMGCR ubiquitination.

UBE2G2 knockout clones derived from two independent gRNAs were identified by immunoblot (**Figure 6.8A**). Consistent with other UBE2G2 knockout clones in my thesis project, I observed an increase in HMGCR steady state expression and a significant block in the sterol-induced degradation of HMGCR (**Figure 6.8B** and **6.8C**). Clone C1 was selected as a knockout clone when I first screened the clones and was used in the experiments shown in Figure 6.6. However, a much longer exposure of the immunoblot revealed a small amount of UBE2G2 protein in the clone C1. I have not sequenced the locus targeted by gRNA #C in this clone, however it would appear that at least one of the alleles has been repaired in-frame but the mutation has resulted in a dramatic decrease in UBE2G2 protein abundance. It is striking that the residual UBE2G2 protein in clone C1 appears to be sufficient to mediate HMGCR degradation (**Figure 6.8C**). However, clone C1 acts as a useful control.

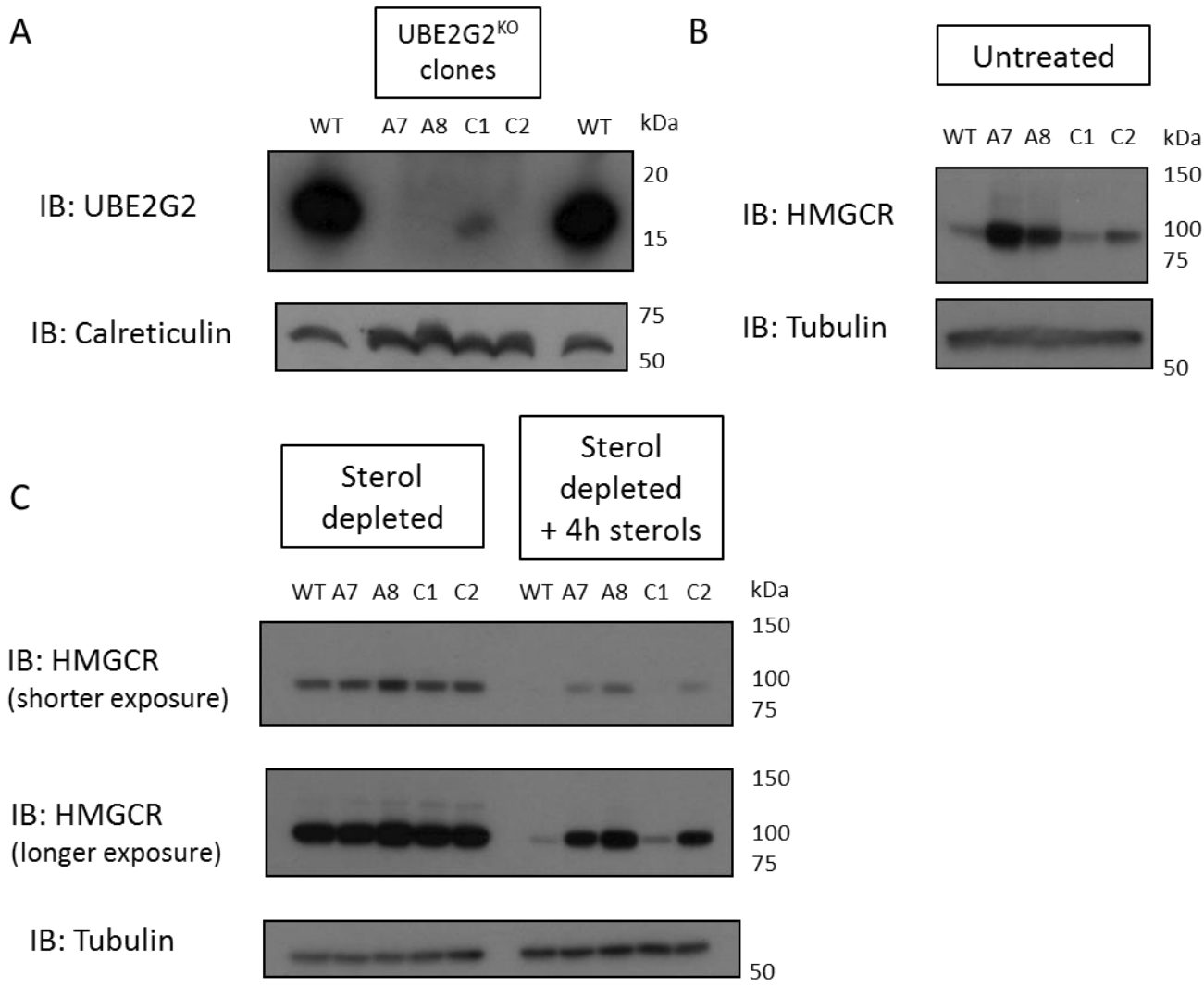

Figure 6.8 UBE2G2 is required for the sterol-induced degradation of HMGCR (A) Wild type HeLa cells were transfected with Cas9 and either UBE2G2 gRNA #A or #C. Transfected cells were selected by puromycin treatment then single cell cloned by serial dilution. UBE2G2 knockout clones were identified by immunoblot. Two clones were selected that were derived from gRNA #A, A7 and A8, and another two clones were selected that were derived from gRNA #C, C1 and C2 (WT, wild type). **(B)** Parental wild-type HeLa cells and UBE2G2 knockout clones were lysed and immunoblotted for HMGCR to analyse steady state HMGCR expression. **(C)** Parental wild-type HeLa cells and UBE2G2 knockout clones were sterol depleted overnight and then cultured for a further four hours in the presence or absence of sterols. The cells were then harvested, lysed and immunoblotted for HMGCR.

6.2.8 Gp78 and RNF145 are required for the sterol-induced ubiquitination of HMGCR

Before assessing HMGCR ubiquitination, I validated the HMGCR immunoprecipitation (**Figure 6.9A**). I observed the efficient enrichment of HMGCR from sterol depleted cells, using untreated cells as a negative control. HMGCR was efficiently eluted from the antibody following a 15-minute incubation at 50^{o}C.

To assess the requirement of gp78 and RNF145 for the sterol-induced ubiquitination of HMGCR, single and double knockout clones were sterol depleted overnight. The cells were treated with 50μM MG132, a proteasome inhibitor, for 30 minutes before a one-hour culture in the presence or absence of sterols. **Figure 6.9B** suggests a small decrease in HMGCR ubiquitination in the absence of gp78 or RNF145, however this was not observed in RNF145 knockout cells in **Figure 6.9C**. In contrast, the combined loss of gp78 and RNF145 caused an almost complete loss of sterol-induced HMGCR ubiquitination (**Figure 6.9C**). As robust sterol-induced degradation of HMGCR was observed in the presence of either gp78 or RNF145, both gp78 and RNF145 can mediate the polyubiquitination of HMGCR. Consistent with previous studies, the loss of UBE2G2 resulted in a significant block to sterol-induced HMGCR ubiquitination (**Figure 6.9B** and **Figure 6.9C**) (Miao et al. 2010).

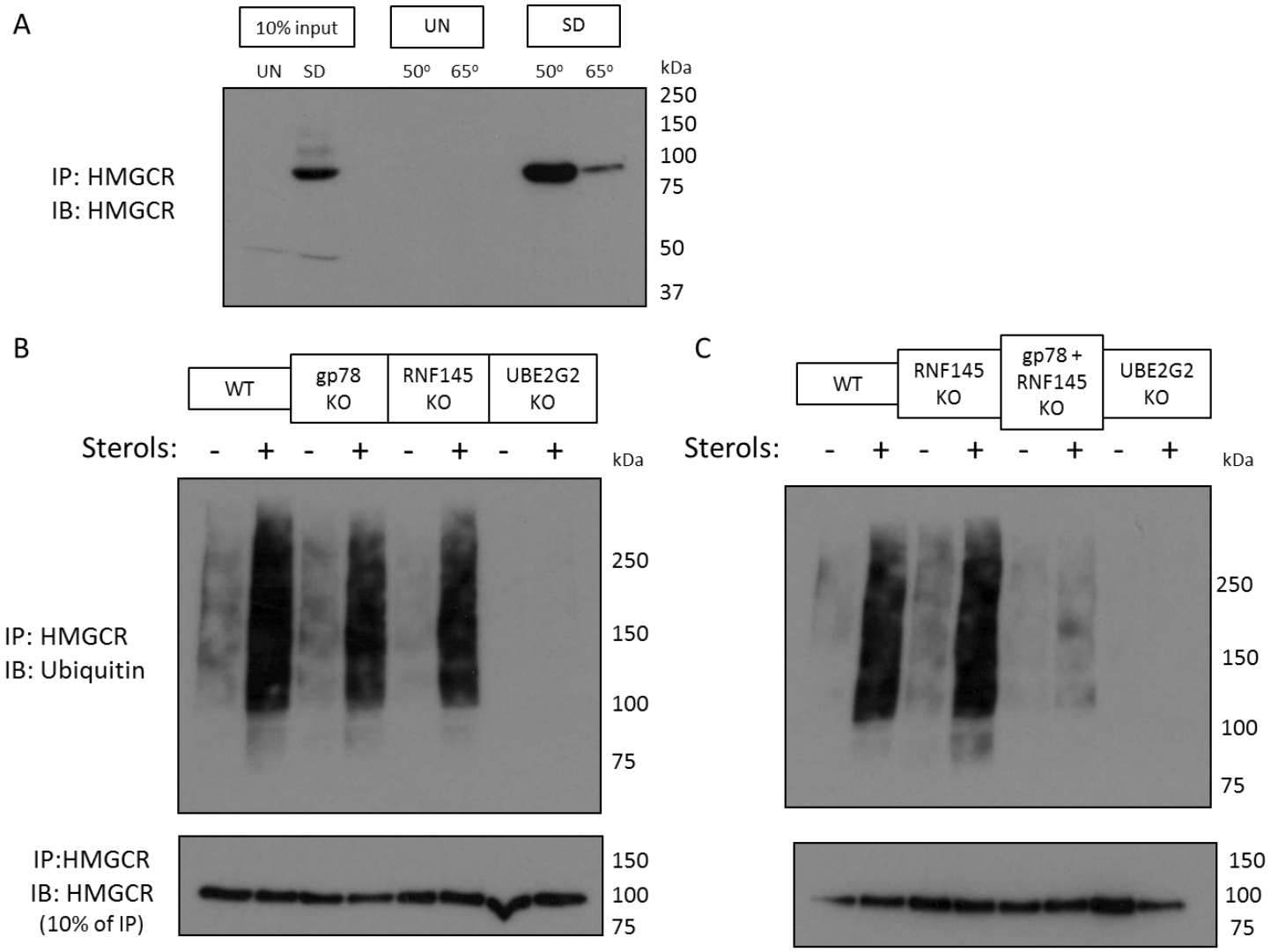

Figure 6.9 Gp78 and RNF145 are required for the sterol-induced ubiquitination of HMGCR
(A) Wild type HeLa cells were left untreated or sterol depleted overnight to induce HMGCR expression. 10^6 cells were lysed and HMGCR was immunoprecipitated with Rb anti-HMGCR and Protein A Sepharose overnight at 4°C. The next day the immunoprecipitation was washed 5 times before resuspending in 20 µl of 2x SDS sample loading buffer. The samples were first incubated at 50°C for 15 minutes. The samples were spun down, the supernatant removed and run out on a gel (50°C). Another 20 µl aliquot of 2x SDS sample loading buffer was added to the pellet followed by a 15-minute incubation at 65°C. The samples were spin down, the supernatant was removed and run out on a gel (65°C). (UN, untreated; SD, sterol depleted) **(B)** Parental wild-type HeLa cells or single knockout clones (gp78 knockout clone 4_2, RNF145 knockout clone 5_7 and UBE2G2 knockout clone A7) were sterol depleted overnight. The following day, all sterol depleted cells were treated with 50µM MG132 for 30 minutes and then for one hour in the presence or absence of sterols. $4x10^6$ cells from each condition were harvested and immunoprecipitated with anti-HMGCR, followed by immunoblot for ubiquitin. **(C)** sterol induced HMGCR ubiquitination was assessed in wild-type HeLa cells, RNF145 knockout clone 5_7, gp78 and RNF145 double knockout clone 5_7 #7 and UBE2G2 knockout clone A7 as described in (B).

6.2.9 RNF145 constitutively associates with Insig1 and Insig2

The model for the sterol-induced degradation of HMGCR revolves around the Insig proteins acting as sterol-sensitive scaffolds to recruit an E3 ubiquitin ligase complex to HMGCR (Goldstein, DeBose-Boyd, and Brown 2006). I therefore wanted to determine whether RNF145 interacts with the Insig proteins and whether this interaction is sensitive to the sterol environment.

Due to the absence of antibodies against endogenous Insig1 and Insig2, epitope-tagged Insig cDNAs were used. To ensure that the exogenous Insig proteins restore HMGCR degradation in Insig knockout cells, Insig knockout HMGCR-Clover cells for each Insig were created by transiently transfecting Cas9 and a pool of four gRNAs. After a prolonged culture (8 days) the knockout cell lines were transduced with a lentiviral construct encoding an Insig. Transduced cells were selected and the sterol-induced degradation of HMGCR-Clover was assessed (**Figure 6.10A**). Re-expression of each myc-tagged Insig restored the steady state expression of HMGCR-Clover as well as the sterol-induced degradation of HMGCR-Clover. Epitope-tagged Insig transgenes are therefore appropriate tools to investigate the mechanism of HMGCR degradation.

Next, I stably expressed myc-tagged Insig1 and myc-tagged Insig2 in the presence or absence of V5-tagged (C-terminus) RING-mutant RNF145 in a gp78 and RNF145 double knockout HeLa clone. Cells were sterol depleted overnight, then treated with 50nM Bortezomib for 30 minutes before a further 2-hour culture in the presence or absence of sterols. Both Insig1 and Insig2 co-precipitated with RNF145 in the presence and absence of sterols (**Figure 6.10B**). The constitutive association of RNF145 with the Insigs should enable RNF145 to be recruited to HMGCR in response to sterols.

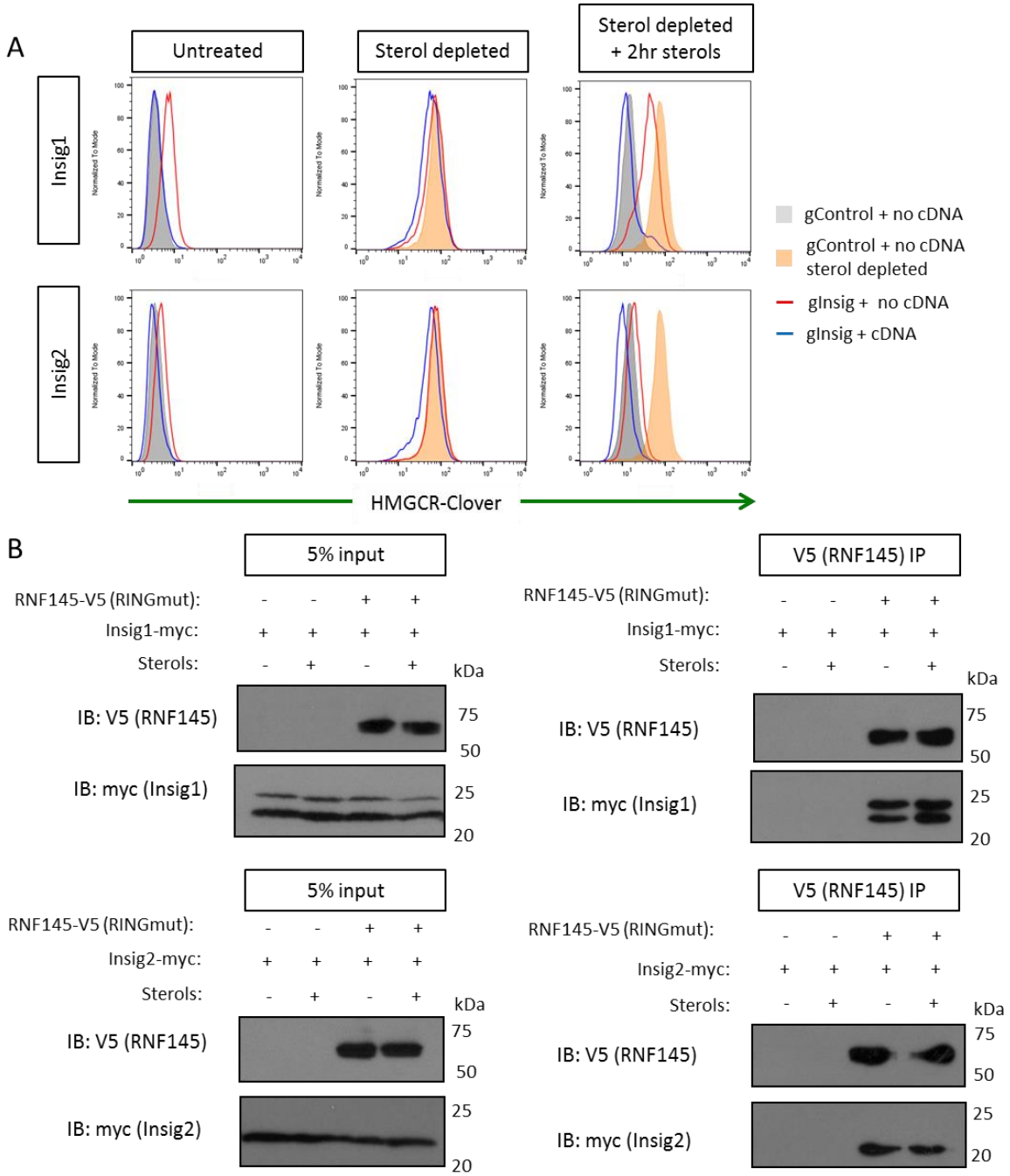

Figure 6.10 RNF145 constitutively associates with Insig1 and Insig2 (A) HMGCR-Clover cells were transiently transfected with Cas9 and a pool of four gRNAs targeting either Insig1 or Insig2. Transfected cells were selected by puromycin treatment. Eight days later, Insig knockout HMGCR-Clover cells were transduced with a lentiviral construct encoding the (myc-tagged) Insig gene that had been disrupted. Transduced cells were selected by puromycin selection. Cells were sterol depleted overnight and then cultured for a further two hours in the presence or absence of sterols. HMGCR-Clover expression was assessed by flow cytometry. **(B)** A gp78 and RNF145 double knockout HeLa clone was transduced with lentiviral constructs encoding either myc-tagged Insig1 or Insig2 with or without V5-tagged RING-mutant RNF145. Transduced cells were selected with puromycin (Insig) or hygromycin (RNF145). Selected cells were sterol depleted overnight. The following day, the sterol depleted samples were treated with 50nM Bortezomib for 30 minutes and then cultured for a further 2 hours in the presence or absence of sterols. Cells were then lysed and RNF145-V5 was immunoprecipitated. Immunoprecipitates were resolved by SDS-PAGE and immunoblotted. Representative of two independent experiments.

6.2.10 Identifying RNF145 binding partners by mass spectrometry

I sought to identify other RNF145 interacting factors by performing an immunoprecipitation followed by mass spectrometry analysis. I stably expressed V5-tagged wild type RNF145 in a RNF145 knockout HeLa clone (5_7). Whilst RNF145 is constitutively associated with the Insig proteins, I predicted that other interactions made with RNF145 would be sensitive to the cellular sterol environment. Three sets of RNF145-V5-expressing cells were sterol depleted overnight. The next day, one sample remained under sterol deplete conditions, one sample was treated with sterols for one hour and the last sample was treated with 50μM MG132 for 30 minutes followed by 1 hour with sterols. I also performed an immunoprecipitation in the RNF145 knockout clone that did not express RNF145-V5 to control for non-specific binding to anti-V5 antibody or Protein A Sepharose beads.

A selection of proteins identified from the RNF145-V5 immunoprecipitations are listed in **Table 6.1** (full list in Appendix 3). It is surprising that HMGCR is identified in the sterol depleted sample (10 peptides). The Insig and HMGCR interaction is dependent on sterols and so it would be expected that the RNF145 and HMGCR interaction would also be sterol dependent (Sever, Song, et al. 2003). Treating sterol depleted cells with sterols for one hour did not increase the abundance of HMGCR in the RNF145-V5 immunoprecipitation and the number of unique peptides identified decreased (7 peptides). However, both the number of unique peptides (16 peptides) and the area (a measure of abundance) of HMGCR increased when the sterol depleted cells were treated with sterols and MG132. This suggests a sterol dependent interaction between HMGCR and RNF145 that is sensitive to proteasome inhibition. It was promising to detect an interaction between HMGCR and RNF145, however proteasome inhibition was not controlled for. It is therefore not possible to exclude a constitutive association between HMGCR and RNF145 that is protected by proteasome inhibition.

Multiple ERAD components and proteasome subunits were identified by mass spectrometry. UBXD8 (FAF2) is a hit in both genome wide CRISPR knockout screens that used sterol depletion to focus on HMGCR degradation. UBXD8 helps to recruit the p97 ATPase complex to the ER membrane (Lee et al. 2008). UBAC2 recruits UBXD8 to gp78, therefore the mass spectrometry data suggests that UBAC2 might also recruit UBXD8 to RNF145 (Christianson et al. 2012). Erlin-2 and Derlin-1 are common interaction partners of ERAD E3 ubiquitin ligases (Christianson et al. 2012). Ubiquilin is proposed to assist delivery of poly-ubiquitinated

substrates to the proteasome (Ko et al. 2004). No E2 conjugating enzyme was identified in the RNF145 immunoprecipitation, however AUP1 was identified. AUP1 recruits UBE2G2 to TRC8 and assists the recruitment of UBE2G2 to gp78 (Jo, Hartman, and DeBose-Boyd 2013). It is therefore likely that AUP1 facilitates the recruitment of UBE2G2 to RNF145.

A striking hit from the RNF145-V5 immunoprecipitation is gp78. The number of unique peptides identified and gp78 abundance is similar in the sterol depleted and sterol treated samples, with an increase in unique peptides and abundance in the sterol treated sample with MG132, a pattern resembling HMGCR. This suggests that gp78 and RNF145 could oligomerise through a direct interaction. Perhaps more likely, gp78 and RNF145 might interact with the same Insig molecule through distinct binding sites. However, the over-expression of the transmembrane domain of gp78 inhibits HMGCR degradation. If correct this might imply that the E3 ubiquitin ligases have a shared binding site on the Insig proteins (Song, Sever, and DeBose-Boyd 2005). No other ERAD E3 ligases were identified in the mass spectrometry analysis.

Several hits are SREBP-2 target genes in the cholesterol biosynthesis pathway, such as HMG-CoA Synthase and 7-dehydrocholesterol reductase (Dooley, Millinder, and Osborne 1998, Prabhu, Sharpe, and Brown 2014). Importantly, the negative control for non-specific immunoprecipitation was not sterol depleted and the protein abundance might be too low without sterol depletion to detect these proteins as non-specific binding partners.

			Sterol depleted (SD)		SD + sterols		SD + sterols +MG132	
Accession	**Gene Name**	**Gene ID**	**Peptides**	**Area**	**Peptides**	**Area**	**Peptides**	**Area**
Q8N766	ER membrane protein complex subunit 1	EMC1	15	1.99	13	2.40	19	3.35
P04035	3-hydroxy-3-methylglutaryl-coenzyme A reductase	HMGCR	10	1.41	7	1.41	16	7.65
Q96MT1	RING finger protein 145	RNF145	15	102.48	14	126.23	15	140.74
O14818	Proteasome subunit alpha type-7	PSMA7	7	2.98	4	2.57	9	8.04
P20618	Proteasome subunit beta type-1	PSMB1	3	0.78	3	0.93	9	3.82
Q14534	Squalene monooxygenase	SQLE	5	1.08	5	1.40	8	2.77
P49720	Proteasome subunit beta type-3	PSMB3	2	1.02	2	0.81	7	3.84
P28074	Proteasome subunit beta type-5	PSMB5	5	0.97	2	0.55	7	4.05
A0A024RA52	Proteasome subunit alpha type-2	PSMA2					7	3.71
Q96CS3	FAS-associated factor 2	FAF2	3	1.53	5	1.98	6	4.70
Q9UKV5	E3 ubiquitin-protein ligase AMFR (gp78)	AMFR	4	0.68	3	0.67	6	1.46
Q8NBM4	Ubiquitin-associated domain-containing protein 2	UBAC2	5	1.60	3	1.04	6	2.92
P28070	Proteasome subunit beta type-4	PSMB4	2	0.58	2	0.42	6	2.67
Q9UMX0	Ubiquilin-1	UBQLN1	2	1.27			6	1.68
Q16850	Lanosterol 14-alpha demethylase	CYP51A1	2	0.58	6	1.21	5	1.31
Q9NPA0	ER membrane protein complex subunit 7	EMC7	2	0.85	2	0.73	5	1.31
O94905	Erlin-2	ERLIN2	2	0.70	4	0.65	5	1.21
Q15738	Sterol-4-alpha-carboxylate 3-dehydrogenase, decarboxylating	NSDHL	1	1.86	1	2.13	4	1.47
P28066	Proteasome subunit alpha type-5	PSMA5	1	0.37	2	1.09	4	4.58
P28072	Proteasome subunit beta type-6	PSMB6	1	1.16	1	0.90	4	3.10
Q9UBV2	Protein sel-1 homolog 1	SEL1L			2	0.40	4	0.76
O14975	Very long-chain acyl-CoA synthetase	SLC27A2	3	1.83	3	0.49	3	0.58
Q9P0I2	ER membrane protein complex subunit 3	EMC3	2	1.60	1	1.61	3	1.48
Q9Y679	Ancient ubiquitous protein 1	AUP1	1	0.43	1	0.17	3	1.12
Q9P035	Very-long-chain (3R)-3-hydroxyacyl-CoA dehydratase 3	HACD3	2	0.92	1	1.61	2	1.17
Q01581	Hydroxymethylglutaryl-CoA synthase, cytoplasmic	HMGCS1	4	0.87	4	1.89	2	0.68
Q9BWD1	Acetyl-CoA acetyltransferase, cytosolic	ACAT2	3	0.78	3	1.33	2	1.04
Q99436	Proteasome subunit beta type-7	PSMB7					2	2.30
Q15006	ER membrane protein complex subunit 2	EMC2	2	0.28	1	1.12	2	1.36
Q9BUN8	Derlin-1	DERL1					2	0.40
Q9UBM7	7-dehydrocholesterol reductase	DHCR7	1	1.00	2	0.79	1	1.18
Q9NR19	Acetyl-coenzyme A synthetase, cytoplasmic	ACSS2			1	1.57	1	1.14
P37268	Squalene synthase	FDFT1	2	0.73	3	0.67	1	1.25
O00767	Acyl-CoA desaturase	SCD					1	2.63

Table 6.1 Selected interaction partners of RNF145. Three sets of RNF145 knockout HeLa cells stably expressing RNF145-V5 were sterol depleted overnight. The next day, one sample remained sterol depleted, another was treated with sterols for one hour and the other sample was treated with 50μM MG132 for 30 minutes before a 1-hour culture with sterols. The RNF145 knockout clone without RNF145-V5 was used as a negative control. $1x10^7$ cells from each condition were lysed and RNF145 was immunoprecipitated with anti-V5 antibody. Immunoprecipitates were analysed by mass spectrometry. Hits were excluded from RNF145-V5 samples if they were detected in the negative control. Proteins are ranked based on the number of unique peptides in the MG132 and sterol treated sample. Area is a measure of abundance. Full list in Appendix 3.

Immunoblot analysis demonstrated that the expression level of RNF145-V5 was only modestly higher than endogenous RNF145 (**Figure 6.6C**). It is therefore unlikely that the interaction partners identified in Table 6.1 are artefacts of protein over-expression. However, a recent analysis of Hrd1-interacting partners observed subtle differences between the immunoprecipitation of endogenous and over-expressed Hrd1 (Hwang, Walczak, et al. 2017).

To further investigate potential RNF145-interacting partners, I immunoprecipitated endogenous RNF145 followed by mass spectrometry analysis. Four sets of wild type HeLa cells were sterol depleted overnight. The next day, one sample remained sterol depleted, and samples were treated with 50 nM Bortezomib for 1.5 hours, sterols for 1 hour or 50 nM Bortezomib for 30 minutes followed by a further hour with sterols. In addition, an RNF145 knockout clone (8_20) was sterol depleted overnight and used as a negative control for non-specific binding to anti-RNF145 antibody and Protein A Sepharose (**Figure 6.11A**).

Of note, the number of unique peptides enriched with endogenous RNF145 was lower when compared with RNF145-V5 immunoprecipitation (full list in Appendix 4). An interpretation of this experiment is further complicated by the identification of RNF145 peptides in the immunoprecipitation from the RNF145 knockout clone (**Figure 6.11B**), presumably owing to the expression of a RNF145 truncated protein not detectable by immunoblot. The truncated protein might be able to associate with RNF145's interaction partners rendering this particular RNF145 knockout clone an inadequate negative control.

The immunoblot analysis of the total lysates and immunoprecipitates suggested there was an equivalent abundance of RNF145 in each sample (**Figure 6.11A**). However, the mass spectrometry identified a greater abundance of RNF145 peptides in Bortezomib treated samples (**Figure 6.11B**), consistent with a previous study (Cook et al. 2017).

HMGCR was identified in each RNF145 immunoprecipitation (**Figure 6.11B**), however the abundance of HMGCR that co-precipitated with RNF145 increased significantly when the cells were treated with sterols in the presence of Bortezomib. This is consistent with the model in which sterols promote the recruitment of RNF145 to HMGCR and HMGCR is then degraded by the proteasome. As this project moves forward, it will be critical to determine whether the interaction between HMGCR and RNF145 is dependent on the Insig proteins.

I also tried to take advantage of the BioID system to identify RNF145 interaction partners (Roux et al. 2012). BirA is a biotin ligase from E. coli that becomes highly promiscuous when arginine 118 is mutated to glycine (R118G). BirA R118G biotinylates proteins in close proximity, which can then be identified by a streptavidin immunoprecipitation and mass spectrometry (Roux et al. 2012). Unfortunately, the C-terminal BirA-tagged RNF145 fusion protein would not express in HeLa cells and the N-terminal BirA tagged RNF145 fusion protein was cleaved. I therefore could not pursue BioID as a method to identify RNF145 interaction partners.

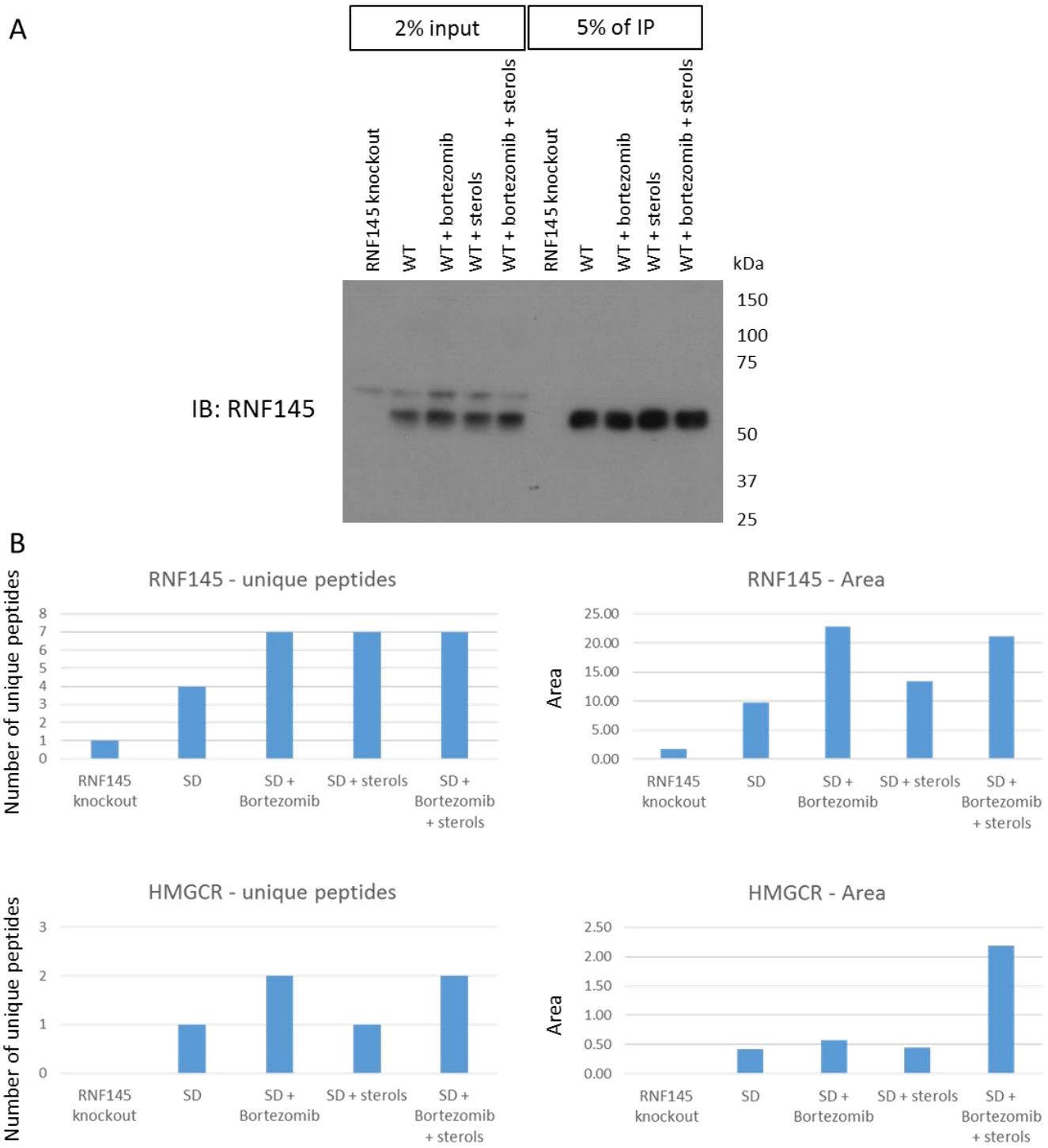

Figure 6.11 Identification of HMGCR as an endogenous RNF145 interaction partner (A) Four sets of wild type HeLa cells were sterol depleted overnight. The following day, one sample remained sterol depleted, one sample was treated with 50nM Bortezomib for 1.5 hours, one sample was treated with sterols for 1 hour and the last sample was treated with 50nM Bortezomib for 30 minutes followed by a 1-hour culture with sterols. An RNF145 knockout clone (8_20) was also sterol depleted overnight. $1x10^7$ cells from each condition were lysed and endogenous RNF145 was immunoprecipitated with anti-RNF145 antibody. Five percent of the immunoprecipitates were resolved by SDS-PAGE to confirm the efficient enrichment of RNF145. The immunoprecipitates were analysed by mass spectrometry. Full list of proteins in Appendix 4. **(B)** The number of unique peptides and the abundance of RNF145 and HMGCR in the immunoprecipitates described in (A) measured by mass spectrometry (SD, sterol depleted).

6.2.11 Gp78 might stabilise RNF145 during sterol-induced HMGCR ubiquitination

The findings in this chapter suggest that gp78 and RNF145 are Insig-associated E3 ubiquitin ligases that ubiquitinate HMGCR. One of the current aims of the project is to determine whether gp78 and RNF145 influence each other's expression or stability. In a preliminary experiment, the expression of RNF145 was analysed in the presence or absence of gp78, in different sterol conditions, with or without the proteasome inhibitor MG132 (**Figure 6.12**).

In wild type HeLa cells, the expression of RNF145 initially appears to be induced by sterol depletion. This experiment has not been repeated and so I cannot rule out the inefficient transfer of RNF145 from the acrylamide gel to the PVDF membrane to account for the reduced RNF145 signal in the outer lanes of this immunoblot (**Figure 6.12**).

In gp78 knockout cells, there is a marked increase in RNF145 expression in MG132-treated cells following the addition of sterols to a sterol-depleted culture (**Figure 6.12**). This suggests that RNF145 is co-degraded following sterol-induced HMGCR ubiquitination. The presence of gp78 might prevent the degradation of RNF145 by sharing the ubiquitination of HMGCR. Alternatively, given that gp78 was identified as a potential RNF145-interaction partner by mass spectrometry (**Table 6.1**), the association of RNF145 with gp78 might stabilise RNF145. This preliminary observation suggests that gp78 and RNF145 influence each other and understanding the relationship between the two E3 ligases is critical. This result (**Figure 6.12**) needs to be repeated and it will be interesting to see if gp78 is affected by the loss of RNF145.

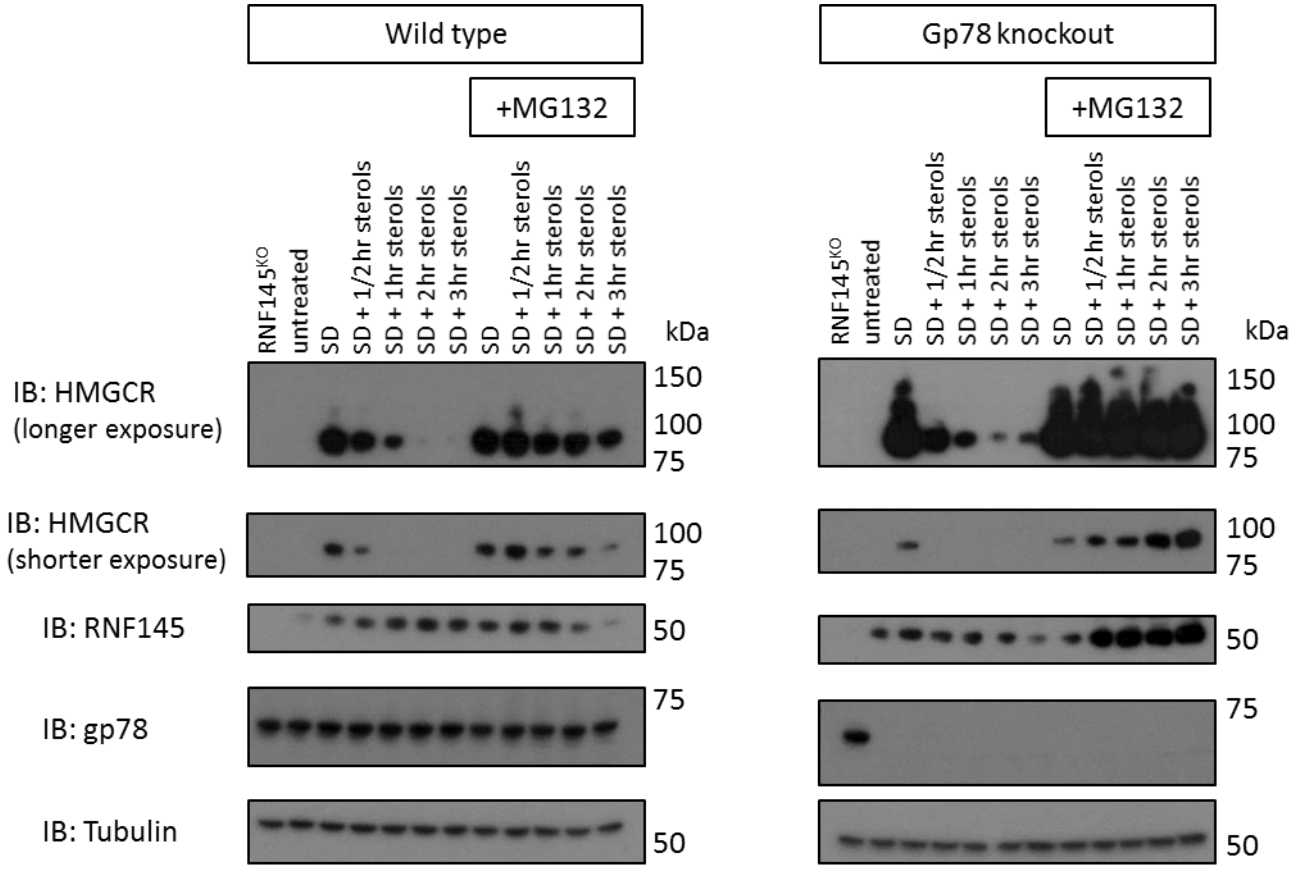

Figure 6.12 RNF145 is degraded in the absence of gp78 by sterol repletion following sterol depletion. Wild type HeLa cells or gp78 knockout (clone 4_2) were sterol depleted overnight. The following day, sterols were added back into the sterol depleted culture for the indicated period. 50 µM MG132 was added to the indicated samples 30 min before the addition of sterols. Cells were lysed and analysed by immunoblot.

6.3 Discussion

6.3.1 CRISPR-mediated gene disruption versus RNA interference

Throughout this thesis project I have used CRISPR-mediated gene disruption to create knockout cell lines for loss-of-function analysis. Previously, projects relied on RNAi to deplete genes of interest. However, gene silencing with siRNA or shRNA is typically incomplete. The UBE2G2 CRISPR clone C1 (**Figure 6.8A**) is extraordinary as it is a heterozygous knockout with extremely low UBE2G2 protein abundance. The difference in UBE2G2 expression between clone C1 and the parental wild-type HeLa cells would represent a very efficient knockdown. However, residual UBE2G2 protein was sufficient to mediate the sterol-induced degradation of HMGCR (**Figure 6.8C**), emphasising the superiority of CRISPR-mediated gene disruption.

A disadvantage of CRISPR-mediated gene disruption is that it takes longer to generate gene knockouts than for a gene to be depleted by RNAi. When I transfected control cells with gp78-targeting siRNA, I observed a decrease in the sterol-induced degradation of HMGCR-Clover (**Figure 6.1**). Depleting gp78 in RNF145 knockout cells resulted in a greater decrease in the sterol-induced degradation of HMGCR-Clover. This raises the question, does the gp78 siRNA cause a phenotype due to the depletion of gp78 or an off-target effect of the siRNA? The Weissman laboratory made a convincing argument that the reduced rate of sterol-induced HMGCR degradation seen by the Debose Boyd laboratory following gp78 depletion is the result of siRNA off-target effects (Tsai et al. 2012). However, I used a different gp78 siRNA sequence to the Debose Boyd laboratory at a lower concentration and so it is unlikely that I observed the consequences of the same off-target effect. This raises the possibility that the acute loss of gp78 leads to a decreased rate of sterol-induced HMGCR degradation (**Figure 6.1**), however over time the cell adapts so that the loss of gp78 does not impair the sterol-induced degradation of HMGCR (**Figure 6.2A**).

The depletion of a gene by RNAi can be readily determined by quantitative real-time (qPCR). The absence of a gene-specific antibody complicates determination of CRISPR-mediated gene knockout efficiency. Alternatively, gene knockouts can be confirmed by sequencing the gRNA-targeted genomic locus to confirm frame-shift insertions or deletions in all alleles, as was initially done to identify RNF145 knockout clones in Chapter 5. However, this method cannot be applied to a heterogenous population.

6.3.2 Gp78 and RNF145 mediate the sterol-induced degradation of HMGCR

Despite identification of RNF145 in two genome-wide CRISPR screens, only a small decrease in HMGCR reporter degradation was observed in CRISPR validation experiments. Consequently, I postulated the existence of an additional E3 ligase mediating the ubiquitination of HMGCR in the absence of RNF145. To test this hypothesis, I used CRISPR-mediated gene disruption and RNA interference to abolish gp78 or TRC8 in the presence or absence of RNF145. I consistently saw a significant decrease in the sterol-induced degradation of HMGCR in the absence of both gp78 and RNF145 (**Figure 6.1, 6.2**, **6.3** and **6.4**). The re-expression of RING-mutant RNF145 could not restore HMGCR degradation in a gp78 and RNF145 double knockout cell line, indicating that the E3 ligase activity of RNF145 is required for HMGCR degradation (**Figure 6.6A**). A gp78 and RNF145 double knockout clone showed a significant reduction in sterol-induced HMGCR ubiquitination, whereas robust ubiquitination of HMGCR was observed in single gp78 or RNF145 knockout clones (**Figure 6.9**). This suggests that gp78 and RNF145 both ubiquitinate HMGCR and these two E3 ligases act in parallel, rather than sequentially. I did not observe any role for TRC8 in HMGCR degradation in HeLa cells (**Figure 6.1** and **Figure 6.2B**).

The sterol-induced degradation of HMGCR is dependent on the Insig proteins, which interact with HMGCR's sterol sensing domain at high cellular cholesterol levels (Sever, Yang, et al. 2003, Sever, Song, et al. 2003). The Debose Boyd laboratory have previously implicated gp78 as the E3 ligase responsible for HMGCR degradation (Song, Sever, and DeBose-Boyd 2005, Jo et al. 2011). They observed the constitutive association of gp78 with Insig1 and a sterol dependent interaction between gp78 and HMGCR that was dependent on Insig1 (Song, Sever, and DeBose-Boyd 2005, Jo et al. 2011). The model for gp78-mediated ubiquitination of HMGCR therefore uses Insig1 as a sterol sensitive scaffold protein to recruit gp78 to HMGCR at high cholesterol levels.

I observed RNF145 interacting with both Insig1 and Insig2 independent of sterols (**Figure 6.10B**). This therefore places RNF145 in the position to be recruited to HMGCR by both Insig proteins in a sterol dependent manner. I identified HMGCR as a RNF145 interaction partner by mass spectrometry. This interaction was enhanced by sterols and proteasome inhibition

(**Table 6.1** and **Figure 6.11**). Future work on this project will aim to determine whether the interaction between HMGCR and RNF145 is dependent on the Insig proteins. However, the evidence presented in this Chapter strongly suggests that RNF145, like gp78, is recruited to HMGCR by the Insig proteins to mediate HMGCR ubiquitination.

6.3.3 ERAD pathways with multiple E3 ligases

Previous reports have also implicated the action of multiple E3 ubiquitin ligases on ERAD substrates. Most cystic fibrosis patients carry the ΔF508 mutation in the Cystic Fibrosis Transmembrane Conductance Regulator (CFTR) protein that inhibits protein folding and leads to the degradation of CFTRΔF508 by the UPS (Kopito 1999). RNF5 (RMA1) and CHIP ubiquitinate CFTRΔF508, however, they recognise different misfolded domains of CFTRΔF508 at different protein quality control checkpoints (Younger et al. 2006).

Gp78 has been shown to ubiquitinate CFTRΔF508 in cooperation with RNF5 in an ERAD pathway independent of CHIP (Morito et al. 2008). RNF5 initiates the degradative pathway by mono-ubiquitinating CFTRΔF508. Gp78 then binds to mono-ubiquitinated CFTRΔF508 via its CUE domain and mediates poly-ubiquitination. Accordingly, gp78 failed to ubiquitinate CFTR when RNF5 had been depleted by RNAi (Morito et al. 2008). It is unlikely that gp78 and RNF145 act sequentially on HMGCR because robust ubiquitination of HMGCR is seen in the single ligase knockout clones (**Figure 6.9B**). The significant block in HMGCR ubiquitination in the absence of both gp78 and RNF145 suggests that the ligases act on HMGCR in parallel.

RNF5 and RNF185 share 70% sequence identity and are functionally redundant for CFTRΔF508 degradation (El Khouri et al. 2013). The knockdown of either ligase caused a small increase in CFTRΔF508 expression, whereas the simultaneous knockdown of both ligases resulted in a dramatic increase in CFTRΔF508 expression and a significant decrease in its post-translational degradation (El Khouri et al. 2013). This ERAD pathway is reminiscent of the combined involvement of gp78 and RNF145 in HMGCR degradation. The loss of one ligase is compensated for by a second E3 ligase and concomitant only the loss of both ligases results in a marked decrease in degradation.

Co-operation between Hrd1 and gp78 has also been reported for the ERAD of model substrates MHC-147 and TCRα (Zhang et al. 2015). However, only Hrd1 depletion reduced ubiquitination of MHC-147 and TCRα. The authors propose that gp78 is required for the correct function of the BAG6 complex, which assists the delivery of aggregate-prone, retrotranslocated ERAD substrates to the proteasome (Wang, Liu, et al. 2011, Liu et al. 2014, Zhang et al. 2015). Given that the loss of RNF145 alone does not cause a significant loss of HMGCR ubiquitination, gp78 must be able to ubiquitinate HMGCR and is not primarily influencing HMGCR ERAD via the BAG6 complex.

6.3.4 Why are multiple E3 ligases required for HMGCR degradation?

My data and previously published data point towards a model in which gp78 and RNF145 are constitutively associated with the Insig proteins (Song, Sever, and DeBose-Boyd 2005). In the presence of sterols, the Insig proteins recruit gp78 and RNF145 to HMGCR leading to the ubiquitination and subsequent degradation of HMGCR. This mechanism is strikingly different from the ubiquitination of the yeast HMGCR ortholog, Hmg2, by Hrd1. A sterol intermediate, farnesyl pyrophosphate, induces a conformational change in Hmg2's sterol sensing domain that is recognised by Hrd1p (Garza, Tran, and Hampton 2009, Shearer and Hampton 2005, Theesfeld and Hampton 2013). In stark contrast to human cells, the Insig ortholog, Nsg1, is stimulated by lanosterol to associate with Hmg2 to block the degradation of Hmg2 (Flury et al. 2005, Theesfeld and Hampton 2013).

The re-purposing of the Insig proteins to act as scaffold factors to promote the sterol-induced degradation of HMGCR might allow the coordination of multiple E3 ubiquitin ligases to give finer control over HMGCR expression in different cell types that have different sterol requirements. All cell types must be able to maintain cholesterol homeostasis by balancing endogenous cholesterol biosynthesis and cholesterol uptake. However, the liver is a major organ for lipid biosynthesis and so hepatic cells might adapt the regulation of the cholesterol biosynthesis pathway to enable greater cholesterol production. Individual ligase knockout HeLa clones shown in this study demonstrate no decrease in sterol-induced degradation of HMGCR. This is consistent with gp78 knockout MEFs and gp78-depleted human fibroblasts (Tsai et al. 2012). In contrast to gp78 knockout MEFs, gp78 knockout mouse hepatocytes show

a significant decrease in sterol-induced HMGCR degradation (Liu et al. 2012). Another striking feature of the gp78 knockout mouse hepatocytes is their significant rescue of Insig2 at steady state and impaired degradation of Insig2 in a cycloheximide chase experiment. Previous studies saw no effect of sterols or gp78 depletion on exogenous Insig2 stability in Chinese Hamster Ovary (CHO) cells or human fibroblasts (Lee, Gong, et al. 2006, Lee, Song, et al. 2006). These observations show that there is a difference between how epithelial cells and hepatocytes regulate HMGCR and the Insig proteins. In this thesis project, I have only assessed HMGCR degradation in HeLa cells. As the project moves forward, it will be interesting to analyse how the relative contribution of gp78 and RNF145 to HMGCR degradation varies between cell types and how this correlates with differential cholesterol metabolism.

In this thesis project, I have induced the degradation of HMGCR by adding cholesterol and 25-hydroxycholesterol to cells that have been sterol depleted overnight. HMGCR degradation can also be induced by other sterol intermediates, such as mevalonate and 24,25-dihydrolanosterol (Song, Javitt, and DeBose-Boyd 2005, Lange et al. 2008). It is possible that different stimuli favour the recruitment of different ubiquitin E3 ligases to HMGCR.

6.4 Summary

In this chapter, I used siRNA-mediated gene depletion and CRISPR-mediated gene disruption to identify gp78 and RNF145 as functionally redundant ubiquitin E3 ligases for the sterol-induced degradation of HMGCR. In the absence of either E3 ligase there is little or no decrease in the sterol-induced ubiquitination and degradation of HMGCR. However, in the absence of both gp78 and RNF145 I observed a significant decrease in the sterol-induced ubiquitination and degradation of HMGCR. The Debose-Boyd laboratory has previously shown that gp78 is recruited to HMGCR by the Insig proteins in response to sterols (Sever, Yang, et al. 2003). Co-precipitation experiments presented in this thesis demonstrate that RNF145 interacts with both Insig1 and Insig2 independent of the cellular sterol conditions. I also observed a sterol sensitive interaction between RNF145 and HMGCR that was enhanced by proteasome inhibition. Together these findings support a model in which both RNF145 and gp78 are recruited to HMGCR by the Insig proteins to mediate the ubiquitination of HMGCR.

Chapter 7: Hrd1-mediated degradation of HMGCR in the absence of gp78 and RNF145

7.1 Introduction

Whilst the loss of gp78 and RNF145 causes a significant block in the sterol-induced degradation of HMGCR, I always observed a lower abundance of HMGCR in cells that were cultured with sterols after sterol depletion compared to cells that remained under sterol deplete conditions. I also consistently observed less sterol-induced degradation of HMGCR in the absence of UBE2G2 than in the absence of both gp78 and RNF145. I hypothesised that there was at least one other ubiquitin E3 ligase that ubiquitinates HMGCR in response to sterols. The aim of this section of my thesis project was to identify more ubiquitin E3 ligases that mediate the sterol-induced degradation of HMGCR and to determine the redundancy with gp78 and RNF145.

7.2 Results

7.2.1 The degradation of HMGCR is mediated by gp78, RNF145 and at least one more elusive E3 ligase

So far, I have assumed that gp78 and RNF145 both use UBE2G2 as the E2 ubiquitin conjugating enzyme to mediate the ubiquitination of HMGCR. To confirm this assumption, I used CRISPR-mediated gene disruption to knockout UBE2G2 in the gp78 and RNF145 double knockout HMGCR-Clover cell line. Surprisingly, this result gave me two significant results (i) a significant increase in HMGCR-Clover at steady state and (ii) a complete block in sterol-induced HMGCR-Clover degradation (**Figure 7.1A**). If two genes are in the same pathway, the combined loss of the two genes will not have an additive effect. In contrast, if the combined loss of two genes has an additive effect, the genes act in at least two independent pathways. Critically, an additive effect does not rule out the possibility that both genes also act in the same pathway. Therefore, the additive effect at both steady state and following sterol depletion of losing UBE2G2 on top of the double ligase knockout leads to two important conclusions. Firstly, there is at least one more E3 ubiquitin ligase that uses UBE2G2 to mediate HMGCR ubiquitination. Secondly, either gp78 or RNF145 can use another E2 ubiquitin conjugating enzyme to mediate HMGCR ubiquitination. If both gp78 and RNF145 only used UBE2G2 to mediate HMGCR degradation, there would not be an additive effect of losing gp78 and RNF145 in combination with the loss of UBE2G2.

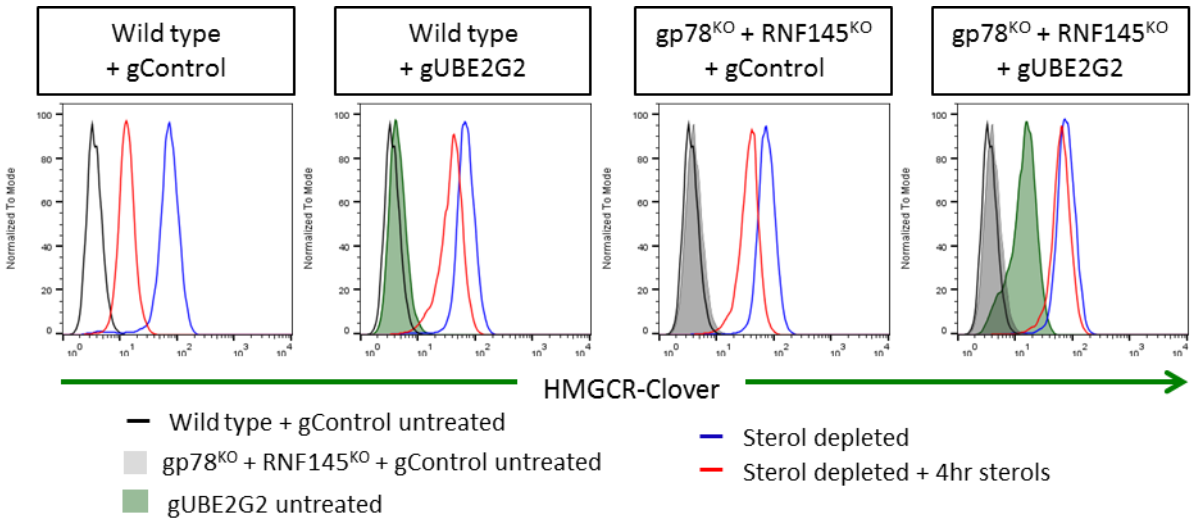

Figure 7.1 An elusive E3 ligase requires UBE2G2 and Insig1 to mediate HMGCR degradation in the absence of gp78 and RNF145. Wild type or gp78 and RNF145 double knockout HMGCR-Clover HeLa cells were transiently transfected with Cas9 and either a control gRNA or a pool of three UBE2G2-targeting gRNAs. Transfected cells were selected by puromycin treatment. The cells were sterol depleted overnight eight days post transfection, then cultured for a further four hours in the presence or absence of sterols. HMGCR-Clover expression was assessed by flow cytometry. Representative of three independent experiments.

I next sought to determine which E3 ligase can use another E2 enzyme. The loss of UBE2G2 and either gp78 or RNF145 resulted in a significant rescue of HMGCR-Clover at steady state (**Figure 7.2A**). However, only the loss of both gp78 and UBE2G2 resulted in a near-complete block in sterol-induced HMGCR-Clover degradation. Whilst this data does not mean that gp78 does not use UBE2G2 to mediate HMGCR ubiquitination, it indicates that gp78 can use another E2 conjugating enzyme.

The model for the sterol-induced degradation of HMGCR is dependent upon the Insig proteins acting as sterol sensitive scaffold factors (Sever, Song, et al. 2003). I next sought to determine whether the elusive E3 ligase is dependent on the Insig proteins to degrade HMGCR. I found that the loss of Insig1 in the gp78 and RNF145 double knockout HMGCR-Clover line lead to a near-complete block in sterol-induced HMGCR-Clover degradation (**Figure 7.2B**). In contrast, the loss of Insig2 in the gp78 and RNF145 double knockout line had no additional effect on the degradation of HMGCR-Clover.

Since there is an additive effect of UBE2G2 and Insig1 in the combined absence of gp78 and RNF145, it is therefore likely that the elusive E3 ligase(s) uses UBE2G2 and Insig1 to mediate the sterol-induced ubiquitination of HMGCR in the absence of gp78 and RNF145.

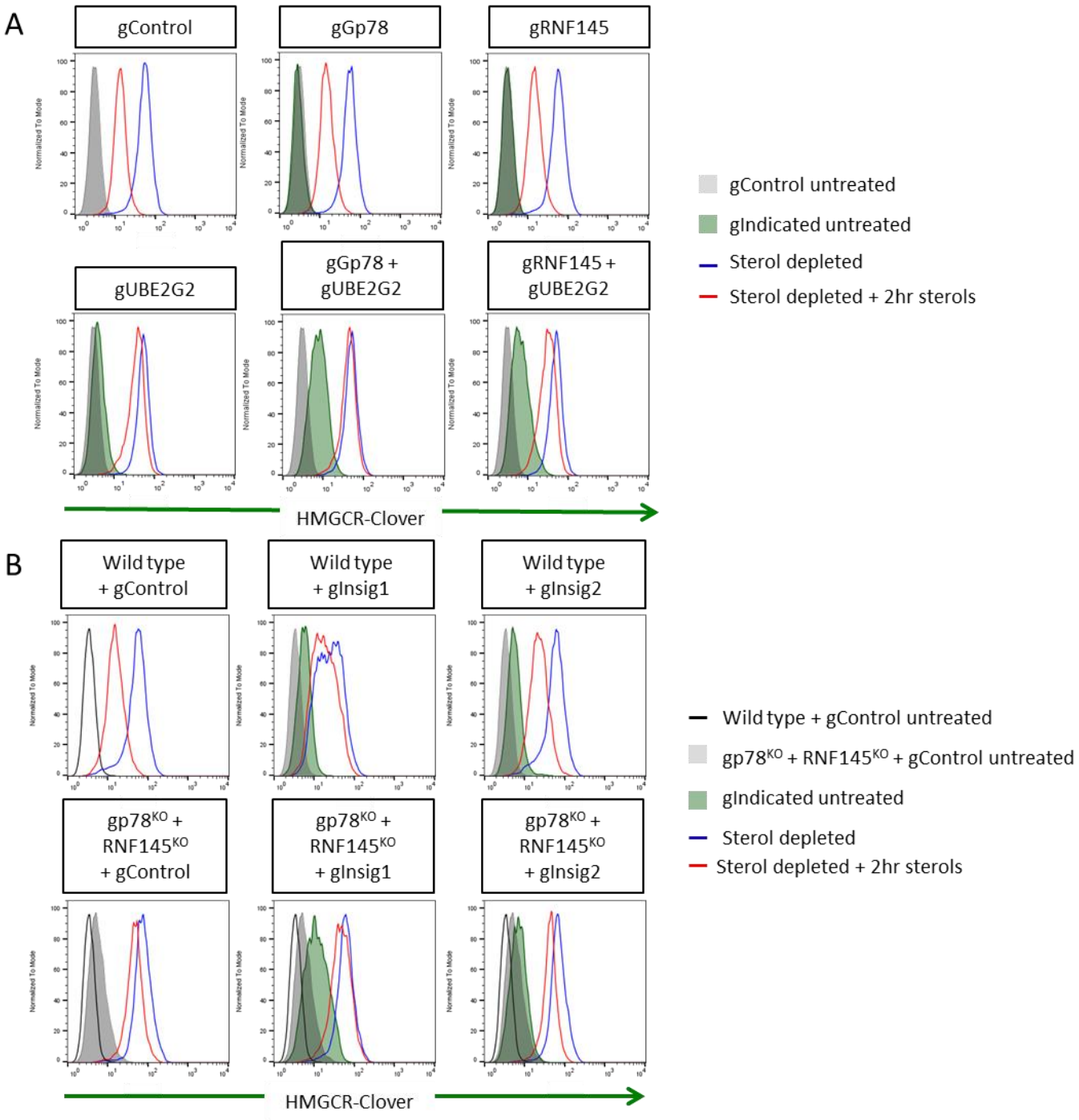

Figure 7.2 The elusive E3 ligase requires UBE2G2 and Insig1 to mediate HMGCR degradation in the absence of gp78 and RNF145 (A) Wild type HMGCR-Clover HeLa cells were transfected with a control gRNA, a pool of three UBE2G2-targeting gRNAs, a pool of four gp78-targeting gRNAs, a pool of four RNF145-targeting gRNAs or a combination of these gRNA pools. Transfected cells were selected with puromycin treatment. Cell were sterol depleted overnight eight days post transfection, then cultured for a further two hours in the presence or absence of sterols. **(B)** Wild type or gp78 and RNF145 double knockout HMGCR-Clover HeLa cells were transiently transfected with a control gRNA, a pool of four Insig1-targeting gRNAs or a pool of four Insig2-targeting gRNAs. Transfected cells were selected with puromycin treatment and HMGCR-Clover degradation was assessed as in (A). Representative of two independent experiments.

7.2.2 TRC8 is not involved in the sterol-induced degradation of HMGCR

The obvious candidate gene for the elusive E3 ligase was TRC8, which associates with Insig1 and uses UBE2G2 to ubiquitinate substrates (Brauweiler et al. 2007, Lee et al. 2010). I have already tested TRC8 as a candidate gene for E3 ligases that might be redundant with RNF145 and observed no requirement for TRC8 (**Figure 6.1** and **Figure 6.2B**). I used the same gRNA from Figure 6.2C, which consistently results in a population of >70% TRC8 knockouts, to knockout TRC8 in the gp78 and RNF145 double knockout HMGCR-Clover cell line. The cells transfected with the TRC8-targeting gRNA were indistinguishable from control cells (**Figure 7.3A**). TRC8 is therefore not the missing ubiquitin E3 ligase.

To confirm that the loss of TRC8 similarly had no effect on wild type HMGCR, I transfected wild type HeLa cells, a gp78 knockout HeLa clone, a RNF145 knockout clone and a gp78 and RNF145 double knockout clone with the TRC8-targeting gRNA. The loss of TRC8 did not result in any difference in sterol-induced HMGCR degradation in any of these genetic backgrounds (**Figure 7.2B**). I have not observed a role for TRC8 in the sterol-induced degradation of HMGCR throughout this thesis project. The US2-mediated down-regulation of MHC-I demonstrated that TRC8 is expressed in HeLa cells (**Figure 6.2C**) (Stagg et al. 2009).

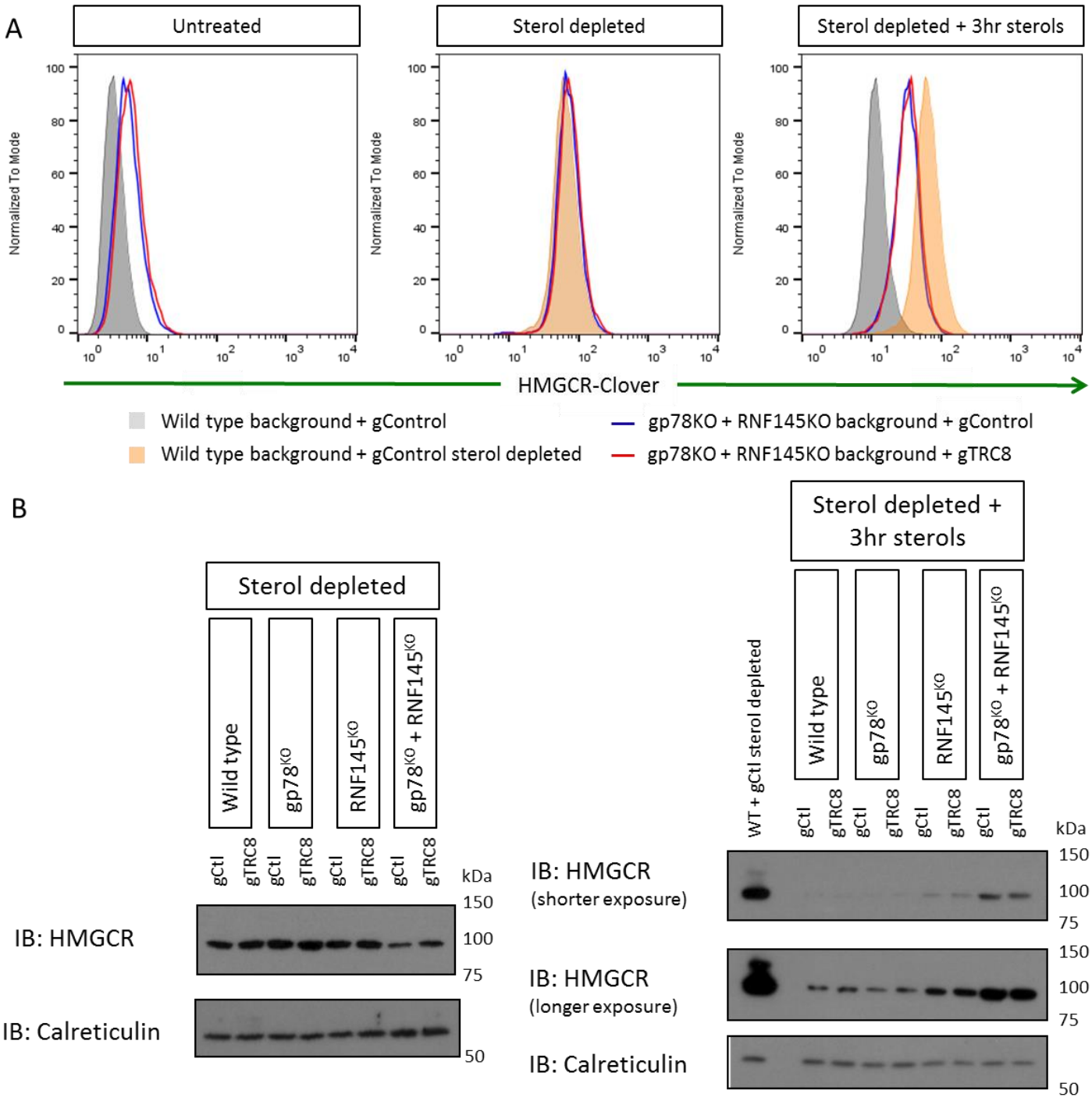

Figure 7.3 TRC8 is not required for the sterol-induced degradation of HMGCR (A) Gp78 and RNF145 double knockout HMGCR-Clover HeLa cells were transfected with Cas9 and either a control gRNA or TRC8-targeting gRNA. Transfected cells were selected with puromycin treatment. Cells were sterol depleted overnight eight days post transfection, then cultured for a further three hours in the presence or absence of sterols. HMGCR-Clover expression was assessed by flow cytometry. **(B)** Wild type HeLa cells, gp78 knockout clone 4_2, RNF145 knockout clone 5_7 and gp78 and RNF145 double knockout clone 5_7 #7 were transiently transfected with Cas9 and either a control gRNA or TRC8-targeting gRNA. Transfected cells were sterol depleted overnight eight days post transfection, then cultured for a further three hours in the presence or absence of sterols. Cells were lysed and immunoblotted for HMGCR (WT, wild type; Ctl, control; KO, knockout).

7.2.3 A focused ubiquitin E3 ligase CRISPR knockout screen identifies Hrd1 and RNF185 as additional E3 ligases required for HMGCR-Clover degradation

The Lehner laboratory, in collaboration with James Nathan's laboratory, has created a gRNA library for ubiquitin-related genes. This library is made up of 6 sub-pools: E1s/E2s, E3 ligases, deubiquitinating enzymes, ubiquitin-binding/-like proteins, proteasome components and control gRNAs. I decided to use the E3 ligase sub-pool to perform a focused CRISPR screen in the gp78 and RNF145 double knockout HMGCR-Clover cell line to identify the elusive E3 ligase that can also mediate HMGCR ERAD. To focus the screen on the sterol-induced degradation of HMGCR, I used the same FACS strategy that identified RNF145 in Figure 5.5. This involved sterol depleting the mutagenised library overnight, then treating the culture with sterols for five hours before selecting HMGCR-Clover^{high} mutants by FACS.

The gp78 and RNF145 double knockout HMGCR-Clover cell line was transduced with the nuclease Cas9 and Cas9 activity was confirmed with the control B2M gRNA. The Cas9-expressing double knockout cell line was transduced at a M.O.I. of 0.3 with the E3 ligase gRNA library. Transduced cells were selected with puromycin and cells with a decreased rate of sterol-induced HMGCR degradation were selected by FACS on day 8 using the FACS strategy described above. Given that the size of the library was significantly smaller than the genome wide libraries (8300 gRNAs compared to 211,695 gRNAs in the Bassik genome wide library) I only carried out one round of FACS and subsequent DNA extraction. I expanded 20,000 cells so that I could test the enrichment from the sorting process. The selected population had a small enrichment, approximately 2%, of mutants that had a reduced ability to degrade HMGCR-Clover in response to sterols (**Figure 7.4A**).

I quantified the gRNAs in the selected cells and unselected library using the Illumina MiniSeq platform. The RSA algorithm identified two significantly enriched genes, RNF185 and Hrd1 (gene name *SYVN1*) (**Figure 7.4B**) (König et al. 2007). Although Hrd1 has previously been shown to be dispensable for HMGCR degradation, the identification of Hrd1 in this screen suggests that Hrd1 is functionally redundant with gp78 and RNF145 (Kikkert et al. 2004). RNF185 is an ER-localised E3 ubiquitin ligase that targets CFTRΔ508 for degradation and ubiquitinates cGAS to promote enzymatic activity (El Khouri et al. 2013, Wang, Huang, et al. 2017).

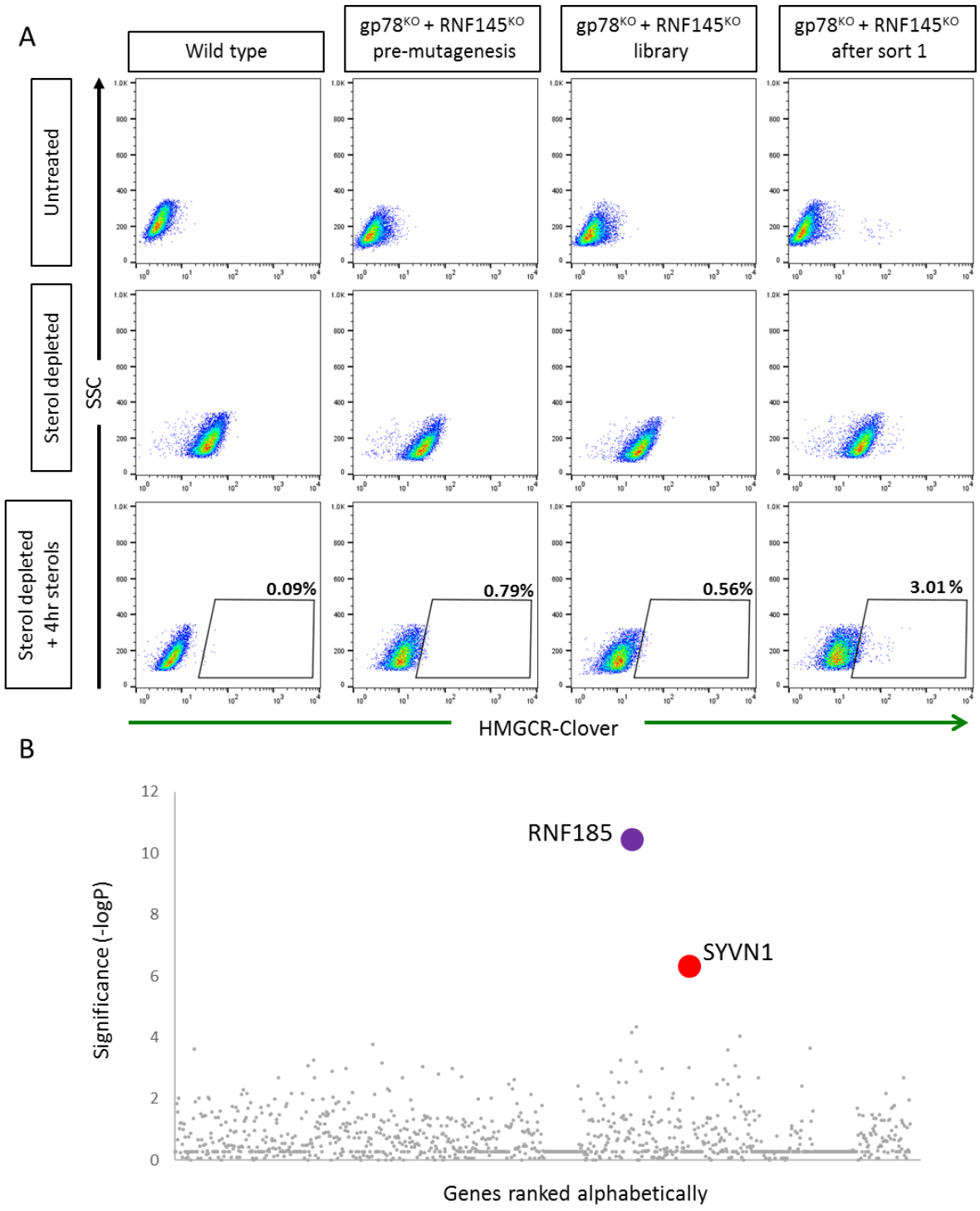

Figure 7.4 E3 ligase CRISPR screen in the gp78 and RNF145 double knockout HMGCR-Clover HeLa cell line (A) Cas9 expressing gp78 and RNF145 double knockout HMGCR-Clover HeLa cells were transduced with the E3 ligase library at an M.O.I. of 0.3. Transduced cells were selected with puromycin treatment. The mutagenised library was sterol depleted overnight eight days post gRNA library transduction. The following day, sterols were added into the sterol depleted culture for five hours and HMGCR-Clover^{high} cells were selected by FACS. 200,000 cells were lysed for genomic DNA extraction and 20,000 cells were expanded in culture. The enrichment of the selected population was tested by sterol depleting wild type, the starting gp78 and RNF145 double knockout, the mutagenised library and the selected HMCR-Clover cells overnight, followed by a four-hour culture in the presence or absence of sterols. HMGCR-Clover expression was assessed by flow cytometry. **(B)** The RSA algorithm identified RNF185 and Hrd1 (König et al. 2007).

7.2.4 Hrd1-mediated degradation of HMGCR in the absence of gp78 and RNF145

I used CRISPR-mediated gene disruption to validate the requirement of Hrd1 and RNF185 in the degradation of HMGCR-Clover in the absence of gp78 and RNF145. The loss of Hrd1 in the gp78 and RNF145 double knockout HMGCR-Clover cell line resulted in a dramatic increase in HMGCR-Clover at steady state, resembling the loss of UBE2G2 in the double knockout line (**Figure 7.5A**). In contrast, the loss of RNF185 alone did not alter steady-state HMGCR-Clover expression. However, loss of either Hrd1 or RNF185 in the absence of gp78 and RNF145 caused a complete block in sterol-dependent HMGCR-Clover degradation (**Figure 7.5A**).

I next sought to confirm that both Hrd1 and RNF185 degraded wild type HMGCR by using CRISPR-mediated gene disruption to knockout Hrd1 or RNF185 in a gp78 and RNF145 double knockout HeLa clone (5_7 #7). The loss of either Hrd1 or RNF185 increased wild type HMGCR steady state expression, with a larger increase in the absence of Hrd1 (**Figure 7.5B**). The loss of Hrd1 in a gp78 and RNF145 double knockout clone resulted in a complete block in sterol-induced HMGCR degradation (**Figure 7.5C**). However, the loss of RNF185 in a gp78 and RNF145 double knockout clone only had a minor effect on the sterol-induced degradation of HMGCR. The inconsistency between the effect of RNF185 on the degradation of HMGCR-Clover and wild type HMGCR suggests that RNF185 is targeting the Clover tag, rather than endogenous HMGCR.

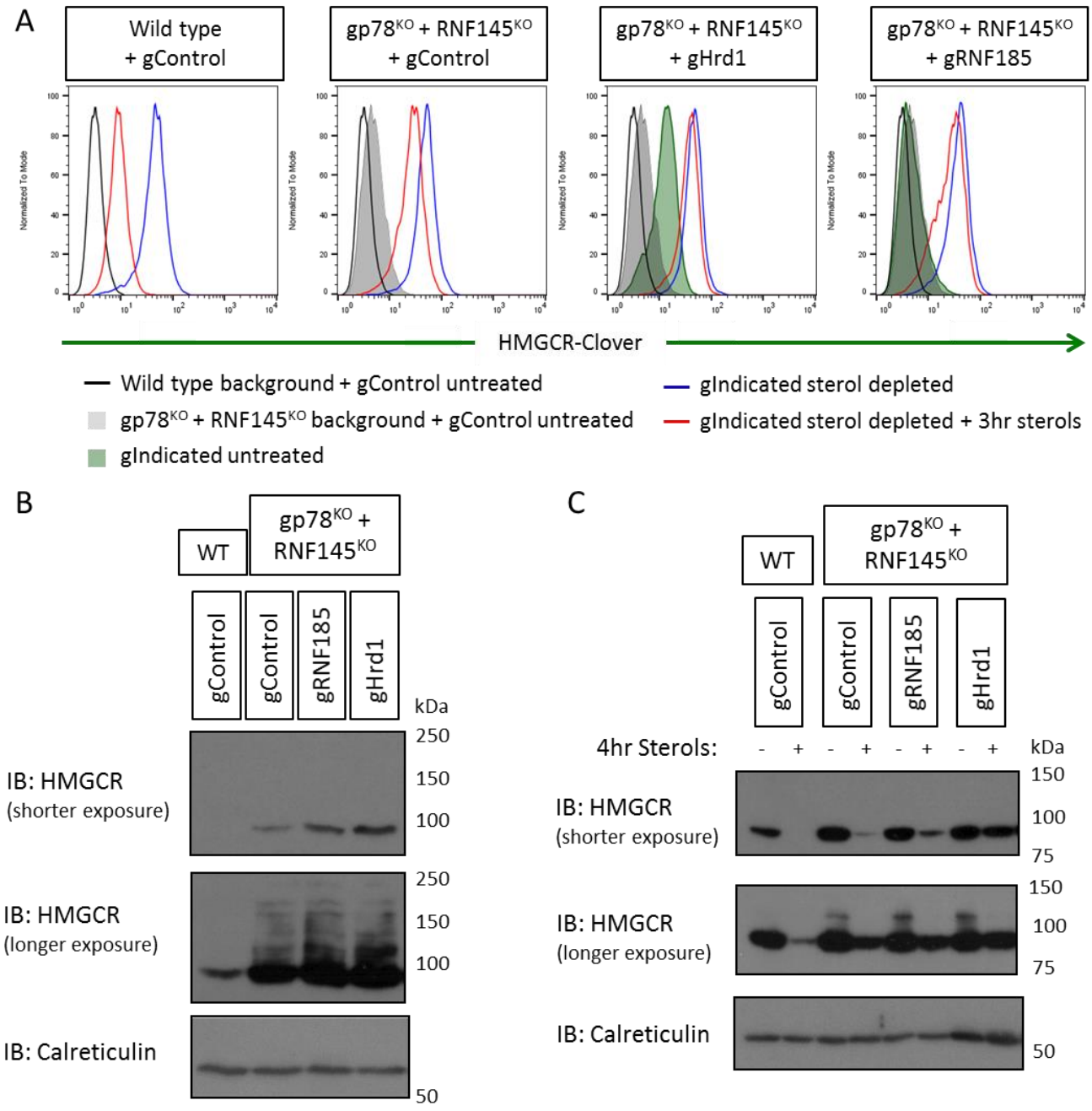

Figure 7.5 Hrd1-mediated degradation of HMGCR in the absence of gp78 and RNF145 (A) The gp78 and RNF145 double knockout HMGCR-Clover cell line was transiently transfect with Cas9 and either a control gRNA, a pool of four Hrd1-targeting gRNAs or a pool of four RNF185-targeting gRNAs. Transfected cells were selected with puromycin treatment. The cells were sterol depleted overnight eight days post transfection then cultured for a further three hours in the presence or absence of sterols. HMGCR-Clover expression was assessed by flow cytometry. **(B)** Wild type HeLa cells were transiently transfected with Cas9 and a control gRNA. A gp78 and RNF145 double knockout HeLa clone (5_7 #7) was transiently transfected with Cas9 and either a control gRNA, a pool of four Hrd1-targeting gRNAs or a pool of four RNF185-targeting gRNAs. Transfected cells were selected with puromycin treatment. Steady state HMGCR expression was determine by immunoblot analysis. (WT, wild type) **(C)** Sterol induced HMGCR degradation was determined of the cells in (B) by overnight sterol depletion eight days post gRNA transfection followed by a four-hour culture in the presence or absence of sterols. Cells were lysed and immunoblotted for HMGCR. Representative of three independent experiments.

To determine the redundancy of Hrd1 with gp78 and RNF145, I knocked-out Hrd1 in combination with gp78 or RNF145. The loss of Hrd1 did not inhibit the degradation of HMGCR-Clover in combination with the loss of gp78 or RNF145 (**Figure 7.6**). The only dual combination of ligases with a significant partial phenotype was the combination of gp78 and RNF145. There are two possibilities that could describe the partial redundancy of Hrd1 with gp78 and RNF145. Firstly, all three ligases can ubiquitinate HMGCR in a wild type cell, however Hrd1-mediated ubiquitination of HMGCR is inefficient and gp78 or RNF145 can ubiquitinate HMGCR efficiently in the absence of Hrd1. Secondly, gp78 and RNF145 are the primary E3 ligases for HMGCR degradation and Hrd1 ubiquitinates HMGCR only in the absence of the primary E3 ligases.

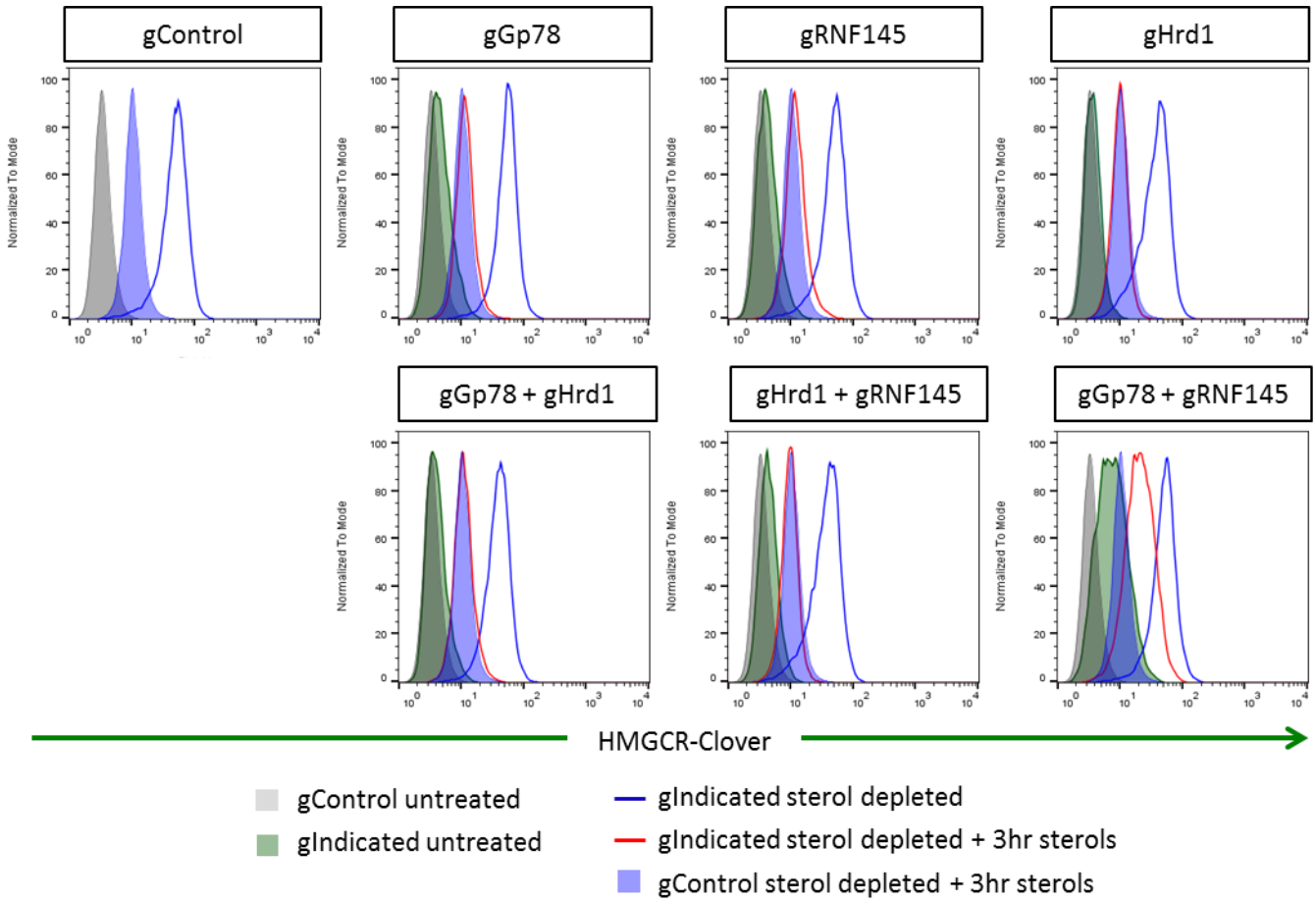

Figure 7.6 Hrd1 redundancy with gp78 and RNF145 in HMGCR-Clover degradation. Wild type HMGCR-Clover HeLa cells were transiently transfected with Cas9 and either a control gRNA or a pool of four gRNAs targeting the indicated gene. The sterol induced HMGCR-Clover degradation was assessed eight days post gRNA transfection.

7.2.5 Generating HMGCR-Clover UBE2G2 knockout clones

I also sought to identify the E2 conjugating enzyme that gp78 can use in addition to UBE2G2 to mediate the ubiquitination of HMGCR. I could have taken a candidate gene approach and knocked out the other E2 conjugating enzymes that have been implicated in ERAD so far, UBE2J1, UBE2J2 and UBE2K. However, I chose to use the E1 and E2 sub-pool of the Lehner and Nathan ubiquitome library in case another E2 was involved that had not previously been implicated in ERAD.

To create a cell line to perform an E2 screen; I generated UBE2G2 knockout HMGCR-Clover clones from two independent gRNAs. The absence of UBE2G2 was confirmed by immunoblot (**Figure 7.7A**). Each UBE2G2 knockout clone showed a significant block in sterol-induced HMGCR-Clover degradation (**Figure 7.7B**).

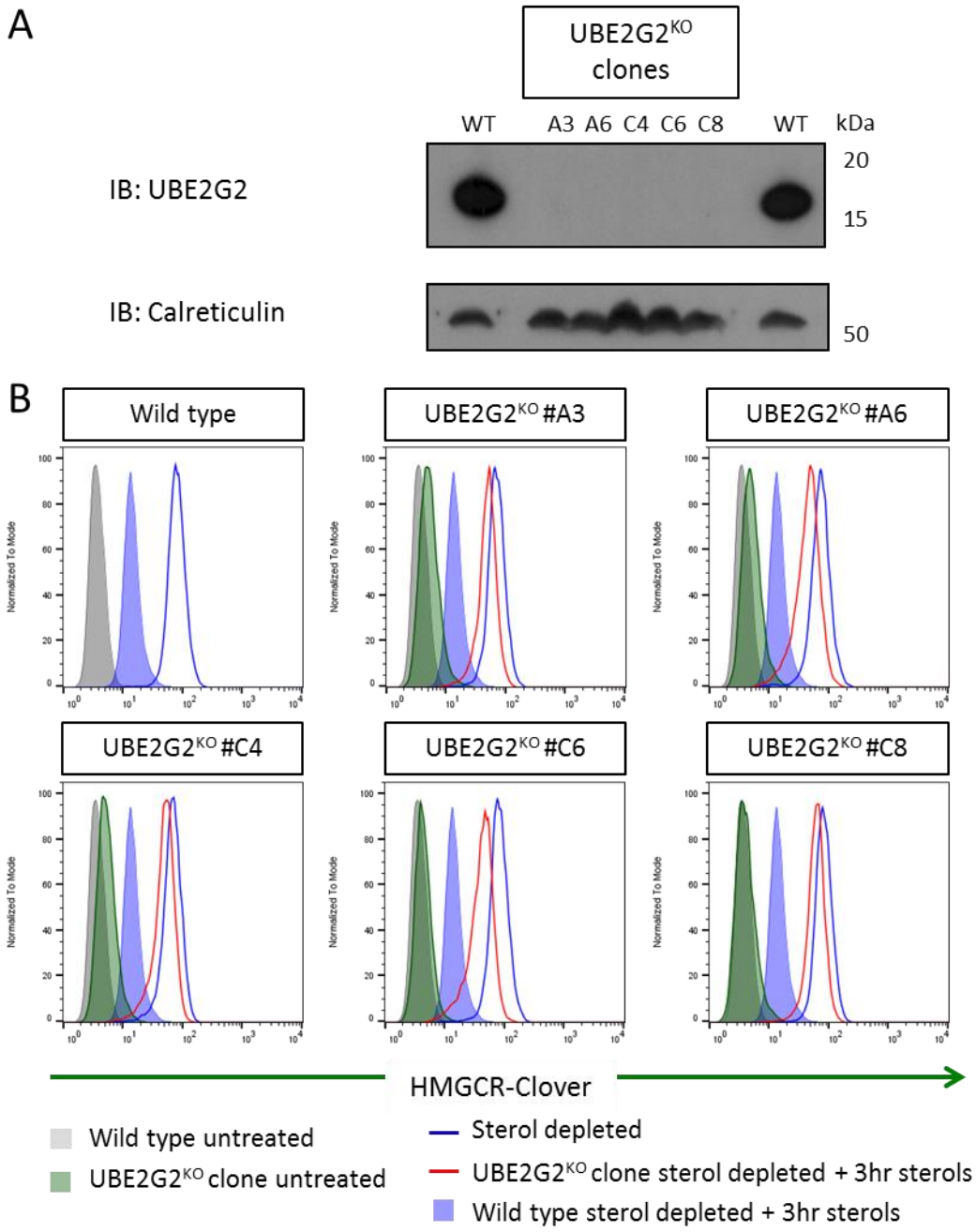

Figure 7.7 Isolating HMGCR-Clover UBE2G2 knockout clones (A) HMGCR-Clover HeLa cells were transiently transfected with Cas9 and a UBE2G2-targeting gRNA (either gRNA A or C). Transfected cells were selected with puromycin selection then single cell cloned by serial dilution. UBE2G2 knockout clones were identified by immunoblot. (WT, wild type) **(B)** Parental wild-type HMGCR-Clover HeLa cells and HMGCR-Clover UBE2G2 knockout clones were sterol depleted overnight then cultured for a further three hours in the presence or absence of sterols. HMGCR-Clover expression was assessed by flow cytometry.

7.2.6 A focused E2 conjugating enzyme CRISPR screen in a UBE2G2 knockout clone

The UBE2G2 knockout clone C8 (**Figure 7.7**) was transduced with a lentiviral vector encoding the nuclease Cas9. The Cas9-expressing C8 clone was transduced at an M.O.I. of 0.3 with the E1 and E2 sub-pool of the Lehner/Nathan ubiquitome gRNA library. The mutagensied library was sterol depleted overnight eight days later. The next day sterols were added to the sterol depleted library for five hours and HMGCR-Clover^{high} cells were selected by FACS. Genomic DNA was extracted from approximately 200,000 cells and 20,000 cells were expanded in culture. The selected population's ability to degrade HMGCR-Clover in response to sterols was tested, revealing a small enrichment of mutants with a reduced rate of sterol-induced HMGCR-Clover degradation (**Figure 7.8A**).

The abundance of the gRNAs in the selected cells was compared to an unselected library using the RSA algorithm (König et al. 2007). The RSA algorithm assigned a significant number of E2 enzymes a very high p-value (**Figure 7.8B**). However, this might be an artefact of using a small library with only 470 gRNAs. Encouragingly the highest ranking E2, UBE2K, has been implicated in ERAD as one of the E2 enzymes required for the downregulation of MHC-I by the human cytomegalovirus protein US11 and likely works with TMEM129 (Flierman et al. 2006, van den Boomen et al. 2014).

A

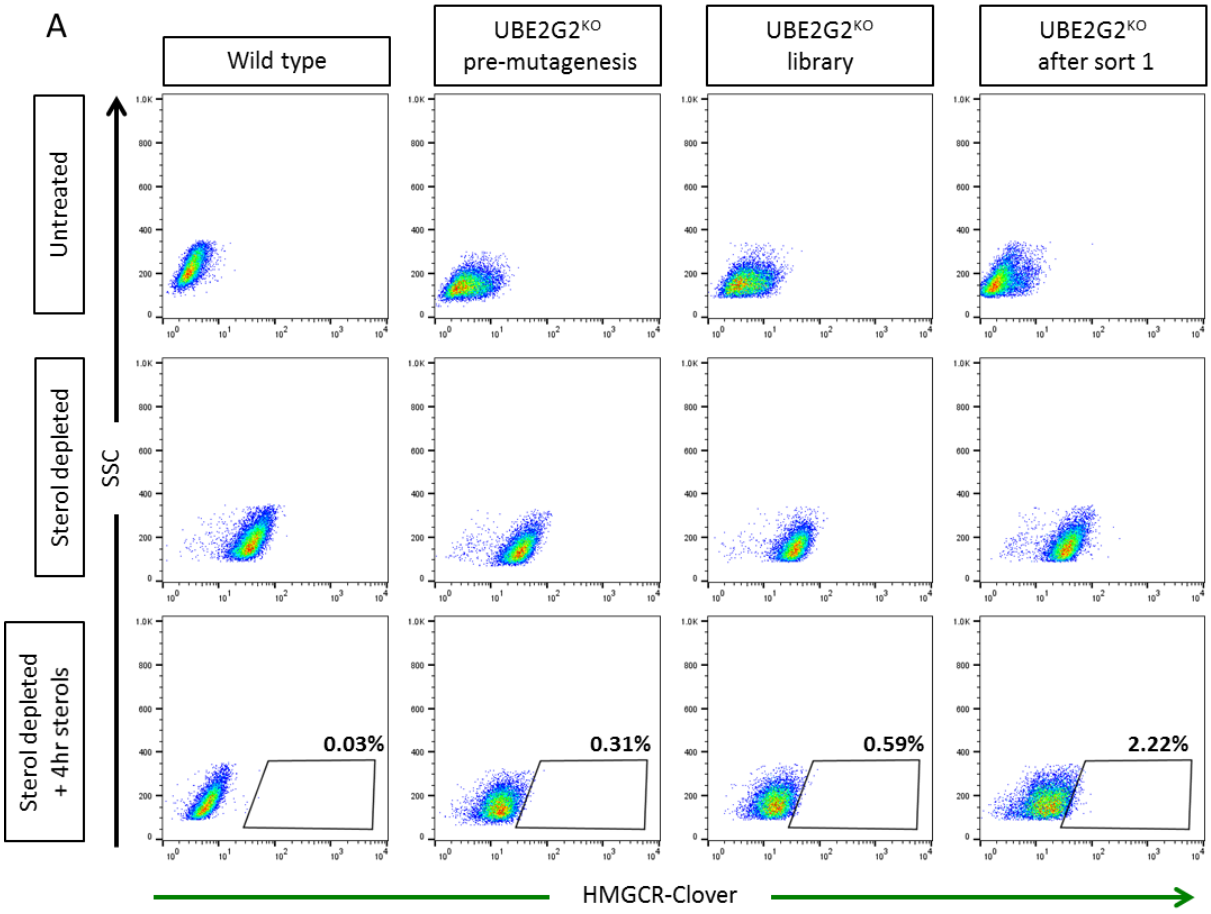

B

Gene_ID	Significance (-logP)
UBE2K	31.973
UBE2D2	20.122
AKTIP	16.577
UBE2N	16.513
UBE2QL1	11.225
UBE2I	10.645
UBA2	9.214
UBE2D3	9.004
UBE2O	8.95
UBE2E1	8.915
UBE2B	8.862
UBE2M	7.022
UBA7	6.934
UBE2E2	6.822
CDC34	6.768
UBA3	6.677
UBE2D1	5.317

Figure 7.8 E2 conjugating enzyme CRISPR screen in a UBE2G2 knockout clone (A) A focused E1/E2 CRISPR screen was performed using a UBE2G2 knockout HMGCR-Clover clone that used sterol depletion to focus on the sterol induced degradation of HMGCR-Clover. To determine the enrichment in the screen, wild type HMGCR-Clover cells, the starting UBE2G2 knockout clone, the mutagensised library and the selected cells were sterol depleted overnight and then cultured for a further four hours in the presence or absence of sterols. HMGCR-Clover expression was assessed by flow cytometry. **(B)** Candidate genes were identified using the RSA algorithm (König et al. 2007).

7.2.7 UBE2K mediates the sterol-induced degradation of HMGCR-Clover inefficiently in the absence of UBE2G2

I chose to knockout the second E2 from the screen, UBE2D2, using CRISPR-mediated gene disruption as well as the top hit, UBE2K (**Figure 7.8B**). The CRISPR validation was carried out in a different UBE2G2 knockout clone (A6) to the clone used in the screen.

The loss of either UBE2D2 or UBE2K in a UBE2G2 knockout background resulted in an increased HMGCR-Clover expression level at steady state (**Figure 7.9**, compare green to grey). At steady state, the combined absence of UBE2K and UBE2G2 resulted in a significantly greater increase in HMGCR-Clover expression than the combined absence of UBE2D2 and UBE2G2 and is similar to the combined loss of gp78, RNF145 and Hrd1. Furthermore, the loss of UBE2K in the UBE2G2 knockout clone completely blocked the sterol-induced degradation of HMGCR-Clover, whereas the loss of UBE2D2 in the UBE2G2 knockout clone did not further impair the sterol-induced degradation of HMGCR-Clover. When UBE2K was knocked out in wild type HMGCR-Clover cells, there was no difference in steady state HMGCR-Clover expression or sterol-induced HMGCR-Clover degradation. The loss of UBE2D2 in wild type HMGCR-Clover cells caused a small increase in steady state HMGCR-Clover expression, but did not affect sterol-induced HMGCR-Clover degradation.

Based on the data presented in Figure 7.2A and Figure 7.9, gp78 can mediate the ubiquitination of HMGCR with UBE2K in the absence of UBE2G2. Whilst UBE2D2 influences the steady state expression of HMGCR-Clover, I did not observe a requirement for UBE2D2 in the sterol-induced degradation of HMGCR-Clover (**Figure 7.9**).

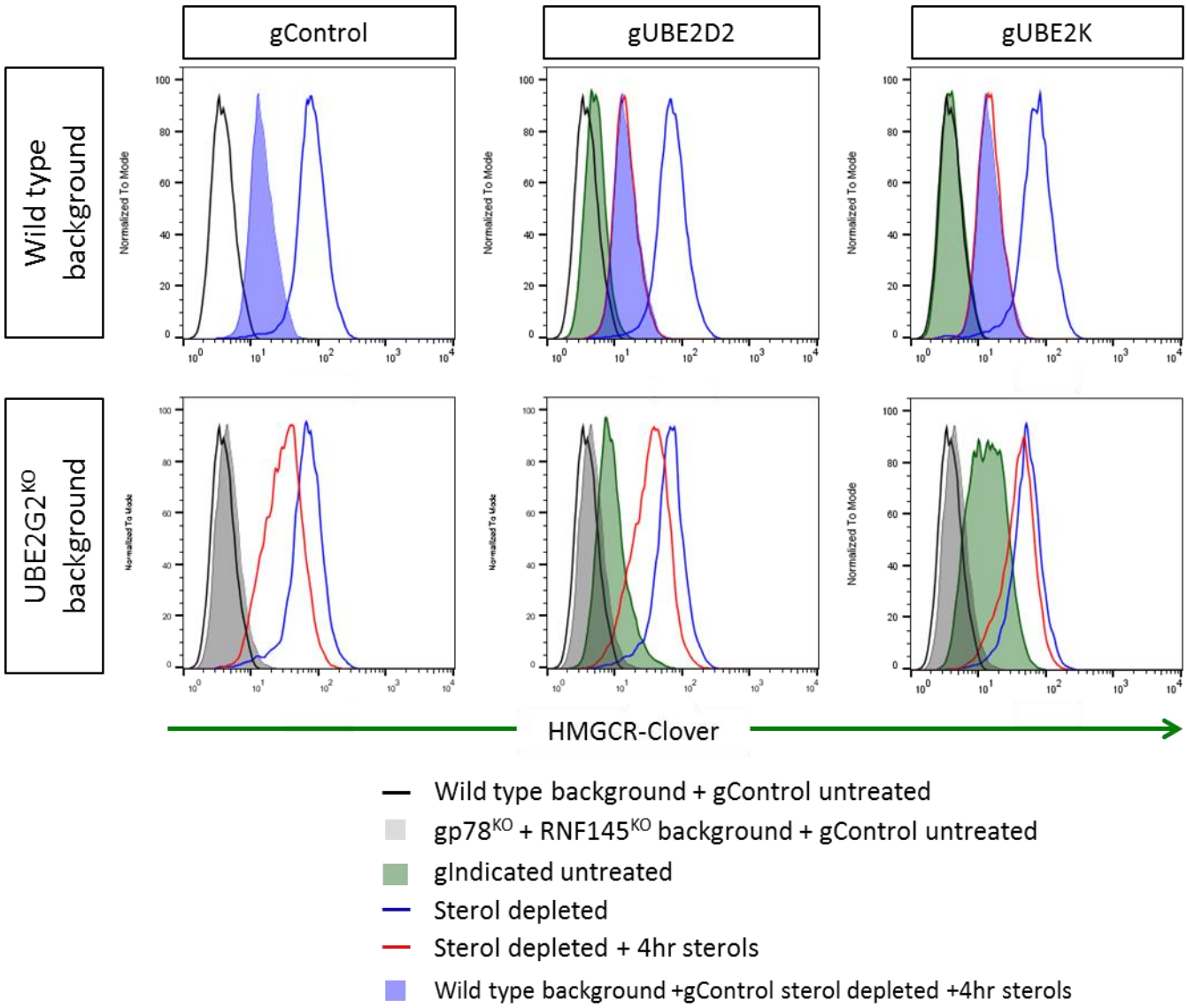

Figure 7.9 CRISPR validation of UBE2D2 and UBE2K (A) Wild type or UBE2G2 knockout (clone A6) HMGCR-Clover cells were transiently transfected with Cas9 and either a control gRNA, a UBE2D2-targeting gRNA or a UBE2K-targeting gRNA. Transfected cells were selected with puromycin treatment. Selected cells were sterol depleted overnight eight days post transfection and then cultured for a further four hours in the presence or absence of sterols. HMGCR-Clover expression was assessed by flow cytometry.

7.3 Discussion

7.3.1 TRC8 is not involved in HMGCR ERAD

The Debose Boyd laboratory reported that TRC8 was required for the degradation of HMGCR (Jo et al. 2011). However, the Weissman laboratory could not reproduce this observation (Tsai et al. 2012). Throughout this thesis project, I have not seen a requirement for TRC8 in the degradation of HMGCR (**Figure 6.1, 6.2B and 7.3**). Even in the absence of gp78 and RNF145, TRC8 did not mediate the degradation of HMGCR. Independent laboratories have shown that exogenous TRC8 associates with both Insig proteins (Lee et al. 2010, Jo et al. 2011). Given the homology between TRC8 and RNF145 as well as TRC8's constitutive binding to the Insig proteins, it is striking that TRC8 cannot ubiquitinate HMGCR, even in the absence of RNF145.

7.3.2 CRISPR knockout screens using focused gRNA libraries

The success of a CRISPR knockout screen is dependent on the ability to enrich mutants with the phenotype of interest. A high enrichment is more likely to be achieved if the phenotype of the mutants of interest is distinct from the starting population. The fluorescent window is small between gp78 and RNF145 double knockout HMGCR-Clover HeLa cells cultured in the presence or absence of sterols following sterol depletion, with a considerable overlap between the two populations on a FACS plot. The aim of the screen was to identify E3 ubiquitin ligases and so I used a focused E3 ligase gRNA library. This ensured that other factors required for the sterol-induced degradation of HMGCR, such as proteasome components, p97 complex components or UBE2G2, would not dilute the enrichment of E3 ligase knockouts.

The ability to rapidly create focused gRNA libraries to sample a specific family of genes is an extremely powerful tool for cell biology research. Focused gRNA libraries are particularly useful if the aim of the screen is to identify a specific component. There are also practical advantages to performing screens with focused gRNA libraries. Focused CRISPR screens are less demanding on reagents and tissue culture time as fewer cells are required to maintain representation of the library. The lower complexity samples from focused gRNA libraries do not need to be sequenced as deeply as genome-wide libraries, therefore making sequencing cheaper and potentially more accessible.

It is worth remembering that all forward genetic screens performed with a library (CRISPR or RNA-interference based) are limited by the construction of the library. A focused library relies on the bioinformatic analysis used to identify all relevant genes. For example, TMEM129 contains an atypical RING domain and so was not included in an siRNA E3 ligase library that was used to try to identify the E3 ligase responsible for US11-mediated MHC-I degradation (van den Boomen et al. 2014). Whereas, TMEM129 was identified by a genome wide library, as it is an annotated open reading frame, and in a retroviral mutagenesis haploid screen (van de Weijer et al. 2014, van den Boomen et al. 2014).

7.3.3 Hrd1-mediated HMGCR degradation

My focused E3 ligase CRISPR screen identified a role for Hrd1 as a ubiquitin E3 ligase that mediates the sterol-induced degradation of HMGCR in the absence of gp78 and RNF145. If either gp78 or RNF145 is present, the loss of Hrd1 had no effect on HMGCR degradation (**Figure 7.6**).

As one of the orthologues of *S cerevisiae* Hrd1p, Hrd1 has already been assessed for its ability to target HMGCR for degradation. So far, there is no evidence to support a role for Hrd1 in the sterol-induced ubiquitination of HMGCR (Kikkert et al. 2004, Song, Sever, and DeBose-Boyd 2005). Consistent with these studies, I did not see a decrease in sterol-induced HMGCR degradation in the absence of Hrd1 alone.

The limited sterol-induced degradation of HMGCR-Clover in the gp78 and RNF145 double knockout HMGCR-Clover cell line could be abolished by the loss of UBE2G2, Insig1 or Hrd1 (**Figure 7.1, 7.2 and 7.5**). This suggests that Hrd1 mediates the ubiquitination of HMGCR using UBE2G2 and Insig1. However, the Debose Boyd laboratory did not see co-precipitation of Hrd1 with the Insig proteins (Jo et al. 2011, Song, Sever, and DeBose-Boyd 2005). These experiments were performed by over-expressing epitope-tagged Hrd1 and Insigs in wild type CHO cells. It is possible that Hrd1 associates with Insig1 with a lower affinity than gp78 and RNF145. In the experiments presented by the Debose Boyd laboratory, endogenous gp78 and RNF145 might out-compete exogenous Hrd1 for Insig1 binding. It would therefore be interesting to see if Insig1 co-immunoprecipitates with Hrd1 in the absence of gp78 and RNF145.

The current model for the sterol-induced degradation of HMGCR revolves around the Insig proteins acting as sterol dependent scaffold proteins to recruit E3 ligase complexes to HMGCR (Jo and Debose-Boyd 2010). HMGCR is reported to be a high confidence interaction partner of Hrd1 (Christianson et al. 2012). If Hrd1 is already bound to HMGCR, it is unlikely that Insig1 is acting as a sterol sensitive Hrd1 recruitment factor. Instead, Hrd1 might only be able to ubiquitinate Insig1 bound HMGCR or Insig1 might recruit another factor required for Hrd1-mediated HMGCR degradation.

7.4 Summary

In this chapter, I used a combinatorial gene knockout approach to demonstrate that the loss of UBE2G2 or Insig1 blocked the sterol-induced degradation of HMGCR-Clover in the absence of gp78 and RNF145. This suggested that there was another E3 ubiquitin ligase that could mediate sterol-induced HMGCR degradation using UBE2G2 and Insig1. I identified Hrd1 and RNF185 in a focused E3 ligase CRISPR screen in a gp78 and RNF145 double knockout HMGCR-Clover cell line. Whilst the loss of either RNF185 or Hrd1 in the gp78 and RNF145 double knockout HMGCR-Clover cell line blocked the sterol-induced degradation of HMGCR-Clover, only the loss of Hrd1 in a gp78 and RNF145 double knockout HeLa clone blocked the sterol-induced degradation of wild type HMGCR. The loss of Hrd1 only affects HMGCR degradation in the absence of both gp78 and RNF145. A focused E2 conjugating enzyme CRISPR screen in a UBE2G2 knockout HMGCR-Clover clone identified UBE2K. It is likely that gp78 can use UBE2K to ubiquitinate HMGCR in the absence of UBE2G2, all be it inefficiently.

Chapter 8: General Discussion

8.1 Summary and model for HMGCR degradation

Fluorescence-based forward genetic screens in human cells are a highly effective approach to identify genes required for a cellular process. The first major aim of my thesis project was to compare the efficacy of retroviral gene-trap mutagenesis haploid screens, the previous gold standard, to genome-wide CRISPR knockout screens. I found that, in KBM7 cells, the two screening methods produced highly concordant results (**Figure 3.2** and **Figure 3.3**). Both screens identified a role for the uncharacterised gene TXNDC11 in glycoprotein ERAD. My collaborators went on to demonstrate that TXNDC11 is an ER-localised disulphide reductase that acts on a component of the ERAD machinery.

HMGCR catalyses the rate-limiting step of the cholesterol biosynthesis pathway. To maintain cholesterol homeostasis, the expression of HMGCR is tightly regulated by transcriptional and post-transcriptional mechanisms. Cholesterol pathway intermediates stimulate the Insig proteins to recruit E3 ligase complexes to HMGCR to mediate ERAD (Sever, Song, et al. 2003, Sever, Yang, et al. 2003). However, the identity of the ERAD E3 ligases responsible for HMGCR ubiquitination was controversial (Tsai et al. 2012). I performed a series of fluorescence-based forward genetic screens as an unbiased approach to identify the E3 ligase responsible for the ubiquitination of HMGCR. My genome-wide CRISPR knockout screens identified a role for the poorly characterised ERAD E3 ligase RNF145 in the sterol-induced degradation of HMGCR (**Figure 4.6** and **Figure 5.5**).

The loss of RNF145 alone only resulted in a small reduction in the sterol-induced degradation of HMGCR-Clover (**Figure 5.6A**), however I could not detect a decrease in the sterol-induced degradation or ubiquitination of wild type HMGCR in the absence of RNF145 (**Figure 5.7** and **Figure 6.9B** and **6.9C**). The loss of gp78, an Insig-associated ERAD E3 ligase previously implicated in the sterol-induced degradation of HMGCR, did not result in a detectable decrease in the sterol-induced degradation or ubiquitination of HMGCR (**Figure 6.7C** and **Figure 6.9B**). However, the combined loss of both gp78 and RNF145 resulted in a pronounced decrease in the sterol-induced degradation and ubiquitination of HMGCR (**Figure 6.4** and **Figure 6.9C**). This indicates that gp78 and RNF145 demonstrate partial functional redundancy

and act in parallel on HMGCR (**Figure 8.1A**). I proceeded to observe the constitutive association of RNF145 with both Insig proteins (**Figure 6.10B**) and a sterol-dependent interaction between RNF145 and HMGCR that was also enhanced by proteasome inhibition (**Table 6.1** and **Figure 6.11B**). This supports a model in which the Insig proteins recruit both gp78 and RNF145 to HMGCR in a sterol-dependent manner (**Figure 8.1A**).

In gp78 and RNF145 double knockout cells, I used a focused ubiquitin E3 ligase CRISPR screen to identify a role for Hrd1 in HMGCR degradation (**Figure 7.4**). The combined loss of gp78, RNF145 and Hrd1 completely blocks the sterol-induced degradation of HMGCR in HeLa cells (**Figure 7.5C)**. Hrd1 is dispensable for sterol-induced HMGCR degradation (Kikkert et al. 2004). Consistent with previous studies, the loss of Hrd1 alone did not affect HMGCR degradation and a requirement for Hrd1 was only observed in the absence of both gp78 and RNF145 (**Figure 7.6**). This suggests that Hrd1 acts as a back-up, secondary E3 ligase to mediate the degradation of HMGCR in the absence of gp78 and RNF145 (**Figure 8.1B**). No interaction between Hrd1 and the Insig proteins is reported (Song, Sever, and DeBose-Boyd 2005, Jo et al. 2011). It is possible that Hrd1 has a lower affinity for the Insig proteins and only interacts with the Insig in the absence of gp78 and RNF145 (**Figure 8.1B**). Alternatively, Hrd1 might not interact directly with the Insigs but recognises and ubiquitinates Insig-bound HMGCR (**Figure 8.1B**).

The loss of gp78 in UBE2G2 knockout cells resulted in a near-complete block in the sterol-induced degradation of HMGCR-Clover, whereas the loss of RNF145 had no additional effect on sterol-induced HMGCR-Clover degradation in UBE2G2 knockout cells (**Figure 7.2A**). This suggests that gp78 can ubiquitinate HMGCR using another E2, in the absence of UBE2G2. A focused E2 screen identified the elusive E2 as UBE2K and the combined loss of both UBE2G2 and UBE2K resulted in a near-complete block in sterol-induced HMGCR-Clover degradation (**Figure 7.8** and **Figure 7.9**). It is therefore likely that gp78 ubiquitinates HMGCR using UBE2K in the absence of UBE2G2, however this process is inefficient (**Figure 8.1A**).

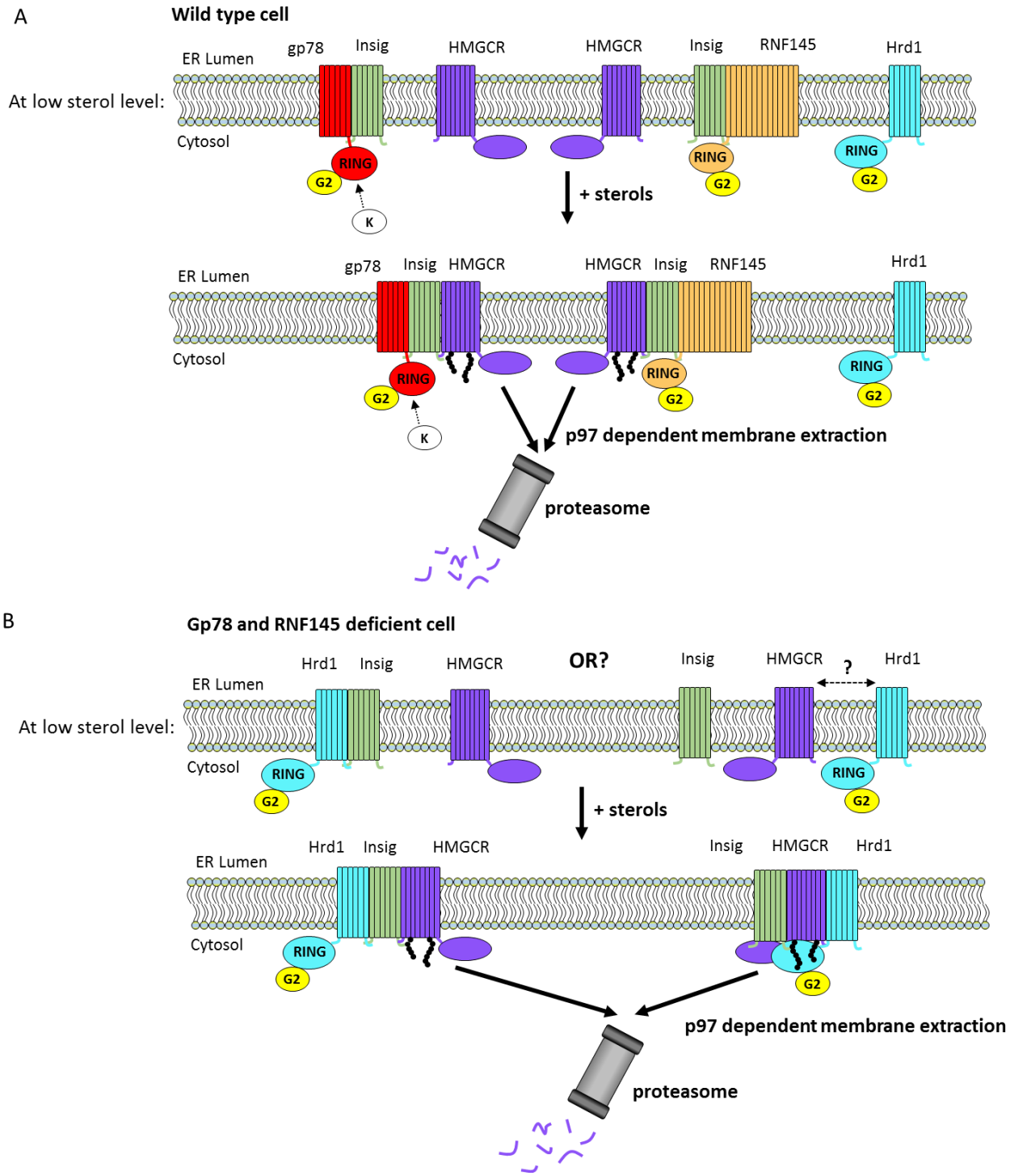

Figure 8.1 The sterol-induced degradation of HMGCR. (A) Insig proteins recruit gp78 and RNF145 to HMGCR in response to sterols. Gp78 and RNF145 mediate the ubiquitination of HMGCR using UBE2G2 (G2). In the absence of UBE2G2, gp78 can use UBE2K (K). Gp78 and RNF145 are functionally redundant; they compensate for the loss of the other to maintain the cell's ability to degrade HMGCR. Ubiquitinated HMGCR is extracted from the ER membrane in a p97 dependent manner and degraded by the proteasome. Ubiquitin is represented by black circles **(B)** HMGCR is degraded in a Hrd1-dependent manner in the absence of gp78 and RNF145. The mechanism of Hrd1-mediated HMGCR degradation is yet to be determined. Hrd1 might interact with Insigs in the absence of gp78 and RNF145 so that it is recruited to HMGCR by the sterol-dependent association of Insigs with HMGCR. Alternatively, Hrd1 might interact directly with HMGCR, however Hrd1 might specifically ubiquitinate Insig-bound HMGCR.

8.2 Future work

A major aim of this project, as it continues beyond my thesis, is to determine whether the RNF145-HMGCR interaction is dependent on the Insig proteins, i.e. similar to the gp78-HMGCR interaction (Song, Sever, and DeBose-Boyd 2005, Jo et al. 2011). This will be tested by performing RNF145 immunoprecipitations in Insig knockout cell lines.

It will be critical to understand the relationship between gp78 and RNF145 to elucidate the mechanism for HMGCR ubiquitination by multiple E3 ubiquitin ligases. The stability of gp78 and RNF145 might be influenced by the loss of an interaction between the E3 ligases or differential Insig occupancy when one E3 ligase is absent. Preliminary data suggests that RNF145 is degraded by the proteasome by sterols in the absence of gp78 (**Figure 6.12**). This result needs to be repeated and it will be interesting to see if gp78 is affected by the loss of RNF145.

CRISPR-mediated gene disruption in the gp78 and RNF145 knockout HMGCR-Clover cell line suggested that the residual degradation of HMGCR is dependent on Hrd1, Insig1 and UBE2G2 (**Figure 7.1, 7.2** and **7.5**). It will be important to determine whether the loss of Hrd1 in combination with gp78 and RNF145 further reduces HMGCR ubiquitination. Hrd1 immunoprecipitations should also be performed in wild type and gp78/RNF145 double knockout cells to determine whether Hrd1 interacts with HMGCR and the Insig proteins (**Figure 8.1B**).

All the work presented in this thesis on HMGCR degradation was performed in HeLa cells. Whilst all cells need to regulate cholesterol homeostasis, different cells have different requirements for cholesterol. For example, hepatocytes are a major cholesterol-producing cell type. We will need to assess the requirement for gp78, RNF145 and Hrd1 in HMGCR degradation in different cells.

8.3 RNF145 as an LXR target gene

RNF145 was identified as a LXR target gene in a transcriptomics screen (Cook et al. 2017). The LXR genetic program aims to reduce cellular cholesterol through several mechanisms, such as inhibiting cholesterol biosynthesis (Sallam et al. 2016). It is plausible for the ubiquitin E3 ligase

responsible for HMGCR degradation to be an LXR target gene. However, if the model for HMGCR degradation is correct and the E3 ubiquitin ligases are recruited to HMGCR by the Insig proteins, it is likely that the Insig proteins are the rate limiting factors (Sever, Yang, et al. 2003, Sever, Song, et al. 2003). Therefore, the upregulation of RNF145 alone is unlikely to affect HMGCR degradation. However, at high cholesterol levels, the Insig1 protein is stabilised (Lee, Song, et al. 2006). The increase in RNF145 transcription and decrease in Insig1 degradation might be coordinated to increase HMGCR degradation. Alternatively, RNF145 might be an LXR target gene to enhance the ubiquitination of a different RNF145 substrate to regulate lipid metabolism.

The work in this thesis shows that RNF145-mediated ubiquitination of HMGCR is sterol-regulated. Given that the transcription of RNF145 is controlled by sterol derivatives (as an LXR target gene), further characterisation of RNF145 should seek to determine whether RNF145 turnover is sterol-regulated. If the expression of RNF145 is induced when the cell is seeking to reduce its cholesterol level, it follows that when the cholesterol level is restored to its desired level either RNF145 activity is stopped or RNF145 is degraded to decrease activity.

8.4 Sterol sensing to induce HMGCR degradation

Sterol sensing domains (SSDs) are a critical feature of proteins involved in maintaining cholesterol homeostasis (Goldstein, DeBose-Boyd, and Brown 2006). SCAP inhibits SREBP processing by associating with Insig proteins in the ER at high ER cholesterol levels (Yang et al. 2002, Yabe, Brown, and Goldstein 2002). The Brown and Goldstein laboratory observed the direct binding of cholesterol to SCAP in an *in vitro* binding assay (Radhakrishnan et al. 2004). The Radhakrishnan laboratory went on to identify a significant cholesterol-induced conformational change in SCAP (Zhang et al. 2016, Gao et al. 2017). Co-precipitation and protease protection assays revealed that the binding of cholesterol to SCAP's SSD induces the transition from a closed to open state, which enables binding to the Insig proteins (Zhang et al. 2016, Gao et al. 2017). The SCAP-Insig interaction can also be induced by the oxysterol 25-hydroxycholesterol. However, *in vitro* binding assays revealed that 25-hydroxycholesterol binds specifically to Insig rather than SCAP (Sun et al. 2007, Radhakrishnan et al. 2007).

In contrast to SCAP, no-one has yet observed the direct binding of cholesterol or other sterols to the SSD of HMGCR (Goldstein, DeBose-Boyd, and Brown 2006). In this thesis project, I used a combination of cholesterol and 25-hydroxycholesterol to induce the degradation of HMGCR. It is tempting to speculate that 25-hydroxycholesterol-bound Insigs can also associate with HMGCR, in the same manner as they can with SCAP (Radhakrishnan et al. 2007). It is yet to be determined how sterols induce the binding of Insigs to HMGCR to recruit E3 ligase complexes and enable the degradation of HMGCR. Sterols might bind to a currently unidentified protein that facilitates the Insig-HMGCR interaction. There are no candidate genes in the CRISPR screens presented in this thesis, however I always used cholesterol and 25-hydroxycholesterol to induce HMGCR degradation. If 25-hydroxycholesterol-bound Insig can bind directly to HMGCR, in a similar way as to SCAP, then the addition of 25-hydroxycholesterol might compensate for the loss of the sterol-binding protein. Using a single sterol to induce HMGCR degradation might enable the identification of the sterol-binding protein.

8.5 CRISPR screen developments

The CRISPR revolution has advanced spectacularly over the last few years. At the beginning of my thesis project, CRISPR technology was in its infancy with enormous potential for both cell biology research and therapeutics (Hsu, Lander, and Zhang 2014). Now, CRISPR technology has been reported to remove proviral HIV DNA from mice and to correct disease-causing mutations in mouse models of conditions such as Duchenne muscular dystrophy and Huntington's disease (Nelson et al. 2016, Yang et al. 2017, Yin et al. 2017). Controversially, Chinese and American laboratories have successfully used CRISPR-mediated genome editing in human embryos (Liang et al. 2015, Ma et al. 2017). However, both studies highlighted the necessity to reduce off-target effects of the Cas9 nuclease to ensure that no unwanted mutations are introduced into the germline.

At the start of my thesis project, only a handful of proof-of-concept CRISPR screens had been reported (Wang et al. 2014, Shalem et al. 2014, Zhou et al. 2014, Koike-Yusa et al. 2014). Early on in this thesis project, I demonstrated that genome-wide CRISPR screens are as effective at identifying candidate genes as the previous gold standard method, retroviral gene-trap

mutagenesis haploid screens. An exciting attraction of CRISPR screens is the potential to perform forward genetic screens in any cell type, as CRISPR-mediated gene disruption is not restricted to a haploid karyotype. This potential has been realised, with CRISPR screens being reported that dissect a range of processes in physiologically relevant cell lines, including hepatic Huh7 cells (Marceau et al. 2016) and T cells (Park et al. 2017), as well as primary cells (Parnas et al. 2015).

CRISPR/Cas9 technology can be readily adapted to alter gene expression by tagging a catalytically inactive Cas9 (dCas9) with effector domains. CRISPR interference (CRISPRi) refers to a system in which dCas9 is tagged with a repressive KRAB effector domain. A gene of interest can be efficiently silenced by targeting the dCas9-KRAB fusion protein to the promoter region of the gene (Gilbert et al. 2013). CRISPRi can be used to perform forward genetic screens using libraries of gRNAs that target the promoter region of all the desired open reading frames (Gilbert et al. 2014). Whilst CRISPRi results in a knockdown of gene expression rather than a gene knockout, there are some potential advantages to using CRISPRi. CRISPR knockout screens are limited to targeting protein-coding open reading frames because the loss of gene expression is dependent on the frame-shift mutations disrupting the amino acid sequence. Whereas, CRISPRi can silence expression of any open reading frame, including long non-coding RNA genes (Liu et al. 2017).

A recent development aims to use the CRISPR/Cas9 system for precise 'base editing' (Komor et al. 2016). Cytidine deaminase enzymes convert cytidine to uridine, which results in a cytosine to thymidine or guanine to adenine mutation following DNA repair (Conticello 2008). Tagging dCas9 with a cytidine deaminase enzyme, such as activation-induced deaminase (AID) or APOBEC3G, efficiently and precisely creates point mutations (Komor et al. 2016). Therefore, using a tiled gRNA library across a gene-of-interest should be able to identify loss of function mutations and regions for gene function.

The CRISPR/Cas9 system can also be adapted to upregulate target gene expression by tagging dCas9 with a transcription activator domain. All the Cas9 activation systems use VP64 as the activating effector domain alone or in combination with additional transcription-activating modules (Gilbert et al. 2013, Chavez et al. 2015, Joung, Konermann, et al. 2017). Genome-wide gain-of-function screens can be performed by using a gRNA library that targets a Cas9-activator fusion protein to the promoter of all annotated open reading frames (Gilbert et al.

2014, Joung, Engreitz, et al. 2017). Previously, gain-of-function screens were performed using the over-expression of cDNA libraries (Grimm 2004). However, gRNA libraries are significantly easier to work with because of the enormous variation in cDNA lengths and sequence features in a cDNA library.

8.6 Concluding remarks

The last decade has seen the extraordinary development of technologies to advance forward genetics in human cells. Retroviral gene-trap mutagenesis screens in near-haploid cells have made a significant contribution to our understanding of the biology of the cell. Custom genome editing with CRISPR/Cas9 technology is now transforming cell biology research. Geneticists can choose from a diverse range of cell types and CRISPR/Cas9 technologies to optimise their forward genetic screens for the cellular process they seek to interrogate.

Acknowledgements

I am enormously grateful to Prof Paul Lehner for his support and guidance throughout my PhD. Paul's mentorship made this project extremely rewarding.

I am also heavily indebted to Dr Richard Timms, who supervised me at the bench during my rotation project in the Lehner laboratory and provided invaluable advice throughout my PhD.

I thank the rest of the Lehner laboratory. In particular, Dr Dick van den Boomen for his advice throughout the project as well as practical support, notably for cloning the Lehner/Nathan ubiquitome gRNA library. I also thank Dr James Williamson for processing and analysing mass spectrometry samples and Stuart Bloor for assistance with Illumina sequencing. I am also grateful to Dr Norbert Volkmar who is continuing this project.

I am grateful for Dr Richard Timms, Dr Iva Tchasovnikarova from Prof Paul Lehner's laboratory and Dr Lea Christensen from Prof Lars Ellgaard's laboratory at the University of Copenhagen, Denmark for their collaboration in completing the TXNDC11 story.

I am grateful to Dr Michael Bassik (Stanford University) for the generous gift of his genome-wide CRISPR gRNA library.

I thank all members of the Cambridge Institute of Medical Research core facilities for their invaluable support, in particular Reiner Schulte, Chiara Cossetti and Michal Maj for FACS.

I thank Dr James Nathan for his collaboration in the Lehner/Nathan ubiquitome gRNA library as well as for providing a MARCH6 knockout clone.

I thank Prof Gordon Dougan for access to the Illumina HiSeq platform, and to Richard Rance, Nathalie Smerdon and the sequencing teams at the Wellcome Trust Sanger Institute.

Finally, I thank my friends and family for their support during my time in Cambridge, and particularly my parents, without whose unwavering support and sacrifice I would not have had this opportunity.

This work was funded by a Wellcome Trust PhD studentship through the Infection & Immunity four-year PhD programme.

References

Adams, C. M., J. L. Goldstein, and M. S. Brown. 2003. "Cholesterol-induced conformational change in SCAP enhanced by Insig proteins and mimicked by cationic amphiphiles." *Proc Natl Acad Sci U S A* 100 (19):10647-52. doi: 10.1073/pnas.1534833100.

Adams, C. M., J. Reitz, J. K. De Brabander, J. D. Feramisco, L. Li, M. S. Brown, and J. L. Goldstein. 2004. "Cholesterol and 25-hydroxycholesterol inhibit activation of SREBPs by different mechanisms, both involving SCAP and Insigs." *J Biol Chem* 279 (50):52772-80. doi: 10.1074/jbc.M410302200.

Aizawa, S., T. Okamoto, Y. Sugiyama, T. Kouwaki, A. Ito, T. Suzuki, C. Ono, T. Fukuhara, M. Yamamoto, M. Okochi, N. Hiraga, M. Imamura, K. Chayama, R. Suzuki, I. Shoji, K. Moriishi, K. Moriya, K. Koike, and Y. Matsuura. 2016. "TRC8-dependent degradation of hepatitis C virus immature core protein regulates viral propagation and pathogenesis." *Nat Commun* 7:11379. doi: 10.1038/ncomms11379.

Altier, C., A. Garcia-Caballero, B. Simms, H. You, L. Chen, J. Walcher, H. W. Tedford, T. Hermosilla, and G. W. Zamponi. 2011. "The Cavβ subunit prevents RFP2-mediated ubiquitination and proteasomal degradation of L-type channels." *Nat Neurosci* 14 (2):173-80. doi: 10.1038/nn.2712.

Andersson, B. S., M. Beran, S. Pathak, A. Goodacre, B. Barlogie, and K. B. McCredie. 1987. "Ph-positive chronic myeloid leukemia with near-haploid conversion in vivo and establishment of a continuously growing cell line with similar cytogenetic pattern." *Cancer Genet Cytogenet* 24 (2):335-43.

Appenzeller-Herzog, C., and L. Ellgaard. 2008. "The human PDI family: versatility packed into a single fold." *Biochim Biophys Acta* 1783 (4):535-48. doi: 10.1016/j.bbamcr.2007.11.010.

Bagola, K., M. von Delbrück, G. Dittmar, M. Scheffner, I. Ziv, M. H. Glickman, A. Ciechanover, and T. Sommer. 2013. "Ubiquitin binding by a CUE domain regulates ubiquitin chain formation by ERAD E3 ligases." *Mol Cell* 50 (4):528-39. doi: 10.1016/j.molcel.2013.04.005.

Baldridge, R. D., and T. A. Rapoport. 2016. "Autoubiquitination of the Hrd1 Ligase Triggers Protein Retrotranslocation in ERAD." *Cell* 166 (2):394-407. doi: 10.1016/j.cell.2016.05.048.

Ballar, P., Y. Shen, H. Yang, and S. Fang. 2006. "The role of a novel p97/valosin-containing protein-interacting motif of gp78 in endoplasmic reticulum-associated degradation." *J Biol Chem* 281 (46):35359-68. doi: 10.1074/jbc.M603355200.

Bassik, M. C., R. J. Lebbink, L. S. Churchman, N. T. Ingolia, W. Patena, E. M. LeProust, M. Schuldiner, J. S. Weissman, and M. T. McManus. 2009. "Rapid creation and quantitative monitoring of high coverage shRNA libraries." *Nat Methods* 6 (6):443-5. doi: 10.1038/nmeth.1330.

Bays, N. W., S. K. Wilhovsky, A. Goradia, K. Hodgkiss-Harlow, and R. Y. Hampton. 2001. "HRD4/NPL4 is required for the proteasomal processing of ubiquitinated ER proteins." *Mol Biol Cell* 12 (12):4114-28.
Bernards, R., T. R. Brummelkamp, and R. L. Beijersbergen. 2006. "shRNA libraries and their use in cancer genetics." *Nat Methods* 3 (9):701-6. doi: 10.1038/nmeth921.

Bernasconi, R., C. Galli, V. Calanca, T. Nakajima, and M. Molinari. 2010. "Stringent requirement for HRD1, SEL1L, and OS-9/XTP3-B for disposal of ERAD-LS substrates." *J Cell Biol* 188 (2):223-35. doi: 10.1083/jcb.200910042.

Bernasconi, R., T. Pertel, J. Luban, and M. Molinari. 2008. "A dual task for the Xbp1-responsive OS-9 variants in the mammalian endoplasmic reticulum: inhibiting secretion of misfolded protein conformers and enhancing their disposal." *J Biol Chem* 283 (24):16446-54. doi: 10.1074/jbc.M802272200.

Bernstein, E., A. A. Caudy, S. M. Hammond, and G. J. Hannon. 2001. "Role for a bidentate ribonuclease in the initiation step of RNA interference." *Nature* 409 (6818):363-6. doi: 10.1038/35053110.

Bieberich, E. 2014. "Synthesis, Processing, and Function of N-glycans in N-glycoproteins." *Adv Neurobiol* 9:47-70. doi: 10.1007/978-1-4939-1154-7_3.

Biederer, T., C. Volkwein, and T. Sommer. 1997. "Role of Cue1p in ubiquitination and degradation at the ER surface." *Science* 278 (5344):1806-9.

Birsoy, K., T. Wang, R. Possemato, O. H. Yilmaz, C. E. Koch, W. W. Chen, A. W. Hutchins, Y. Gultekin, T. R. Peterson, J. E. Carette, T. R. Brummelkamp, C. B. Clish, and D. M. Sabatini. 2013. "MCT1-mediated transport of a toxic molecule is an effective strategy for targeting glycolytic tumors." *Nat Genet* 45 (1):104-8. doi: 10.1038/ng.2471.

Boden, G. 2011. "Obesity, insulin resistance and free fatty acids." *Curr Opin Endocrinol Diabetes Obes* 18 (2):139-43. doi: 10.1097/MED.0b013e3283444b09.

Boname, J. M., S. Bloor, M. P. Wandel, J. A. Nathan, R. Antrobus, K. S. Dingwell, T. L. Thurston, D. L. Smith, J. C. Smith, F. Randow, and P. J. Lehner. 2014. "Cleavage by signal peptide peptidase is required for the degradation of selected tail-anchored proteins." *J Cell Biol* 205 (6):847-62. doi: 10.1083/jcb.201312009.

Boname, J. M., M. Thomas, H. R. Stagg, P. Xu, J. Peng, and P. J. Lehner. 2010. "Efficient internalization of MHC I requires lysine-11 and lysine-63 mixed linkage polyubiquitin chains." *Traffic* 11 (2):210-20. doi: 10.1111/j.1600-0854.2009.01011.x.

Borgese, N., S. Colombo, and E. Pedrazzini. 2003. "The tale of tail-anchored proteins: coming from the cytosol and looking for a membrane." *J Cell Biol* 161 (6):1013-9. doi: 10.1083/jcb.200303069.

Braulke, T., and J. S. Bonifacino. 2009. "Sorting of lysosomal proteins." *Biochim Biophys Acta* 1793 (4):605-14. doi: 10.1016/j.bbamcr.2008.10.016.

Brauweiler, A., K. L. Lorick, J. P. Lee, Y. C. Tsai, D. Chan, A. M. Weissman, H. A. Drabkin, and R. M. Gemmill. 2007. "RING-dependent tumor suppression and G2/M arrest induced by the TRC8 hereditary kidney cancer gene." *Oncogene* 26 (16):2263-71. doi: 10.1038/sj.onc.1210017.

Brodsky, J. L. 2012. "Cleaning up: ER-associated degradation to the rescue." *Cell* 151 (6):1163-7. doi: 10.1016/j.cell.2012.11.012.

Brown, M. S., R. G. Anderson, and J. L. Goldstein. 1983. "Recycling receptors: the round-trip itinerary of migrant membrane proteins." *Cell* 32 (3):663-7.

Brown, M. S., and J. L. Goldstein. 1986. "A receptor-mediated pathway for cholesterol homeostasis." *Science* 232 (4746):34-47.

Brown, M. S., and J. L. Goldstein. 1997. "The SREBP pathway: regulation of cholesterol metabolism by proteolysis of a membrane-bound transcription factor." *Cell* 89 (3):331-40.

Burr, M. L., F. Cano, S. Svobodova, L. H. Boyle, J. M. Boname, and P. J. Lehner. 2011. "HRD1 and UBE2J1 target misfolded MHC class I heavy chains for endoplasmic reticulum-associated degradation." *Proc Natl Acad Sci U S A* 108 (5):2034-9. doi: 10.1073/pnas.1016229108.

Burr, M. L., D. J. van den Boomen, H. Bye, R. Antrobus, E. J. Wiertz, and P. J. Lehner. 2013. "MHC class I molecules are preferentially ubiquitinated on endoplasmic reticulum luminal residues during HRD1 ubiquitin E3 ligase-mediated dislocation." *Proc Natl Acad Sci U S A* 110 (35):14290-5. doi: 10.1073/pnas.1303380110.

Cadwell, K., and L. Coscoy. 2005. "Ubiquitination on nonlysine residues by a viral E3 ubiquitin ligase." *Science* 309 (5731):127-30. doi: 10.1126/science.1110340.

Cao, J., J. Wang, W. Qi, H. H. Miao, L. Ge, R. A. DeBose-Boyd, J. J. Tang, B. L. Li, and B. L. Song. 2007. "Ufd1 is a cofactor of gp78 and plays a key role in cholesterol metabolism by regulating the stability of HMG-CoA reductase." *Cell Metab* 6 (2):115-28. doi: 10.1016/j.cmet.2007.07.002.

Carette, J. E., C. P. Guimaraes, M. Varadarajan, A. S. Park, I. Wuethrich, A. Godarova, M. Kotecki, B. H. Cochran, E. Spooner, H. L. Ploegh, and T. R. Brummelkamp. 2009. "Haploid genetic screens in human cells identify host factors used by pathogens." *Science* 326 (5957):1231-5. doi: 10.1126/science.1178955.

Carette, J. E., C. P. Guimaraes, I. Wuethrich, V. A. Blomen, M. Varadarajan, C. Sun, G. Bell, B. Yuan, M. K. Muellner, S. M. Nijman, H. L. Ploegh, and T. R. Brummelkamp. 2011. "Global gene disruption in human cells to assign genes to phenotypes by deep sequencing." *Nat Biotechnol* 29 (6):542-6. doi: 10.1038/nbt.1857.

Carette, J. E., M. Raaben, A. C. Wong, A. S. Herbert, G. Obernosterer, N. Mulherkar, A. I. Kuehne, P. J. Kranzusch, A. M. Griffin, G. Ruthel, P. Dal Cin, J. M. Dye, S. P. Whelan, K. Chandran, and T. R. Brummelkamp. 2011. "Ebola virus entry requires the cholesterol transporter Niemann-Pick C1." *Nature* 477 (7364):340-3. doi: 10.1038/nature10348.

Carroll, D. 2011. "Genome engineering with zinc-finger nucleases." *Genetics* 188 (4):773-82. doi: 10.1534/genetics.111.131433.

Carvalho, A. F., M. P. Pinto, C. P. Grou, I. S. Alencastre, M. Fransen, C. Sá-Miranda, and J. E. Azevedo. 2007. "Ubiquitination of mammalian Pex5p, the peroxisomal import receptor." *J Biol Chem* 282 (43):31267-72. doi: 10.1074/jbc.M706325200.

Carvalho, P., V. Goder, and T. A. Rapoport. 2006. "Distinct ubiquitin-ligase complexes define convergent pathways for the degradation of ER proteins." *Cell* 126 (2):361-73. doi: 10.1016/j.cell.2006.05.043.

Carvalho, P., A. M. Stanley, and T. A. Rapoport. 2010. "Retrotranslocation of a misfolded luminal ER protein by the ubiquitin-ligase Hrd1p." *Cell* 143 (4):579-91. doi: 10.1016/j.cell.2010.10.028.

Chambers, J. E., T. J. Tavender, O. B. Oka, S. Warwood, D. Knight, and N. J. Bulleid. 2010. "The reduction potential of the active site disulfides of human protein disulfide isomerase limits oxidation of the enzyme by Ero1α." *J Biol Chem* 285 (38):29200-7. doi: 10.1074/jbc.M110.156596.

Chang, K., S. J. Elledge, and G. J. Hannon. 2006. "Lessons from Nature: microRNA-based shRNA libraries." *Nat Methods* 3 (9):707-14. doi: 10.1038/nmeth923.

Chang, T. Y., C. C. Chang, and D. Cheng. 1997. "Acyl-coenzyme A:cholesterol acyltransferase." *Annu Rev Biochem* 66:613-38. doi: 10.1146/annurev.biochem.66.1.613.

Chang, T. Y., C. C. Chang, N. Ohgami, and Y. Yamauchi. 2006. "Cholesterol sensing, trafficking, and esterification." *Annu Rev Cell Dev Biol* 22:129-57. doi: 10.1146/annurev.cellbio.22.010305.104656.

Chavez, A., J. Scheiman, S. Vora, B. W. Pruitt, M. Tuttle, E. P R Iyer, S. Lin, S. Kiani, C. D. Guzman, D. J. Wiegand, D. Ter-Ovanesyan, J. L. Braff, N. Davidsohn, B. E. Housden, N. Perrimon, R. Weiss, J. Aach, J. J. Collins, and G. M. Church. 2015. "Highly efficient Cas9-mediated transcriptional programming." *Nat Methods* 12 (4):326-8. doi: 10.1038/nmeth.3312.

Chawla, A., W. A. Boisvert, C. H. Lee, B. A. Laffitte, Y. Barak, S. B. Joseph, D. Liao, L. Nagy, P. A. Edwards, L. K. Curtiss, R. M. Evans, and P. Tontonoz. 2001. "A PPAR gamma-LXR-ABCA1 pathway in macrophages is involved in cholesterol efflux and atherogenesis." *Mol Cell* 7 (1):161-71.

Chen, B., J. Mariano, Y. C. Tsai, A. H. Chan, M. Cohen, and A. M. Weissman. 2006. "The activity of a human endoplasmic reticulum-associated degradation E3, gp78, requires its Cue domain, RING finger, and an E2-binding site." *Proc Natl Acad Sci U S A* 103 (2):341-6. doi: 10.1073/pnas.0506618103.

Chen, X., H. Tukachinsky, C. H. Huang, C. Jao, Y. R. Chu, H. Y. Tang, B. Mueller, S. Schulman, T. A. Rapoport, and A. Salic. 2011. "Processing and turnover of the Hedgehog protein in the endoplasmic reticulum." *J Cell Biol* 192 (5):825-38. doi: 10.1083/jcb.201008090.

Chia, N. Y., Y. S. Chan, B. Feng, X. Lu, Y. L. Orlov, D. Moreau, P. Kumar, L. Yang, J. Jiang, M. S. Lau, M. Huss, B. S. Soh, P. Kraus, P. Li, T. Lufkin, B. Lim, N. D. Clarke, F. Bard, and H. H. Ng. 2010. "A genome-wide RNAi screen reveals determinants of human embryonic stem cell identity." *Nature* 468 (7321):316-20. doi: 10.1038/nature09531.

Chiruvella, K. K., Z. Liang, and T. E. Wilson. 2013. "Repair of double-strand breaks by end joining." *Cold Spring Harb Perspect Biol* 5 (5):a012757. doi: 10.1101/cshperspect.a012757.

Chivers, P. T., M. C. Laboissière, and R. T. Raines. 1996. "The CXXC motif: imperatives for the formation of native disulfide bonds in the cell." *EMBO J* 15 (11):2659-67.

Choi, K., H. Kim, H. Kang, S. Y. Lee, S. J. Lee, S. H. Back, S. H. Lee, M. S. Kim, J. E. Lee, J. Y. Park, J. Kim, S. Kim, J. H. Song, Y. Choi, S. Lee, H. J. Lee, J. H. Kim, and S. Cho. 2014. "Regulation of diacylglycerol acyltransferase 2 protein stability by gp78-associated endoplasmic-reticulum-associated degradation." *FEBS J* 281 (13):3048-60. doi: 10.1111/febs.12841.

Christianson, J. C., J. A. Olzmann, T. A. Shaler, M. E. Sowa, E. J. Bennett, C. M. Richter, R. E. Tyler, E. J. Greenblatt, J. W. Harper, and R. R. Kopito. 2012. "Defining human ERAD networks through an integrative mapping strategy." *Nat Cell Biol* 14 (1):93-105. doi: 10.1038/ncb2383.

Christianson, J. C., T. A. Shaler, R. E. Tyler, and R. R. Kopito. 2008. "OS-9 and GRP94 deliver mutant alpha1-antitrypsin to the Hrd1-SEL1L ubiquitin ligase complex for ERAD." *Nat Cell Biol* 10 (3):272-82. doi: 10.1038/ncb1689.

Christianson, J. C., and Y. Ye. 2014. "Cleaning up in the endoplasmic reticulum: ubiquitin in charge." *Nat Struct Mol Biol* 21 (4):325-35. doi: 10.1038/nsmb.2793.

Ciechanover, A., H. Heller, R. Katz-Etzion, and A. Hershko. 1981. "Activation of the heat-stable polypeptide of the ATP-dependent proteolytic system." *Proc Natl Acad Sci U S A* 78 (2):761-5.

Conticello, S. G. 2008. "The AID/APOBEC family of nucleic acid mutators." *Genome Biol* 9 (6):229. doi: 10.1186/gb-2008-9-6-229.

Cook, E. C., J. K. Nelson, V. Sorrentino, D. Koenis, M. Moeton, S. Scheij, R. Ottenhoff, B. Bleijlevens, A. Loregger, and N. Zelcer. 2017. "Identification of the ER-resident E3 ubiquitin ligase RNF145 as a novel LXR-regulated gene." *PLoS One* 12 (2):e0172721. doi: 10.1371/journal.pone.0172721.

Cormier, J. H., T. Tamura, J. C. Sunryd, and D. N. Hebert. 2009. "EDEM1 recognition and delivery of misfolded proteins to the SEL1L-containing ERAD complex." *Mol Cell* 34 (5):627-33. doi: 10.1016/j.molcel.2009.05.018.

D'Alessio, C., J. J. Caramelo, and A. J. Parodi. 2010. "UDP-GlC:glycoprotein glucosyltransferase-glucosidase II, the ying-yang of the ER quality control." *Semin Cell Dev Biol* 21 (5):491-9. doi: 10.1016/j.semcdb.2009.12.014.

Demaison, C., K. Parsley, G. Brouns, M. Scherr, K. Battmer, C. Kinnon, M. Grez, and A. J. Thrasher. 2002. "High-level transduction and gene expression in hematopoietic repopulating cells using a human immunodeficiency [correction of imunodeficiency] virus type 1-based lentiviral vector containing an internal spleen focus forming virus promoter." *Hum Gene Ther* 13 (7):803-13. doi: 10.1089/10430340252898984.

Denic, V., E. M. Quan, and J. S. Weissman. 2006. "A luminal surveillance complex that selects misfolded glycoproteins for ER-associated degradation." *Cell* 126 (2):349-59. doi: 10.1016/j.cell.2006.05.045.
Deshaies, R. J., and C. A. Joazeiro. 2009. "RING domain E3 ubiquitin ligases." *Annu Rev Biochem* 78:399-434. doi: 10.1146/annurev.biochem.78.101807.093809.

Dhar, M. K., A. Koul, and S. Kaul. 2013. "Farnesyl pyrophosphate synthase: a key enzyme in isoprenoid biosynthetic pathway and potential molecular target for drug development." *N Biotechnol* 30 (2):114-23. doi: 10.1016/j.nbt.2012.07.001.

Dong, M., J. P. Bridges, K. Apsley, Y. Xu, and T. E. Weaver. 2008. "ERdj4 and ERdj5 are required for endoplasmic reticulum-associated protein degradation of misfolded surfactant protein C." *Mol Biol Cell* 19 (6):2620-30. doi: 10.1091/mbc.E07-07-0674.

Dong, X. Y., and S. Q. Tang. 2010. "Insulin-induced gene: a new regulator in lipid metabolism." *Peptides* 31 (11):2145-50. doi: 10.1016/j.peptides.2010.07.020.

Dooley, K. A., S. Millinder, and T. F. Osborne. 1998. "Sterol regulation of 3-hydroxy-3-methylglutaryl-coenzyme A synthase gene through a direct interaction between sterol regulatory element binding protein and the trimeric CCAAT-binding factor/nuclear factor Y." *J Biol Chem* 273 (3):1349-56.

Duncan, E. A., M. S. Brown, J. L. Goldstein, and J. Sakai. 1997. "Cleavage site for sterol-regulated protease localized to a leu-Ser bond in the lumenal loop of sterol regulatory element-binding protein-2." *J Biol Chem* 272 (19):12778-85.

Duncan, E. A., U. P. Davé, J. Sakai, J. L. Goldstein, and M. S. Brown. 1998. "Second-site cleavage in sterol regulatory element-binding protein occurs at transmembrane junction as determined by cysteine panning." *J Biol Chem* 273 (28):17801-9.

Duncan, L. M., R. T. Timms, E. Zavodszky, F. Cano, G. Dougan, F. Randow, and P. J. Lehner. 2012. "Fluorescence-based phenotypic selection allows forward genetic screens in haploid human cells." *PLoS One* 7 (6):e39651. doi: 10.1371/journal.pone.0039651.

Edwards, P. A., S. F. Lan, and A. M. Fogelman. 1983. "Alterations in the rates of synthesis and degradation of rat liver 3-hydroxy-3-methylglutaryl coenzyme A reductase produced by cholestyramine and mevinolin." *J Biol Chem* 258 (17):10219-22.

El Khouri, E., G. Le Pavec, M. B. Toledano, and A. Delaunay-Moisan. 2013. "RNF185 is a novel E3 ligase of endoplasmic reticulum-associated degradation (ERAD) that targets cystic fibrosis transmembrane conductance regulator (CFTR)." *J Biol Chem* 288 (43):31177-91. doi: 10.1074/jbc.M113.470500.

Eletr, Z. M., D. T. Huang, D. M. Duda, B. A. Schulman, and B. Kuhlman. 2005. "E2 conjugating enzymes must disengage from their E1 enzymes before E3-dependent ubiquitin and ubiquitin-like transfer." *Nat Struct Mol Biol* 12 (10):933-4. doi: 10.1038/nsmb984.

Evers, B., K. Jastrzebski, J. P. Heijmans, W. Grernrum, R. L. Beijersbergen, and R. Bernards. 2016. "CRISPR knockout screening outperforms shRNA and CRISPRi in identifying essential genes." *Nat Biotechnol* 34 (6):631-3. doi: 10.1038/nbt.3536.

Fang, S., M. Ferrone, C. Yang, J. P. Jensen, S. Tiwari, and A. M. Weissman. 2001. "The tumor autocrine motility factor receptor, gp78, is a ubiquitin protein ligase implicated in degradation from the endoplasmic reticulum." *Proc Natl Acad Sci U S A* 98 (25):14422-7. doi: 10.1073/pnas.251401598.

Faust, J. R., K. L. Luskey, D. J. Chin, J. L. Goldstein, and M. S. Brown. 1982. "Regulation of synthesis and degradation of 3-hydroxy-3-methylglutaryl-coenzyme A reductase by low density lipoprotein and 25-hydroxycholesterol in UT-1 cells." *Proc Natl Acad Sci U S A* 79 (17):5205-9.

Feramisco, J. D., J. L. Goldstein, and M. S. Brown. 2004. "Membrane topology of human insig-1, a protein regulator of lipid synthesis." *J Biol Chem* 279 (9):8487-96. doi: 10.1074/jbc.M312623200.

Finley, D. 2009. "Recognition and processing of ubiquitin-protein conjugates by the proteasome." *Annu Rev Biochem* 78:477-513. doi: 10.1146/annurev.biochem.78.081507.101607.

Fire, A., S. Xu, M. K. Montgomery, S. A. Kostas, S. E. Driver, and C. C. Mello. 1998. "Potent and specific genetic interference by double-stranded RNA in Caenorhabditis elegans." *Nature* 391 (6669):806-11. doi: 10.1038/35888.

Fisher, E. A., and H. N. Ginsberg. 2002. "Complexity in the secretory pathway: the assembly and secretion of apolipoprotein B-containing lipoproteins." *J Biol Chem* 277 (20):17377-80. doi: 10.1074/jbc.R100068200.

Fisher, E. A., N. A. Khanna, and R. S. McLeod. 2011. "Ubiquitination regulates the assembly of VLDL in HepG2 cells and is the committing step of the apoB-100 ERAD pathway." *J Lipid Res* 52 (6):1170-80. doi: 10.1194/jlr.M011726.

Flierman, D., C. S. Coleman, C. M. Pickart, T. A. Rapoport, and V. Chau. 2006. "E2-25K mediates US11-triggered retro-translocation of MHC class I heavy chains in a permeabilized cell system." *Proc Natl Acad Sci U S A* 103 (31):11589-94. doi: 10.1073/pnas.0605215103.

Flierman, D., Y. Ye, M. Dai, V. Chau, and T. A. Rapoport. 2003. "Polyubiquitin serves as a recognition signal, rather than a ratcheting molecule, during retrotranslocation of proteins across the endoplasmic reticulum membrane." *J Biol Chem* 278 (37):34774-82. doi: 10.1074/jbc.M303360200.

Flury, I., R. Garza, A. Shearer, J. Rosen, S. Cronin, and R. Y. Hampton. 2005. "INSIG: a broadly conserved transmembrane chaperone for sterol-sensing domain proteins." *EMBO J* 24 (22):3917-26. doi: 10.1038/sj.emboj.7600855.

Foresti, O., A. Ruggiano, H. K. Hannibal-Bach, C. S. Ejsing, and P. Carvalho. 2013. "Sterol homeostasis requires regulated degradation of squalene monooxygenase by the ubiquitin ligase Doa10/Teb4." *Elife* 2:e00953. doi: 10.7554/eLife.00953.

Forsburg, S. L. 2001. "The art and design of genetic screens: yeast." *Nat Rev Genet* 2 (9):659-68. doi: 10.1038/35088500.

Frickel, E. M., P. Frei, M. Bouvier, W. F. Stafford, A. Helenius, R. Glockshuber, and L. Ellgaard. 2004. "ERp57 is a multifunctional thiol-disulfide oxidoreductase." *J Biol Chem* 279 (18):18277-87. doi: 10.1074/jbc.M314089200.

Fry, W. H., C. Simion, C. Sweeney, and K. L. Carraway. 2011. "Quantity control of the ErbB3 receptor tyrosine kinase at the endoplasmic reticulum." *Mol Cell Biol* 31 (14):3009-18. doi: 10.1128/MCB.05105-11.

Fröhlich, F., C. Petit, N. Kory, R. Christiano, H. K. Hannibal-Bach, M. Graham, X. Liu, C. S. Ejsing, R. V. Farese, and T. C. Walther. 2015. "The GARP complex is required for cellular sphingolipid homeostasis." *Elife* 4. doi: 10.7554/eLife.08712.

Gao, Y., Y. Zhou, J. L. Goldstein, M. S. Brown, and A. Radhakrishnan. 2017. "Cholesterol-induced conformational changes in the sterol-sensing domain of the Scap protein suggest feedback mechanism to control cholesterol synthesis." *J Biol Chem* 292 (21):8729-8737. doi: 10.1074/jbc.M117.783894.

Gardner, R. G., and R. Y. Hampton. 1999. "A highly conserved signal controls degradation of 3-hydroxy-3-methylglutaryl-coenzyme A (HMG-CoA) reductase in eukaryotes." *J Biol Chem* 274 (44):31671-8.

Gardner, R. G., G. M. Swarbrick, N. W. Bays, S. R. Cronin, S. Wilhovsky, L. Seelig, C. Kim, and R. Y. Hampton. 2000. "Endoplasmic reticulum degradation requires lumen to cytosol signaling. Transmembrane control of Hrd1p by Hrd3p." *J Cell Biol* 151 (1):69-82.

Garza, R. M., B. K. Sato, and R. Y. Hampton. 2009. "In vitro analysis of Hrd1p-mediated retrotranslocation of its multispanning membrane substrate 3-hydroxy-3-methylglutaryl (HMG)-CoA reductase." *J Biol Chem* 284 (22):14710-22. doi: 10.1074/jbc.M809607200.

Garza, R. M., P. N. Tran, and R. Y. Hampton. 2009. "Geranylgeranyl pyrophosphate is a potent regulator of HRD-dependent 3-Hydroxy-3-methylglutaryl-CoA reductase degradation in yeast." *J Biol Chem* 284 (51):35368-80. doi: 10.1074/jbc.M109.023994.

Gauss, R., E. Jarosch, T. Sommer, and C. Hirsch. 2006. "A complex of Yos9p and the HRD ligase integrates endoplasmic reticulum quality control into the degradation machinery." *Nat Cell Biol* 8 (8):849-54. doi: 10.1038/ncb1445.

Gibson, D. G., L. Young, R. Y. Chuang, J. C. Venter, C. A. Hutchison, and H. O. Smith. 2009. "Enzymatic assembly of DNA molecules up to several hundred kilobases." *Nat Methods* 6 (5):343-5. doi: 10.1038/nmeth.1318.

Gil, G., J. R. Faust, D. J. Chin, J. L. Goldstein, and M. S. Brown. 1985. "Membrane-bound domain of HMG CoA reductase is required for sterol-enhanced degradation of the enzyme." *Cell* 41 (1):249-58.

Gilbert, L. A., M. A. Horlbeck, B. Adamson, J. E. Villalta, Y. Chen, E. H. Whitehead, C. Guimaraes, B. Panning, H. L. Ploegh, M. C. Bassik, L. S. Qi, M. Kampmann, and J. S. Weissman. 2014. "Genome-Scale CRISPR-Mediated Control of Gene Repression and Activation." *Cell* 159 (3):647-61. doi: 10.1016/j.cell.2014.09.029.

Gilbert, L. A., M. H. Larson, L. Morsut, Z. Liu, G. A. Brar, S. E. Torres, N. Stern-Ginossar, O. Brandman, E. H. Whitehead, J. A. Doudna, W. A. Lim, J. S. Weissman, and L. S. Qi. 2013. "CRISPR-mediated modular RNA-guided regulation of transcription in eukaryotes." *Cell* 154 (2):442-51. doi: 10.1016/j.cell.2013.06.044.

Gill, S., J. Stevenson, I. Kristiana, and A. J. Brown. 2011. "Cholesterol-dependent degradation of squalene monooxygenase, a control point in cholesterol synthesis beyond HMG-CoA reductase." *Cell Metab* 13 (3):260-73. doi: 10.1016/j.cmet.2011.01.015.

Gnann, A., J. R. Riordan, and D. H. Wolf. 2004. "Cystic fibrosis transmembrane conductance regulator degradation depends on the lectins Htm1p/EDEM and the Cdc48 protein complex in yeast." *Mol Biol Cell* 15 (9):4125-35. doi: 10.1091/mbc.E04-01-0024.

Goeckeler, J. L., and J. L. Brodsky. 2010. "Molecular chaperones and substrate ubiquitination control the efficiency of endoplasmic reticulum-associated degradation." *Diabetes Obes Metab* 12 Suppl 2:32-8. doi: 10.1111/j.1463-1326.2010.01273.x.

Goldstein, J. L., and M. S. Brown. 1990. "Regulation of the mevalonate pathway." *Nature* 343 (6257):425-30. doi: 10.1038/343425a0.

Goldstein, J. L., R. A. DeBose-Boyd, and M. S. Brown. 2006. "Protein sensors for membrane sterols." *Cell* 124 (1):35-46. doi: 10.1016/j.cell.2005.12.022.

Goldstein, J. L., R. B. Rawson, and M. S. Brown. 2002. "Mutant mammalian cells as tools to delineate the sterol regulatory element-binding protein pathway for feedback regulation of lipid synthesis." *Arch Biochem Biophys* 397 (2):139-48. doi: 10.1006/abbi.2001.2615.

Gong, Y., J. N. Lee, P. C. Lee, J. L. Goldstein, M. S. Brown, and J. Ye. 2006. "Sterol-regulated ubiquitination and degradation of Insig-1 creates a convergent mechanism for feedback control of cholesterol synthesis and uptake." *Cell Metab* 3 (1):15-24. doi: 10.1016/j.cmet.2005.11.014.

Graham, D. B., C. E. Becker, A. Doan, G. Goel, E. J. Villablanca, D. Knights, A. Mok, A. C. Ng, J. G. Doench, D. E. Root, C. B. Clish, and R. J. Xavier. 2015. "Functional genomics identifies negative regulatory nodes controlling phagocyte oxidative burst." *Nat Commun* 6:7838. doi: 10.1038/ncomms8838.

Greenblatt, E. J., J. A. Olzmann, and R. R. Kopito. 2011. "Derlin-1 is a rhomboid pseudoprotease required for the dislocation of mutant α-1 antitrypsin from the endoplasmic reticulum." *Nat Struct Mol Biol* 18 (10):1147-52. doi: 10.1038/nsmb.2111.

Grimm, S. 2004. "The art and design of genetic screens: mammalian culture cells." *Nat Rev Genet* 5 (3):179-89. doi: 10.1038/nrg1291.

Guimaraes, C. P., J. E. Carette, M. Varadarajan, J. Antos, M. W. Popp, E. Spooner, T. R. Brummelkamp, and H. L. Ploegh. 2011. "Identification of host cell factors required for intoxication through use of modified cholera toxin." *J Cell Biol* 195 (5):751-64. doi: 10.1083/jcb.201108103.

Guo, X., S. Shen, S. Song, S. He, Y. Cui, G. Xing, J. Wang, Y. Yin, L. Fan, F. He, and L. Zhang. 2011. "The E3 ligase Smurf1 regulates Wolfram syndrome protein stability at the endoplasmic reticulum." *J Biol Chem* 286 (20):18037-47. doi: 10.1074/jbc.M111.225615.

Guo, Y., T. C. Walther, M. Rao, N. Stuurman, G. Goshima, K. Terayama, J. S. Wong, R. D. Vale, P. Walter, and R. V. Farese. 2008. "Functional genomic screen reveals genes involved in lipid-droplet formation and utilization." *Nature* 453 (7195):657-61. doi: 10.1038/nature06928.

Haas, A. L., and I. A. Rose. 1982. "The mechanism of ubiquitin activating enzyme. A kinetic and equilibrium analysis." *J Biol Chem* 257 (17):10329-37.

Hagiwara, M., K. Maegawa, M. Suzuki, R. Ushioda, K. Araki, Y. Matsumoto, J. Hoseki, K. Nagata, and K. Inaba. 2011. "Structural basis of an ERAD pathway mediated by the ER-resident protein disulfide reductase ERdj5." *Mol Cell* 41 (4):432-44. doi: 10.1016/j.molcel.2011.01.021.

Hampton, R. Y., R. G. Gardner, and J. Rine. 1996. "Role of 26S proteasome and HRD genes in the degradation of 3-hydroxy-3-methylglutaryl-CoA reductase, an integral endoplasmic reticulum membrane protein." *Mol Biol Cell* 7 (12):2029-44.

Hampton, R. Y., and R. M. Garza. 2009. "Protein quality control as a strategy for cellular regulation: lessons from ubiquitin-mediated regulation of the sterol pathway." *Chem Rev* 109 (4):1561-74. doi: 10.1021/cr800544v.

Hartwell, L. H., J. Culotti, and B. Reid. 1970. "Genetic control of the cell-division cycle in yeast. I. Detection of mutants." *Proc Natl Acad Sci U S A* 66 (2):352-9.

Hebert, D. N., R. Bernasconi, and M. Molinari. 2010. "ERAD substrates: which way out?" *Semin Cell Dev Biol* 21 (5):526-32. doi: 10.1016/j.semcdb.2009.12.007.

Hebert, D. N., B. Foellmer, and A. Helenius. 1995. "Glucose trimming and reglucosylation determine glycoprotein association with calnexin in the endoplasmic reticulum." *Cell* 81 (3):425-33.

Hebert, D. N., S. C. Garman, and M. Molinari. 2005. "The glycan code of the endoplasmic reticulum: asparagine-linked carbohydrates as protein maturation and quality-control tags." *Trends Cell Biol* 15 (7):364-70. doi: 10.1016/j.tcb.2005.05.007.

Hegde, R. S., and H. L. Ploegh. 2010. "Quality and quantity control at the endoplasmic reticulum." *Curr Opin Cell Biol* 22 (4):437-46. doi: 10.1016/j.ceb.2010.05.005.

Hershko, A., and A. Ciechanover. 1998. "The ubiquitin system." *Annu Rev Biochem* 67:425-79. doi: 10.1146/annurev.biochem.67.1.425.

Hicke, L., H. L. Schubert, and C. P. Hill. 2005. "Ubiquitin-binding domains." *Nat Rev Mol Cell Biol* 6 (8):610-21. doi: 10.1038/nrm1701.

Hiller, M. M., A. Finger, M. Schweiger, and D. H. Wolf. 1996. "ER degradation of a misfolded luminal protein by the cytosolic ubiquitin-proteasome pathway." *Science* 273 (5282):1725-8.

Hirao, K., Y. Natsuka, T. Tamura, I. Wada, D. Morito, S. Natsuka, P. Romero, B. Sleno, L. O. Tremblay, A. Herscovics, K. Nagata, and N. Hosokawa. 2006. "EDEM3, a soluble EDEM homolog, enhances glycoprotein endoplasmic reticulum-associated degradation and mannose trimming." *J Biol Chem* 281 (14):9650-8. doi: 10.1074/jbc.M512191200.

Horton, J. D., J. C. Cohen, and H. H. Hobbs. 2007. "Molecular biology of PCSK9: its role in LDL metabolism." *Trends Biochem Sci* 32 (2):71-7. doi: 10.1016/j.tibs.2006.12.008.

Horton, J. D., J. L. Goldstein, and M. S. Brown. 2002. "SREBPs: activators of the complete program of cholesterol and fatty acid synthesis in the liver." *J Clin Invest* 109 (9):1125-31. doi: 10.1172/JCI15593.

Hosokawa, N., Y. Kamiya, D. Kamiya, K. Kato, and K. Nagata. 2009. "Human OS-9, a lectin required for glycoprotein endoplasmic reticulum-associated degradation, recognizes mannose-trimmed N-glycans." *J Biol Chem* 284 (25):17061-8. doi: 10.1074/jbc.M809725200.

Hosokawa, N., I. Wada, K. Nagasawa, T. Moriyama, K. Okawa, and K. Nagata. 2008. "Human XTP3-B forms an endoplasmic reticulum quality control scaffold with the HRD1-SEL1L ubiquitin ligase complex and BiP." *J Biol Chem* 283 (30):20914-24. doi: 10.1074/jbc.M709336200.

Housden, B. E., M. Muhar, M. Gemberling, C. A. Gersbach, D. Y. Stainier, G. Seydoux, S. E. Mohr, J. Zuber, and N. Perrimon. 2017. "Loss-of-function genetic tools for animal models: cross-species and cross-platform differences." *Nat Rev Genet* 18 (1):24-40. doi: 10.1038/nrg.2016.118.

Hsu, J. L., D. J. van den Boomen, P. Tomasec, M. P. Weekes, R. Antrobus, R. J. Stanton, E. Ruckova, D. Sugrue, G. S. Wilkie, A. J. Davison, G. W. Wilkinson, and P. J. Lehner. 2015. "Plasma membrane profiling defines an expanded class of cell surface proteins selectively targeted for degradation by HCMV US2 in cooperation with UL141." *PLoS Pathog* 11 (4):e1004811. doi: 10.1371/journal.ppat.1004811.

Hsu, P. D., E. S. Lander, and F. Zhang. 2014. "Development and Applications of CRISPR-Cas9 for Genome Engineering." *Cell* 157 (6):1262-1278. doi: 10.1016/j.cell.2014.05.010.

Hua, X., A. Nohturfft, J. L. Goldstein, and M. S. Brown. 1996. "Sterol resistance in CHO cells traced to point mutation in SREBP cleavage-activating protein." *Cell* 87 (3):415-26.

Husnjak, K., S. Elsasser, N. Zhang, X. Chen, L. Randles, Y. Shi, K. Hofmann, K. J. Walters, D. Finley, and I. Dikic. 2008. "Proteasome subunit Rpn13 is a novel ubiquitin receptor." *Nature* 453 (7194):481-8. doi: 10.1038/nature06926.

Hutvágner, G., J. McLachlan, A. E. Pasquinelli, E. Bálint, T. Tuschl, and P. D. Zamore. 2001. "A cellular function for the RNA-interference enzyme Dicer in the maturation of the let-7 small temporal RNA." *Science* 293 (5531):834-8. doi: 10.1126/science.1062961.

Huyer, G., W. F. Piluek, Z. Fansler, S. G. Kreft, M. Hochstrasser, J. L. Brodsky, and S. Michaelis. 2004. "Distinct machinery is required in Saccharomyces cerevisiae for the endoplasmic reticulum-associated degradation of a multispanning membrane protein and a soluble luminal protein." *J Biol Chem* 279 (37):38369-78. doi: 10.1074/jbc.M402468200.

Hwang, J., C. P. Walczak, T. A. Shaler, J. A. Olzmann, L. Zhang, J. E. Elias, and R. R. Kopito. 2017. "Characterization of protein complexes of the endoplasmic reticulum-associated degradation E3 ubiquitin ligase Hrd1." *J Biol Chem* 292 (22):9104-9116. doi: 10.1074/jbc.M117.785055.

Hwang, S., A. D. Nguyen, Y. Jo, L. J. Engelking, J. Brugarolas, and R. A. DeBose-Boyd. 2017. "Hypoxia-inducible factor 1α activates insulin-induced gene 2 (Insig-2) transcription for degradation of 3-hydroxy-3-methylglutaryl (HMG)-CoA reductase in the liver." *J Biol Chem* 292 (22):9382-9393. doi: 10.1074/jbc.M117.788562.

Imai, Y., M. Soda, S. Hatakeyama, T. Akagi, T. Hashikawa, K. I. Nakayama, and R. Takahashi. 2002. "CHIP is associated with Parkin, a gene responsible for familial Parkinson's disease, and enhances its ubiquitin ligase activity." *Mol Cell* 10 (1):55-67.

Infante, R. E., M. L. Wang, A. Radhakrishnan, H. J. Kwon, M. S. Brown, and J. L. Goldstein. 2008. "NPC2 facilitates bidirectional transfer of cholesterol between NPC1 and lipid bilayers, a step in cholesterol egress from lysosomes." *Proc Natl Acad Sci U S A* 105 (40):15287-92. doi: 10.1073/pnas.0807328105.

Irisawa, M., J. Inoue, N. Ozawa, K. Mori, and R. Sato. 2009. "The sterol-sensing endoplasmic reticulum (ER) membrane protein TRC8 hampers ER to Golgi transport of sterol regulatory element-binding protein-2 (SREBP-2)/SREBP cleavage-activated protein and reduces SREBP-2 cleavage." *J Biol Chem* 284 (42):28995-9004. doi: 10.1074/jbc.M109.041376.

Isakov, E., and A. Stanhill. 2011. "Stalled proteasomes are directly relieved by P97 recruitment." *J Biol Chem* 286 (35):30274-83. doi: 10.1074/jbc.M111.240309.

Jackson, A. L., S. R. Bartz, J. Schelter, S. V. Kobayashi, J. Burchard, M. Mao, B. Li, G. Cavet, and P. S. Linsley. 2003. "Expression profiling reveals off-target gene regulation by RNAi." *Nat Biotechnol* 21 (6):635-7. doi: 10.1038/nbt831.

Jackson, A. L., J. Burchard, J. Schelter, B. N. Chau, M. Cleary, L. Lim, and P. S. Linsley. 2006. "Widespread siRNA "off-target" transcript silencing mediated by seed region sequence complementarity." *RNA* 12 (7):1179-87. doi: 10.1261/rna.25706.

Jae, L. T., M. Raaben, M. Riemersma, E. van Beusekom, V. A. Blomen, A. Velds, R. M. Kerkhoven, J. E. Carette, H. Topaloglu, P. Meinecke, M. W. Wessels, D. J. Lefeber, S. P. Whelan, H. van Bokhoven, and T. R. Brummelkamp. 2013. "Deciphering the glycosylome of dystroglycanopathies using haploid screens for lassa virus entry." *Science* 340 (6131):479-83. doi: 10.1126/science.1233675.

Janowski, B. A. 2002. "The hypocholesterolemic agent LY295427 up-regulates INSIG-1, identifying the INSIG-1 protein as a mediator of cholesterol homeostasis through SREBP." *Proc Natl Acad Sci U S A* 99 (20):12675-80. doi: 10.1073/pnas.202471599.

Janowski, B. A., P. J. Willy, T. R. Devi, J. R. Falck, and D. J. Mangelsdorf. 1996. "An oxysterol signalling pathway mediated by the nuclear receptor LXR alpha." *Nature* 383 (6602):728-31. doi: 10.1038/383728a0.

Jarosch, E., C. Taxis, C. Volkwein, J. Bordallo, D. Finley, D. H. Wolf, and T. Sommer. 2002. "Protein dislocation from the ER requires polyubiquitination and the AAA-ATPase Cdc48." *Nat Cell Biol* 4 (2):134-9. doi: 10.1038/ncb746.

Jo, Y., and R. A. Debose-Boyd. 2010. "Control of cholesterol synthesis through regulated ER-associated degradation of HMG CoA reductase." *Crit Rev Biochem Mol Biol* 45 (3):185-98. doi: 10.3109/10409238.2010.485605.

Jo, Y., I. Z. Hartman, and R. A. DeBose-Boyd. 2013. "Ancient ubiquitous protein-1 mediates sterol-induced ubiquitination of 3-hydroxy-3-methylglutaryl CoA reductase in lipid droplet-associated endoplasmic reticulum membranes." *Mol Biol Cell* 24 (3):169-83. doi: 10.1091/mbc.E12-07-0564.

Jo, Y., P. C. Lee, P. V. Sguigna, and R. A. DeBose-Boyd. 2011. "Sterol-induced degradation of HMG CoA reductase depends on interplay of two Insigs and two ubiquitin ligases, gp78 and Trc8." *Proc Natl Acad Sci U S A* 108 (51):20503-8. doi: 10.1073/pnas.1112831108.

Johnson, A. E., and M. A. van Waes. 1999. "The translocon: a dynamic gateway at the ER membrane." *Annu Rev Cell Dev Biol* 15:799-842. doi: 10.1146/annurev.cellbio.15.1.799.

Joung, J., J. M. Engreitz, S. Konermann, O. O. Abudayyeh, V. K. Verdine, F. Aguet, J. S. Gootenberg, N. E. Sanjana, J. B. Wright, C. P. Fulco, Y. Y. Tseng, C. H. Yoon, J. S. Boehm, E. S. Lander, and F. Zhang. 2017. "Genome-scale activation screen identifies a lncRNA locus regulating a gene neighbourhood." *Nature*. doi: 10.1038/nature23451.

Joung, J. K., and J. D. Sander. 2013. "TALENs: a widely applicable technology for targeted genome editing." *Nat Rev Mol Cell Biol* 14 (1):49-55. doi: 10.1038/nrm3486.

Joung, J., S. Konermann, J. S. Gootenberg, O. O. Abudayyeh, R. J. Platt, M. D. Brigham, N. E. Sanjana, and F. Zhang. 2017. "Genome-scale CRISPR-Cas9 knockout and transcriptional activation screening." *Nat Protoc* 12 (4):828-863. doi: 10.1038/nprot.2017.016.

Kanapin, A., S. Batalov, M. J. Davis, J. Gough, S. Grimmond, H. Kawaji, M. Magrane, H. Matsuda, C. Schönbach, R. D. Teasdale, Z. Yuan, RIKEN GER Group, and GSL Members. 2003. "Mouse proteome analysis." *Genome Res* 13 (6B):1335-44. doi: 10.1101/gr.978703.

Kaneko, M., I. Iwase, Y. Yamasaki, T. Takai, Y. Wu, S. Kanemoto, K. Matsuhisa, R. Asada, Y. Okuma, T. Watanabe, K. Imaizumi, and Y. Nomura. 2016. "Genome-wide identification and gene expression profiling of ubiquitin ligases for endoplasmic reticulum protein degradation." *Sci Rep* 6:30955. doi: 10.1038/srep30955.

Kaneko, M., H. Koike, R. Saito, Y. Kitamura, Y. Okuma, and Y. Nomura. 2010. "Loss of HRD1-mediated protein degradation causes amyloid precursor protein accumulation and amyloid-beta generation." *J Neurosci* 30 (11):3924-32. doi: 10.1523/JNEUROSCI.2422-09.2010.

Karlas, A., N. Machuy, Y. Shin, K. P. Pleissner, A. Artarini, D. Heuer, D. Becker, H. Khalil, L. A. Ogilvie, S. Hess, A. P. Mäurer, E. Müller, T. Wolff, T. Rudel, and T. F. Meyer. 2010. "Genome-wide RNAi screen identifies human host factors crucial for influenza virus replication." *Nature* 463 (7282):818-22. doi: 10.1038/nature08760.

Kelley, L. A., S. Mezulis, C. M. Yates, M. N. Wass, and M. J. Sternberg. 2015. "The Phyre2 web portal for protein modeling, prediction and analysis." *Nat Protoc* 10 (6):845-58. doi: 10.1038/nprot.2015.053.

Kennedy, M. A., A. Venkateswaran, P. T. Tarr, I. Xenarios, J. Kudoh, N. Shimizu, and P. A. Edwards. 2001. "Characterization of the human ABCG1 gene: liver X receptor activates an internal promoter that produces a novel transcript encoding an alternative form of the protein." *J Biol Chem* 276 (42):39438-47. doi: 10.1074/jbc.M105863200.

Kikkert, M., R. Doolman, M. Dai, R. Avner, G. Hassink, S. van Voorden, S. Thanedar, J. Roitelman, V. Chau, and E. Wiertz. 2004. "Human HRD1 is an E3 ubiquitin ligase involved in degradation of proteins from the endoplasmic reticulum." *J Biol Chem* 279 (5):3525-34. doi: 10.1074/jbc.M307453200.

Kim, H., and J. S. Kim. 2014. "A guide to genome engineering with programmable nucleases." *Nat Rev Genet* 15 (5):321-34. doi: 10.1038/nrg3686.

Kirisako, T., K. Kamei, S. Murata, M. Kato, H. Fukumoto, M. Kanie, S. Sano, F. Tokunaga, K. Tanaka, and K. Iwai. 2006. "A ubiquitin ligase complex assembles linear polyubiquitin chains." *EMBO J* 25 (20):4877-87. doi: 10.1038/sj.emboj.7601360.

Kleinfelter, L. M., R. K. Jangra, L. T. Jae, A. S. Herbert, E. Mittler, K. M. Stiles, A. S. Wirchnianski, M. Kielian, T. R. Brummelkamp, J. M. Dye, and K. Chandran. 2015. "Haploid Genetic Screen Reveals a Profound and Direct Dependence on Cholesterol for Hantavirus Membrane Fusion." *MBio* 6 (4):e00801. doi: 10.1128/mBio.00801-15.

Klemm, E. J., E. Spooner, and H. L. Ploegh. 2011. "Dual role of ancient ubiquitous protein 1 (AUP1) in lipid droplet accumulation and endoplasmic reticulum (ER) protein quality control." *J Biol Chem* 286 (43):37602-14. doi: 10.1074/jbc.M111.284794.

Ko, H. S., T. Uehara, K. Tsuruma, and Y. Nomura. 2004. "Ubiquilin interacts with ubiquitylated proteins and proteasome through its ubiquitin-associated and ubiquitin-like domains." *FEBS Lett* 566 (1-3):110-4. doi: 10.1016/j.febslet.2004.04.031.

Koegl, M., T. Hoppe, S. Schlenker, H. D. Ulrich, T. U. Mayer, and S. Jentsch. 1999. "A novel ubiquitination factor, E4, is involved in multiubiquitin chain assembly." *Cell* 96 (5):635-44.

Koike-Yusa, H., Y. Li, E. P. Tan, M.el C Velasco-Herrera, and K. Yusa. 2014. "Genome-wide recessive genetic screening in mammalian cells with a lentiviral CRISPR-guide RNA library." *Nat Biotechnol* 32 (3):267-73. doi: 10.1038/nbt.2800.

Komander, D., and M. Rape. 2012. "The ubiquitin code." *Annu Rev Biochem* 81:203-29. doi: 10.1146/annurev-biochem-060310-170328.

Komor, A. C., Y. B. Kim, M. S. Packer, J. A. Zuris, and D. R. Liu. 2016. "Programmable editing of a target base in genomic DNA without double-stranded DNA cleavage." *Nature* 533 (7603):420-4. doi: 10.1038/nature17946.

Kong, S., Y. Yang, Y. Xu, Y. Wang, Y. Zhang, J. Melo-Cardenas, X. Xu, B. Gao, E. B. Thorp, D. D. Zhang, B. Zhang, J. Song, K. Zhang, J. Zhang, H. Li, and D. Fang. 2016. "Endoplasmic reticulum-resident E3 ubiquitin ligase Hrd1 controls B-cell immunity through degradation of the death receptor CD95/Fas." *Proc Natl Acad Sci U S A* 113 (37):10394-9. doi: 10.1073/pnas.1606742113.

Kopito, R. R. 1999. "Biosynthesis and degradation of CFTR." *Physiol Rev* 79 (1 Suppl):S167-73.

Kostova, Z., J. Mariano, S. Scholz, C. Koenig, and A. M. Weissman. 2009. "A Ubc7p-binding domain in Cue1p activates ER-associated protein degradation." *J Cell Sci* 122 (Pt 9):1374-81. doi: 10.1242/jcs.044255.

Kotecki, M., P. S. Reddy, and B. H. Cochran. 1999. "Isolation and characterization of a near-haploid human cell line." *Exp Cell Res* 252 (2):273-80. doi: 10.1006/excr.1999.4656.

Kravtsova-Ivantsiv, Y., and A. Ciechanover. 2012. "Non-canonical ubiquitin-based signals for proteasomal degradation." *J Cell Sci* 125 (Pt 3):539-48. doi: 10.1242/jcs.093567.

Kreft, S. G., L. Wang, and M. Hochstrasser. 2006. "Membrane topology of the yeast endoplasmic reticulum-localized ubiquitin ligase Doa10 and comparison with its human ortholog TEB4 (MARCH-VI)." *J Biol Chem* 281 (8):4646-53. doi: 10.1074/jbc.M512215200.

Kuwabara, P. E., and M. Labouesse. 2002. "The sterol-sensing domain: multiple families, a unique role?" *Trends Genet* 18 (4):193-201.

Kwon, H. J., L. Abi-Mosleh, M. L. Wang, J. Deisenhofer, J. L. Goldstein, M. S. Brown, and R. E. Infante. 2009. "Structure of N-terminal domain of NPC1 reveals distinct subdomains for binding and transfer of cholesterol." *Cell* 137 (7):1213-24. doi: 10.1016/j.cell.2009.03.049.

König, R., C. Y. Chiang, B. P. Tu, S. F. Yan, P. D. DeJesus, A. Romero, T. Bergauer, A. Orth, U. Krueger, Y. Zhou, and S. K. Chanda. 2007. "A probability-based approach for the analysis of large-scale RNAi screens." *Nat Methods* 4 (10):847-9. doi: 10.1038/nmeth1089.

Lagace, T. A., D. E. Curtis, R. Garuti, M. C. McNutt, S. W. Park, H. B. Prather, N. N. Anderson, Y. K. Ho, R. E. Hammer, and J. D. Horton. 2006. "Secreted PCSK9 decreases the number of LDL receptors in hepatocytes and in livers of parabiotic mice." *J Clin Invest* 116 (11):2995-3005. doi: 10.1172/JCI29383.

Lange, Y., D. S. Ory, J. Ye, M. H. Lanier, F. F. Hsu, and T. L. Steck. 2008. "Effectors of rapid homeostatic responses of endoplasmic reticulum cholesterol and 3-hydroxy-3-methylglutaryl-CoA reductase." *J Biol Chem* 283 (3):1445-55. doi: 10.1074/jbc.M706967200.

Langmead, B., C. Trapnell, M. Pop, and S. L. Salzberg. 2009. "Ultrafast and memory-efficient alignment of short DNA sequences to the human genome." *Genome Biol* 10 (3):R25. doi: 10.1186/gb-2009-10-3-r25.

Lee, J. G., and Y. Ye. 2013. "Bag6/Bat3/Scythe: a novel chaperone activity with diverse regulatory functions in protein biogenesis and degradation." *Bioessays* 35 (4):377-85. doi: 10.1002/bies.201200159.

Lee, J. N., Y. Gong, X. Zhang, and J. Ye. 2006. "Proteasomal degradation of ubiquitinated Insig proteins is determined by serine residues flanking ubiquitinated lysines." *Proc Natl Acad Sci U S A* 103 (13):4958-63. doi: 10.1073/pnas.0600422103.

Lee, J. N., B. Song, R. A. DeBose-Boyd, and J. Ye. 2006. "Sterol-regulated degradation of Insig-1 mediated by the membrane-bound ubiquitin ligase gp78." *J Biol Chem* 281 (51):39308-15. doi: 10.1074/jbc.M608999200.

Lee, J. N., and J. Ye. 2004. "Proteolytic activation of sterol regulatory element-binding protein induced by cellular stress through depletion of Insig-1." *J Biol Chem* 279 (43):45257-65. doi: 10.1074/jbc.M408235200.

Lee, J. N., X. Zhang, J. D. Feramisco, Y. Gong, and J. Ye. 2008. "Unsaturated fatty acids inhibit proteasomal degradation of Insig-1 at a postubiquitination step." *J Biol Chem* 283 (48):33772-83. doi: 10.1074/jbc.M806108200.

Lee, J. P., A. Brauweiler, M. Rudolph, J. E. Hooper, H. A. Drabkin, and R. M. Gemmill. 2010. "The TRC8 ubiquitin ligase is sterol regulated and interacts with lipid and protein biosynthetic pathways." *Mol Cancer Res* 8 (1):93-106. doi: 10.1158/1541-7786.MCR-08-0491.

Lee, Y., C. Ahn, J. Han, H. Choi, J. Kim, J. Yim, J. Lee, P. Provost, O. Rådmark, S. Kim, and V. N. Kim. 2003. "The nuclear RNase III Drosha initiates microRNA processing." *Nature* 425 (6956):415-9. doi: 10.1038/nature01957.

Lees, W. U., and G. M. Whitesides. 1993. Equilibrium constants for thiol-disulphide interchange reactions: a coherent, corrected set. The Journal of Organic Chemistry.

Lemberg, M. K. 2013. "Sampling the membrane: function of rhomboid-family proteins." *Trends Cell Biol* 23 (5):210-7. doi: 10.1016/j.tcb.2013.01.002.

Lerner, M., M. Corcoran, D. Cepeda, M. L. Nielsen, R. Zubarev, F. Pontén, M. Uhlén, S. Hober, D. Grandér, and O. Sangfelt. 2007. "The RBCC gene RFP2 (Leu5) encodes a novel transmembrane E3 ubiquitin ligase involved in ERAD." *Mol Biol Cell* 18 (5):1670-82. doi: 10.1091/mbc.E06-03-0248.

Liang, J. S., T. Kim, S. Fang, J. Yamaguchi, A. M. Weissman, E. A. Fisher, and H. N. Ginsberg. 2003. "Overexpression of the tumor autocrine motility factor receptor Gp78, a ubiquitin protein ligase, results in increased ubiquitinylation and decreased secretion of apolipoprotein B100 in HepG2 cells." *J Biol Chem* 278 (26):23984-8. doi: 10.1074/jbc.M302683200.

Liang, P., Y. Xu, X. Zhang, C. Ding, R. Huang, Z. Zhang, J. Lv, X. Xie, Y. Chen, Y. Li, Y. Sun, Y. Bai, Z. Songyang, W. Ma, C. Zhou, and J. Huang. 2015. "CRISPR/Cas9-mediated gene editing in human tripronuclear zygotes." *Protein Cell* 6 (5):363-372. doi: 10.1007/s13238-015-0153-5.

Lilley, B. N., and H. L. Ploegh. 2005. "Multiprotein complexes that link dislocation, ubiquitination, and extraction of misfolded proteins from the endoplasmic reticulum membrane." *Proc Natl Acad Sci U S A* 102 (40):14296-301. doi: 10.1073/pnas.0505014102.

Liscum, L., J. Finer-Moore, R. M. Stroud, K. L. Luskey, M. S. Brown, and J. L. Goldstein. 1985. "Domain structure of 3-hydroxy-3-methylglutaryl coenzyme A reductase, a glycoprotein of the endoplasmic reticulum." *J Biol Chem* 260 (1):522-30.

Liu, S. J., M. A. Horlbeck, S. W. Cho, H. S. Birk, M. Malatesta, D. He, F. J. Attenello, J. E. Villalta, M. Y. Cho, Y. Chen, M. A. Mandegar, M. P. Olvera, L. A. Gilbert, B. R. Conklin, H. Y. Chang, J. S. Weissman, and D. A. Lim. 2017. "CRISPRi-based genome-scale identification of functional long noncoding RNA loci in human cells." *Science* 355 (6320). doi: 10.1126/science.aah7111.

Liu, T. F., J. J. Tang, P. S. Li, Y. Shen, J. G. Li, H. H. Miao, B. L. Li, and B. L. Song. 2012. "Ablation of gp78 in liver improves hyperlipidemia and insulin resistance by inhibiting SREBP to decrease lipid biosynthesis." *Cell Metab* 16 (2):213-25. doi: 10.1016/j.cmet.2012.06.014.

Liu, Y., N. Soetandyo, J. G. Lee, L. Liu, Y. Xu, W. M. Clemons, and Y. Ye. 2014. "USP13 antagonizes gp78 to maintain functionality of a chaperone in ER-associated degradation." *Elife* 3:e01369. doi: 10.7554/eLife.01369.

Loregger, A., E. C. Cook, J. K. Nelson, M. Moeton, L. J. Sharpe, S. Engberg, M. Karimova, G. Lambert, A. J. Brown, and N. Zelcer. 2015. "A MARCH6 and IDOL E3 Ubiquitin Ligase Circuit Uncouples Cholesterol Synthesis from Lipoprotein Uptake in Hepatocytes." *Mol Cell Biol* 36 (2):285-94. doi: 10.1128/MCB.00890-15.

Lu, J. P., Y. Wang, D. A. Sliter, M. M. Pearce, and R. J. Wojcikiewicz. 2011. "RNF170 protein, an endoplasmic reticulum membrane ubiquitin ligase, mediates inositol 1,4,5-trisphosphate receptor ubiquitination and degradation." *J Biol Chem* 286 (27):24426-33. doi: 10.1074/jbc.M111.251983.

Ma, H., N. Marti-Gutierrez, S. W. Park, J. Wu, Y. Lee, K. Suzuki, A. Koski, D. Ji, T. Hayama, R. Ahmed, H. Darby, C. Van Dyken, Y. Li, E. Kang, A. R. Park, D. Kim, S. T. Kim, J. Gong, Y. Gu, X. Xu, D. Battaglia, S. A. Krieg, D. M. Lee, D. H. Wu, D. P. Wolf, S. B. Heitner, J. C. I. Belmonte, P. Amato, J. S. Kim, S. Kaul, and S. Mitalipov. 2017. "Correction of a pathogenic gene mutation in human embryos." *Nature*. doi: 10.1038/nature23305.

Maeda, Y., S. Tanaka, J. Hino, K. Kangawa, and T. Kinoshita. 2000. "Human dolichol-phosphate-mannose synthase consists of three subunits, DPM1, DPM2 and DPM3." *EMBO J* 19 (11):2475-82. doi: 10.1093/emboj/19.11.2475.

Marceau, C. D., A. S. Puschnik, K. Majzoub, Y. S. Ooi, S. M. Brewer, G. Fuchs, K. Swaminathan, M. A. Mata, J. E. Elias, P. Sarnow, and J. E. Carette. 2016. "Genetic dissection of Flaviviridae host factors through genome-scale CRISPR screens." *Nature* 535 (7610):159-63. doi: 10.1038/nature18631.

Martín, V., G. Carrillo, C. Torroja, and I. Guerrero. 2001. "The sterol-sensing domain of Patched protein seems to control Smoothened activity through Patched vesicular trafficking." *Curr Biol* 11 (8):601-7.

Maxson, M. E., and S. Grinstein. 2014. "The vacuolar-type H^+-ATPase at a glance - more than a proton pump." *J Cell Sci* 127 (Pt 23):4987-93. doi: 10.1242/jcs.158550.

McFie, P. J., S. L. Banman, S. Kary, and S. J. Stone. 2011. "Murine diacylglycerol acyltransferase-2 (DGAT2) can catalyze triacylglycerol synthesis and promote lipid droplet formation independent of its localization to the endoplasmic reticulum." *J Biol Chem* 286 (32):28235-46. doi: 10.1074/jbc.M111.256008.

Meacham, G. C., C. Patterson, W. Zhang, J. M. Younger, and D. M. Cyr. 2001. "The Hsc70 co-chaperone CHIP targets immature CFTR for proteasomal degradation." *Nat Cell Biol* 3 (1):100-5. doi: 10.1038/35050509.

Medicherla, B., Z. Kostova, A. Schaefer, and D. H. Wolf. 2004. "A genomic screen identifies Dsk2p and Rad23p as essential components of ER-associated degradation." *EMBO Rep* 5 (7):692-7. doi: 10.1038/sj.embor.7400164.

Metzger, M. B., V. A. Hristova, and A. M. Weissman. 2012. "HECT and RING finger families of E3 ubiquitin ligases at a glance." *J Cell Sci* 125 (Pt 3):531-7. doi: 10.1242/jcs.091777.

Meyer, H. H., Y. Wang, and G. Warren. 2002. "Direct binding of ubiquitin conjugates by the mammalian p97 adaptor complexes, p47 and Ufd1-Npl4." *EMBO J* 21 (21):5645-52.

Miao, H., W. Jiang, L. Ge, B. Li, and B. Song. 2010. "Tetra-glutamic acid residues adjacent to Lys248 in HMG-CoA reductase are critical for the ubiquitination mediated by gp78 and UBE2G2." *Acta Biochim Biophys Sin (Shanghai)* 42 (5):303-10.

Millard, E. E., S. E. Gale, N. Dudley, J. Zhang, J. E. Schaffer, and D. S. Ory. 2005. "The sterol-sensing domain of the Niemann-Pick C1 (NPC1) protein regulates trafficking of low density lipoprotein cholesterol." *J Biol Chem* 280 (31):28581-90. doi: 10.1074/jbc.M414024200.

Moffat, J., D. A. Grueneberg, X. Yang, S. Y. Kim, A. M. Kloepfer, G. Hinkle, B. Piqani, T. M. Eisenhaure, B. Luo, J. K. Grenier, A. E. Carpenter, S. Y. Foo, S. A. Stewart, B. R. Stockwell, N. Hacohen, W. C. Hahn, E. S. Lander, D. M. Sabatini, and D. E. Root. 2006. "A lentiviral RNAi library for human and mouse genes applied to an arrayed viral high-content screen." *Cell* 124 (6):1283-98. doi: 10.1016/j.cell.2006.01.040.

Mohorko, E., R. Glockshuber, and M. Aebi. 2011. "Oligosaccharyltransferase: the central enzyme of N-linked protein glycosylation." *J Inherit Metab Dis* 34 (4):869-78. doi: 10.1007/s10545-011-9337-1.

Moon, Y. A., and J. D. Horton. 2003. "Identification of two mammalian reductases involved in the two-carbon fatty acyl elongation cascade." *J Biol Chem* 278 (9):7335-43. doi: 10.1074/jbc.M211684200.

Morgens, D. W., R. M. Deans, A. Li, and M. C. Bassik. 2016. "Systematic comparison of CRISPR/Cas9 and RNAi screens for essential genes." *Nat Biotechnol* 34 (6):634-6. doi: 10.1038/nbt.3567.

Morgens, D. W., M. Wainberg, E. A. Boyle, O. Ursu, C. L. Araya, C. K. Tsui, M. S. Haney, G. T. Hess, K. Han, E. E. Jeng, A. Li, M. P. Snyder, W. J. Greenleaf, A. Kundaje, and M. C. Bassik. 2017. "Genome-scale measurement of off-target activity using Cas9 toxicity in high-throughput screens." *Nat Commun* 8:15178. doi: 10.1038/ncomms15178.

Morito, D., K. Hirao, Y. Oda, N. Hosokawa, F. Tokunaga, D. M. Cyr, K. Tanaka, K. Iwai, and K. Nagata. 2008. "Gp78 cooperates with RMA1 in endoplasmic reticulum-associated degradation of CFTRDeltaF508." *Mol Biol Cell* 19 (4):1328-36. doi: 10.1091/mbc.E07-06-0601.

Morris, L. L., I. Z. Hartman, D. J. Jun, J. Seemann, and R. A. DeBose-Boyd. 2014. "Sequential actions of the AAA-ATPase valosin-containing protein (VCP)/p97 and the proteasome 19 S regulatory particle in sterol-accelerated, endoplasmic reticulum (ER)-associated degradation of 3-hydroxy-3-methylglutaryl-coenzyme A reductase." *J Biol Chem* 289 (27):19053-66. doi: 10.1074/jbc.M114.576652.

Muller, H. J. 1927. "ARTIFICIAL TRANSMUTATION OF THE GENE." *Science* 66 (1699):84-7. doi: 10.1126/science.66.1699.84.

Nadav, E., A. Shmueli, H. Barr, H. Gonen, A. Ciechanover, and Y. Reiss. 2003. "A novel mammalian endoplasmic reticulum ubiquitin ligase homologous to the yeast Hrd1." *Biochem Biophys Res Commun* 303 (1):91-7.

Nakanishi, M., J. L. Goldstein, and M. S. Brown. 1988. "Multivalent control of 3-hydroxy-3-methylglutaryl coenzyme A reductase. Mevalonate-derived product inhibits translation of mRNA and accelerates degradation of enzyme." *J Biol Chem* 263 (18):8929-37.

Nakatsukasa, K., and J. L. Brodsky. 2008. "The recognition and retrotranslocation of misfolded proteins from the endoplasmic reticulum." *Traffic* 9 (6):861-70. doi: 10.1111/j.1600-0854.2008.00729.x.

Nakatsukasa, K., G. Huyer, S. Michaelis, and J. L. Brodsky. 2008. "Dissecting the ER-associated degradation of a misfolded polytopic membrane protein." *Cell* 132 (1):101-12. doi: 10.1016/j.cell.2007.11.023.

Nandi, D., P. Tahiliani, A. Kumar, and D. Chandu. 2006. "The ubiquitin-proteasome system." *J Biosci* 31 (1):137-55.

Naslavsky, N., and S. Caplan. 2011. "EHD proteins: key conductors of endocytic transport." *Trends Cell Biol* 21 (2):122-31. doi: 10.1016/j.tcb.2010.10.003.

Naslavsky, N., J. Rahajeng, D. Rapaport, M. Horowitz, and S. Caplan. 2007. "EHD1 regulates cholesterol homeostasis and lipid droplet storage." *Biochem Biophys Res Commun* 357 (3):792-9. doi: 10.1016/j.bbrc.2007.04.022.

Nasmyth, K., and D. Shore. 1987. "Transcriptional regulation in the yeast life cycle." *Science* 237 (4819):1162-70.

Nelson, C. E., C. H. Hakim, D. G. Ousterout, P. I. Thakore, E. A. Moreb, R. M. Castellanos Rivera, S. Madhavan, X. Pan, F. A. Ran, W. X. Yan, A. Asokan, F. Zhang, D. Duan, and C. A. Gersbach. 2016. "In vivo genome editing improves muscle function in a mouse model of Duchenne muscular dystrophy." *Science* 351 (6271):403-7. doi: 10.1126/science.aad5143.

Neuber, O., E. Jarosch, C. Volkwein, J. Walter, and T. Sommer. 2005. "Ubx2 links the Cdc48 complex to ER-associated protein degradation." *Nat Cell Biol* 7 (10):993-8. doi: 10.1038/ncb1298.

Neutzner, A., M. Neutzner, A. S. Benischke, S. W. Ryu, S. Frank, R. J. Youle, and M. Karbowski. 2011. "A systematic search for endoplasmic reticulum (ER) membrane-associated RING finger proteins identifies Nixin/ZNRF4 as a regulator of calnexin stability and ER homeostasis." *J Biol Chem* 286 (10):8633-43. doi: 10.1074/jbc.M110.197459.

Ninagawa, S., T. Okada, Y. Sumitomo, Y. Kamiya, K. Kato, S. Horimoto, T. Ishikawa, S. Takeda, T. Sakuma, T. Yamamoto, and K. Mori. 2014. "EDEM2 initiates mammalian glycoprotein ERAD by catalyzing the first mannose trimming step." *J Cell Biol* 206 (3):347-56. doi: 10.1083/jcb.201404075.

Nishimasu, H., F. A. Ran, P. D. Hsu, S. Konermann, S. I. Shehata, N. Dohmae, R. Ishitani, F. Zhang, and O. Nureki. 2014. "Crystal structure of Cas9 in complex with guide RNA and target DNA." *Cell* 156 (5):935-49. doi: 10.1016/j.cell.2014.02.001.

Nohturfft, A., M. S. Brown, and J. L. Goldstein. 1998a. "Sterols regulate processing of carbohydrate chains of wild-type SREBP cleavage-activating protein (SCAP), but not sterol-resistant mutants Y298C or D443N." *Proc Natl Acad Sci U S A* 95 (22):12848-53.

Nohturfft, A., M. S. Brown, and J. L. Goldstein. 1998b. "Topology of SREBP cleavage-activating protein, a polytopic membrane protein with a sterol-sensing domain." *J Biol Chem* 273 (27):17243-50.

Novick, P., C. Field, and R. Schekman. 1980. "Identification of 23 complementation groups required for post-translational events in the yeast secretory pathway." *Cell* 21 (1):205-15.

Nüsslein-Volhard, C., and E. Wieschaus. 1980. "Mutations affecting segment number and polarity in Drosophila." *Nature* 287 (5785):795-801.

Oda, Y., N. Hosokawa, I. Wada, and K. Nagata. 2003. "EDEM as an acceptor of terminally misfolded glycoproteins released from calnexin." *Science* 299 (5611):1394-7. doi: 10.1126/science.1079181.

Okuda-Shimizu, Y., and L. M. Hendershot. 2007. "Characterization of an ERAD pathway for nonglycosylated BiP substrates, which require Herp." *Mol Cell* 28 (4):544-54. doi: 10.1016/j.molcel.2007.09.012.

Olivari, S., and M. Molinari. 2007. "Glycoprotein folding and the role of EDEM1, EDEM2 and EDEM3 in degradation of folding-defective glycoproteins." *FEBS Lett* 581 (19):3658-64. doi: 10.1016/j.febslet.2007.04.070.

Otero, J. H., B. Lizák, and L. M. Hendershot. 2010. "Life and death of a BiP substrate." *Semin Cell Dev Biol* 21 (5):472-8. doi: 10.1016/j.semcdb.2009.12.008.

Papatheodorou, P., J. E. Carette, G. W. Bell, C. Schwan, G. Guttenberg, T. R. Brummelkamp, and K. Aktories. 2011. "Lipolysis-stimulated lipoprotein receptor (LSR) is the host receptor for the binary toxin Clostridium difficile transferase (CDT)." *Proc Natl Acad Sci U S A* 108 (39):16422-7. doi: 10.1073/pnas.1109772108.

Park, R. J., T. Wang, D. Koundakjian, J. F. Hultquist, P. Lamothe-Molina, B. Monel, K. Schumann, H. Yu, K. M. Krupzcak, W. Garcia-Beltran, A. Piechocka-Trocha, N. J. Krogan, A. Marson, D. M. Sabatini, E. S. Lander, N. Hacohen, and B. D. Walker. 2017. "A genome-wide CRISPR screen identifies a restricted set of HIV host dependency factors." *Nat Genet* 49 (2):193-203. doi: 10.1038/ng.3741.

Parnas, O., M. Jovanovic, T. M. Eisenhaure, R. H. Herbst, A. Dixit, C. J. Ye, D. Przybylski, R. J. Platt, I. Tirosh, N. E. Sanjana, O. Shalem, R. Satija, R. Raychowdhury, P. Mertins, S. A. Carr, F. Zhang, N. Hacohen, and A. Regev. 2015. "A Genome-wide CRISPR Screen in Primary Immune Cells to Dissect Regulatory Networks." *Cell*. doi: 10.1016/j.cell.2015.06.059.

Peth, A., H. C. Besche, and A. L. Goldberg. 2009. "Ubiquitinated proteins activate the proteasome by binding to Usp14/Ubp6, which causes 20S gate opening." *Mol Cell* 36 (5):794-804. doi: 10.1016/j.molcel.2009.11.015.

Peth, A., T. Uchiki, and A. L. Goldberg. 2010. "ATP-dependent steps in the binding of ubiquitin conjugates to the 26S proteasome that commit to degradation." *Mol Cell* 40 (4):671-81. doi: 10.1016/j.molcel.2010.11.002.

Pickart, C. M. 2001. "Mechanisms underlying ubiquitination." *Annu Rev Biochem* 70:503-33. doi: 10.1146/annurev.biochem.70.1.503.

Prabhu, A. V., L. J. Sharpe, and A. J. Brown. 2014. "The sterol-based transcriptional control of human 7-dehydrocholesterol reductase (DHCR7): Evidence of a cooperative regulatory program in cholesterol synthesis." *Biochim Biophys Acta* 1842 (10):1431-9. doi: 10.1016/j.bbalip.2014.07.006.

Qian, Y., I. Lee, W. S. Lee, M. Qian, M. Kudo, W. M. Canfield, P. Lobel, and S. Kornfeld. 2010. "Functions of the alpha, beta, and gamma subunits of UDP-GlcNAc:lysosomal enzyme N-acetylglucosamine-1-phosphotransferase." *J Biol Chem* 285 (5):3360-70. doi: 10.1074/jbc.M109.068650.

Quan, E. M., Y. Kamiya, D. Kamiya, V. Denic, J. Weibezahn, K. Kato, and J. S. Weissman. 2008. "Defining the glycan destruction signal for endoplasmic reticulum-associated degradation." *Mol Cell* 32 (6):870-7. doi: 10.1016/j.molcel.2008.11.017.

Rabinovich, E., A. Kerem, K. U. Fröhlich, N. Diamant, and S. Bar-Nun. 2002. "AAA-ATPase p97/Cdc48p, a cytosolic chaperone required for endoplasmic reticulum-associated protein degradation." *Mol Cell Biol* 22 (2):626-34.

Radhakrishnan, A., Y. Ikeda, H. J. Kwon, M. S. Brown, and J. L. Goldstein. 2007. "Sterol-regulated transport of SREBPs from endoplasmic reticulum to Golgi: oxysterols block transport by binding to Insig." *Proc Natl Acad Sci U S A* 104 (16):6511-8. doi: 10.1073/pnas.0700899104.

Radhakrishnan, A., L. P. Sun, H. J. Kwon, M. S. Brown, and J. L. Goldstein. 2004. "Direct binding of cholesterol to the purified membrane region of SCAP: mechanism for a sterol-sensing domain." *Mol Cell* 15 (2):259-68. doi: 10.1016/j.molcel.2004.06.019.

Ran, F. A., P. D. Hsu, J. Wright, V. Agarwala, D. A. Scott, and F. Zhang. 2013. "Genome engineering using the CRISPR-Cas9 system." *Nat Protoc* 8 (11):2281-308. doi: 10.1038/nprot.2013.143.

Ravid, T., R. Doolman, R. Avner, D. Harats, and J. Roitelman. 2000. "The ubiquitin-proteasome pathway mediates the regulated degradation of mammalian 3-hydroxy-3-methylglutaryl-coenzyme A reductase." *J Biol Chem* 275 (46):35840-7. doi: 10.1074/jbc.M004793200.

Reichardt, J. K. 2007. "Quo vadis, genoma? A call to pipettes for biochemists." *Trends Biochem Sci* 32 (12):529-30. doi: 10.1016/j.tibs.2007.10.001.

Reiling, J. H., C. B. Clish, J. E. Carette, M. Varadarajan, T. R. Brummelkamp, and D. M. Sabatini. 2011. "A haploid genetic screen identifies the major facilitator domain containing 2A (MFSD2A) transporter as a key mediator in the response to tunicamycin." *Proc Natl Acad Sci U S A* 108 (29):11756-65. doi: 10.1073/pnas.1018098108.

Riblett, A. M., V. A. Blomen, L. T. Jae, L. A. Altamura, R. W. Doms, T. R. Brummelkamp, and J. A. Wojcechowskyj. 2015. "A Haploid Genetic Screen Identifies Heparan Sulfate Proteoglycans Supporting Rift Valley Fever Virus Infection." *J Virol* 90 (3):1414-23. doi: 10.1128/JVI.02055-15.

Roitelman, J., E. H. Olender, S. Bar-Nun, W. A. Dunn, and R. D. Simoni. 1992. "Immunological evidence for eight spans in the membrane domain of 3-hydroxy-3-methylglutaryl coenzyme A reductase: implications for enzyme degradation in the endoplasmic reticulum." *J Cell Biol* 117 (5):959-73.

Root, D. E., N. Hacohen, W. C. Hahn, E. S. Lander, and D. M. Sabatini. 2006. "Genome-scale loss-of-function screening with a lentiviral RNAi library." *Nat Methods* 3 (9):715-9. doi: 10.1038/nmeth924.

Rosmarin, D. M., J. E. Carette, A. J. Olive, M. N. Starnbach, T. R. Brummelkamp, and H. L. Ploegh. 2012. "Attachment of Chlamydia trachomatis L2 to host cells requires sulfation." *Proc Natl Acad Sci U S A* 109 (25):10059-64. doi: 10.1073/pnas.1120244109.

Roux, K. J., D. I. Kim, M. Raida, and B. Burke. 2012. "A promiscuous biotin ligase fusion protein identifies proximal and interacting proteins in mammalian cells." *J Cell Biol* 196 (6):801-10. doi: 10.1083/jcb.201112098.

Rubin, G. M., and E. B. Lewis. 2000. "A brief history of Drosophila's contributions to genome research." *Science* 287 (5461):2216-8.

Rudenko, G., L. Henry, K. Henderson, K. Ichtchenko, M. S. Brown, J. L. Goldstein, and J. Deisenhofer. 2002. "Structure of the LDL receptor extracellular domain at endosomal pH." *Science* 298 (5602):2353-8. doi: 10.1126/science.1078124.

Saeed, M., R. Suzuki, N. Watanabe, T. Masaki, M. Tomonaga, A. Muhammad, T. Kato, Y. Matsuura, H. Watanabe, T. Wakita, and T. Suzuki. 2011. "Role of the endoplasmic reticulum-associated degradation (ERAD) pathway in degradation of hepatitis C virus envelope proteins and production of virus particles." *J Biol Chem* 286 (43):37264-73. doi: 10.1074/jbc.M111.259085.

Sakai, J., A. Nohturfft, D. Cheng, Y. K. Ho, M. S. Brown, and J. L. Goldstein. 1997. "Identification of complexes between the COOH-terminal domains of sterol regulatory element-binding proteins (SREBPs) and SREBP cleavage-activating protein." *J Biol Chem* 272 (32):20213-21.

Sakai, J., R. B. Rawson, P. J. Espenshade, D. Cheng, A. C. Seegmiller, J. L. Goldstein, and M. S. Brown. 1998. "Molecular identification of the sterol-regulated luminal protease that cleaves SREBPs and controls lipid composition of animal cells." *Mol Cell* 2 (4):505-14.

Sallam, T., M. C. Jones, T. Gilliland, L. Zhang, X. Wu, A. Eskin, J. Sandhu, D. Casero, T. Q. Vallim, C. Hong, M. Katz, R. Lee, J. Whitelegge, and P. Tontonoz. 2016. "Feedback modulation of cholesterol metabolism by the lipid-responsive non-coding RNA LeXis." *Nature* 534 (7605):124-8. doi: 10.1038/nature17674.

Sanjana, N. E., O. Shalem, and F. Zhang. 2014. "Improved vectors and genome-wide libraries for CRISPR screening." *Nat Methods* 11 (8):783-4. doi: 10.1038/nmeth.3047.

Sato, B. K., and R. Y. Hampton. 2006. "Yeast Derlin Dfm1 interacts with Cdc48 and functions in ER homeostasis." *Yeast* 23 (14-15):1053-64. doi: 10.1002/yea.1407.

Schoebel, S., W. Mi, A. Stein, S. Ovchinnikov, R. Pavlovicz, F. DiMaio, D. Baker, M. G. Chambers, H. Su, D. Li, T. A. Rapoport, and M. Liao. 2017. "Cryo-EM structure of the protein-conducting ERAD channel Hrd1 in complex with Hrd3." *Nature*. doi: 10.1038/nature23314.

Schreiner, P., X. Chen, K. Husnjak, L. Randles, N. Zhang, S. Elsasser, D. Finley, I. Dikic, K. J. Walters, and M. Groll. 2008. "Ubiquitin docking at the proteasome through a novel pleckstrin-homology domain interaction." *Nature* 453 (7194):548-52. doi: 10.1038/nature06924.

Schuberth, C., and A. Buchberger. 2005. "Membrane-bound Ubx2 recruits Cdc48 to ubiquitin ligases and their substrates to ensure efficient ER-associated protein degradation." *Nat Cell Biol* 7 (10):999-1006. doi: 10.1038/ncb1299.

Schulze, A., S. Standera, E. Buerger, M. Kikkert, S. van Voorden, E. Wiertz, F. Koning, P. M. Kloetzel, and M. Seeger. 2005. "The ubiquitin-domain protein HERP forms a complex with components of the endoplasmic reticulum associated degradation pathway." *J Mol Biol* 354 (5):1021-7. doi: 10.1016/j.jmb.2005.10.020.

Schumacher, M. M., R. Elsabrouty, J. Seemann, Y. Jo, and R. A. DeBose-Boyd. 2015. "The prenyltransferase UBIAD1 is the target of geranylgeraniol in degradation of HMG CoA reductase." *Elife* 4. doi: 10.7554/eLife.05560.

Schweitzer, J. K., A. E. Sedgwick, and C. D'Souza-Schorey. 2011. "ARF6-mediated endocytic recycling impacts cell movement, cell division and lipid homeostasis." *Semin Cell Dev Biol* 22 (1):39-47. doi: 10.1016/j.semcdb.2010.09.002.

Schwientek, T., E. P. Bennett, C. Flores, J. Thacker, M. Hollmann, C. A. Reis, J. Behrens, U. Mandel, B. Keck, M. A. Schäfer, K. Haselmann, R. Zubarev, P. Roepstorff, J. M. Burchell, J. Taylor-Papadimitriou, M. A. Hollingsworth, and H. Clausen. 2002. "Functional conservation of subfamilies of putative UDP-N-acetylgalactosamine:polypeptide N-acetylgalactosaminyltransferases in Drosophila, Caenorhabditis elegans, and mammals. One subfamily composed of l(2)35Aa is essential in Drosophila." *J Biol Chem* 277 (25):22623-38. doi: 10.1074/jbc.M202684200.

Sekijima, Y., J. W. Kelly, and S. Ikeda. 2008. "Pathogenesis of and therapeutic strategies to ameliorate the transthyretin amyloidoses." *Curr Pharm Des* 14 (30):3219-30.

Sever, N., B. L. Song, D. Yabe, J. L. Goldstein, M. S. Brown, and R. A. DeBose-Boyd. 2003. "Insig-dependent ubiquitination and degradation of mammalian 3-hydroxy-3-methylglutaryl-CoA reductase stimulated by sterols and geranylgeraniol." *J Biol Chem* 278 (52):52479-90. doi: 10.1074/jbc.M310053200.

Sever, N., T. Yang, M. S. Brown, J. L. Goldstein, and R. A. DeBose-Boyd. 2003. "Accelerated degradation of HMG CoA reductase mediated by binding of insig-1 to its sterol-sensing domain." *Mol Cell* 11 (1):25-33.

Shalem, O., N. E. Sanjana, E. Hartenian, X. Shi, D. A. Scott, T. S. Mikkelsen, D. Heckl, B. L. Ebert, D. E. Root, J. G. Doench, and F. Zhang. 2014. "Genome-scale CRISPR-Cas9 knockout screening in human cells." *Science* 343 (6166):84-7. doi: 10.1126/science.1247005.

Sharpe, L. J., and A. J. Brown. 2013. "Controlling cholesterol synthesis beyond 3-hydroxy-3-methylglutaryl-CoA reductase (HMGCR)." *J Biol Chem* 288 (26):18707-15. doi: 10.1074/jbc.R113.479808.

Shearer, A. G., and R. Y. Hampton. 2005. "Lipid-mediated, reversible misfolding of a sterol-sensing domain protein." *EMBO J* 24 (1):149-59. doi: 10.1038/sj.emboj.7600498.

Shimizu, Y., Y. Okuda-Shimizu, and L. M. Hendershot. 2010. "Ubiquitylation of an ERAD substrate occurs on multiple types of amino acids." *Mol Cell* 40 (6):917-26. doi: 10.1016/j.molcel.2010.11.033.

Shmueli, A., Y. C. Tsai, M. Yang, M. A. Braun, and A. M. Weissman. 2009. "Targeting of gp78 for ubiquitin-mediated proteasomal degradation by Hrd1: cross-talk between E3s in the endoplasmic reticulum." *Biochem Biophys Res Commun* 390 (3):758-62. doi: 10.1016/j.bbrc.2009.10.045.

Smith, D. M., S. C. Chang, S. Park, D. Finley, Y. Cheng, and A. L. Goldberg. 2007. "Docking of the proteasomal ATPases' carboxyl termini in the 20S proteasome's alpha ring opens the gate for substrate entry." *Mol Cell* 27 (5):731-44. doi: 10.1016/j.molcel.2007.06.033.

Smith, D. M., H. Fraga, C. Reis, G. Kafri, and A. L. Goldberg. 2011. "ATP binds to proteasomal ATPases in pairs with distinct functional effects, implying an ordered reaction cycle." *Cell* 144 (4):526-38. doi: 10.1016/j.cell.2011.02.005.

Sommer, T., and S. Jentsch. 1993. "A protein translocation defect linked to ubiquitin conjugation at the endoplasmic reticulum." *Nature* 365 (6442):176-9. doi: 10.1038/365176a0.

Song, B. L., N. B. Javitt, and R. A. DeBose-Boyd. 2005. "Insig-mediated degradation of HMG CoA reductase stimulated by lanosterol, an intermediate in the synthesis of cholesterol." *Cell Metab* 1 (3):179-89. doi: 10.1016/j.cmet.2005.01.001.

Song, B. L., N. Sever, and R. A. DeBose-Boyd. 2005. "Gp78, a membrane-anchored ubiquitin ligase, associates with Insig-1 and couples sterol-regulated ubiquitination to degradation of HMG CoA reductase." *Mol Cell* 19 (6):829-40. doi: 10.1016/j.molcel.2005.08.009.

Song, J. J., S. K. Smith, G. J. Hannon, and L. Joshua-Tor. 2004. "Crystal structure of Argonaute and its implications for RISC slicer activity." *Science* 305 (5689):1434-7. doi: 10.1126/science.1102514.

Sousa, M., and A. J. Parodi. 1995. "The molecular basis for the recognition of misfolded glycoproteins by the UDP-Glc:glycoprotein glucosyltransferase." *EMBO J* 14 (17):4196-203.

Spann, N. J., L. X. Garmire, J. G. McDonald, D. S. Myers, S. B. Milne, N. Shibata, D. Reichart, J. N. Fox, I. Shaked, D. Heudobler, C. R. Raetz, E. W. Wang, S. L. Kelly, M. C. Sullards, R. C. Murphy, A. H. Merrill, H. A. Brown, E. A. Dennis, A. C. Li, K. Ley, S. Tsimikas, E. Fahy, S. Subramaniam, O. Quehenberger, D. W. Russell, and C. K. Glass. 2012. "Regulated accumulation of desmosterol integrates macrophage lipid metabolism and inflammatory responses." *Cell* 151 (1):138-52. doi: 10.1016/j.cell.2012.06.054.

St Johnston, D. 2002. "The art and design of genetic screens: Drosophila melanogaster." *Nat Rev Genet* 3 (3):176-88. doi: 10.1038/nrg751.

Stagg, H. R., M. Thomas, D. van den Boomen, E. J. Wiertz, H. A. Drabkin, R. M. Gemmill, and P. J. Lehner. 2009. "The TRC8 E3 ligase ubiquitinates MHC class I molecules before dislocation from the ER." *J Cell Biol* 186 (5):685-92.

Stanley, A. M., P. Carvalho, and T. Rapoport. 2011. "Recognition of an ERAD-L substrate analyzed by site-specific in vivo photocrosslinking." *FEBS Lett* 585 (9):1281-6. doi: 10.1016/j.febslet.2011.04.009.

Steinberg, D. 2006. "Thematic review series: the pathogenesis of atherosclerosis. An interpretive history of the cholesterol controversy, part V: the discovery of the statins and the end of the controversy." *J Lipid Res* 47 (7):1339-51. doi: 10.1194/jlr.R600009-JLR200.

Sternberg, S. H., S. Redding, M. Jinek, E. C. Greene, and J. A. Doudna. 2014. "DNA interrogation by the CRISPR RNA-guided endonuclease Cas9." *Nature* 507 (7490):62-7. doi: 10.1038/nature13011.

Sudbery, I., A. J. Enright, A. G. Fraser, and I. Dunham. 2010. "Systematic analysis of off-target effects in an RNAi screen reveals microRNAs affecting sensitivity to TRAIL-induced apoptosis." *BMC Genomics* 11:175. doi: 10.1186/1471-2164-11-175.

Sugii, S., P. C. Reid, N. Ohgami, H. Du, and T. Y. Chang. 2003. "Distinct endosomal compartments in early trafficking of low density lipoprotein-derived cholesterol." *J Biol Chem* 278 (29):27180-9. doi: 10.1074/jbc.M300542200.

Sun, L. P., L. Li, J. L. Goldstein, and M. S. Brown. 2005. "Insig required for sterol-mediated inhibition of Scap/SREBP binding to COPII proteins in vitro." *J Biol Chem* 280 (28):26483-90. doi: 10.1074/jbc.M504041200.

Sun, L. P., J. Seemann, J. L. Goldstein, and M. S. Brown. 2007. "Sterol-regulated transport of SREBPs from endoplasmic reticulum to Golgi: Insig renders sorting signal in Scap inaccessible to COPII proteins." *Proc Natl Acad Sci U S A* 104 (16):6519-26. doi: 10.1073/pnas.0700907104.

Suzuki, M., T. Otsuka, Y. Ohsaki, J. Cheng, T. Taniguchi, H. Hashimoto, H. Taniguchi, and T. Fujimoto. 2012. "Derlin-1 and UBXD8 are engaged in dislocation and degradation of lipidated ApoB-100 at lipid droplets." *Mol Biol Cell* 23 (5):800-10. doi: 10.1091/mbc.E11-11-0950.

Swanson, R., M. Locher, and M. Hochstrasser. 2001. "A conserved ubiquitin ligase of the nuclear envelope/endoplasmic reticulum that functions in both ER-associated and Matalpha2 repressor degradation." *Genes Dev* 15 (20):2660-74. doi: 10.1101/gad.933301.

Tait, S. W., E. de Vries, C. Maas, A. M. Keller, C. S. D'Santos, and J. Borst. 2007. "Apoptosis induction by Bid requires unconventional ubiquitination and degradation of its N-terminal fragment." *J Cell Biol* 179 (7):1453-66. doi: 10.1083/jcb.200707063.

Taxis, C., R. Hitt, S. H. Park, P. M. Deak, Z. Kostova, and D. H. Wolf. 2003. "Use of modular substrates demonstrates mechanistic diversity and reveals differences in chaperone requirement of ERAD." *J Biol Chem* 278 (38):35903-13. doi: 10.1074/jbc.M301080200.

Tchasovnikarova, I. A., R. T. Timms, N. J. Matheson, K. Wals, R. Antrobus, B. Göttgens, G. Dougan, M. A. Dawson, and P. J. Lehner. 2015. "GENE SILENCING. Epigenetic silencing by the HUSH complex mediates position-effect variegation in human cells." *Science* 348 (6242):1481-5. doi: 10.1126/science.aaa7227.

Theesfeld, C. L., and R. Y. Hampton. 2013. "Insulin-induced gene protein (INSIG)-dependent sterol regulation of Hmg2 endoplasmic reticulum-associated degradation (ERAD) in yeast." *J Biol Chem* 288 (12):8519-30. doi: 10.1074/jbc.M112.404517.

Thrower, J. S., L. Hoffman, M. Rechsteiner, and C. M. Pickart. 2000. "Recognition of the polyubiquitin proteolytic signal." *EMBO J* 19 (1):94-102. doi: 10.1093/emboj/19.1.94.

Timms, R. T., L. M. Duncan, I. A. Tchasovnikarova, R. Antrobus, D. L. Smith, G. Dougan, M. P. Weekes, and P. J. Lehner. 2013. "Haploid genetic screens identify an essential role for PLP2 in the downregulation of novel plasma membrane targets by viral E3 ubiquitin ligases." *PLoS Pathog* 9 (11):e1003772. doi: 10.1371/journal.ppat.1003772.

Tsai, Y. C., G. S. Leichner, M. M. Pearce, G. L. Wilson, R. J. Wojcikiewicz, J. Roitelman, and A. M. Weissman. 2012. "Differential regulation of HMG-CoA reductase and Insig-1 by enzymes of the ubiquitin-proteasome system." *Mol Biol Cell* 23 (23):4484-94. doi: 10.1091/mbc.E12-08-0631.

Tsai, Y. C., A. Mendoza, J. M. Mariano, M. Zhou, Z. Kostova, B. Chen, T. Veenstra, S. M. Hewitt, L. J. Helman, C. Khanna, and A. M. Weissman. 2007. "The ubiquitin ligase gp78 promotes sarcoma metastasis by targeting KAI1 for degradation." *Nat Med* 13 (12):1504-9. doi: 10.1038/nm1686.

Tyler, R. E., M. M. Pearce, T. A. Shaler, J. A. Olzmann, E. J. Greenblatt, and R. R. Kopito. 2012. "Unassembled CD147 is an endogenous endoplasmic reticulum-associated degradation substrate." *Mol Biol Cell* 23 (24):4668-78. doi: 10.1091/mbc.E12-06-0428.

Urano, Y., H. Watanabe, S. R. Murphy, Y. Shibuya, Y. Geng, A. A. Peden, C. C. Chang, and T. Y. Chang. 2008. "Transport of LDL-derived cholesterol from the NPC1 compartment to the ER involves the trans-Golgi network and the SNARE protein complex." *Proc Natl Acad Sci U S A* 105 (43):16513-8. doi: 10.1073/pnas.0807450105.

Ushioda, R., J. Hoseki, K. Araki, G. Jansen, D. Y. Thomas, and K. Nagata. 2008. "ERdj5 is required as a disulfide reductase for degradation of misfolded proteins in the ER." *Science* 321 (5888):569-72. doi: 10.1126/science.1159293.

van de Weijer, M. L., M. C. Bassik, R. D. Luteijn, C. M. Voorburg, M. A. Lohuis, E. Kremmer, R. C. Hoeben, E. M. LeProust, S. Chen, H. Hoelen, M. E. Ressing, W. Patena, J. S. Weissman, M. T. McManus, E. J. Wiertz, and R. J. Lebbink. 2014. "A high-coverage shRNA screen identifies TMEM129 as an E3 ligase involved in ER-associated protein degradation." *Nat Commun* 5:3832. doi: 10.1038/ncomms4832.

van den Boomen, D. J., R. T. Timms, G. L. Grice, H. R. Stagg, K. Skødt, G. Dougan, J. A. Nathan, and P. J. Lehner. 2014. "TMEM129 is a Derlin-1 associated ERAD E3 ligase essential for virus-induced degradation of MHC-I." *Proc Natl Acad Sci U S A* 111 (31):11425-30. doi: 10.1073/pnas.1409099111.

VanDemark, A. P., R. M. Hofmann, C. Tsui, C. M. Pickart, and C. Wolberger. 2001. "Molecular insights into polyubiquitin chain assembly: crystal structure of the Mms2/Ubc13 heterodimer." *Cell* 105 (6):711-20.

Vanier, M. T., and G. Millat. 2003. "Niemann-Pick disease type C." *Clin Genet* 64 (4):269-81.

Vashist, S., and D. T. Ng. 2004. "Misfolded proteins are sorted by a sequential checkpoint mechanism of ER quality control." *J Cell Biol* 165 (1):41-52. doi: 10.1083/jcb.200309132.

Vembar, S. S., and J. L. Brodsky. 2008. "One step at a time: endoplasmic reticulum-associated degradation." *Nat Rev Mol Cell Biol* 9 (12):944-57. doi: 10.1038/nrm2546.

Venkateswaran, A., B. A. Laffitte, S. B. Joseph, P. A. Mak, D. C. Wilpitz, P. A. Edwards, and P. Tontonoz. 2000. "Control of cellular cholesterol efflux by the nuclear oxysterol receptor LXR alpha." *Proc Natl Acad Sci U S A* 97 (22):12097-102. doi: 10.1073/pnas.200367697.

Venken, K. J., and H. J. Bellen. 2014. "Chemical mutagens, transposons, and transgenes to interrogate gene function in Drosophila melanogaster." *Methods* 68 (1):15-28. doi: 10.1016/j.ymeth.2014.02.025.

Verma, R., S. Chen, R. Feldman, D. Schieltz, J. Yates, J. Dohmen, and R. J. Deshaies. 2000. "Proteasomal proteomics: identification of nucleotide-sensitive proteasome-interacting proteins by mass spectrometric analysis of affinity-purified proteasomes." *Mol Biol Cell* 11 (10):3425-39.

Wahlman, J., G. N. DeMartino, W. R. Skach, N. J. Bulleid, J. L. Brodsky, and A. E. Johnson. 2007. "Real-time fluorescence detection of ERAD substrate retrotranslocation in a mammalian in vitro system." *Cell* 129 (5):943-55. doi: 10.1016/j.cell.2007.03.046.

Wang, D., X. De Deken, M. Milenkovic, Y. Song, I. Pirson, J. E. Dumont, and F. Miot. 2005. "Identification of a novel partner of duox: EFP1, a thioredoxin-related protein." *J Biol Chem* 280 (4):3096-103. doi: 10.1074/jbc.M407709200.

Wang, H., Q. Li, Y. Shen, A. Sun, X. Zhu, and S. Fang. 2011. "The ubiquitin ligase Hrd1 promotes degradation of the Z variant alpha 1-antitrypsin and increases its solubility." *Mol Cell Biochem* 346 (1-2):137-45. doi: 10.1007/s11010-010-0600-9.

Wang, M. L., M. Motamed, R. E. Infante, L. Abi-Mosleh, H. J. Kwon, M. S. Brown, and J. L. Goldstein. 2010. "Identification of surface residues on Niemann-Pick C2 essential for hydrophobic handoff of cholesterol to NPC1 in lysosomes." *Cell Metab* 12 (2):166-73. doi: 10.1016/j.cmet.2010.05.016.

Wang, Q., L. Huang, Z. Hong, Z. Lv, Z. Mao, Y. Tang, X. Kong, S. Li, Y. Cui, H. Liu, L. Zhang, X. Zhang, L. Jiang, C. Wang, and Q. Zhou. 2017. "The E3 ubiquitin ligase RNF185 facilitates the cGAS-mediated innate immune response." *PLoS Pathog* 13 (3):e1006264. doi: 10.1371/journal.ppat.1006264.

Wang, Q., Y. Liu, N. Soetandyo, K. Baek, R. Hegde, and Y. Ye. 2011. "A ubiquitin ligase-associated chaperone holdase maintains polypeptides in soluble states for proteasome degradation." *Mol Cell* 42 (6):758-70. doi: 10.1016/j.molcel.2011.05.010.

Wang, T., K. Birsoy, N. W. Hughes, K. M. Krupczak, Y. Post, J. J. Wei, E. S. Lander, and D. M. Sabatini. 2015. "Identification and characterization of essential genes in the human genome." *Science* 350 (6264):1096-101. doi: 10.1126/science.aac7041.

Wang, T., J. J. Wei, D. M. Sabatini, and E. S. Lander. 2014. "Genetic screens in human cells using the CRISPR-Cas9 system." *Science* 343 (6166):80-4. doi: 10.1126/science.1246981.

Wang, X., R. A. Herr, W. J. Chua, L. Lybarger, E. J. Wiertz, and T. H. Hansen. 2007. "Ubiquitination of serine, threonine, or lysine residues on the cytoplasmic tail can induce ERAD of MHC-I by viral E3 ligase mK3." *J Cell Biol* 177 (4):613-24. doi: 10.1083/jcb.200611063.

Wang, Y. J., Y. Bian, J. Luo, M. Lu, Y. Xiong, S. Y. Guo, H. Y. Yin, X. Lin, Q. Li, C. C. Y. Chang, T. Y. Chang, B. L. Li, and B. L. Song. 2017. "Cholesterol and fatty acids regulate cysteine ubiquitylation of ACAT2 through competitive oxidation." *Nat Cell Biol* 19 (7):808-819. doi: 10.1038/ncb3551.

Webb, B., and A. Sali. 2014. "Comparative Protein Structure Modeling Using MODELLER." *Curr Protoc Bioinformatics* 47:5.6.1-32. doi: 10.1002/0471250953.bi0506s47.

Weber, A., I. Cohen, O. Popp, G. Dittmar, Y. Reiss, T. Sommer, T. Ravid, and E. Jarosch. 2016. "Sequential Poly-ubiquitylation by Specialized Conjugating Enzymes Expands the Versatility of a Quality Control Ubiquitin Ligase." *Mol Cell* 63 (5):827-39. doi: 10.1016/j.molcel.2016.07.020.

Wei, J., Y. Y. Zhang, J. Luo, J. Q. Wang, Y. X. Zhou, H. H. Miao, X. J. Shi, Y. X. Qu, J. Xu, B. L. Li, and B. L. Song. 2017. "The GARP Complex Is Involved in Intracellular Cholesterol Transport via Targeting NPC2 to Lysosomes." *Cell Rep* 19 (13):2823-2835. doi: 10.1016/j.celrep.2017.06.012.

Whitby, F. G., J. D. Phillips, J. P. Kushner, and C. P. Hill. 1998. "Crystal structure of human uroporphyrinogen decarboxylase." *EMBO J* 17 (9):2463-71. doi: 10.1093/emboj/17.9.2463.

Wiertz, E. J., T. R. Jones, L. Sun, M. Bogyo, H. J. Geuze, and H. L. Ploegh. 1996. "The human cytomegalovirus US11 gene product dislocates MHC class I heavy chains from the endoplasmic reticulum to the cytosol." *Cell* 84 (5):769-79.

Williams, J. M., T. Inoue, L. Banks, and B. Tsai. 2013. "The ERdj5-Sel1L complex facilitates cholera toxin retrotranslocation." *Mol Biol Cell* 24 (6):785-95. doi: 10.1091/mbc.E12-07-0522.

Wright, F. A., J. P. Lu, D. A. Sliter, N. Dupré, G. A. Rouleau, and R. J. Wojcikiewicz. 2015. "A Point Mutation in the Ubiquitin Ligase RNF170 That Causes Autosomal Dominant Sensory Ataxia Destabilizes the Protein and Impairs Inositol 1,4,5-Trisphosphate Receptor-mediated Ca2+ Signaling." *J Biol Chem* 290 (22):13948-57. doi: 10.1074/jbc.M115.655043.

Yabe, D., M. S. Brown, and J. L. Goldstein. 2002. "Insig-2, a second endoplasmic reticulum protein that binds SCAP and blocks export of sterol regulatory element-binding proteins." *Proc Natl Acad Sci U S A* 99 (20):12753-8. doi: 10.1073/pnas.162488899.

Yabe, D., R. Komuro, G. Liang, J. L. Goldstein, and M. S. Brown. 2003. "Liver-specific mRNA for Insig-2 down-regulated by insulin: implications for fatty acid synthesis." *Proc Natl Acad Sci U S A* 100 (6):3155-60. doi: 10.1073/pnas.0130116100.

Yabe, D., Z. P. Xia, C. M. Adams, and R. B. Rawson. 2002. "Three mutations in sterol-sensing domain of SCAP block interaction with insig and render SREBP cleavage insensitive to sterols." *Proc Natl Acad Sci U S A* 99 (26):16672-7. doi: 10.1073/pnas.262669399.

Yamaguchi, D., D. Hu, N. Matsumoto, and K. Yamamoto. 2010. "Human XTP3-B binds to alpha1-antitrypsin variant null(Hong Kong) via the C-terminal MRH domain in a glycan-dependent manner." *Glycobiology* 20 (3):348-55. doi: 10.1093/glycob/cwp182.

Yamasaki, S., N. Yagishita, T. Sasaki, M. Nakazawa, Y. Kato, T. Yamadera, E. Bae, S. Toriyama, R. Ikeda, L. Zhang, K. Fujitani, E. Yoo, K. Tsuchimochi, T. Ohta, N. Araya, H. Fujita, S. Aratani, K. Eguchi, S. Komiya, I. Maruyama, N. Higashi, M. Sato, H. Senoo, T. Ochi, S. Yokoyama, T. Amano, J. Kim, S. Gay, A. Fukamizu, K. Nishioka, K. Tanaka, and T. Nakajima. 2007. "Cytoplasmic destruction of p53 by the endoplasmic reticulum-resident ubiquitin ligase 'Synoviolin'." *EMBO J* 26 (1):113-22. doi: 10.1038/sj.emboj.7601490.

Yang, C., J. G. McDonald, A. Patel, Y. Zhang, M. Umetani, F. Xu, E. J. Westover, D. F. Covey, D. J. Mangelsdorf, J. C. Cohen, and H. H. Hobbs. 2006. "Sterol intermediates from cholesterol biosynthetic pathway as liver X receptor ligands." *J Biol Chem* 281 (38):27816-26. doi: 10.1074/jbc.M603781200.

Yang, J., R. Yan, A. Roy, D. Xu, J. Poisson, and Y. Zhang. 2015. "The I-TASSER Suite: protein structure and function prediction." *Nat Methods* 12 (1):7-8. doi: 10.1038/nmeth.3213.

Yang, S., R. Chang, H. Yang, T. Zhao, Y. Hong, H. E. Kong, X. Sun, Z. Qin, P. Jin, S. Li, and X. J. Li. 2017. "CRISPR/Cas9-mediated gene editing ameliorates neurotoxicity in mouse model of Huntington's disease." *J Clin Invest* 127 (7):2719-2724. doi: 10.1172/JCI92087.

Yang, T., P. J. Espenshade, M. E. Wright, D. Yabe, Y. Gong, R. Aebersold, J. L. Goldstein, and M. S. Brown. 2002. "Crucial step in cholesterol homeostasis: sterols promote binding of SCAP to INSIG-1, a membrane protein that facilitates retention of SREBPs in ER." *Cell* 110 (4):489-500.

Ye, Y., H. H. Meyer, and T. A. Rapoport. 2001. "The AAA ATPase Cdc48/p97 and its partners transport proteins from the ER into the cytosol." *Nature* 414 (6864):652-6. doi: 10.1038/414652a.

Ye, Y., H. H. Meyer, and T. A. Rapoport. 2003. "Function of the p97-Ufd1-Npl4 complex in retrotranslocation from the ER to the cytosol: dual recognition of nonubiquitinated polypeptide segments and polyubiquitin chains." *J Cell Biol* 162 (1):71-84. doi: 10.1083/jcb.200302169.

Ye, Y., and M. Rape. 2009. "Building ubiquitin chains: E2 enzymes at work." *Nat Rev Mol Cell Biol* 10 (11):755-64. doi: 10.1038/nrm2780.

Ye, Y., Y. Shibata, M. Kikkert, S. van Voorden, E. Wiertz, and T. A. Rapoport. 2005. "Recruitment of the p97 ATPase and ubiquitin ligases to the site of retrotranslocation at the endoplasmic reticulum membrane." *Proc Natl Acad Sci U S A* 102 (40):14132-8. doi: 10.1073/pnas.0505006102.

Ye, Y., Y. Shibata, C. Yun, D. Ron, and T. A. Rapoport. 2004. "A membrane protein complex mediates retro-translocation from the ER lumen into the cytosol." *Nature* 429 (6994):841-7. doi: 10.1038/nature02656.

Yeung, H. O., P. Kloppsteck, H. Niwa, R. L. Isaacson, S. Matthews, X. Zhang, and P. S. Freemont. 2008. "Insights into adaptor binding to the AAA protein p97." *Biochem Soc Trans* 36 (Pt 1):62-7. doi: 10.1042/BST0360062.

Yin, C., T. Zhang, X. Qu, Y. Zhang, R. Putatunda, X. Xiao, F. Li, W. Xiao, H. Zhao, S. Dai, X. Qin, X. Mo, W. B. Young, K. Khalili, and W. Hu. 2017. "In Vivo Excision of HIV-1 Provirus by saCas9 and Multiplex Single-Guide RNAs in Animal Models." *Mol Ther* 25 (5):1168-1186. doi: 10.1016/j.ymthe.2017.03.012.

Yoshida, Y., T. Chiba, F. Tokunaga, H. Kawasaki, K. Iwai, T. Suzuki, Y. Ito, K. Matsuoka, M. Yoshida, K. Tanaka, and T. Tai. 2002. "E3 ubiquitin ligase that recognizes sugar chains." *Nature* 418 (6896):438-42. doi: 10.1038/nature00890.

Yoshida, Y., F. Tokunaga, T. Chiba, K. Iwai, K. Tanaka, and T. Tai. 2003. "Fbs2 is a new member of the E3 ubiquitin ligase family that recognizes sugar chains." *J Biol Chem* 278 (44):43877-84. doi: 10.1074/jbc.M304157200.

Younger, J. M., L. Chen, H. Y. Ren, M. F. Rosser, E. L. Turnbull, C. Y. Fan, C. Patterson, and D. M. Cyr. 2006. "Sequential quality-control checkpoints triage misfolded cystic fibrosis transmembrane conductance regulator." *Cell* 126 (3):571-82. doi: 10.1016/j.cell.2006.06.041.

Zelcer, N., C. Hong, R. Boyadjian, and P. Tontonoz. 2009. "LXR regulates cholesterol uptake through Idol-dependent ubiquitination of the LDL receptor." *Science* 325 (5936):100-4. doi: 10.1126/science.1168974.

Zelcer, N., L. J. Sharpe, A. Loregger, I. Kristiana, E. C. Cook, L. Phan, J. Stevenson, and A. J. Brown. 2014. "The E3 ubiquitin ligase MARCH6 degrades squalene monooxygenase and affects 3-hydroxy-3-methyl-glutaryl coenzyme A reductase and the cholesterol synthesis pathway." *Mol Cell Biol* 34 (7):1262-70. doi: 10.1128/MCB.01140-13.

Zelcer, N., and P. Tontonoz. 2006. "Liver X receptors as integrators of metabolic and inflammatory signaling." *J Clin Invest* 116 (3):607-14. doi: 10.1172/JCI27883.

Zhang, T., Y. Xu, Y. Liu, and Y. Ye. 2015. "gp78 functions downstream of Hrd1 to promote degradation of misfolded proteins of the endoplasmic reticulum." *Mol Biol Cell* 26 (24):4438-50. doi: 10.1091/mbc.E15-06-0354.

Zhang, X., A. Shaw, P. A. Bates, R. H. Newman, B. Gowen, E. Orlova, M. A. Gorman, H. Kondo, P. Dokurno, J. Lally, G. Leonard, H. Meyer, M. van Heel, and P. S. Freemont. 2000. "Structure of the AAA ATPase p97." *Mol Cell* 6 (6):1473-84.

Zhang, Y., K. M. Lee, L. N. Kinch, L. Clark, N. V. Grishin, D. M. Rosenbaum, M. S. Brown, J. L. Goldstein, and A. Radhakrishnan. 2016. "Direct Demonstration That Loop1 of Scap Binds to Loop7: A CRUCIAL EVENT IN CHOLESTEROL HOMEOSTASIS." *J Biol Chem* 291 (24):12888-96. doi: 10.1074/jbc.M116.729798.

Zhou, Y., S. Zhu, C. Cai, P. Yuan, C. Li, Y. Huang, and W. Wei. 2014. "High-throughput screening of a CRISPR/Cas9 library for functional genomics in human cells." *Nature* 509 (7501):487-91. doi: 10.1038/nature13166.

Appendix 1: gRNA and RNAi sequences

1. gRNA target sequences

Target gene	gRNA sequence
EDEM2	TATCTGACCGGCTCTCCCAG
PDI	GCGGAAAAGCAACTTCGCGG
ALG3	GGAGAAGAAACAGTAACCCA
DPM3	GAGGACTTCCTGGCAGGACAA
TXNDC11 #1	GTCAAGGACTGGAGACCTCA
TXNDC11 #2	AAGAAGGTCAAATAACCAGG
UPF2	GCTGGTGAAAGAGAGAGCAG
SMG6	GCGGGTACTTCCAATGGGAG
ALG12	TGACTGACTTACCTAAACAG
SMG7	AGGTCCACTCACCATTGGAG
UROD #1	GCACCAGCAAAGCCAATCAG
UROD #2	ACACGTGCTGAAAAAGTCCT
UBE2G2 #A	CATGGGCTACGAGAGCAGCG
UBE2G2 #C	TTACCTGCTACAATTCCTTC
UBE2G2 #D	AGAATTAACACTGAATCCTC
RNF145 #1	TGTTAAATGTGGCCCTG
RNF145 #2	TTGGATGTCCTGTACAGAT
RNF145 #3	GGAATTCAGAAAAGAGCCAG
RNF145 #4	GGCTGCAAAGGAGAAACTGG
RNF145 #5	TCATAGGCTTACCTGAAGAG
RNF145 #8	AGTGTTAAATGTGGCCCTGA
HMGCR C-terminus	TCAGAACTGTCGGGCTATTC
ATP6V1B2 #1	CTCCCGAGCTCCCACCGC
ATP6V1B2 #2	GAGGAGACAAGATGGCGCTG
EHD1 #1	TGCTGTACTGCCCCACG
EHD1 #2	GCTCCGGCTCCTTCTTGCGG
EHD1 #3	GAGAAGCAGCGGATCAGCAG
EHD1 #4	GCAGAAGCTGCTACCCCTGG
GNPTAB #1	GGTCAGAGAACAGATGGAGG
GNPTAB #2	GTGGAGGTGGACACAAGGGA
GALNT11 #1	ATCAAGAGTTGAGAGACTT
GALNT11 #2	GGTGTGCCGGTCCTCACGGA
GALNT11 #3	AGTGGCATGGATATCTGGGG
GALNT11 #4	GGTCAGGAGGATCCCAGCAG
LDLR #1	GAGGTGCGATGGCCAAG
LDLR #2	GAATGCTTGGACAACAACGG
LDLR #3	GAATGCTTGGACAACAACGG
LDLR #4	GTGGCCCAGCGAAGATGCGA
NPC #1	GTGCAGTTCGTGTTATA
NPC #2	GGGCAGAACATGGTGTGCGG

NPC #3	GTAGCAGCAGGAGGAGGCCA
NPC #4	AGATTTTCCAGTCCATGGGA
Insig1 #1	CGTAGCTAGAAAAGCTA
Insig1 #2	GCTGCTGTCCCGCAGCAGGG
Insig1 #3	GCAGCCCCTACCCCAACACC
Insig1 #4	TCAACCTGCTGCAGATCCAG
Insig2 #1	AAGGAGAGACAGAGTCACCT
Insig2 #2	CTAGATGTCTGTCAATGCAG
Insig2 #3	GAATCATCAAGTTCACACTC
Insig2 #4	AAAAGTCCACCACAGTCCAA
TECR #1	CGCAAAGGCATAGTGCCAT
TECR #2	GAGGTTCTTGATCTCCGCAA
TECR #3	GTTCTGCAGAAGCTGCCCGT
TECR #4	ATGAGTGACAGATGCAGGCG
gp78 #1	GTTAGCTGGTCCGGCTCGCC
gp78 #2	GCGGCGAGCCGGACCAGCTAA
gp78 #3	GACTGGGCCACATCGCGGGCC
gp78 #4	GTGAGGCCCGTGTAGGTGCGG
TRC8	GGCGTCGATGATGTAAAGGC
Control (B2M)	GGCCGAGATGTCTCGCTCCG
RNF185 #1	GGCGCTGGCGAGAGCGGA
RNF185 #2	GGCTGATGACGGCATCCT
RNF185 #3	GCTGGCGAGAGCGGAGGGC
RNF185 #4	GATGCCGTCATCAGCCTGTG
Hrd1 #1	GGTGTTCTTTGGGCAACTGA
Hrd1 #2	GCACGGCAGTGATGATGG
Hrd1 #3	GTCATCCCGAAAAACGGTGA
Hrd1 #4	GACCAAGTCCAGCCCCAGCA
UBE2D2 #1	CACCGGGCAAGCTACAATAATG
UBE2D2 #2	GTTTGAAGGGGTAATCTGTT
UBE2D2 #3	GTAGATCCGAGCAATCTC
UBE2D2 #4	GTGTTCAGCAGGTCCTGT
UBE2K #1	GAATTAAGAGGAGAAATAGC
UBE2K #2	GGATTAAATGGGTATGTTTC
UBE2K #3	GTGACGGAACTAATATT
UBE2K #4	GCTGTCTGTTTGAACATTTC

2. siRNA target sequences

Target gene	**siRNA sequence**
gp78	GACGGAUUCAAGUACCUUU
MARCHVI	UCAUAGAUCUCGUCGCUUA
TRC8	GGGAGCCGCUUACAAGAAA

3. shRNA forward oligo sequences (5’-3’)

Target gene	**Forward oligo sequence (5'-3')**
Control	GATCCGGGTATCGACGATTACAAATTCAAGAGATTTGTAATCGTCGATACCCTTTTTTG
TXNDC11 #1	GATCCGCGGCAATTGTTGACGTGAATTCAAGAGATTCACGTCAACAATTGCCGTTTTTTG
TXNDC11 #2	GATCCGTGGCTAACTCTCCTACCAATTCAAGAGATTGGTAGGAGAGTTAGCCATTTTTTG
UROD #1	GATCCGGTCCGATCATGTGATCTTCTTCAAGAGAGAAGATCACATGATCGGACTTTTTTG
UROD #2	GATCCGCTCCGACATCCTTGTTGTATTCAAGAGATACAACAAGGATGTCGGAGTTTTTTG
UROD #3	GATCCGCCCAGAGCCATTAAGAGAATTCAAGAGATTCTCTTAATGGCTCTGGGTTTTTTG
UROD #4	GATCCGCATGGACCCTGATGACATATTCAAGAGATATGTCATCAGGGTCCATGTTTTTTG

Appendix 1. gRNA and siRNA target sequences. shRNA forward oligo sequence cloned into pSIREN

Appendix 2: Oligonucleotides for screen preparation

Retroviral LAM-PCR	
	Sequence 5'-3'
Digested gDNA adaptor	CCTATAGTGAGTCGTATTATATGAGTAGTACCATGGGAAC
Digested gDNA adaptor	GTTCCCATGGTACTACTCATATAATACGACTCACTATAGG
Linear PCR primer	[Biotin]-GGTCTCCAAATCTCGGTGGAAC
P5-VirusZ	AATGATACGGCGACCACCGAGATCTACACTCTTTCCCTACACGACGCTCTTCC GATCTCTATACGAAGTTATGGGCCCTAGCTC
P7-Index5-Ad1	CAAGCAGAAGACGGCATACGAGA*nnnnnnn*TGACTGGAGTTCAGACGTGTGC TCTTCCGATCTGTTCCCATGGTACTACTCATATAATACG
Illumina sequencing primer	AGCTCAGTACAAACCTACAGGTGGGGTCTTTCA
CRISPR screen analysis	
GeCKO library	
	Sequence 5'-3'
sgRNA_outer_F	GCTTACCGTAACTTGAAAGTATTTCG
sgRNA_outer_R	GTCTGTTGCTATTATGTCTACTATTCTTTCC
P5-sgRNA_inner_F	AATGATACGGCGACCACCGAGATCTACACTCTCTTGTGGAAAGGACGAAACA CCG
P7-index-sgRNA_inner_R	CAAGCAGAAGACGGCATACGAGA*nnnnnnn*GTGACTGGAGTTCAGACGTGT GCTCTTCCGATCTTCTACTATTCTTTCCCCTGCACTGT
Illumina sequencing primer	ACACTCTCTTGTGGAAAGGACGAAACACCG
Bassik library	
	Sequence 5'-3'
sgRNA_outer_F	AGGCTTGGATTTCTATAACTTCGTATAGCATACATTATAC
sgRNA_outer_R	ACATGCATGGCGGTAATACGGTTATC
P5-sgRNA_inner_F	AATGATACGGCGACCACCGAGATCTACACGCACAAAAGGAAACTCACCCT
P7-index-sgRNA_inner_R	CAAGCAGAAGACGGCATACGAGAT*nnnnnnn*GTGACTGGAGTTCAGACGTGT GCTCTTCCGATCCGACTCGGTGCCACTTTTTC
Illumina sequencing primer	AGACTATAAGTATCCCTTGGAGAACCACCTTGTTGG
Ubiquitome library	
	Sequence 5'-3'
sgRNA_outer_F	GCTTACCGTAACTTGAAAGTATTTCG
sgRNA_outer_R	CGAGACTAGTGAGACGTGCTAC
P5-sgRNA_inner_F	AATGATACGGCGACCACCGAGATCTACACTCTCTTGTGGAAAGGACGAAACA CCG

P7-index-sgRNA_inner_R	CAAGCAGAAGACGGCATACGAGAT*nnnnnnn*GTGACTGGAGTTCAGACGTGT GCTCTTCCGATCT CCATTTGTCACGTCCTGCACG
Illumina sequencing primer	CTTGTGGAAAGGACGAAACACCG

Appendix 2. Primer and adapter sequences used to prepare samples from forward genetic screens for Illumina sequencing

Appendix 3: RNF145-V5 immunoprecipitation

SD: sterol depleted, sterols: sterol depleted + 1 hr sterols, sterols + MG132: sterol depleted + 30 min 50 µM MG132 treatment followed by 1 hr sterols.

#: number of unique peptides, A: Area

Accession	Gene name	Gene ID	SD		sterols		sterols + MG132	
			#	A	#	A	#	A
Q8N766	ER membrane protein complex subunit 1	EMC1	15	1.99	13.00	2.40	19.00	3.35
O75955	Flotillin-1	FLOT1	17	3.90	19.00	7.35	16.00	3.54
P04035	3-hydroxy-3-methylglutaryl-coenzyme A reductase	HMGCR	10	1.41	7.00	1.41	16.00	7.65
Q96MT1	RING finger protein 145	RNF145	15	102.48	14.00	126.23	15.00	140.74
P32004	Neural cell adhesion molecule L1	L1CAM	13	4.64	19.00	13.80	14.00	5.85
O15031	Plexin-B2	PLXNB2	12	1.50	21.00	3.61	14.00	1.42
P00533	Epidermal growth factor receptor	EGFR	14	2.54	17.00	5.63	13.00	2.10
O96005	Cleft lip and palate transmembrane protein 1	CLPTM1	6	2.40	7.00	2.44	11.00	4.24
Q86VI3	Ras GTPase-activating-like protein IQGAP3	IQGAP3	3	0.54	3.00	0.52	11.00	1.32
Q12907	Vesicular integral-membrane protein VIP36	LMAN2	10	5.36	7.00	3.63	10.00	5.70
P04844	Dolichyl-diphosphooligosaccharide--protein glycosyltransferase subunit 2	RPN2	5	1.52	9.00	2.07	10.00	2.25
O14980	Exportin-1	XPO1	9	1.78	14.00	2.59	10.00	1.26
O14818	Proteasome subunit alpha type-7	PSMA7	7	2.98	4.00	2.57	9.00	8.04
Q9UNQ0	ATP-binding cassette sub-family G member 2	ABCG2	10	3.16	10.00	6.11	9.00	3.53
Q6YHK3	CD109 antigen	CD109	9	1.82	17.00	3.84	9.00	1.34
P20618	Proteasome subunit beta type-1	PSMB1	3	0.78	3.00	0.93	9.00	3.82
P20020	Plasma membrane calcium-transporting ATPase 1	ATP2B1	5	1.23	9.00	2.56	9.00	1.01
P10586	Receptor-type tyrosine-protein phosphatase F	PTPRF	9	0.87	19.00	2.60	9.00	0.74
Q9UJS0	Calcium-binding mitochondrial carrier protein Aralar2	SLC25A13	7	0.98	12.00	1.35	9.00	0.77
Q7L576	Cytoplasmic FMR1-interacting protein 1	CYFIP1	3	0.96	9.00	1.19	9.00	0.68
Q92621	Nuclear pore complex protein Nup205	NUP205	5	0.63	13.00	1.13	9.00	0.74
Q14677	Clathrin interactor 1	CLINT1	5	0.49	7.00	0.52	9.00	0.86
Q96AD5	Patatin-like phospholipase domain-containing protein 2	PNPLA2	6	2.95	7.00	4.35	8.00	2.32
Q14534	Squalene monooxygenase	SQLE	5	1.08	5.00	1.40	8.00	2.77
P49720	Proteasome subunit beta type-3	PSMB3	2	1.02	2.00	0.81	7.00	3.84
P28074	Proteasome subunit beta type-5	PSMB5	5	0.97	2.00	0.55	7.00	4.05
Q9UKS6	Protein kinase C and casein kinase substrate in neurons protein 3	PACSIN3	5	1.13	7.00	2.41	7.00	1.16
A0A024RA52	Proteasome subunit alpha type	PSMA2					7.00	3.71
Q5T5U3	Rho GTPase-activating protein 21	ARHGAP21	1	0.20	5.00	0.20	7.00	0.42
Q96CS3	FAS-associated factor 2	FAF2	3	1.53	5.00	1.98	6.00	4.70
Q14254	Flotillin-2	FLOT2	7	1.84	12.00	4.58	6.00	1.74
Q8NBM4	Ubiquitin-associated domain-containing protein 2	UBAC2	5	1.60	3.00	1.04	6.00	2.92
Q6DD88	Atlastin-3	ATL3	3	0.65	7.00	2.23	6.00	2.04
P28070	Proteasome subunit beta type-4	PSMB4	2	0.58	2.00	0.42	6.00	2.67
Q9UMX0	Ubiquilin-1	UBQLN1	2	1.27			6.00	1.68
O60237	Protein phosphatase 1 regulatory subunit 12B	PPP1R12B	1	0.81	2.00	1.16	6.00	0.90
Q9UKV5	E3 ubiquitin-protein ligase AMFR	AMFR	4	0.68	3.00	0.67	6.00	1.46
Q6P2E9	Enhancer of mRNA-decapping protein 4	EDC4	3	0.46	6.00	1.10	6.00	0.78
Q9Y2L1	Exosome complex exonuclease RRP44	DIS3	5	0.56	6.00	0.85	6.00	0.53

F1T0I1	Protein transport protein Sec16A	SEC16A	7	21.71	7.00	14.12	5.00	13.74
P16070	CD44 antigen	CD44	4	6.60	6.00	16.10	5.00	7.36
Q15758	Neutral amino acid transporter B(0)	SLC1A5	5	3.75	8.00	8.48	5.00	4.72
Q9H9B4	Sideroflexin-1	SFXN1	9	1.67	10.00	2.45	5.00	2.07
Q9NR30	Nucleolar RNA helicase 2	DDX21	3	0.82	8.00	2.98	5.00	1.48
Q96SB3	Neurabin-2	PPP1R9B	9	1.92	7.00	2.01	5.00	0.80
O14964	Hepatocyte growth factor-regulated tyrosine kinase substrate	HGS	1	1.43	1.00	2.21	5.00	1.08
P51648	Fatty aldehyde dehydrogenase	ALDH3A2	3	0.95	3.00	0.86	5.00	2.29
P01130	Low-density lipoprotein receptor	LDLR	4	1.00	8.00	1.83	5.00	1.05
Q14160	Protein scribble homolog	SCRIB	2	0.48	9.00	2.06	5.00	0.57
Q16850	Lanosterol 14-alpha demethylase	CYP51A1	2	0.58	6.00	1.21	5.00	1.31
Q9NPA0	ER membrane protein complex subunit 7	EMC7	2	0.85	2.00	0.73	5.00	1.31
P52789	Hexokinase-2	HK2	7	0.57	10.00	1.38	5.00	0.87
Q96FS4	Signal-induced proliferation-associated protein 1	SIPA1	3	0.69	5.00	0.86	5.00	1.22
O94905	Erlin-2	ERLIN2	2	0.70	4.00	0.65	5.00	1.21
Q7L014	Probable ATP-dependent RNA helicase DDX46	DDX46	1	0.72	2.00	0.63	5.00	0.53
P78346	Ribonuclease P protein subunit p30	RPP30	1	0.57	3.00	0.36	5.00	0.71
O00231	26S proteasome non-ATPase regulatory subunit 11	PSMD11	1	0.38	5.00	0.59	5.00	0.30
Q6P4F7	Rho GTPase-activating protein 11A	ARHGAP11A			2.00	0.44	5.00	0.47
Q13769	THO complex subunit 5 homolog	THOC5			3.00	0.33	5.00	0.24
P39656	Dolichyl-diphosphooligosaccharide--protein glycosyltransferase 48 kDa subunit	DDOST	3	0.42	4.00	5.82	4.00	3.10
P43121	Cell surface glycoprotein MUC18	MCAM	8	1.92	10.00	5.66	4.00	1.46
P28066	Proteasome subunit alpha type-5	PSMA5	1	0.37	2.00	1.09	4.00	4.58
Q15738	Sterol-4-alpha-carboxylate 3-dehydrogenase, decarboxylating	NSDHL	1	1.86	1.00	2.13	4.00	1.47
P28072	Proteasome subunit beta type-6	PSMB6	1	1.16	1.00	0.90	4.00	3.10
Q14152	Eukaryotic translation initiation factor 3 subunit A	EIF3A	4	0.39	14.00	3.17	4.00	0.86
P25788	Proteasome subunit alpha type-3	PSMA3	3	0.86	3.00	0.82	4.00	2.54
Q9NXW2	DnaJ homolog subfamily B member 12	DNAJB12	3	0.89	3.00	0.61	4.00	1.68
Q6PJ61	F-box only protein 46	FBXO46	2	0.25	5.00	0.80	4.00	1.09
Q9NRG9	Aladin	AAAS	2	0.34	4.00	1.10	4.00	0.66
O14579	Coatomer subunit epsilon	COPE	2	0.50	1.00	0.50	4.00	0.85
Q7L5D6	Golgi to ER traffic protein 4 homolog	GET4					4.00	1.75
P00387	NADH-cytochrome b5 reductase 3	CYB5R3	1	0.19	4.00	0.60	4.00	0.77
P57678	Gem-associated protein 4	GEMIN4	2	0.41	6.00	0.62	4.00	0.51
Q7Z478	ATP-dependent RNA helicase DHX29	DHX29	1	0.50	4.00	0.52	4.00	0.46
Q9UBV2	Protein sel-1 homolog 1	SEL1L			2.00	0.40	4.00	0.76
P09884	DNA polymerase alpha catalytic subunit	POLA1	2	0.52	1.00	0.17	4.00	0.38
O75128	Protein cordon-bleu	COBL	4	0.25	6.00	0.33	4.00	0.23
P80723	Brain acid soluble protein 1	BASP1	3	1.87	2.00	6.99	3.00	1.08
Q15149-3	Isoform 3 of Plectin	PLEC			4.00	4.12	3.00	5.74
P53985	Monocarboxylate transporter 1	SLC16A1	4	1.76	6.00	5.03	3.00	1.60
O00560	Syntenin-1	SDCBP	4	1.34	4.00	2.97	3.00	1.80
P83731	60S ribosomal protein L24	RPL24	2	1.38	2.00	2.33	3.00	1.93
P63000	Ras-related C3 botulinum toxin substrate 1	RAC1	6	1.82	5.00	2.37	3.00	1.22
P40692	DNA mismatch repair protein Mlh1	MLH1	2	1.39	1.00	3.50	3.00	0.26
Q9Y6M5	Zinc transporter 1	SLC30A1	2	0.99	3.00	2.56	3.00	1.49
Q9Y320	Thioredoxin-related transmembrane protein 2	TMX2	4	3.35	4.00	0.72	3.00	0.87
P32969	60S ribosomal protein L9	RPL9	3	0.95	4.00	2.45	3.00	1.49

Q9P0I2	ER membrane protein complex subunit 3	EMC3	2	1.60	1.00	1.61	3.00	1.48
Q14118	Dystroglycan	DAG1	1	1.77	6.00	2.17	3.00	0.69
P06756	Integrin alpha-V	ITGAV	5	0.94	10.00	2.24	3.00	0.95
O75396	Vesicle-trafficking protein SEC22b	SEC22B	2	1.06	3.00	1.14	3.00	1.60
Q8TC12	Retinol dehydrogenase 11	RDH11	1	1.50	2.00	1.47	3.00	0.68
P53007	Tricarboxylate transport protein, mitochondrial	SLC25A1	3	1.38	4.00	1.56	3.00	0.71
P62070	Ras-related protein R-Ras2	RRAS2	3	1.09	4.00	1.84	3.00	0.69
P13073	Cytochrome c oxidase subunit 4 isoform 1, mitochondrial	COX4I1	2	1.42	3.00	1.15	3.00	0.74
Q02543	60S ribosomal protein L18a	RPL18A	2	0.71	4.00	1.54	3.00	1.01
O95297	Myelin protein zero-like protein 1	MPZL1	2	0.65	3.00	1.53	3.00	0.75
O14975	Very long-chain acyl-CoA synthetase	SLC27A2	3	1.83	3.00	0.49	3.00	0.58
Q96A33	Coiled-coil domain-containing protein 47	CCDC47	1	0.94	2.00	0.83	3.00	1.03
P08574	Cytochrome c1, heme protein, mitochondrial	CYC1	2	1.60	3.00	0.61	3.00	0.58
Q92542	Nicastrin	NCSTN	3	0.43	6.00	1.68	3.00	0.55
Q9NR12	PDZ and LIM domain protein 7	PDLIM7	1	0.64	2.00	0.44	3.00	1.48
P46777	60S ribosomal protein L5	RPL5	2	0.74	3.00	1.20	3.00	0.53
Q9UBX3	Mitochondrial dicarboxylate carrier	SLC25A10	2	0.88	3.00	0.84	3.00	0.59
P55263	Adenosine kinase	ADK	5	0.74	2.00	0.72	3.00	0.62
P46977	Dolichyl-diphosphooligosaccharide--protein glycosyltransferase subunit STT3A	STT3A	1	0.58	1.00	0.81	3.00	0.66
O15381	Nuclear valosin-containing protein-like	NVL	1	0.84	2.00	0.76	3.00	0.42
Q14558	Phosphoribosyl pyrophosphate synthase-associated protein 1	PRPSAP1	2	0.45	3.00	0.66	3.00	0.85
Q5ZPR3	CD276 antigen	CD276	2	0.43	3.00	1.01	3.00	0.49
P62873	Guanine nucleotide-binding protein G(I)/G(S)/G(T) subunit beta-1	GNB1					3.00	1.89
P51812	Ribosomal protein S6 kinase alpha-3	RPS6KA3	4	0.99	3.00	0.42	3.00	0.42
P46060	Ran GTPase-activating protein 1	RANGAP1	3	0.50	5.00	0.77	3.00	0.50
Q9Y679	Ancient ubiquitous protein 1	AUP1	1	0.43	1.00	0.17	3.00	1.12
Q7L2E3	Putative ATP-dependent RNA helicase DHX30	DHX30	1	0.60	2.00	0.70	3.00	0.37
Q86YQ8	Copine-8	CPNE8	1	0.29	4.00	0.75	3.00	0.53
Q9Y5Y2	Cytosolic Fe-S cluster assembly factor NUBP2	NUBP2	1	0.47	2.00	0.39	3.00	0.54
Q9NSE4	Isoleucine--tRNA ligase, mitochondrial	IARS2	3	0.39	2.00	0.38	3.00	0.63
Q9HC35	Echinoderm microtubule-associated protein-like 4	EML4	4	0.41	4.00	0.53	3.00	0.44
Q15149-4	Isoform 4 of Plectin	PLEC					3.00	1.24
Q14643	Inositol 1,4,5-trisphosphate receptor type 1	ITPR1	2	0.23	4.00	0.55	3.00	0.40
Q9Y4P3	Transducin beta-like protein 2	TBL2	1	0.30	4.00	0.39	3.00	0.47
P18031	Tyrosine-protein phosphatase non-receptor type 1	PTPN1	1	0.37	2.00	0.18	3.00	0.43
O95347	Structural maintenance of chromosomes protein 2	SMC2	3	0.31	2.00	0.21	3.00	0.47
P55061	Bax inhibitor 1	TMBIM6					3.00	0.90
Q96RT1	Erbin	ERBIN	1		2.00	0.55	3.00	0.30
Q96KA5	Cleft lip and palate transmembrane protein 1-like protein	CLPTM1L	1	0.27	2.00	0.13	3.00	0.44
Q86TM6	E3 ubiquitin-protein ligase synoviolin	SYVN1			1.00	0.34	3.00	0.50
A5YKK6	CCR4-NOT transcription complex subunit 1	CNOT1	1	0.26	4.00	0.34	3.00	0.21
Q9UN37	Vacuolar protein sorting-associated protein 4A	VPS4A					3.00	0.74
Q92620	Pre-mRNA-splicing factor ATP-dependent RNA helicase PRP16	DHX38			3.00	0.35	3.00	0.33
Q9NX61	Transmembrane protein 161A	TMEM161A					3.00	0.63
Q13619	Cullin-4A	CUL4A			2.00	0.32	3.00	0.25
O60826	Coiled-coil domain-containing protein 22	CCDC22	1	0.22	1.00		3.00	0.21
Q14839	Chromodomain-helicase-DNA-binding protein 4	CHD4					3.00	0.33
O75150	E3 ubiquitin-protein ligase BRE1B	RNF40	1		1.00		3.00	0.24

Q96CW5	Gamma-tubulin complex component 3	TUBGCP3					3.00	0.16
Q9NRZ9	Lymphoid-specific helicase	HELLS					3.00	0.14
P12270	Nucleoprotein TPR	TPR	1				3.00	
A0A087WW89	Protein IGHV3-72	IGHV3-72	3	54.95	2.00	63.66	2.00	32.52
Q9NQC3	Reticulon-4	RTN4	1	2.38	4.00	5.23	2.00	2.32
Q10589	Bone marrow stromal antigen 2	BST2	1	2.77	1.00	3.93	2.00	1.62
P11233	Ras-related protein Ral-A	RALA	5	1.93	6.00	3.41	2.00	2.15
P22695	Cytochrome b-c1 complex subunit 2, mitochondrial	UQCRC2	4	1.26	8.00	4.68	2.00	1.01
Q8WTV0	Scavenger receptor class B member 1	SCARB1	1	2.14	3.00	1.80	2.00	1.44
Q9H2H9	Sodium-coupled neutral amino acid transporter 1	SLC38A1	2	1.78	3.00	2.06	2.00	1.34
Q14126	Desmoglein-2	DSG2	4	0.51	11.00	4.07	2.00	0.58
P07947	Tyrosine-protein kinase Yes	YES1	3	1.21	4.00	2.24	2.00	1.01
Q8NBI5	Solute carrier family 43 member 3	SLC43A3	2	1.70	3.00	0.91	2.00	1.68
Q9NRR5	Ubiquilin-4	UBQLN4			1.00	2.32	2.00	1.74
Q99808	Equilibrative nucleoside transporter 1	SLC29A1	2	0.78	2.00	2.47	2.00	0.80
O14828	Secretory carrier-associated membrane protein 3	SCAMP3	2	1.36	3.00	1.24	2.00	1.42
P20645	Cation-dependent mannose-6-phosphate receptor	M6PR	2	0.78	1.00	1.92	2.00	1.29
P36897	TGF-beta receptor type-1	TGFBR1	2	0.93	3.00	2.10	2.00	0.87
Q9P035	Very-long-chain (3R)-3-hydroxyacyl-CoA dehydratase 3	HACD3	2	0.92	1.00	1.61	2.00	1.17
P06241	Tyrosine-protein kinase Fyn	FYN	3	1.12	5.00	1.36	2.00	1.20
P35268	60S ribosomal protein L22	RPL22					2.00	3.66
Q6NUK1	Calcium-binding mitochondrial carrier protein SCaMC-1	SLC25A24	4	0.97	7.00	2.08	2.00	0.54
P39023	60S ribosomal protein L3	RPL3			4.00	2.21	2.00	1.37
P11166	Solute carrier family 2, facilitated glucose transporter member 1	SLC2A1	2	0.31	3.00	1.83	2.00	1.34
Q01581	Hydroxymethylglutaryl-CoA synthase, cytoplasmic	HMGCS1	4	0.87	4.00	1.89	2.00	0.68
P01111	GTPase NRas	NRAS	1	0.97	1.00	1.67	2.00	0.64
O75695	Protein XRP2	RP2	1	0.82	1.00	1.76	2.00	0.69
O00592	Podocalyxin	PODXL	1		2.00	1.96	2.00	1.23
P61254	60S ribosomal protein L26	RPL26	2	1.45	2.00	0.98	2.00	0.73
Q9BWD1	Acetyl-CoA acetyltransferase, cytosolic	ACAT2	3	0.78	3.00	1.33	2.00	1.04
Q8NBM8	Prenylcysteine oxidase-like	PCYOX1L	1	1.06	2.00	0.63	2.00	1.07
Q15006	ER membrane protein complex subunit 2	EMC2	2	0.28	1.00	1.12	2.00	1.36
Q9Y4W6	AFG3-like protein 2	AFG3L2	2	1.64	3.00	0.56	2.00	0.54
P51114	Fragile X mental retardation syndrome-related protein 1	FXR1	2	0.82	3.00	1.28	2.00	0.60
H3BQK9	Microtubule-actin cross-linking factor 1, isoforms 1/2/3/5	MACF1	1	1.16	1.00	0.21	2.00	1.27
P02794	Ferritin heavy chain	FTH1	3	0.78	4.00	1.21	2.00	0.62
P12277	Creatine kinase B-type	CKB	2	1.15	2.00	0.67	2.00	0.77
P07948	Tyrosine-protein kinase Lyn	LYN	2	0.30	5.00	1.37	2.00	0.88
P62995	Transformer-2 protein homolog beta	TRA2B	1	0.72	3.00	0.85	2.00	0.78
Q96N66	Lysophospholipid acyltransferase 7	MBOAT7			2.00	1.22	2.00	1.10
Q99436	Proteasome subunit beta type-7	PSMB7					2.00	2.30
Q6PJ69	Tripartite motif-containing protein 65	TRIM65			1.00	1.33	2.00	0.87
O75915	PRA1 family protein 3	ARL6IP5	1	0.44	1.00	0.97	2.00	0.67
Q04721	Neurogenic locus notch homolog protein 2	NOTCH2	3	0.59	8.00	1.23	2.00	0.25
Q8IX12	Cell division cycle and apoptosis regulator protein 1	CCAR1	1	0.73	1.00	0.73	2.00	0.46
Q14240	Eukaryotic initiation factor 4A-II	EIF4A2	1	0.08	2.00	0.84	2.00	0.98
Q9Y3E0	Vesicle transport protein GOT1B	GOLT1B			2.00	1.21	2.00	0.68
Q9HCE1	Putative helicase MOV-10	MOV10	2	0.53	4.00	0.79	2.00	0.51
Q01780	Exosome component 10	EXOSC10	1	0.64	2.00	0.86	2.00	0.30

Q00341	Vigilin	HDLBP	3	0.25	7.00	0.94	2.00	0.61
P43007	Neutral amino acid transporter A	SLC1A4	1	0.30	2.00	1.09	2.00	0.37
Q9BXS9	Solute carrier family 26 member 6	SLC26A6	1	0.32	1.00	0.86	2.00	0.51
Q5T0V7	Dystonin (Fragment)	DST			1.00	0.73	2.00	0.88
Q9BZH6	WD repeat-containing protein 11	WDR11	2	0.52	2.00	0.57	2.00	0.52
Q9H0U4	Ras-related protein Rab-1B	RAB1B			1.00	0.08	2.00	1.53
Q9Y2A7	Nck-associated protein 1	NCKAP1	1	0.29	1.00	1.08	2.00	0.23
Q93052	Lipoma-preferred partner	LPP	4	0.52	4.00	0.68	2.00	0.34
Q86TC9	Myopalladin	MYPN	2	0.56	3.00	0.53	2.00	0.44
Q9P2B2	Prostaglandin F2 receptor negative regulator	PTGFRN	2	0.16	3.00	0.96	2.00	0.36
Q15717	ELAV-like protein 1	ELAVL1	3	0.80			2.00	0.68
Q9BTW9	Tubulin-specific chaperone D	TBCD	2	0.24	5.00	0.80	2.00	0.42
Q9P0L0	Vesicle-associated membrane protein-associated protein A	VAPA			1.00	0.90	2.00	0.55
P29317	Ephrin type-A receptor 2	EPHA2			4.00	1.02	2.00	0.41
Q15021	Condensin complex subunit 1	NCAPD2			3.00	0.95	2.00	0.42
Q99459	Cell division cycle 5-like protein	CDC5L	1	0.34	3.00	0.53	2.00	0.48
P82650	28S ribosomal protein S22, mitochondrial	MRPS22	1	0.18	2.00	0.73	2.00	0.42
Q86UP2	Kinectin	KTN1	1	0.33	1.00	0.65	2.00	0.34
P35658	Nuclear pore complex protein Nup214	NUP214	1	0.45	1.00	0.43	2.00	0.43
Q15036	Sorting nexin-17	SNX17			2.00	0.87	2.00	0.44
Q08345	Epithelial discoidin domain-containing receptor 1	DDR1			1.00	0.73	2.00	0.58
P46087	Probable 28S rRNA (cytosine(4447)-C(5))-methyltransferase	NOP2	2	0.39	4.00	0.62	2.00	0.29
Q9P2R3	Rabankyrin-5	ANKFY1	1	0.33	1.00	0.38	2.00	0.57
Q14108	Lysosome membrane protein 2	SCARB2			4.00	0.96	2.00	0.31
Q9HAV4	Exportin-5	XPO5	2	0.45	4.00	0.50	2.00	0.25
A1L0T0	Acetolactate synthase-like protein	ILVBL	3	0.20	3.00	0.62	2.00	0.35
P04183	Thymidine kinase, cytosolic	TK1			1.00	0.54	2.00	0.61
Q92615	La-related protein 4B	LARP4B			1.00	0.68	2.00	0.45
O60610	Protein diaphanous homolog 1	DIAPH1	3	0.19	5.00	0.64	2.00	0.30
Q9H0D6	5'-3' exoribonuclease 2	XRN2			1.00	0.57	2.00	0.51
Q8N7H5	RNA polymerase II-associated factor 1 homolog	PAF1			3.00	0.49	2.00	0.60
Q08752	Peptidyl-prolyl cis-trans isomerase D	PPID	3	0.38	3.00	0.40	2.00	0.25
Q96J02	E3 ubiquitin-protein ligase Itchy homolog	ITCH			6.00	0.70	2.00	0.33
Q9UNN8	Endothelial protein C receptor	PROCR	1	0.54			2.00	0.48
Q96DG6	Carboxymethylenebutenolidase homolog	CMBL	1	0.11	1.00	0.56	2.00	0.32
P49755	Transmembrane emp24 domain-containing protein 10	TMED10	1	0.47			2.00	0.51
Q14738	Serine/threonine-protein phosphatase 2A 56 kDa regulatory subunit delta isoform	PPP2R5D	1	0.30	1.00	0.32	2.00	0.33
Q8NHH9	Atlastin-2	ATL2			4.00	0.58	2.00	0.36
P50402	Emerin	EMD	1	0.46			2.00	0.45
P37198	Nuclear pore glycoprotein p62	NUP62	1	0.32	2.00	0.25	2.00	0.32
P11182	Lipoamide acyltransferase component of branched-chain alpha-keto acid dehydrogenase complex, mitochondrial	DBT			3.00	0.41	2.00	0.42
Q8N4V1	Membrane magnesium transporter 1	MMGT1			1.00	0.17	2.00	0.64
Q92692	Nectin-2	NECTIN2			2.00	0.60	2.00	0.21
P18858	DNA ligase 1	LIG1	1	0.46	2.00	0.15	2.00	0.21
P11908	Ribose-phosphate pyrophosphokinase 2	PRPS2					2.00	0.80
Q96PE2	Rho guanine nucleotide exchange factor 17	ARHGEF17	1	0.15	1.00	0.29	2.00	0.35
Q9H0S4	Probable ATP-dependent RNA helicase DDX47	DDX47	1		3.00	0.46	2.00	0.31
Q12972	Nuclear inhibitor of protein phosphatase 1	PPP1R8			2.00	0.23	2.00	0.46
Q92556	Engulfment and cell motility protein 1	ELMO1					2.00	0.68

Q96DZ1	Endoplasmic reticulum lectin 1	ERLEC1					2.00	0.65
Q8TEX9	Importin-4	IPO4	2	0.11	3.00	0.31	2.00	0.20
Q5SRD1	Putative mitochondrial import inner membrane translocase subunit Tim23B	TIMM23B					2.00	0.63
A0FGR8	Extended synaptotagmin-2	ESYT2			2.00	0.27	2.00	0.35
Q9NQW6	Anillin	ANLN			1.00	0.13	2.00	0.48
Q13614	Myotubularin-related protein 2	MTMR2			1.00	0.36	2.00	0.24
A3KMH1	von Willebrand factor A domain-containing protein 8	VWA8			1.00	0.28	2.00	0.32
Q9P2R7	Succinate--CoA ligase [ADP-forming] subunit beta, mitochondrial	SUCLA2	1	0.19	1.00	0.19	2.00	0.21
O15127	Secretory carrier-associated membrane protein 2	SCAMP2			1.00	0.21	2.00	0.37
O15294	UDP-N-acetylglucosamine--peptide N-acetylglucosaminyltransferase 110 kDa subunit	OGT	1	0.24	1.00	0.14	2.00	0.16
Q86V48	Leucine zipper protein 1	LUZP1			1.00		2.00	0.51
Q9UDY2	Tight junction protein ZO-2	TJP2	1		2.00	0.20	2.00	0.28
O15118	Niemann-Pick C1 protein	NPC1					2.00	0.47
Q5GLZ8	Probable E3 ubiquitin-protein ligase HERC4	HERC4					2.00	0.46
Q07157	Tight junction protein ZO-1	TJP1			2.00	0.35	2.00	0.09
Q14678	KN motif and ankyrin repeat domain-containing protein 1	KANK1					2.00	0.44
Q9BUN8	Derlin-1	DERL1					2.00	0.40
Q8NEZ5	F-box only protein 22	FBXO22					2.00	0.35
Q8IZH2	5'-3' exoribonuclease 1	XRN1					2.00	0.34
Q8N6R0	Methyltransferase-like protein 13	METTL13					2.00	0.30
Q10570	Cleavage and polyadenylation specificity factor subunit 1	CPSF1					2.00	0.29
Q9UBN7	Histone deacetylase 6	HDAC6					2.00	0.23
Q96JH7	Deubiquitinating protein VCIP135	VCPIP1					2.00	0.16
A0A075B7B8	Protein IGHV3OR16-12 (Fragment)	IGHV3OR16-12	1	24.24	1.00	21.64	1.00	6.94
A0A075B6R9	Protein IGKV2D-24 (Fragment)	IGKV2D-24	2	17.18	1.00	17.11	1.00	13.71
Q13576	Ras GTPase-activating-like protein IQGAP2	IQGAP2					1.00	21.35
A0A0B4J2D9	Protein IGKV1D-13 (Fragment)	IGKV1D-13	1	8.95	1.00	6.86	1.00	2.96
Q86YR7	Probable guanine nucleotide exchange factor MCF2L2	MCF2L2					1.00	12.59
H7C144	Alpha-actinin-4 (Fragment)	ACTN4			1.00	5.67	1.00	6.72
P04211	Immunoglobulin lambda variable 7-43	IGLV7-43	1	5.37	1.00	3.68	1.00	1.95
P21926	CD9 antigen	CD9	2	2.36	2.00	4.51	1.00	2.86
Q16563	Synaptophysin-like protein 1	SYPL1	1	2.48	1.00	4.27	1.00	2.94
P01704	Immunoglobulin lambda variable 2-14	IGLV2-14	1	4.20	1.00	3.10	1.00	1.91
P01817	Immunoglobulin heavy variable 2-5	IGHV2-5	1	3.63	1.00	3.60	1.00	1.15
G8JLA2	Myosin light polypeptide 6	MYL6					1.00	6.67
P46776	60S ribosomal protein L27a	RPL27A	1	0.19	2.00	3.89	1.00	2.58
Q86Y46	Keratin, type II cytoskeletal 73	KRT73					1.00	6.42
P05556	Integrin beta-1	ITGB1	1	1.71	3.00	2.95	1.00	1.26
P01601	Immunoglobulin kappa variable 1D-16 (Fragment)	IGKV1D-16	1	3.04	1.00	1.94	1.00	0.94
P01891	HLA class I histocompatibility antigen, A-68 alpha chain	HLA-A	3	1.08	4.00	2.54	1.00	2.21
P46778	60S ribosomal protein L21	RPL21	1	0.94	1.00	2.76	1.00	1.99
Q9P2E9	Ribosome-binding protein 1	RRBP1	3	0.82	2.00	1.43	1.00	2.95
P04899	Guanine nucleotide-binding protein G(i) subunit alpha-2	GNAI2	1	1.79	2.00	1.78	1.00	1.43
Q96S97	Myeloid-associated differentiation marker	MYADM	1	1.05	1.00	2.56	1.00	1.31
Q8NFJ5	Retinoic acid-induced protein 3	GPRC5A	1	1.32	3.00	2.47	1.00	1.11
Q1KMD3	Heterogeneous nuclear ribonucleoprotein U-like protein 2	HNRNPUL2	1	2.17	2.00	0.95	1.00	1.47
A0A087WSZ0	Protein IGKV1D-8 (Fragment)	IGKV1D-8	1	2.10	1.00	1.48	1.00	0.78
P01764	Immunoglobulin heavy variable 3-23	IGHV3-23	1	1.89	1.00	1.79	1.00	0.66

P09496-2	Isoform Non-brain of Clathrin light chain A	CLTA	1	2.02			1.00	1.96
P09382	Galectin-1	LGALS1	1	1.20	2.00	1.41	1.00	1.34
Q6IWH7	Anoctamin-7	ANO7					1.00	3.74
P14174	Macrophage migration inhibitory factor	MIF			1.00	1.93	1.00	1.68
Q04941	Proteolipid protein 2	PLP2	1	1.03	1.00	1.88	1.00	0.66
Q03135	Caveolin-1	CAV1	1	2.02	2.00	1.40	1.00	0.11
Q8TDN6	Ribosome biogenesis protein BRX1 homolog	BRIX1	1	0.14			1.00	3.39
Q9NQC3-2	Isoform 2 of Reticulon-4	RTN4			1.00	2.15	1.00	1.08
Q9BUP3	Oxidoreductase HTATIP2	HTATIP2					1.00	3.20
Q9UBM7	7-dehydrocholesterol reductase	DHCR7	1	1.00	2.00	0.79	1.00	1.18
P10155	60 kDa SS-A/Ro ribonucleoprotein	TROVE2	4	0.69	4.00	1.23	1.00	1.01
Q9UHD9	Ubiquilin-2	UBQLN2					1.00	2.75
Q9NR19	Acetyl-coenzyme A synthetase, cytoplasmic	ACSS2			1.00	1.57	1.00	1.14
H7BZJ3	Protein disulfide-isomerase A3 (Fragment)	PDIA3			1.00	1.92	1.00	0.75
P37268	Squalene synthase	FDFT1	2	0.73	3.00	0.67	1.00	1.25
O00767	Acyl-CoA desaturase	SCD					1.00	2.63
A0A0B4J1V2	Immunoglobulin heavy variable 2-26	IGHV2-26	2	1.22	2.00	0.97	1.00	0.43
Q969X1	Protein lifeguard 3	TMBIM1	1	0.82	1.00	1.36	1.00	0.44
P62899	60S ribosomal protein L31	RPL31	1	0.28	2.00	1.96	1.00	0.28
Q96KR1	Zinc finger RNA-binding protein	ZFR	2	0.30	3.00	0.74	1.00	1.46
P15529	Membrane cofactor protein	CD46	1	0.41	1.00	1.38	1.00	0.67
P61026	Ras-related protein Rab-10	RAB10	1	0.84	2.00	0.76	1.00	0.85
Q9BT67	NEDD4 family-interacting protein 1	NDFIP1			1.00	1.89	1.00	0.55
O60759	Cytohesin-interacting protein	CYTIP					1.00	2.42
P29992	Guanine nucleotide-binding protein subunit alpha-11	GNA11	2	0.59	3.00	1.05	1.00	0.77
P15151	Poliovirus receptor	PVR	1	0.51	2.00	1.26	1.00	0.53
Q9NXE4	Sphingomyelin phosphodiesterase 4	SMPD4	1	0.77	1.00	0.98	1.00	0.47
Q99536	Synaptic vesicle membrane protein VAT-1 homolog	VAT1	1	0.91	5.00	0.99	1.00	0.30
O43653	Prostate stem cell antigen	PSCA			1.00	1.62	1.00	0.50
Q99595	Mitochondrial import inner membrane translocase subunit Tim17-A	TIMM17A	1	0.75	1.00	0.55	1.00	0.81
Q8NFW8	N-acylneuraminate cytidylyltransferase	CMAS			1.00	0.61	1.00	1.44
Q07955	Serine/arginine-rich splicing factor 1	SRSF1	2	0.59	1.00	0.96	1.00	0.49
Q8WYA6	Beta-catenin-like protein 1	CTNNBL1	1	0.55	2.00	0.65	1.00	0.84
P62753	40S ribosomal protein S6	RPS6			1.00	1.26	1.00	0.76
Q14181	DNA polymerase alpha subunit B	POLA2	1	0.40	1.00	0.86	1.00	0.73
Q9BPX3	Condensin complex subunit 3	NCAPG	2	0.73	3.00	0.95	1.00	0.29
P30825	High affinity cationic amino acid transporter 1	SLC7A1			2.00	1.30	1.00	0.66
Q8IWR0	Zinc finger CCCH domain-containing protein 7A	ZC3H7A					1.00	1.93
O75781	Paralemmin-1	PALM	2	0.62	3.00	1.01	1.00	0.29
Q92783	Signal transducing adapter molecule 1	STAM			1.00	1.10	1.00	0.82
P05362	Intercellular adhesion molecule 1	ICAM1	2	0.47	5.00	1.11	1.00	0.32
Q5JWF2	Guanine nucleotide-binding protein G(s) subunit alpha isoforms XLas	GNAS	2	0.46	5.00	0.90	1.00	0.52
P63027	Vesicle-associated membrane protein 2	VAMP2			1.00	1.09	1.00	0.76
P31942	Heterogeneous nuclear ribonucleoprotein H3	HNRNPH3	2	0.78	1.00	0.45	1.00	0.61
Q9GZT3	SRA stem-loop-interacting RNA-binding protein, mitochondrial	SLIRP	2	0.51	2.00	0.65	1.00	0.68
Q6P1M3	Lethal(2) giant larvae protein homolog 2	LLGL2	1	0.16	2.00	0.16	1.00	1.49
P23634	Plasma membrane calcium-transporting ATPase 4	ATP2B4	3	0.49	4.00	1.08	1.00	0.24
Q9UI26	Importin-11	IPO11	1	0.44	1.00	0.93	1.00	0.44

P62258	14-3-3 protein epsilon	YWHAE	2	0.40	2.00	1.09	1.00	0.30
P14649	Myosin light chain 6B	MYL6B	2	0.57	1.00	0.44	1.00	0.76
Q687X5	Metalloreductase STEAP4	STEAP4	2	0.42	2.00	0.64	1.00	0.70
Q9Y639	Neuroplastin	NPTN	1	0.27	3.00	1.10	1.00	0.38
Q16836	Hydroxyacyl-coenzyme A dehydrogenase, mitochondrial	HADH	1	0.55	1.00	0.52	1.00	0.68
Q9P287	BRCA2 and CDKN1A-interacting protein	BCCIP			2.00	0.75	1.00	0.97
P31946	14-3-3 protein beta/alpha	YWHAB	1	1.01	1.00	0.30	1.00	0.41
Q9Y3L5	Ras-related protein Rap-2c	RAP2C	3	0.48	2.00	0.72	1.00	0.51
Q6NUM9	All-trans-retinol 13,14-reductase	RETSAT	1	0.44	2.00	0.45	1.00	0.80
O95671	N-acetylserotonin O-methyltransferase-like protein	ASMTL			1.00	0.92	1.00	0.77
P11216	Glycogen phosphorylase, brain form	PYGB	2	0.39	2.00	0.69	1.00	0.61
P17252	Protein kinase C alpha type	PRKCA			3.00	0.66	1.00	0.99
Q8TEM1	Nuclear pore membrane glycoprotein 210	NUP210	1	0.51	4.00	0.98	1.00	0.16
Q96EK6	Glucosamine 6-phosphate N-acetyltransferase	GNPNAT1	1	0.44	1.00	0.60	1.00	0.61
Q9UH65	Switch-associated protein 70	SWAP70	1	0.62	2.00	0.47	1.00	0.55
Q92544	Transmembrane 9 superfamily member 4	TM9SF4					1.00	1.63
P48651	Phosphatidylserine synthase 1	PTDSS1			1.00	0.90	1.00	0.72
Q9Y450	HBS1-like protein	HBS1L	1	0.21	4.00	0.76	1.00	0.65
P52594	Arf-GAP domain and FG repeat-containing protein 1	AGFG1			2.00	0.42	1.00	1.19
P61289	Proteasome activator complex subunit 3	PSME3	1	0.65	1.00	0.49	1.00	0.45
O60888	Protein CutA	CUTA	2	0.64	1.00	0.60	1.00	0.33
P20674	Cytochrome c oxidase subunit 5A, mitochondrial	COX5A	1	0.49	2.00	0.75	1.00	0.32
Q15043	Zinc transporter ZIP14	SLC39A14	1	0.52	3.00	0.79	1.00	0.23
Q5JPE7	Nodal modulator 2	NOMO2	2	0.45	2.00	0.58	1.00	0.50
O75717	WD repeat and HMG-box DNA-binding protein 1	WDHD1	1	0.43	1.00	0.74	1.00	0.33
Q8NF37	Lysophosphatidylcholine acyltransferase 1	LPCAT1	1	0.27	1.00	0.73	1.00	0.50
P08240	Signal recognition particle receptor subunit alpha	SRPRA	1	0.26	2.00	0.50	1.00	0.73
P51571	Translocon-associated protein subunit delta	SSR4	1	0.92			1.00	0.55
O15260	Surfeit locus protein 4	SURF4	1	0.29	2.00	0.52	1.00	0.66
Q13123	Protein Red	IK	1	0.61	2.00	0.27	1.00	0.59
P13798	Acylamino-acid-releasing enzyme	APEH	1	0.45	1.00	0.39	1.00	0.62
P07954	Fumarate hydratase, mitochondrial	FH	2	0.73	4.00	0.63	1.00	0.09
P20700	Lamin-B1	LMNB1	5	0.75	5.00	0.52	1.00	0.16
P19256	Lymphocyte function-associated antigen 3	CD58			1.00	1.17	1.00	0.25
Q8WY22	BRI3-binding protein	BRI3BP					1.00	1.42
E9PLY5	Microtubule-actin cross-linking factor 1, isoforms 1/2/3/5 (Fragment)	MACF1					1.00	1.40
Q92890	Ubiquitin fusion degradation protein 1 homolog	UFD1L			1.00	0.68	1.00	0.72
Q9H2P9	Diphthine methyl ester synthase	DPH5	2	0.45	1.00	0.38	1.00	0.57
P19971	Thymidine phosphorylase	TYMP	1	0.23	1.00	0.74	1.00	0.42
Q02809	Procollagen-lysine,2-oxoglutarate 5-dioxygenase 1	PLOD1	2	0.52	1.00	0.71	1.00	0.15
Q08722	Leukocyte surface antigen CD47	CD47	1	0.74			1.00	0.63
Q9ULV4	Coronin-1C	CORO1C			1.00	0.93	1.00	0.44
Q13509	Tubulin beta-3 chain	TUBB3	2	0.60	3.00	0.77	1.00	
Q9H6S0	Probable ATP-dependent RNA helicase YTHDC2	YTHDC2	2	0.18	3.00	0.97	1.00	0.21
O43760	Synaptogyrin-2	SYNGR2					1.00	1.34
Q96C36	Pyrroline-5-carboxylate reductase 2	PYCR2	1	1.00			1.00	0.30
Q02978	Mitochondrial 2-oxoglutarate/malate carrier protein	SLC25A11	1	0.42	4.00	0.58	1.00	0.30
Q9ULC4	Malignant T-cell-amplified sequence 1	MCTS1	3	0.38	2.00	0.43	1.00	0.48
O95834	Echinoderm microtubule-associated protein-like 2	EML2	1	0.16	1.00	1.00	1.00	0.13

Q9H8Y5	Ankyrin repeat and zinc finger domain-containing protein 1	ANKZF1	1	0.35	3.00	0.47	1.00	0.47
Q14247	Src substrate cortactin	CTTN	1	0.48	5.00	0.55	1.00	0.23
P36404	ADP-ribosylation factor-like protein 2	ARL2	2	0.81	1.00	0.45	1.00	
Q9HB07	UPF0160 protein MYG1, mitochondrial	C12orf10					1.00	1.24
Q9Y4W2	Ribosomal biogenesis protein LAS1L	LAS1L	1	0.34	1.00	0.45	1.00	0.43
P55039	Developmentally-regulated GTP-binding protein 2	DRG2	2	0.55	1.00	0.56	1.00	0.10
Q9BTX1	Nucleoporin NDC1	NDC1	1	0.39	2.00	0.32	1.00	0.50
Q8NFH3	Nucleoporin Nup43	NUP43	1	0.42	1.00	0.44	1.00	0.34
Q5VYK3	Proteasome-associated protein ECM29 homolog	ECM29	1	0.19	3.00	0.54	1.00	0.46
Q8WWM7	Ataxin-2-like protein	ATXN2L	1	0.28	1.00	0.36	1.00	0.55
Q9BSH4	Translational activator of cytochrome c oxidase 1	TACO1	1	0.09			1.00	1.08
P00492	Hypoxanthine-guanine phosphoribosyltransferase	HPRT1	1	0.62			1.00	0.53
Q9BT78	COP9 signalosome complex subunit 4	COPS4	1	0.78			1.00	0.38
Q96PY5	Formin-like protein 2	FMNL2	1	0.10	2.00	0.81	1.00	0.24
P51553	Isocitrate dehydrogenase [NAD] subunit gamma, mitochondrial	IDH3G	1	0.11	1.00	0.68	1.00	0.36
O60216	Double-strand-break repair protein rad21 homolog	RAD21					1.00	1.14
O60547	GDP-mannose 4,6 dehydratase	GMDS	1	0.40	2.00	0.30	1.00	0.45
P08581	Hepatocyte growth factor receptor	MET	1	0.26	4.00	0.63	1.00	0.26
Q9Y6M7	Sodium bicarbonate cotransporter 3	SLC4A7			2.00	0.91	1.00	0.22
O95470	Sphingosine-1-phosphate lyase 1	SGPL1			1.00	0.60	1.00	0.52
Q8NI27	THO complex subunit 2	THOC2	1	0.32	2.00	0.38	1.00	0.40
P08582	Melanotransferrin	MELTF	1	0.25	4.00	0.72	1.00	0.13
O43688	Phospholipid phosphatase 2	PLPP2			2.00	0.80	1.00	0.29
Q8NCG7	Sn1-specific diacylglycerol lipase beta	DAGLB	2	0.27	5.00	0.50	1.00	0.29
P47755	F-actin-capping protein subunit alpha-2	CAPZA2	1	0.36			1.00	0.71
P61006	Ras-related protein Rab-8A	RAB8A			1.00	1.06	1.00	
Q96FC9	ATP-dependent DNA helicase DDX11	DDX11	1	0.27	1.00	0.63	1.00	0.16
Q06136	3-ketodihydrosphingosine reductase	KDSR					1.00	1.05
O43402	ER membrane protein complex subunit 8	EMC8	1	0.47			1.00	0.58
O75306	NADH dehydrogenase [ubiquinone] iron-sulfur protein 2, mitochondrial	NDUFS2			4.00	0.63	1.00	0.40
O14639-5	Isoform 5 of Actin-binding LIM protein 1	ABLIM1					1.00	1.02
P42025	Beta-centractin	ACTR1B			1.00	0.79	1.00	0.23
P21912	Succinate dehydrogenase [ubiquinone] iron-sulfur subunit, mitochondrial	SDHB	2	0.55			1.00	0.47
Q8NE86	Calcium uniporter protein, mitochondrial	MCU	1	0.51			1.00	0.50
Q96G46	tRNA-dihydrouridine(47) synthase [NAD(P)(+)]-like	DUS3L	1	0.63	1.00	0.23	1.00	0.15
P69905	Hemoglobin subunit alpha	HBA1					1.00	1.01
Q00765	Receptor expression-enhancing protein 5	REEP5	1	0.13	1.00	0.53	1.00	0.35
Q86X29	Lipolysis-stimulated lipoprotein receptor	LSR			1.00	0.68	1.00	0.31
Q9Y315	Deoxyribose-phosphate aldolase	DERA			1.00	0.37	1.00	0.62
Q8IZ69	tRNA (uracil-5-)-methyltransferase homolog A	TRMT2A			1.00	0.46	1.00	0.51
P33897	ATP-binding cassette sub-family D member 1	ABCD1	1	0.34			1.00	0.62
Q5VZK9	F-actin-uncapping protein LRRC16A	LRRC16A			1.00	0.45	1.00	0.50
Q8WU90	Zinc finger CCCH domain-containing protein 15	ZC3H15			1.00	0.61	1.00	0.33
P51665	26S proteasome non-ATPase regulatory subunit 7	PSMD7			2.00	0.50	1.00	0.43
O14763	Tumor necrosis factor receptor superfamily member 10B	TNFRSF10B			1.00	0.61	1.00	0.31
O15084	Serine/threonine-protein phosphatase 6 regulatory ankyrin repeat subunit A	ANKRD28	2	0.40	2.00	0.14	1.00	0.33
Q96S52	GPI transamidase component PIG-S	PIGS	1	0.26	1.00	0.23	1.00	0.35
Q15813	Tubulin-specific chaperone E	TBCE			2.00	0.41	1.00	0.43

Q9BTU6	Phosphatidylinositol 4-kinase type 2-alpha	PI4K2A			3.00	0.53	1.00	0.30
Q13618	Cullin-3	CUL3	1	0.25	3.00	0.33	1.00	0.24
Q9Y613	FH1/FH2 domain-containing protein 1	FHOD1					1.00	0.81
Q05655	Protein kinase C delta type	PRKCD					1.00	0.81
Q9HBL0	Tensin-1	TNS1	1	0.44			1.00	0.36
Q9NPQ8	Synembryn-A	RIC8A	1	0.51	2.00	0.30	1.00	
P52788	Spermine synthase	SMS	1	0.34	1.00	0.24	1.00	0.23
A1X283	SH3 and PX domain-containing protein 2B	SH3PXD2B			2.00	0.40	1.00	0.41
Q9UNM6	26S proteasome non-ATPase regulatory subunit 13	PSMD13					1.00	0.79
Q9HCE7	E3 ubiquitin-protein ligase SMURF1	SMURF1					1.00	0.79
Q9P265	Disco-interacting protein 2 homolog B	DIP2B	3	0.21	1.00	0.39	1.00	0.18
Q8NC42	E3 ubiquitin-protein ligase RNF149	RNF149			1.00	0.42	1.00	0.36
Q9NQR4	Omega-amidase NIT2	NIT2	1	0.33	1.00	0.26	1.00	0.18
P24043	Laminin subunit alpha-2	LAMA2					1.00	0.75
Q9BQI0	Allograft inflammatory factor 1-like	AIF1L	1	0.27	1.00		1.00	0.48
Q5TA45	Integrator complex subunit 11	CPSF3L	1	0.18	1.00	0.25	1.00	0.31
Q9C0H2	Protein tweety homolog 3	TTYH3			1.00	0.53	1.00	0.20
Q9P0J7	E3 ubiquitin-protein ligase KCMF1	KCMF1	1	0.20	1.00	0.35	1.00	0.18
Q6NVY1	3-hydroxyisobutyryl-CoA hydrolase, mitochondrial	HIBCH	1	0.38			1.00	0.34
P51151	Ras-related protein Rab-9A	RAB9A	1	0.46			1.00	0.25
P42224	Signal transducer and activator of transcription 1-alpha/beta	STAT1	1	0.36	3.00	0.35	1.00	
P11717	Cation-independent mannose-6-phosphate receptor	IGF2R	1	0.26	4.00	0.45	1.00	
P49589	Cysteine--tRNA ligase, cytoplasmic	CARS	1	0.13	2.00	0.41	1.00	0.17
P62424	60S ribosomal protein L7a	RPL7A	1		1.00	0.42	1.00	0.28
Q8TAA9	Vang-like protein 1	VANGL1			4.00	0.70	1.00	
P23975	Sodium-dependent noradrenaline transporter	SLC6A2					1.00	0.70
P35251	Replication factor C subunit 1	RFC1			1.00	0.35	1.00	0.34
P30460	HLA class I histocompatibility antigen, B-8 alpha chain	HLA-B					1.00	0.69
Q13283	Ras GTPase-activating protein-binding protein 1	G3BP1	1	0.22	3.00	0.30	1.00	0.15
Q8WVC0	RNA polymerase-associated protein LEO1	LEO1			1.00	0.09	1.00	0.57
P68402	Platelet-activating factor acetylhydrolase IB subunit beta	PAFAH1B2	1	0.20	1.00	0.27	1.00	0.19
Q8WUY1	Protein THEM6	THEM6					1.00	0.65
P32970	CD70 antigen	CD70			1.00	0.48	1.00	0.16
Q8N2G8	GH3 domain-containing protein	GHDC			1.00	0.18	1.00	0.44
Q9P0K7	Ankycorbin	RAI14	1	0.38			1.00	0.25
Q14764	Major vault protein	MVP	1	0.17	2.00	0.46	1.00	
P04920	Anion exchange protein 2	SLC4A2	1		1.00	0.45	1.00	0.16
Q5SRE5	Nucleoporin NUP188 homolog	NUP188	2	0.13	4.00	0.28	1.00	0.19
Q9UNF0	Protein kinase C and casein kinase substrate in neurons protein 2	PACSIN2	1	0.20	2.00	0.26	1.00	0.14
P53350	Serine/threonine-protein kinase PLK1	PLK1			1.00	0.29	1.00	0.31
O00750	Phosphatidylinositol 4-phosphate 3-kinase C2 domain-containing subunit beta	PIK3C2B			1.00	0.31	1.00	0.27
P06213	Insulin receptor	INSR			3.00	0.44	1.00	0.15
P52732	Kinesin-like protein KIF11	KIF11			2.00	0.31	1.00	0.25
P98196	Probable phospholipid-transporting ATPase IH	ATP11A					1.00	0.56
P38606	V-type proton ATPase catalytic subunit A	ATP6V1A	1	0.16	2.00	0.23	1.00	0.16
Q15477	Helicase SKI2W	SKIV2L			1.00	0.30	1.00	0.24
Q9UP95	Solute carrier family 12 member 4	SLC12A4	1	0.10	2.00	0.31	1.00	0.12
Q3MIP1	Inositol 1,4,5-trisphosphate receptor-interacting protein-like 2	ITPRIPL2	1		1.00	0.09	1.00	0.44

Q9Y3T9	Nucleolar complex protein 2 homolog	NOC2L			1.00	0.31	1.00	0.22
Q13610	Periodic tryptophan protein 1 homolog	PWP1					1.00	0.53
Q13131	5'-AMP-activated protein kinase catalytic subunit alpha-1	PRKAA1					1.00	0.52
Q7RTV0	PHD finger-like domain-containing protein 5A	PHF5A					1.00	0.52
Q8IU81	Interferon regulatory factor 2-binding protein 1	IRF2BP1					1.00	0.52
O15397	Importin-8	IPO8			2.00	0.30	1.00	0.22
Q99447	Ethanolamine-phosphate cytidylyltransferase	PCYT2					1.00	0.51
Q9Y5Q8	General transcription factor 3C polypeptide 5	GTF3C5					1.00	0.51
P11441	Ubiquitin-like protein 4A	UBL4A					1.00	0.50
Q96ST3	Paired amphipathic helix protein Sin3a	SIN3A			2.00	0.24	1.00	0.26
P10620	Microsomal glutathione S-transferase 1	MGST1	1	0.24			1.00	0.26
Q15063	Periostin	POSTN					1.00	0.49
Q8N122	Regulatory-associated protein of mTOR	RPTOR			1.00	0.25	1.00	0.24
Q9UM54-6	Isoform 6 of Unconventional myosin-VI	MYO6					1.00	0.47
O94972	E3 ubiquitin-protein ligase TRIM37	TRIM37					1.00	0.46
Q09161	Nuclear cap-binding protein subunit 1	NCBP1			1.00	0.20	1.00	0.26
Q8TCJ2	Dolichyl-diphosphooligosaccharide--protein glycosyltransferase subunit STT3B	STT3B	1	0.09	1.00	0.16	1.00	0.21
O60427	Fatty acid desaturase 1	FADS1					1.00	0.46
Q9H0A0	RNA cytidine acetyltransferase	NAT10			1.00	0.28	1.00	0.17
Q13564	NEDD8-activating enzyme E1 regulatory subunit	NAE1			1.00	0.27	1.00	0.17
Q9HCK5	Protein argonaute-4	AGO4					1.00	0.43
Q86X55	Histone-arginine methyltransferase CARM1	CARM1	1	0.18	1.00	0.17	1.00	0.08
O15258	Protein RER1	RER1	1	0.09	1.00	0.18	1.00	0.16
Q15773	Myeloid leukemia factor 2	MLF2					1.00	0.42
O14981	TATA-binding protein-associated factor 172	BTAF1			1.00	0.37	1.00	0.05
P50336	Protoporphyrinogen oxidase	PPOX			1.00	0.22	1.00	0.20
P20585	DNA mismatch repair protein Msh3	MSH3	1	0.22			1.00	0.19
Q14573	Inositol 1,4,5-trisphosphate receptor type 3	ITPR3	1	0.26			1.00	0.15
Q8TEP8	Centrosomal protein of 192 kDa	CEP192					1.00	0.40
Q14147	Probable ATP-dependent RNA helicase DHX34	DHX34			1.00	0.18	1.00	0.22
O15344	E3 ubiquitin-protein ligase Midline-1	MID1			1.00	0.18	1.00	0.22
Q7Z3C6	Autophagy-related protein 9A	ATG9A			2.00	0.25	1.00	0.15
Q9UNL2	Translocon-associated protein subunit gamma	SSR3					1.00	0.40
Q12899	Tripartite motif-containing protein 26	TRIM26					1.00	0.38
Q9NWT1	p21-activated protein kinase-interacting protein 1	PAK1IP1					1.00	0.38
Q6IA86	Elongator complex protein 2	ELP2			1.00	0.38	1.00	
P11117	Lysosomal acid phosphatase	ACP2			1.00	0.23	1.00	0.14
Q8WUD6	Cholinephosphotransferase 1	CHPT1					1.00	0.37
Q8NEY8	Periphilin-1	PPHLN1			1.00	0.12	1.00	0.25
Q92636	Protein FAN	NSMAF					1.00	0.37
Q9NQX4	Unconventional myosin-Vc	MYO5C	1	0.12			1.00	0.25
O15091	Mitochondrial ribonuclease P protein 3	KIAA0391			1.00	0.16	1.00	0.20
Q9Y6D9	Mitotic spindle assembly checkpoint protein MAD1	MAD1L1					1.00	0.36
Q8NC60	Nitric oxide-associated protein 1	NOA1					1.00	0.36
Q8TAQ2	SWI/SNF complex subunit SMARCC2	SMARCC2					1.00	0.36
Q9NVN8	Guanine nucleotide-binding protein-like 3-like protein	GNL3L			2.00	0.25	1.00	0.10
Q4G176	Acyl-CoA synthetase family member 3, mitochondrial	ACSF3					1.00	0.35
Q53G44	Interferon-induced protein 44-like	IFI44L					1.00	0.34
P30626	Sorcin	SRI					1.00	0.34

P49137	MAP kinase-activated protein kinase 2	MAPKAPK2			1.00	0.21	1.00	0.13
Q15291	Retinoblastoma-binding protein 5	RBBP5			1.00	0.20	1.00	0.13
P02671	Fibrinogen alpha chain	FGA					1.00	0.33
Q9Y6K5	2'-5'-oligoadenylate synthase 3	OAS3					1.00	0.33
P46019	Phosphorylase b kinase regulatory subunit alpha, liver isoform	PHKA2					1.00	0.33
Q8N8S7	Protein enabled homolog	ENAH			1.00	0.19	1.00	0.13
O43292	Glycosylphosphatidylinositol anchor attachment 1 protein	GPAA1					1.00	0.32
O43592	Exportin-T	XPOT					1.00	0.31
Q8NCW5	NAD(P)H-hydrate epimerase	NAXE					1.00	0.31
A6NNE9	E3 ubiquitin-protein ligase MARCH11	MARCH11					1.00	0.31
P33981	Dual specificity protein kinase TTK	TTK					1.00	0.31
Q8NBJ9	SID1 transmembrane family member 2	SIDT2					1.00	0.31
Q96FX7	tRNA (adenine(58)-N(1))-methyltransferase catalytic subunit TRMT61A	TRMT61A	1	0.17			1.00	0.14
Q9Y2R5	28S ribosomal protein S17, mitochondrial	MRPS17	1				1.00	0.29
O15357	Phosphatidylinositol 3,4,5-trisphosphate 5-phosphatase 2	INPPL1			1.00	0.16	1.00	0.13
Q96HB5	Coiled-coil domain-containing protein 120	CCDC120					1.00	0.29
Q9BTE6	Alanyl-tRNA editing protein Aarsd1	AARSD1					1.00	0.29
Q13286	Battenin	CLN3					1.00	0.28
Q9BTE3	Mini-chromosome maintenance complex-binding protein	MCMBP					1.00	0.28
P61296	Heart- and neural crest derivatives-expressed protein 2	HAND2					1.00	0.28
P48556	26S proteasome non-ATPase regulatory subunit 8	PSMD8	2	0.28			1.00	
Q8IY17	Neuropathy target esterase	PNPLA6			1.00		1.00	0.27
Q7Z5K2	Wings apart-like protein homolog	WAPL					1.00	0.27
Q9H1A4	Anaphase-promoting complex subunit 1	ANAPC1			1.00	0.12	1.00	0.15
Q5SWA1	Protein phosphatase 1 regulatory subunit 15B	PPP1R15B					1.00	0.26
O95996	Adenomatous polyposis coli protein 2	APC2					1.00	0.26
Q86WB0	Nuclear-interacting partner of ALK	ZC3HC1					1.00	0.25
Q13724	Mannosyl-oligosaccharide glucosidase	MOGS					1.00	0.25
Q9BUQ8	Probable ATP-dependent RNA helicase DDX23	DDX23			1.00	0.16	1.00	0.08
Q8NBU5	ATPase family AAA domain-containing protein 1	ATAD1					1.00	0.23
Q6Q0C0	E3 ubiquitin-protein ligase TRAF7	TRAF7					1.00	0.23
O76013	Keratin, type I cuticular Ha6	KRT36					1.00	0.23
Q9BVQ7	Spermatogenesis-associated protein 5-like protein 1	SPATA5L1					1.00	0.23
Q15334	Lethal(2) giant larvae protein homolog 1	LLGL1					1.00	0.23
Q9UPQ9	Trinucleotide repeat-containing gene 6B protein	TNRC6B					1.00	0.23
Q96I99	Succinate--CoA ligase [GDP-forming] subunit beta, mitochondrial	SUCLG2					1.00	0.23
Q9UBQ0	Vacuolar protein sorting-associated protein 29	VPS29					1.00	0.22
P11234	Ras-related protein Ral-B	RALB					1.00	0.22
Q13671	Ras and Rab interactor 1	RIN1			1.00		1.00	0.22
Q9UNY4	Transcription termination factor 2	TTF2	2	0.08			1.00	0.13
Q9ULH0	Kinase D-interacting substrate of 220 kDa	KIDINS220			1.00	0.08	1.00	0.13
O75934	Pre-mRNA-splicing factor SPF27	BCAS2	1	0.15	1.00		1.00	0.06
Q5T9L3	Protein wntless homolog	WLS					1.00	0.21
Q13438	Protein OS-9	OS9					1.00	0.21
Q6P3X3	Tetratricopeptide repeat protein 27	TTC27					1.00	0.20
P17480	Nucleolar transcription factor 1	UBTF			1.00		1.00	0.20
Q92665	28S ribosomal protein S31, mitochondrial	MRPS31					1.00	0.20
P20930	Filaggrin	FLG					1.00	0.20

P54852	Epithelial membrane protein 3	EMP3					1.00	0.20
Q96T51	RUN and FYVE domain-containing protein 1	RUFY1					1.00	0.19
Q5VT66	Mitochondrial amidoxime-reducing component 1	MARC1					1.00	0.19
Q12986	Transcriptional repressor NF-X1	NFX1	1		1.00	0.09	1.00	0.09
Q9BSV6	tRNA-splicing endonuclease subunit Sen34	TSEN34			1.00		1.00	0.18
O15372	Eukaryotic translation initiation factor 3 subunit H	EIF3H					1.00	0.18
Q9Y2F9	BTB/POZ domain-containing protein 3	BTBD3					1.00	0.18
O14976	Cyclin-G-associated kinase	GAK					1.00	0.17
Q9NSI2	Protein FAM207A	FAM207A					1.00	0.17
O75608	Acyl-protein thioesterase 1	LYPLA1					1.00	0.17
P61073	C-X-C chemokine receptor type 4	CXCR4			1.00	0.10	1.00	0.06
P61313	60S ribosomal protein L15	RPL15	1	0.04	1.00	0.09	1.00	0.03
P53990	IST1 homolog	IST1			1.00		1.00	0.15
Q9BRX2	Protein pelota homolog	PELO					1.00	0.15
Q05397	Focal adhesion kinase 1	PTK2					1.00	0.14
Q9H0J9	Poly [ADP-ribose] polymerase 12	PARP12					1.00	0.14
Q7RTP6	Protein-methionine sulfoxide oxidase MICAL3	MICAL3					1.00	0.14
Q9NTJ3	Structural maintenance of chromosomes protein 4	SMC4					1.00	0.14
Q9P253	Vacuolar protein sorting-associated protein 18 homolog	VPS18					1.00	0.13
Q99653	Calcineurin B homologous protein 1	CHP1	1	0.13			1.00	
Q6SPF0	Atherin	SAMD1			1.00		1.00	0.12
Q86X76	Nitrilase homolog 1	NIT1					1.00	0.12
P28370	Probable global transcription activator SNF2L1	SMARCA1					1.00	0.12
O95905	Protein ecdysoneless homolog	ECD					1.00	0.11
P12955	Xaa-Pro dipeptidase	PEPD					1.00	0.09
Q5T5X7	BEN domain-containing protein 3	BEND3					1.00	0.09
Q96GD0	Pyridoxal phosphate phosphatase	PDXP					1.00	0.08
Q9H0M0	NEDD4-like E3 ubiquitin-protein ligase WWP1	WWP1					1.00	0.07
Q13188	Serine/threonine-protein kinase 3	STK3			1.00		1.00	0.06
Q8TC07	TBC1 domain family member 15	TBC1D15					1.00	0.06
P10319	HLA class I histocompatibility antigen, B-58 alpha chain	HLA-B					1.00	0.01
Q3SY69	Mitochondrial 10-formyltetrahydrofolate dehydrogenase	ALDH1L2					1.00	
Q96P48	Arf-GAP with Rho-GAP domain, ANK repeat and PH domain-containing protein 1	ARAP1					1.00	
P21281	V-type proton ATPase subunit B, brain isoform	ATP6V1B2					1.00	
P02452	Collagen alpha-1(I) chain	COL1A1			1.00		1.00	
Q9UQB3	Catenin delta-2	CTNND2					1.00	
Q14999	Cullin-7	CUL7					1.00	
Q5UCC4	ER membrane protein complex subunit 10	EMC10					1.00	
Q99999	Galactosylceramide sulfotransferase	GAL3ST1					1.00	
Q01415	N-acetylgalactosamine kinase	GALK2					1.00	
Q2TB90	Putative hexokinase HKDC1	HKDC1					1.00	
Q5JSJ4	Integrator complex subunit 6-like	INTS6L					1.00	
Q9Y6N6	Laminin subunit gamma-3	LAMC3					1.00	
Q7L5Y9	Macrophage erythroblast attacher	MAEA					1.00	
Q14165	Malectin	MLEC	1				1.00	
Q6ZNB6	NF-X1-type zinc finger protein NFXL1	NFXL1					1.00	
Q93100	Phosphorylase b kinase regulatory subunit beta	PHKB					1.00	
Q7Z3K3	Pogo transposable element with ZNF domain	POGZ					1.00	
Q9BY42	Protein RTF2 homolog	RTFDC1					1.00	

Q92966	snRNA-activating protein complex subunit 3	SNAPC3				1.00
Q08170	Serine/arginine-rich splicing factor 4	SRSF4				1.00
Q5VSL9	Striatin-interacting protein 1	STRIP1				1.00
Q96IR7	4-hydroxyphenylpyruvate dioxygenase-like protein	HPDL			1.00	432.34
A0A075B6S6	Immunoglobulin kappa variable 2D-30	IGKV2D-30	2	89.40		
A0M8Q6	Ig lambda-7 chain C region	IGLC7	1	4.02	2.00	72.96
P01597	Immunoglobulin kappa variable 1-39	IGKV1-39	1	8.62	2.00	30.54
O95425-4	Isoform SV4 of Supervillin	SVIL	1	15.80	1.00	20.62
Q8NBR6	Ubiquitin carboxyl-terminal hydrolase MINDY-2	FAM63B	1	26.55		
A0A0B4J1V1	Immunoglobulin heavy variable 3-21	IGHV3-21			2.00	17.49
Q96JN8	Neuralized-like protein 4	NEURL4			1.00	14.85
Q8WWI1-3	Isoform 3 of LIM domain only protein 7	LMO7	4	5.46	3.00	6.25
A0A075B7D0	Protein IGHV1OR15-1 (Fragment)	IGHV1OR15-1			1.00	9.96
Q8IZ13	Protein ZBED8	ZBED8	1	9.96		
A0A0C4DH35	Protein IGHV3-35 (Fragment)	IGHV3-35			1.00	9.60
P08123	Collagen alpha-2(I) chain	COL1A2			1.00	9.11
A0A075B6H7	Protein IGKV3-7 (Fragment)	IGKV3-7			1.00	8.67
P04430	Immunoglobulin kappa variable 1-16	IGKV1-16	2	4.32	2.00	2.99
P08865	40S ribosomal protein SA	RPSA	3	1.58	6.00	5.47
O15085	Rho guanine nucleotide exchange factor 11	ARHGEF11			1.00	6.93
P62879	Guanine nucleotide-binding protein G(I)/G(S)/G(T) subunit beta-2	GNB2	4	2.41	4.00	2.58
Q86UX2	Inter-alpha-trypsin inhibitor heavy chain H5	ITIH5	2	4.84		
Q15286	Ras-related protein Rab-35	RAB35	2	1.97	3.00	2.87
Q8NF86	Serine protease 33	PRSS33			1.00	4.79
Q53H12	Acylglycerol kinase, mitochondrial	AGK	1	2.28	2.00	2.35
Q01469	Fatty acid-binding protein, epidermal	FABP5	5	3.21	1.00	1.27
P15814	Immunoglobulin lambda-like polypeptide 1	IGLL1	1	2.46	1.00	1.85
A0A0B4J1Y8	Protein IGLV9-49	IGLV9-49	1	2.40	1.00	1.62
Q5JST6	EF-hand domain-containing family member C2	EFHC2			1.00	3.77
Q7Z7M9	Polypeptide N-acetylgalactosaminyltransferase 5	GALNT5			1.00	3.76
A6NIK2	Leucine-rich repeat-containing protein 10B	LRRC10B	1	2.48	1.00	1.10
P62820	Ras-related protein Rab-1A	RAB1A	2	0.95	1.00	2.56
P61224	Ras-related protein Rap-1b	RAP1B	1	1.16	2.00	2.18
Q9Y226	Solute carrier family 22 member 13	SLC22A13			1.00	3.23
Q58FF6	Putative heat shock protein HSP 90-beta 4	HSP90AB4P	1	1.50	1.00	1.63
Q9Y566	SH3 and multiple ankyrin repeat domains protein 1	SHANK1	1	3.13		
P48668	Keratin, type II cytoskeletal 6C	KRT6C	1	3.03		
A0A0C4DH69	Protein IGKV1-9 (Fragment)	IGKV1-9	1	3.00		
O00217	NADH dehydrogenase [ubiquinone] iron-sulfur protein 8, mitochondrial	NDUFS8	1	2.15	2.00	0.84
P18825	Alpha-2C adrenergic receptor	ADRA2C			1.00	2.96
P49454	Centromere protein F	CENPF	1	2.78		
A0A075B7E8	Protein IGHV3OR16-13 (Fragment)	IGHV3OR16-13	1	1.41	1.00	1.33
Q99613	Eukaryotic translation initiation factor 3 subunit C	EIF3C	9	1.29	10.00	1.42
P11279	Lysosome-associated membrane glycoprotein 1	LAMP1	3	1.03	3.00	1.67
Q2Q1W2	E3 ubiquitin-protein ligase TRIM71	TRIM71			1.00	2.64
Q99497	Protein deglycase DJ-1	PARK7	2	1.54	2.00	1.07
Q9NUU7	ATP-dependent RNA helicase DDX19A	DDX19A			4.00	2.60
A0A0B4J1V0	Immunoglobulin heavy variable 3-15	IGHV3-15	1	2.60		

A0A0B4J2H0	Protein IGHV1-69-2 (Fragment)	IGHV1-69-2			1.00	2.60
P0CJ78	Zinc finger protein 865	ZNF865			1.00	2.58
Q86YR6	POTE ankyrin domain family member D	POTED			1.00	2.56
E9PAV3	Nascent polypeptide-associated complex subunit alpha, muscle-specific form	NACA	1	0.96	1.00	1.57
Q8TDB8	Solute carrier family 2, facilitated glucose transporter member 14	SLC2A14	1	0.42	2.00	2.08
A0A0C4DH29	Protein IGHV1-3 (Fragment)	IGHV1-3	1	2.48		
P63096	Guanine nucleotide-binding protein G(i) subunit alpha-1	GNAI1	1	1.26	2.00	1.21
P09496	Clathrin light chain A	CLTA	2	1.31	1.00	1.15
A0A075B6Q5	Immunoglobulin heavy variable 3-64	IGHV3-64	1	1.30	1.00	1.09
P53384	Cytosolic Fe-S cluster assembly factor NUBP1	NUBP1	1	1.14	1.00	1.18
P01762	Immunoglobulin heavy variable 3-11	IGHV3-11	1	2.30		
Q9H3K2	Growth hormone-inducible transmembrane protein	GHITM	1	1.91	3.00	0.34
P04908	Histone H2A type 1-B/E	HIST1H2AB			3.00	2.17
Q9Y4R8	Telomere length regulation protein TEL2 homolog	TELO2	1	1.61	2.00	0.55
Q14318	Peptidyl-prolyl cis-trans isomerase FKBP8	FKBP8	1	0.83	1.00	1.31
P78310	Coxsackievirus and adenovirus receptor	CXADR	5	0.72	6.00	1.41
Q8IZF6	Adhesion G-protein coupled receptor G4	ADGRG4	1	2.10		
K7EKE6	Lon protease homolog, mitochondrial	LONP1	1	0.85	1.00	1.24
Q5TD94	Radial spoke head protein 4 homolog A	RSPH4A	1	2.08		
Q06945	Transcription factor SOX-4	SOX4			1.00	1.97
Q6ZUX3	Crescerin-2	FAM179A	1	1.94		
Q9P0J0	NADH dehydrogenase [ubiquinone] 1 alpha subcomplex subunit 13	NDUFA13	1	0.66	1.00	1.20
Q8NCB2	CaM kinase-like vesicle-associated protein	CAMKV			1.00	1.81
Q96GE9	Transmembrane protein 261	TMEM261	1	1.71		
O15126	Secretory carrier-associated membrane protein 1	SCAMP1	1	0.91	1.00	0.80
P12111	Collagen alpha-3(VI) chain	COL6A3	1	1.70		
P00505	Aspartate aminotransferase, mitochondrial	GOT2	2	0.75	1.00	0.94
P18084	Integrin beta-5	ITGB5	2	0.31	5.00	1.34
Q9UDV7	Zinc finger protein 282	ZNF282			1.00	1.62
Q8NDY3	[Protein ADP-ribosylarginine] hydrolase-like protein 1	ADPRHL1			1.00	1.61
O14925	Mitochondrial import inner membrane translocase subunit Tim23	TIMM23	2	0.57	2.00	1.03
Q15125	3-beta-hydroxysteroid-Delta(8),Delta(7)-isomerase	EBP	1	0.77	1.00	0.82
O94925	Glutaminase kidney isoform, mitochondrial	GLS	1	0.72	3.00	0.88
P56975	Pro-neuregulin-3, membrane-bound isoform	NRG3			1.00	1.57
P30508	HLA class I histocompatibility antigen, Cw-12 alpha chain	HLA-C	3	0.45	3.00	1.11
Q9BVC6	Transmembrane protein 109	TMEM109	1	1.54		
A0A0U1RRN1	UDP-galactose translocator	SLC35A2			1.00	1.49
P17813	Endoglin	ENG			1.00	1.48
P49903	Selenide, water dikinase 1	SEPHS1	1	0.54	2.00	0.92
O75351	Vacuolar protein sorting-associated protein 4B	VPS4B	2	0.64	4.00	0.82
Q9HCC9	Lateral signaling target protein 2 homolog	ZFYVE28			1.00	1.44
Q5T2W1	Na(+)/H(+) exchange regulatory cofactor NHE-RF3	PDZK1			1.00	1.44
Q96PU5	E3 ubiquitin-protein ligase NEDD4-like	NEDD4L			6.00	1.42
P54577	Tyrosine--tRNA ligase, cytoplasmic	YARS	1	0.45	2.00	0.96
P50895	Basal cell adhesion molecule	BCAM	2	0.36	5.00	1.03
P27348	14-3-3 protein theta	YWHAQ	1	1.05	1.00	0.30
P43487	Ran-specific GTPase-activating protein	RANBP1	2	1.32		
Q9NZL9	Methionine adenosyltransferase 2 subunit beta	MAT2B	2	0.66	2.00	0.65

P53582	Methionine aminopeptidase 1	METAP1	1	0.54	1.00	0.78
A6NDZ8	Putative methyl-CpG-binding domain protein 3-like 4	MBD3L4	1	1.30		
A0A0A0MS14	Immunoglobulin heavy variable 1-45	IGHV1-45	1	0.68	1.00	0.61
O75147	Obscurin-like protein 1	OBSL1	1		3.00	1.28
P23468	Receptor-type tyrosine-protein phosphatase delta	PTPRD			2.00	1.27
Q9Y266	Nuclear migration protein nudC	NUDC	1	0.44	1.00	0.80
O96000	NADH dehydrogenase [ubiquinone] 1 beta subcomplex subunit 10	NDUFB10	2	0.57	2.00	0.67
P49748	Very long-chain specific acyl-CoA dehydrogenase, mitochondrial	ACADVL			3.00	1.23
P35237	Serpin B6	SERPINB6	1	0.76	3.00	0.46
Q8WUM9	Sodium-dependent phosphate transporter 1	SLC20A1	1	0.37	1.00	0.84
P38159	RNA-binding motif protein, X chromosome	RBMX	2	0.59	4.00	0.61
P51398	28S ribosomal protein S29, mitochondrial	DAP3	1	0.49	2.00	0.70
O60664	Perilipin-3	PLIN3	1	0.40	2.00	0.77
Q9Y295	Developmentally-regulated GTP-binding protein 1	DRG1	2	0.53	5.00	0.63
P60033	CD81 antigen	CD81			1.00	1.16
P62745	Rho-related GTP-binding protein RhoB	RHOB			2.00	1.15
Q8WWL2	Protein spire homolog 2	SPIRE2			1.00	1.13
P40763	Signal transducer and activator of transcription 3	STAT3	1	0.40	1.00	0.72
Q9P289	Serine/threonine-protein kinase 26	STK26	3	0.38	3.00	0.74
O60443	Non-syndromic hearing impairment protein 5	DFNA5			2.00	1.12
Q6ZW76	Ankyrin repeat and SAM domain-containing protein 3	ANKS3	1	1.11		
Q9H845	Acyl-CoA dehydrogenase family member 9, mitochondrial	ACAD9	1	0.35	2.00	0.75
P30044	Peroxiredoxin-5, mitochondrial	PRDX5	1	0.61	1.00	0.49
P07910-2	Isoform C1 of Heterogeneous nuclear ribonucleoproteins C1/C2	HNRNPC			1.00	1.10
Q6ZU35	Uncharacterized protein KIAA1211	KIAA1211	1	0.54	2.00	0.55
Q9BSJ2	Gamma-tubulin complex component 2	TUBGCP2	1	0.55	1.00	0.54
P49821	NADH dehydrogenase [ubiquinone] flavoprotein 1, mitochondrial	NDUFV1	1	0.51	5.00	0.58
O43169	Cytochrome b5 type B	CYB5B	1	1.09		
P48067	Sodium- and chloride-dependent glycine transporter 1	SLC6A9			2.00	1.08
Q9BY32	Inosine triphosphate pyrophosphatase	ITPA			1.00	1.08
Q71U36	Tubulin alpha-1A chain	TUBA1A			1.00	1.07
Q04725	Transducin-like enhancer protein 2	TLE2			2.00	1.05
O75832	26S proteasome non-ATPase regulatory subunit 10	PSMD10	1	1.05		
Q8IWS0	PHD finger protein 6	PHF6	1		1.00	1.04
P23284	Peptidyl-prolyl cis-trans isomerase B	PPIB	1	0.54	2.00	0.49
O75533	Splicing factor 3B subunit 1	SF3B1	3	0.33	7.00	0.70
P84550	SKI family transcriptional corepressor 1	SKOR1			1.00	1.02
P02788	Lactotransferrin	LTF	1	0.99		
O95278	Laforin	EPM2A			1.00	0.98
Q9Y4F1	FERM, RhoGEF and pleckstrin domain-containing protein 1	FARP1	1	0.16	5.00	0.81
Q15643	Thyroid receptor-interacting protein 11	TRIP11	1	0.97		
P15328	Folate receptor alpha	FOLR1	2	0.44	3.00	0.52
O43681	ATPase ASNA1	ASNA1	1	0.36	1.00	0.60
O94855	Protein transport protein Sec24D	SEC24D	1	0.85	1.00	0.11
Q9Y5M8	Signal recognition particle receptor subunit beta	SRPRB			2.00	0.96
Q9Y3E5	Peptidyl-tRNA hydrolase 2, mitochondrial	PTRH2	1	0.28	1.00	0.67
P28838	Cytosol aminopeptidase	LAP3	1	0.36	1.00	0.59
Q92747	Actin-related protein 2/3 complex subunit 1A	ARPC1A	4	0.43	4.00	0.51

Q12846	Syntaxin-4	STX4	1	0.36	1.00	0.58
P19404	NADH dehydrogenase [ubiquinone] flavoprotein 2, mitochondrial	NDUFV2	1	0.30	1.00	0.64
Q8N142	Adenylosuccinate synthetase isozyme 1	ADSSL1	1	0.93		
P49642	DNA primase small subunit	PRIM1	1	0.45	2.00	0.47
Q01844	RNA-binding protein EWS	EWSR1	2	0.21	2.00	0.71
Q15008	26S proteasome non-ATPase regulatory subunit 6	PSMD6	1	0.39	1.00	0.52
P25787	Proteasome subunit alpha type-2	PSMA2	1	0.91		
O43663	Protein regulator of cytokinesis 1	PRC1	1	0.90		
Q6XQN6	Nicotinate phosphoribosyltransferase	NAPRT	1	0.43	1.00	0.46
Q5RI15	Cytochrome c oxidase protein 20 homolog	COX20			1.00	0.89
Q8NEM2	SHC SH2 domain-binding protein 1	SHCBP1	1	0.36	1.00	0.53
Q8IZ81	ELMO domain-containing protein 2	ELMOD2			1.00	0.89
Q86VM9	Zinc finger CCCH domain-containing protein 18	ZC3H18	2	0.35	3.00	0.53
Q9Y3D9	28S ribosomal protein S23, mitochondrial	MRPS23	2	0.43	1.00	0.44
Q13217	DnaJ homolog subfamily C member 3	DNAJC3	3	0.26	3.00	0.61
Q6PD62	RNA polymerase-associated protein CTR9 homolog	CTR9			1.00	0.87
P0DME0	Protein SETSIP	SETSIP			2.00	0.86
O75947	ATP synthase subunit d, mitochondrial	ATP5H			1.00	0.86
Q06265	Exosome complex component RRP45	EXOSC9	1	0.24	1.00	0.62
Q9P0K9	DOMON domain-containing protein FRRS1L	FRRS1L			1.00	0.85
Q9Y5Z0	Beta-secretase 2	BACE2			1.00	0.84
Q53EL6	Programmed cell death protein 4	PDCD4			1.00	0.84
O00308	NEDD4-like E3 ubiquitin-protein ligase WWP2	WWP2			1.00	0.83
P98194	Calcium-transporting ATPase type 2C member 1	ATP2C1			1.00	0.83
O75390	Citrate synthase, mitochondrial	CS	1	0.83		
O43491	Band 4.1-like protein 2	EPB41L2	1	0.38	3.00	0.44
Q6NZY4	Zinc finger CCHC domain-containing protein 8	ZCCHC8			1.00	0.82
Q05519	Serine/arginine-rich splicing factor 11	SRSF11			1.00	0.81
P61019	Ras-related protein Rab-2A	RAB2A			2.00	0.80
Q16222	UDP-N-acetylhexosamine pyrophosphorylase	UAP1			1.00	0.80
O75449	Katanin p60 ATPase-containing subunit A1	KATNA1			1.00	0.79
P09429	High mobility group protein B1	HMGB1	1	0.45	1.00	0.33
P40925	Malate dehydrogenase, cytoplasmic	MDH1	2	0.29	2.00	0.50
P42167	Lamina-associated polypeptide 2, isoforms beta/gamma	TMPO			3.00	0.79
Q6S8J3	POTE ankyrin domain family member E	POTEE	1	0.78		
P61769	Beta-2-microglobulin	B2M	1	0.78		
Q9P2I0	Cleavage and polyadenylation specificity factor subunit 2	CPSF2			1.00	0.78
P55854	Small ubiquitin-related modifier 3	SUMO3			1.00	0.77
P50395	Rab GDP dissociation inhibitor beta	GDI2			3.00	0.77
Q99798	Aconitate hydratase, mitochondrial	ACO2	1	0.32	1.00	0.45
Q9H6B4	CXADR-like membrane protein	CLMP			2.00	0.76
P50148	Guanine nucleotide-binding protein G(q) subunit alpha	GNAQ			2.00	0.75
A4FU49	SH3 domain-containing protein 21	SH3D21			1.00	0.75
Q8TCT8	Signal peptide peptidase-like 2A	SPPL2A			2.00	0.75
Q9UHG3	Prenylcysteine oxidase 1	PCYOX1	1	0.34	1.00	0.40
A0A075B6S9	Protein IGKV1-37 (Fragment)	IGKV1D-37			1.00	0.75
P11766	Alcohol dehydrogenase class-3	ADH5	1	0.43	2.00	0.32
O43813	LanC-like protein 1	LANCL1			1.00	0.74
P36957	Dihydrolipoyllysine-residue succinyltransferase component of 2-oxoglutarate dehydrogenase complex, mitochondrial	DLST			4.00	0.74

Q13011	Delta(3,5)-Delta(2,4)-dienoyl-CoA isomerase, mitochondrial	ECH1	1	0.37	2.00	0.37
Q13617	Cullin-2	CUL2	2	0.19	3.00	0.54
P08183	Multidrug resistance protein 1	ABCB1	1	0.18	1.00	0.55
P02461	Collagen alpha-1(III) chain	COL3A1			1.00	0.73
Q9H0X4	Protein FAM234A	FAM234A			3.00	0.72
P42702	Leukemia inhibitory factor receptor	LIFR			1.00	0.72
Q9UGP8	Translocation protein SEC63 homolog	SEC63			1.00	0.71
E7EX90	Dynactin subunit 1	DCTN1			1.00	0.70
Q9Y570	Protein phosphatase methylesterase 1	PPME1	2	0.25	2.00	0.45
Q7KZN9	Cytochrome c oxidase assembly protein COX15 homolog	COX15			1.00	0.70
Q9HAB3	Solute carrier family 52, riboflavin transporter, member 2	SLC52A2			1.00	0.70
Q6UVK1	Chondroitin sulfate proteoglycan 4	CSPG4			1.00	0.68
Q969S3	Zinc finger protein 622	ZNF622	1	0.23	1.00	0.45
A0A0B4J1U7	Protein IGHV6-1 (Fragment)	IGHV6-1			1.00	0.68
Q3MHD2	Protein LSM12 homolog	LSM12			1.00	0.68
Q5JTV8	Torsin-1A-interacting protein 1	TOR1AIP1	1	0.28	1.00	0.40
P48960	CD97 antigen	CD97	1	0.34	2.00	0.33
Q68CZ2	Tensin-3	TNS3			2.00	0.67
P17301	Integrin alpha-2	ITGA2			2.00	0.67
P57737	Coronin-7	CORO7	1		1.00	0.67
Q13459	Unconventional myosin-IXb	MYO9B			1.00	0.66
Q9Y224	UPF0568 protein C14orf166	C14orf166	1	0.35	1.00	0.31
O60902-3	Isoform 3 of Short stature homeobox protein 2	SHOX2			2.00	0.65
Q9Y2G3	Probable phospholipid-transporting ATPase IF	ATP11B	1	0.18	1.00	0.48
P47985	Cytochrome b-c1 complex subunit Rieske, mitochondrial	UQCRFS1			3.00	0.65
P12235	ADP/ATP translocase 1	SLC25A4	1	0.36	1.00	0.28
Q2TAL8	Glutamine-rich protein 1	QRICH1	1	0.36	3.00	0.28
Q9Y6M4	Casein kinase I isoform gamma-3	CSNK1G3			3.00	0.64
P01714	Immunoglobulin lambda variable 3-19	IGLV3-19			1.00	0.64
P07099	Epoxide hydrolase 1	EPHX1			3.00	0.64
P40429	60S ribosomal protein L13a	RPL13A	1	0.25	1.00	0.38
Q969E2	Secretory carrier-associated membrane protein 4	SCAMP4			2.00	0.64
Q13547	Histone deacetylase 1	HDAC1			2.00	0.63
P63165	Small ubiquitin-related modifier 1	SUMO1	1	0.27	1.00	0.37
P21399	Cytoplasmic aconitate hydratase	ACO1			1.00	0.63
O94925-3	Isoform 3 of Glutaminase kidney isoform, mitochondrial	GLS	1	0.63		
Q14156	Protein EFR3 homolog A	EFR3A			2.00	0.63
Q96T76	MMS19 nucleotide excision repair protein homolog	MMS19			1.00	0.62
Q13595	Transformer-2 protein homolog alpha	TRA2A	1	0.62		
Q9HDC9	Adipocyte plasma membrane-associated protein	APMAP	1	0.24	1.00	0.38
P23588	Eukaryotic translation initiation factor 4B	EIF4B	1	0.19	1.00	0.43
Q8IXT5	RNA-binding protein 12B	RBM12B	2	0.62		
P62495	Eukaryotic peptide chain release factor subunit 1	ETF1			3.00	0.62
Q9H223	EH domain-containing protein 4	EHD4			1.00	0.61
P28702	Retinoic acid receptor RXR-beta	RXRB	1		1.00	0.60
Q9Y3D7	Mitochondrial import inner membrane translocase subunit TIM16	PAM16	1	0.59		
Q6ZVX7	F-box only protein 50	NCCRP1	2	0.58		
Q9GZP0	Platelet-derived growth factor D	PDGFD			1.00	0.58
P10606	Cytochrome c oxidase subunit 5B, mitochondrial	COX5B	1	0.25	1.00	0.33

P56134	ATP synthase subunit f, mitochondrial	ATP5J2			1.00	0.57
Q96MC5	Uncharacterized protein C16orf45	C16orf45	1	0.57		
Q15907	Ras-related protein Rab-11B	RAB11B	1	0.26	1.00	0.31
O43615	Mitochondrial import inner membrane translocase subunit TIM44	TIMM44	1	0.13	1.00	0.43
P15559	NAD(P)H dehydrogenase [quinone] 1	NQO1	1	0.28	3.00	0.28
O75127	Pentatricopeptide repeat-containing protein 1, mitochondrial	PTCD1	1	0.29	1.00	0.28
Q8IWA5	Choline transporter-like protein 2	SLC44A2			1.00	0.56
O95208	Epsin-2	EPN2			1.00	0.56
Q8N3E9	1-phosphatidylinositol 4,5-bisphosphate phosphodiesterase delta-3	PLCD3			1.00	0.55
Q14344	Guanine nucleotide-binding protein subunit alpha-13	GNA13			3.00	0.55
O00232	26S proteasome non-ATPase regulatory subunit 12	PSMD12			1.00	0.55
O96008	Mitochondrial import receptor subunit TOM40 homolog	TOMM40	1	0.36	1.00	0.19
Q93050	V-type proton ATPase 116 kDa subunit a isoform 1	ATP6V0A1	1	0.13	3.00	0.41
P22570	NADPH:adrenodoxin oxidoreductase, mitochondrial	FDXR	1	0.24	3.00	0.30
A0A0G2JR96	Cytoplasmic FMR1-interacting protein 1 (Fragment)	CYFIP1			1.00	0.54
Q8WVM8	Sec1 family domain-containing protein 1	SCFD1			1.00	0.54
Q15287	RNA-binding protein with serine-rich domain 1	RNPS1			1.00	0.54
P26038	Moesin	MSN			3.00	0.53
Q5JXC2	Migration and invasion-inhibitory protein	MIIP	1	0.53		
P22681	E3 ubiquitin-protein ligase CBL	CBL			1.00	0.53
P61964	WD repeat-containing protein 5	WDR5	1	0.31	1.00	0.22
Q8WX92	Negative elongation factor B	NELFB	1	0.21	1.00	0.32
Q9H9T3	Elongator complex protein 3	ELP3			1.00	0.52
Q13098	COP9 signalosome complex subunit 1	GPS1			1.00	0.52
Q14966	Zinc finger protein 638	ZNF638	1	0.22	1.00	0.30
Q9Y6G9	Cytoplasmic dynein 1 light intermediate chain 1	DYNC1LI1			4.00	0.51
Q9P2D1	Chromodomain-helicase-DNA-binding protein 7	CHD7			1.00	0.51
P49753	Acyl-coenzyme A thioesterase 2, mitochondrial	ACOT2			2.00	0.51
Q96BM9	ADP-ribosylation factor-like protein 8A	ARL8A			1.00	0.51
Q8NA72	Centrosomal protein POC5	POC5	1	0.51		
Q9Y6E2	Basic leucine zipper and W2 domain-containing protein 2	BZW2	2	0.20	1.00	0.31
Q9BV40	Vesicle-associated membrane protein 8	VAMP8	1	0.18	1.00	0.33
Q13554	Calcium/calmodulin-dependent protein kinase type II subunit beta	CAMK2B			3.00	0.50
Q9NTK5	Obg-like ATPase 1	OLA1			1.00	0.50
P51809	Vesicle-associated membrane protein 7	VAMP7			1.00	0.50
Q96P70	Importin-9	IPO9	2	0.29	2.00	0.21
Q13162	Peroxiredoxin-4	PRDX4	1	0.13	3.00	0.37
P27695	DNA-(apurinic or apyrimidinic site) lyase	APEX1	1	0.27	2.00	0.23
Q9NX74	tRNA-dihydrouridine(20) synthase [NAD(P)+]-like	DUS2			1.00	0.50
Q15691	Microtubule-associated protein RP/EB family member 1	MAPRE1	1	0.26	1.00	0.24
P61604	10 kDa heat shock protein, mitochondrial	HSPE1			2.00	0.49
P18206	Vinculin	VCL			2.00	0.49
P67870	Casein kinase II subunit beta	CSNK2B	2	0.22	1.00	0.27
Q13363	C-terminal-binding protein 1	CTBP1			1.00	0.48
Q9Y289	Sodium-dependent multivitamin transporter	SLC5A6			2.00	0.48
O94776	Metastasis-associated protein MTA2	MTA2			1.00	0.48
Q9P1D2	PRO2472				1.00	0.47
Q9Y276	Mitochondrial chaperone BCS1	BCS1L	1	0.47		

O00268	Transcription initiation factor TFIID subunit 4	TAF4			1.00	0.47
Q6P4Q7	Metal transporter CNNM4	CNNM4			2.00	0.47
O14617	AP-3 complex subunit delta-1	AP3D1			1.00	0.46
Q9Y5Q9	General transcription factor 3C polypeptide 3	GTF3C3			1.00	0.46
P54762	Ephrin type-B receptor 1	EPHB1			1.00	0.46
O95251	Histone acetyltransferase KAT7	KAT7	2	0.45		
Q8IX29	F-box only protein 16	FBXO16			1.00	0.45
Q9NYF8	Bcl-2-associated transcription factor 1	BCLAF1	1	0.44		
P12268	Inosine-5'-monophosphate dehydrogenase 2	IMPDH2			2.00	0.43
Q9P258	Protein RCC2	RCC2			3.00	0.43
Q9H4A3	Serine/threonine-protein kinase WNK1	WNK1	1	0.24	2.00	0.19
Q9ULX6	A-kinase anchor protein 8-like	AKAP8L	1	0.43		
P52888	Thimet oligopeptidase	THOP1			1.00	0.43
Q9NVE4	Coiled-coil domain-containing protein 87	CCDC87			1.00	0.43
O75190	DnaJ homolog subfamily B member 6	DNAJB6			1.00	0.43
Q9BRJ6	Uncharacterized protein C7orf50	C7orf50			1.00	0.42
Q6P1N0	Coiled-coil and C2 domain-containing protein 1A	CC2D1A	1	0.22	2.00	0.20
P50750-2	Isoform 2 of Cyclin-dependent kinase 9	CDK9			1.00	0.42
P16989	Y-box-binding protein 3	YBX3	1	0.41		
P55786	Puromycin-sensitive aminopeptidase	NPEPPS			3.00	0.41
Q8N183	Mimitin, mitochondrial	NDUFAF2			2.00	0.41
O95154	Aflatoxin B1 aldehyde reductase member 3	AKR7A3			1.00	0.41
Q96S21	Ras-related protein Rab-40C	RAB40C	1	0.40		
O75165	DnaJ homolog subfamily C member 13	DNAJC13			2.00	0.39
Q9Y6C9	Mitochondrial carrier homolog 2	MTCH2			3.00	0.39
P40121	Macrophage-capping protein	CAPG	1	0.23	1.00	0.16
O60763	General vesicular transport factor p115	USO1	1	0.24	3.00	0.15
O60502	Protein O-GlcNAcase	MGEA5			1.00	0.39
Q29983	MHC class I polypeptide-related sequence A	MICA			1.00	0.39
Q9Y490	Talin-1	TLN1			3.00	0.38
P48507	Glutamate--cysteine ligase regulatory subunit	GCLM			1.00	0.38
O60266	Adenylate cyclase type 3	ADCY3			1.00	0.38
P08758	Annexin A5	ANXA5			2.00	0.38
P84098	60S ribosomal protein L19	RPL19	1		1.00	0.38
Q9UBS4	DnaJ homolog subfamily B member 11	DNAJB11			1.00	0.38
Q9BVC4	Target of rapamycin complex subunit LST8	MLST8	1	0.38		
P27144	Adenylate kinase 4, mitochondrial	AK4	2	0.19	1.00	0.18
A7KAX9	Rho GTPase-activating protein 32	ARHGAP32			1.00	0.37
Q9GZT9	Egl nine homolog 1	EGLN1			2.00	0.37
P61011	Signal recognition particle 54 kDa protein	SRP54			1.00	0.37
Q6ZRR9	Doublecortin domain-containing protein 5	DCDC5			1.00	0.37
Q9UM54	Unconventional myosin-VI	MYO6			1.00	0.37
P51858	Hepatoma-derived growth factor	HDGF			1.00	0.37
Q9UBB4	Ataxin-10	ATXN10			2.00	0.36
Q5VST6	Protein ABHD17B	ABHD17B			1.00	0.36
Q9BTT6	Leucine-rich repeat-containing protein 1	LRRC1	1	0.36	1.00	
Q9BTV4	Transmembrane protein 43	TMEM43	1	0.36		
O15162	Phospholipid scramblase 1	PLSCR1	1	0.11	1.00	0.25
Q5R3I4	Tetratricopeptide repeat protein 38	TTC38			1.00	0.35

O14802	DNA-directed RNA polymerase III subunit RPC1	POLR3A			1.00	0.35
O75419	Cell division control protein 45 homolog	CDC45			1.00	0.35
Q93008	Probable ubiquitin carboxyl-terminal hydrolase FAF-X	USP9X	1		3.00	0.34
A6NDG6	Glycerol-3-phosphate phosphatase	PGP	1	0.34		
P35659	Protein DEK	DEK			1.00	0.34
P49257	Protein ERGIC-53	LMAN1			1.00	0.34
O14773	Tripeptidyl-peptidase 1	TPP1			2.00	0.34
P41240	Tyrosine-protein kinase CSK	CSK	2	0.34		
Q9H4L4	Sentrin-specific protease 3	SENP3			1.00	0.34
Q9Y6N7	Roundabout homolog 1	ROBO1			3.00	0.34
Q8IWV8	E3 ubiquitin-protein ligase UBR2	UBR2			1.00	0.33
Q9H6X2	Anthrax toxin receptor 1	ANTXR1	1		3.00	0.33
Q7Z417	Nuclear fragile X mental retardation-interacting protein 2	NUFIP2	1	0.33		
Q86Y56	Dynein assembly factor 5, axonemal	DNAAF5	1	0.14	1.00	0.19
P55011	Solute carrier family 12 member 2	SLC12A2			1.00	0.33
Q15434	RNA-binding motif, single-stranded-interacting protein 2	RBMS2			1.00	0.32
Q8NBS9	Thioredoxin domain-containing protein 5	TXNDC5	1	0.14	1.00	0.18
P46736	Lys-63-specific deubiquitinase BRCC36	BRCC3	1	0.32		
P23368	NAD-dependent malic enzyme, mitochondrial	ME2			1.00	0.32
P35270	Sepiapterin reductase	SPR			1.00	0.32
Q9BYG5	Partitioning defective 6 homolog beta	PARD6B	1	0.32		
P63208	S-phase kinase-associated protein 1	SKP1	1	0.32		
Q8TDI0	Chromodomain-helicase-DNA-binding protein 5	CHD5			1.00	0.32
Q96JG6	Syndetin	VPS50			1.00	0.32
A0AV96	RNA-binding protein 47	RBM47	1	0.32		
Q9NX58	Cell growth-regulating nucleolar protein	LYAR			2.00	0.31
P01766	Immunoglobulin heavy variable 3-13	IGHV3-13	1	0.31		
Q96BZ8	Leukocyte receptor cluster member 1	LENG1			1.00	0.31
Q96K21	Abscission/NoCut checkpoint regulator	ZFYVE19			1.00	0.31
O75223	Gamma-glutamylcyclotransferase	GGCT	1	0.30		
Q9NRY6	Phospholipid scramblase 3	PLSCR3			1.00	0.30
O75116	Rho-associated protein kinase 2	ROCK2			1.00	0.30
Q5T750	Skin-specific protein 32	XP32	1	0.30		
Q8NE01	Metal transporter CNNM3	CNNM3	1	0.08	3.00	0.22
Q9Y4D8	Probable E3 ubiquitin-protein ligase HECTD4	HECTD4	1	0.29		
Q9NYK5	39S ribosomal protein L39, mitochondrial	MRPL39	1	0.29		
P33947	ER lumen protein-retaining receptor 2	KDELR2	1	0.29		
Q96I59	Probable asparagine--tRNA ligase, mitochondrial	NARS2			2.00	0.29
P15291	Beta-1,4-galactosyltransferase 1	B4GALT1			1.00	0.29
Q6RW13	Type-1 angiotensin II receptor-associated protein	AGTRAP			1.00	0.29
P46934	E3 ubiquitin-protein ligase NEDD4	NEDD4			2.00	0.28
Q9UIW2	Plexin-A1	PLXNA1			2.00	0.28
Q92575	UBX domain-containing protein 4	UBXN4			1.00	0.28
Q15904	V-type proton ATPase subunit S1	ATP6AP1			1.00	0.28
O00139	Kinesin-like protein KIF2A	KIF2A	1		1.00	0.28
P61106	Ras-related protein Rab-14	RAB14	1	0.28		
Q9P0S9	Transmembrane protein 14C	TMEM14C	1	0.28		
Q96JM3	Chromosome alignment-maintaining phosphoprotein 1	CHAMP1			1.00	0.28
Q16698	2,4-dienoyl-CoA reductase, mitochondrial	DECR1			1.00	0.28

Q9H3S7	Tyrosine-protein phosphatase non-receptor type 23	PTPN23			1.00	0.28
Q14241	Transcription elongation factor B polypeptide 3	TCEB3			1.00	0.27
Q8NGU2	Olfactory receptor 9A4	OR9A4	1	0.26		
P01705	Immunoglobulin lambda variable 2-23	IGLV2-23	1	0.26		
O00203	AP-3 complex subunit beta-1	AP3B1			1.00	0.26
Q06124	Tyrosine-protein phosphatase non-receptor type 11	PTPN11			2.00	0.26
Q9NXF1	Testis-expressed sequence 10 protein	TEX10			1.00	0.25
P53701	Cytochrome c-type heme lyase	HCCS			1.00	0.25
Q9H0X9	Oxysterol-binding protein-related protein 5	OSBPL5			1.00	0.25
Q5VT25	Serine/threonine-protein kinase MRCK alpha	CDC42BPA			4.00	0.25
O60264	SWI/SNF-related matrix-associated actin-dependent regulator of chromatin subfamily A member 5	SMARCA5			1.00	0.25
Q6UWE0	E3 ubiquitin-protein ligase LRSAM1	LRSAM1			1.00	0.24
Q969N2	GPI transamidase component PIG-T	PIGT			1.00	0.24
Q12834	Cell division cycle protein 20 homolog	CDC20			1.00	0.24
Q9UBF2	Coatomer subunit gamma-2	COPG2	1	0.07	2.00	0.17
Q07065	Cytoskeleton-associated protein 4	CKAP4			1.00	0.24
Q9Y5L0	Transportin-3	TNPO3			2.00	0.24
Q96FZ2	Embryonic stem cell-specific 5-hydroxymethylcytosine-binding protein	HMCES	1	0.24		
Q99816	Tumor susceptibility gene 101 protein	TSG101			1.00	0.24
Q6PJT7	Zinc finger CCCH domain-containing protein 14	ZC3H14			1.00	0.24
O60341	Lysine-specific histone demethylase 1A	KDM1A			1.00	0.24
O94906	Pre-mRNA-processing factor 6	PRPF6			2.00	0.23
Q99543	DnaJ homolog subfamily C member 2	DNAJC2			1.00	0.23
Q8NC51	Plasminogen activator inhibitor 1 RNA-binding protein	SERBP1			2.00	0.23
Q12800	Alpha-globin transcription factor CP2	TFCP2			2.00	0.23
P29966	Myristoylated alanine-rich C-kinase substrate	MARCKS			2.00	0.23
Q6P1M0	Long-chain fatty acid transport protein 4	SLC27A4			1.00	0.22
P19387	DNA-directed RNA polymerase II subunit RPB3	POLR2C			1.00	0.22
P98175	RNA-binding protein 10	RBM10			1.00	0.22
P50552	Vasodilator-stimulated phosphoprotein	VASP			3.00	0.22
Q9ULF5	Zinc transporter ZIP10	SLC39A10			1.00	0.21
O75143	Autophagy-related protein 13	ATG13			1.00	0.21
Q96TC7	Regulator of microtubule dynamics protein 3	RMDN3	1	0.21		
O95861	3'(2'),5'-bisphosphate nucleotidase 1	BPNT1			1.00	0.21
Q9UI10	Translation initiation factor eIF-2B subunit delta	EIF2B4			1.00	0.21
P30086	Phosphatidylethanolamine-binding protein 1	PEBP1	1	0.21		
Q96IJ6	Mannose-1-phosphate guanyltransferase alpha	GMPPA	2	0.20		
Q9NTJ5	Phosphatidylinositide phosphatase SAC1	SACM1L	1	0.06	1.00	0.14
Q53H96	Pyrroline-5-carboxylate reductase 3	PYCRL	1	0.06	2.00	0.14
Q9NP72	Ras-related protein Rab-18	RAB18			1.00	0.20
Q96GD4	Aurora kinase B	AURKB	1	0.20		
P50570	Dynamin-2	DNM2			2.00	0.20
P25490	Transcriptional repressor protein YY1	YY1	1	0.20		
Q9Y287	Integral membrane protein 2B	ITM2B			1.00	0.20
Q9NRW7	Vacuolar protein sorting-associated protein 45	VPS45			1.00	0.20
Q7Z2Z2	Elongation factor-like GTPase 1	EFL1			1.00	0.19
Q96A26	Protein FAM162A	FAM162A			1.00	0.19
Q8N4T0	Carboxypeptidase A6	CPA6	1	0.19		
Q9NV96	Cell cycle control protein 50A	TMEM30A			1.00	0.19

Q13409	Cytoplasmic dynein 1 intermediate chain 2	DYNC1I2			1.00	0.19
P49756	RNA-binding protein 25	RBM25			1.00	0.19
P30048	Thioredoxin-dependent peroxide reductase, mitochondrial	PRDX3	1	0.19		
P34741	Syndecan-2	SDC2			1.00	0.18
Q9NX00	Transmembrane protein 160	TMEM160			1.00	0.18
Q63ZY3	KN motif and ankyrin repeat domain-containing protein 2	KANK2			1.00	0.18
Q96Q06	Perilipin-4	PLIN4			1.00	0.18
O43395	U4/U6 small nuclear ribonucleoprotein Prp3	PRPF3			1.00	0.18
Q06323	Proteasome activator complex subunit 1	PSME1			1.00	0.18
Q969Z0	Protein TBRG4	TBRG4			2.00	0.18
Q9NUM4	Transmembrane protein 106B	TMEM106B			2.00	0.18
Q9H444	Charged multivesicular body protein 4b	CHMP4B			1.00	0.18
Q969X5	Endoplasmic reticulum-Golgi intermediate compartment protein 1	ERGIC1	1	0.17		
P53597	Succinate--CoA ligase [ADP/GDP-forming] subunit alpha, mitochondrial	SUCLG1			1.00	0.17
O00469	Procollagen-lysine,2-oxoglutarate 5-dioxygenase 2	PLOD2			2.00	0.17
P43307	Translocon-associated protein subunit alpha	SSR1			1.00	0.17
Q92995	Ubiquitin carboxyl-terminal hydrolase 13	USP13			2.00	0.17
Q5QGS0	Protein KIAA2022	KIAA2022	1	0.17		
Q5SSJ5	Heterochromatin protein 1-binding protein 3	HP1BP3			1.00	0.17
P03905	NADH-ubiquinone oxidoreductase chain 4	MT-ND4			1.00	0.17
Q9NPL8	Complex I assembly factor TIMMDC1, mitochondrial	TIMMDC1			1.00	0.16
Q9NY91	Low affinity sodium-glucose cotransporter	SLC5A4	1	0.16		
Q13228	Selenium-binding protein 1	SELENBP1			1.00	0.16
Q9Y4L1	Hypoxia up-regulated protein 1	HYOU1	1		2.00	0.16
Q9H0J4	Glutamine-rich protein 2	QRICH2			1.00	0.16
O00273	DNA fragmentation factor subunit alpha	DFFA	3	0.16		
P53794	Sodium/myo-inositol cotransporter	SLC5A3			1.00	0.16
Q5H9R7	Serine/threonine-protein phosphatase 6 regulatory subunit 3	PPP6R3	1	0.16		
P56199	Integrin alpha-1	ITGA1			1.00	0.16
O00505	Importin subunit alpha-4	KPNA3	1	0.16	1.00	
Q9Y6I3	Epsin-1	EPN1			1.00	0.16
Q92896	Golgi apparatus protein 1	GLG1	1	0.16		
Q9UFC0	Leucine-rich repeat and WD repeat-containing protein 1	LRWD1			1.00	0.16
A6NK53	Zinc finger protein 233	ZNF233	1	0.16		
Q9NVM9	Protein asunder homolog	ASUN			1.00	0.15
Q86TI2	Dipeptidyl peptidase 9	DPP9			1.00	0.15
Q99569	Plakophilin-4	PKP4			2.00	0.15
O43929	Origin recognition complex subunit 4	ORC4			1.00	0.15
Q96FN4	Copine-2	CPNE2	1	0.15		
Q9UL03	Integrator complex subunit 6	INTS6			1.00	0.15
Q9NZ01	Very-long-chain enoyl-CoA reductase	TECR			1.00	0.15
Q9H3Z4	DnaJ homolog subfamily C member 5	DNAJC5			1.00	0.15
O15194	CTD small phosphatase-like protein	CTDSPL			1.00	0.14
O43379	WD repeat-containing protein 62	WDR62			1.00	0.14
Q96K76	Ubiquitin carboxyl-terminal hydrolase 47	USP47			2.00	0.14
Q6P996	Pyridoxal-dependent decarboxylase domain-containing protein 1	PDXDC1			1.00	0.14
Q15149-8	Isoform 8 of Plectin	PLEC	1	0.14		
P61619	Protein transport protein Sec61 subunit alpha isoform 1	SEC61A1			1.00	0.14

P25098	Beta-adrenergic receptor kinase 1	GRK2			1.00	0.14
P40222	Alpha-taxilin	TXLNA			1.00	0.13
Q9H6T0	Epithelial splicing regulatory protein 2	ESRP2			1.00	0.13
O95359	Transforming acidic coiled-coil-containing protein 2	TACC2	1	0.13		
P32121	Beta-arrestin-2	ARRB2			1.00	0.13
Q9P0U3	Sentrin-specific protease 1	SENP1			1.00	0.12
P47895	Aldehyde dehydrogenase family 1 member A3	ALDH1A3			3.00	0.12
Q7Z4F1	Low-density lipoprotein receptor-related protein 10	LRP10			1.00	0.12
Q96I51	RCC1-like G exchanging factor-like protein	RCC1L			1.00	0.12
P25963	NF-kappa-B inhibitor alpha	NFKBIA			1.00	0.12
Q00535	Cyclin-dependent-like kinase 5	CDK5	1	0.11		
Q9UMZ2	Synergin gamma	SYNRG			1.00	0.11
P36941	Tumor necrosis factor receptor superfamily member 3	LTBR			1.00	0.11
Q16851	UTP--glucose-1-phosphate uridylyltransferase	UGP2			1.00	0.11
Q9UPT9	Ubiquitin carboxyl-terminal hydrolase 22	USP22			1.00	0.11
Q9H8M5	Metal transporter CNNM2	CNNM2			1.00	0.11
Q8IVS2	Malonyl-CoA-acyl carrier protein transacylase, mitochondrial	MCAT			1.00	0.11
P54727	UV excision repair protein RAD23 homolog B	RAD23B			1.00	0.11
Q9NPF5	DNA methyltransferase 1-associated protein 1	DMAP1			1.00	0.11
Q9NVD7	Alpha-parvin	PARVA			1.00	0.10
Q9UKX7	Nuclear pore complex protein Nup50	NUP50			2.00	0.10
Q6IPR3	tRNA wybutosine-synthesizing protein 3 homolog	TYW3	1	0.10		
Q9NNW5	WD repeat-containing protein 6	WDR6	1	0.10		
Q5TCZ1	SH3 and PX domain-containing protein 2A	SH3PXD2A	1	0.10		
Q8IX18	Probable ATP-dependent RNA helicase DHX40	DHX40			1.00	0.09
Q9Y4B5	Microtubule cross-linking factor 1	MTCL1			1.00	0.09
Q5VW36	Focadhesin	FOCAD			1.00	0.09
Q9BV44	THUMP domain-containing protein 3	THUMPD3			1.00	0.09
O15111	Inhibitor of nuclear factor kappa-B kinase subunit alpha	CHUK	1	0.08		
P82675	28S ribosomal protein S5, mitochondrial	MRPS5			1.00	0.08
P56937	3-keto-steroid reductase	HSD17B7	1	0.08		
P36507	Dual specificity mitogen-activated protein kinase kinase 2	MAP2K2			1.00	0.08
Q9UBH6	Xenotropic and polytropic retrovirus receptor 1	XPR1			1.00	0.08
Q53HL2	Borealin	CDCA8			1.00	0.08
Q9H6R4	Nucleolar protein 6	NOL6	1	0.07		
Q13451	Peptidyl-prolyl cis-trans isomerase FKBP5	FKBP5			1.00	0.07
O14684	Prostaglandin E synthase	PTGES	1	0.07		
Q9BTZ2	Dehydrogenase/reductase SDR family member 4	DHRS4			1.00	0.07
Q12824	SWI/SNF-related matrix-associated actin-dependent regulator of chromatin subfamily B member 1	SMARCB1			1.00	0.07
Q9H788	SH2 domain-containing protein 4A	SH2D4A	1	0.07		
Q9Y520	Protein PRRC2C	PRRC2C			1.00	0.07
Q8IYB3	Serine/arginine repetitive matrix protein 1	SRRM1			1.00	0.07
P54760	Ephrin type-B receptor 4	EPHB4			1.00	0.06
Q30201	Hereditary hemochromatosis protein	HFE			1.00	0.06
Q8WYL5	Protein phosphatase Slingshot homolog 1	SSH1	1	0.06		
P68400	Casein kinase II subunit alpha	CSNK2A1	1	0.02	1.00	0.03
Q86VI4	Lysosomal-associated transmembrane protein 4B	LAPTM4B	1	0.06		
Q8IUR0	Trafficking protein particle complex subunit 5	TRAPPC5			1.00	0.05
Q9H2C0	Gigaxonin	GAN			1.00	0.05

Q9NX46	Poly(ADP-ribose) glycohydrolase ARH3	ADPRHL2	1	0.04		
P31947	14-3-3 protein sigma	SFN	1	0.04		
Q9NX57	Ras-related protein Rab-20	RAB20			1.00	0.02
Q13443	Disintegrin and metalloproteinase domain-containing protein 9	ADAM9	1			
O95622	Adenylate cyclase type 5	ADCY5			1.00	
F8VVT9	Arf-GAP with GTPase, ANK repeat and PH domain-containing protein 2	AGAP2			1.00	
Q9BSE5	Agmatinase, mitochondrial	AGMAT	1			
Q02252	Methylmalonate-semialdehyde dehydrogenase [acylating], mitochondrial	ALDH6A1			1.00	
O75179	Ankyrin repeat domain-containing protein 17	ANKRD17	1			
Q13535	Serine/threonine-protein kinase ATR	ATR	1			
Q8N8U9	BMP-binding endothelial regulator protein	BMPER			1.00	
Q8IYS8	Biorientation of chromosomes in cell division protein 1-like 2	BOD1L2			1.00	
Q9HA77	Probable cysteine--tRNA ligase, mitochondrial	CARS2			1.00	
Q567U6	Coiled-coil domain-containing protein 93	CCDC93			1.00	
O60583	Cyclin-T2	CCNT2			1.00	
Q9H3R5	Centromere protein H	CENPH			1.00	
Q13112	Chromatin assembly factor 1 subunit B	CHAF1B	1			
Q8WVB6	Chromosome transmission fidelity protein 18 homolog	CHTF18			1.00	
Q9Y696	Chloride intracellular channel protein 4	CLIC4	1			
P29400-2	Isoform 2 of Collagen alpha-5(IV) chain	COL4A5			1.00	
P14384	Carboxypeptidase M	CPM	1			
O60231	Putative pre-mRNA-splicing factor ATP-dependent RNA helicase DHX16	DHX16			2.00	
Q8WXX0	Dynein heavy chain 7, axonemal	DNAH7	1			
Q16610	Extracellular matrix protein 1	ECM1	1			
Q6PJG2	ELM2 and SANT domain-containing protein 1	ELMSAN1	1			
Q15303	Receptor tyrosine-protein kinase erbB-4	ERBB4			1.00	
Q7Z6J4	FYVE, RhoGEF and PH domain-containing protein 2	FGD2			1.00	
Q9Y5Y0	Feline leukemia virus subgroup C receptor-related protein 1	FLVCR1			1.00	
Q8TAX9	Gasdermin-B	GSDMB			1.00	
Q86YV9	Hermansky-Pudlak syndrome 6 protein	HPS6			1.00	
Q12906-5	Isoform 5 of Interleukin enhancer-binding factor 3	ILF3			1.00	
Q96ST2	Protein IWS1 homolog	IWS1			1.00	
H0YBM7	La-related protein 1 (Fragment)	LARP1			1.00	
Q6ICC9	Protein LDOC1L	LDOC1L	1			
P48449	Lanosterol synthase	LSS			1.00	
P20794	Serine/threonine-protein kinase MAK	MAK			1.00	
P27816	Microtubule-associated protein 4	MAP4			1.00	
O60244	Mediator of RNA polymerase II transcription subunit 14	MED14	1			
Q86W50	Methyltransferase-like protein 16	METTL16			1.00	
Q9BUA6	Myosin regulatory light chain 10	MYL10			1.00	
Q8IVL1	Neuron navigator 2	NAV2			1.00	
Q8NFP9	Neurobeachin	NBEA			1.00	
O75251	NADH dehydrogenase [ubiquinone] iron-sulfur protein 7, mitochondrial	NDUFS7	1			
P04150	Glucocorticoid receptor	NR3C1			1.00	
O60890	Oligophrenin-1	OPHN1	1			
Q9H074	Polyadenylate-binding protein-interacting protein 1	PAIP1	1			
O95263	High affinity cAMP-specific and IBMX-insensitive 3',5'-cyclic phosphodiesterase 8B	PDE8B			1.00	

P13667	Protein disulfide-isomerase A4	PDIA4		1.00
O00443	Phosphatidylinositol 4-phosphate 3-kinase C2 domain-containing subunit alpha	PIK3C2A		2.00
Q99959	Plakophilin-2	PKP2		1.00
O43157	Plexin-B1	PLXNB1	1	
Q7Z3J3	RanBP2-like and GRIP domain-containing protein 4	RGPD4	1	
Q6P3W7	SCY1-like protein 2	SCYL2	1	
Q15019	Septin-2	SEPT2		1.00
O75387	Large neutral amino acids transporter small subunit 3	SLC43A1		1.00
Q658P3	Metalloreductase STEAP3	STEAP3		1.00
Q8WVM0	Dimethyladenosine transferase 1, mitochondrial	TFB1M		1.00
P19438	Tumor necrosis factor receptor superfamily member 1A	TNFRSF1A		1.00
Q9NS69	Mitochondrial import receptor subunit TOM22 homolog	TOMM22	1	
Q9P2K2	Thioredoxin domain-containing protein 16	TXNDC16		1.00
Q5T124	UBX domain-containing protein 11	UBXN11		1.00
O94874	E3 UFM1-protein ligase 1	UFL1		1.00
P52735	Guanine nucleotide exchange factor VAV2	VAV2		1.00
A6NGB9	WAS/WASL-interacting protein family member 3	WIPF3	1	
Q96S55	ATPase WRNIP1	WRNIP1		1.00
Q9Y2X9	Zinc finger protein 281	ZNF281		1.00

Appendix 4: Endogenous RNF145 immunoprecipitation

KO: knockout, SD: sterol depleted, SD + B: sterol depleted + 1.5 hr 50 nM Bortezomib, sterols: sterol depleted + 1 hr sterols, sterols + B: sterol depleted + 30 min 50 nM Bortezomib treatment followed by 1 hr with sterols. #: number of unique peptides, A: Area

Accession	Gene name	Gene ID	KO		SD		SD + B		Sterols		Sterols + B	
			#	A	#	A	#	A	#	A	#	A
Q9H2G2	STE20-like serine/threonine-protein kinase	SLK			1	7.26	1	0.31	1	5.44	1	4.56
P09874	Poly [ADP-ribose] polymerase 1	PARP1					1	0.33	4	0.74	10	3.34
Q01813	ATP-dependent 6-phosphofructokinase, platelet type	PFKP			1	0.40	1	0.32	2	4.39	1	2.42
P61254	60S ribosomal protein L26	RPL26					1	0.11	1	0.68	1	0.70
P35268	60S ribosomal protein L22	RPL22			1	0.64	1	0.47	1	0.71	1	2.64
P78527	DNA-dependent protein kinase catalytic subunit	PRKDC					1	0.34	4	0.96	7	1.86
P05090	Apolipoprotein D	APOD	1	0.53			1	0.23	3	0.81	3	1.23
P04035	3-hydroxy-3-methylglutaryl-coenzyme A reductase	HMGCR			1	0.42	2	0.58	1	0.45	2	2.18
P43490	Nicotinamide phosphoribosyltransferase	NAMPT			1	0.20	1	0.38	2	1.90	2	1.38
Q96DR8	Mucin-like protein 1	MUCL1	1	3.56	1	2.51	1	0.98	1	1.86	1	3.51
P17480	Nucleolar transcription factor 1	UBTF			1	0.57	1	0.86	2	1.92	3	2.95
P11387	DNA topoisomerase 1	TOP1			1	0.68	3	0.72	3	2.01	4	2.41
P41091	Eukaryotic translation initiation factor 2 subunit 3	EIF2S3					1	0.59			2	1.97
P68363	Tubulin alpha-1B chain	TUBA1B	2	1.58	3	1.40	4	1.83	6	5.91	10	5.65
B9A064	Immunoglobulin lambda-like polypeptide 5	IGLL5			1	0.21	1	0.20	1	0.29	1	0.59
P02768	Serum albumin	ALB	4	1.91	1	1.40	3	0.82	4	1.63	5	2.32
P13489	Ribonuclease inhibitor	RNH1			1	0.43	1	0.35	1	0.83	1	0.98
Q9BUJ2	Heterogeneous nuclear ribonucleoprotein U-like protein 1	HNRNPUL1					1	0.59	7	2.71	1	1.58
P62280	40S ribosomal protein S11	RPS11	1	0.42	1	1.61	1	1.48	2	2.67	1	3.87
P01834	Ig kappa chain C region	IGKC	1	23.04	1	34.76	1	24.17	1	41.83	1	62.40
P25786	Proteasome subunit alpha type-1	PSMA1					2	1.62			4	4.03
P42357	Histidine ammonia-lyase	HAL	1	0.64	3	1.03	3	0.43	5	1.73	6	1.07
P42677	40S ribosomal protein S27	RPS27	1	0.46	1	1.16	1	0.97	1	2.41	1	2.38
Q7Z2W4	Zinc finger CCCH-type antiviral protein 1	ZC3HAV1	1	0.39			3	0.81	6	2.84	6	1.95
P62263	40S ribosomal protein S14	RPS14	1	1.06	1	2.83	1	3.13	1	6.26	1	7.10
P50502	Hsc70-interacting protein	ST13					2	0.53	2	0.95	1	1.20
Q6UWP8	Suprabasin	SBSN	2	0.29	2	0.35	2	0.18	1	0.23	2	0.40
P57721	Poly(rC)-binding protein 3	PCBP3	1	0.50	1	0.57	2	1.37			2	2.94
P33993	DNA replication licensing factor MCM7	MCM7			1	0.28	1	0.59	2	1.73	1	1.22
Q93034	Cullin-5	CUL5			1	0.77	3	0.62	3	0.88	4	1.23
P61247	40S ribosomal protein S3a	RPS3A					1	2.79	1	5.26	1	5.50
Q8WWI1	LIM domain only protein 7	LMO7			5	0.90	12	2.27	21	10.86	16	4.40
P42704	Leucine-rich PPR motif-containing protein, mitochondrial	LRPPRC			2	0.69	2	0.70	2	2.12	2	1.32
P35579	Myosin-9	MYH9	11	2.14	23	11.41	27	14.55	67	94.38	36	27.23

P08575	Receptor-type tyrosine-protein phosphatase C	PTPRC	1	1.49	1	2.15	1	0.84	1	1.13	1	1.52
P35637	RNA-binding protein FUS	FUS					2	0.98	2	2.69	2	1.75
P43686	26S protease regulatory subunit 6B	PSMC4					1	0.53			1	0.94
P49368	T-complex protein 1 subunit gamma	CCT3	1	0.16			1	0.38	2	0.93	2	0.67
Q6Y7W6	PERQ amino acid-rich with GYF domain-containing protein 2	GIGYF2			1	1.16	2	0.94	5	5.20	3	1.65
Q15369	Transcription elongation factor B polypeptide 1	TCEB1			2	0.21	1	0.22			1	0.37
P62805	Histone H4	HIST1H4A	4	2.10	4	0.92	3	0.99	5	1.96	2	1.68
P61313	60S ribosomal protein L15	RPL15			1	0.30	1	0.48	1	1.01	1	0.81
P35232	Prohibitin	PHB	1	0.68	2	1.78	4	2.23	7	12.22	4	3.72
O14950	Myosin regulatory light chain 12B	MYL12B	1	0.57	1	3.47	3	2.10	3	16.50	3	3.45
Q9UBQ5	Eukaryotic translation initiation factor 3 subunit K	EIF3K					1	0.48	1	0.66	1	0.78
Q5D862	Filaggrin-2	FLG2	5	3.65	7	5.52	2	1.75	4	1.75	4	2.77
Q9UHD9	Ubiquilin-2	UBQLN2					1	1.31			1	2.04
Q96EY1	DnaJ homolog subfamily A member 3, mitochondrial	DNAJA3	1	0.40			2	0.72	2	1.21	1	1.11
P18621	60S ribosomal protein L17	RPL17					1	2.15	1	3.84	1	3.33
P01903	HLA class II histocompatibility antigen, DR alpha chain	HLA-DRA	1	1.63	1	2.01	1	0.96			1	1.48
P54727	UV excision repair protein RAD23 homolog B	RAD23B					1	0.83			2	1.28
Q14134	Tripartite motif-containing protein 29	TRIM29					1	0.28	6	2.23	1	0.44
P20618	Proteasome subunit beta type-1	PSMB1					1	0.40			1	0.62
P31151	Protein S100-A7	S100A7	5	17.01	4	3.69	3	3.92	4	6.42	4	5.98
P63104	14-3-3 protein zeta/delta	YWHAZ	1	0.53	1	1.55	1	0.51	1	0.71	1	0.77
P41252	Isoleucine--tRNA ligase, cytoplasmic	IARS					1	0.66	1	1.29	1	1.00
Q9Y320	Thioredoxin-related transmembrane protein 2	TMX2			1	0.93	1	1.45	2	0.99	1	2.19
P14923	Junction plakoglobin	JUP	2	1.01	5	1.85	2	0.71	1	0.71	1	1.07
Q9UI42	Carboxypeptidase A4	CPA4	2	0.68	1	0.97	1	0.56	3	0.44	1	0.84
Q9Y383	Putative RNA-binding protein Luc7-like 2	LUC7L2	2	0.50	1	1.63	1	1.86	1	4.27	1	2.78
Q08J23	tRNA (cytosine(34)-C(5))-methyltransferase	NSUN2			2	0.52	4	1.02	9	6.47	6	1.51
Q9Y496	Kinesin-like protein KIF3A	KIF3A					3	0.32	2	0.30	2	0.47
P61978	Heterogeneous nuclear ribonucleoprotein K	HNRNPK	1	0.67	1	0.48	1	0.77	2	1.06	1	1.11
P31943	Heterogeneous nuclear ribonucleoprotein H	HNRNPH1			1	0.58	1	0.56	2	0.86	2	0.82
Q02241	Kinesin-like protein KIF23	KIF23					1	0.17			1	0.24
P50454	Serpin H1	SERPINH1			1	0.57	1	1.45	3	1.21	1	1.98
Q86YZ3	Hornerin	HRNR	4	2.47	7	8.24	6	2.61	5	2.22	6	3.57
P02786	Transferrin receptor protein 1	TFRC	2	1.18	3	0.98	2	1.75	2	2.19	1	2.36
O60814	Histone H2B type 1-K	HIST1H2BK	2	1.49	3	0.74	2	0.53	2	1.23	2	0.71
A4UGR9	Xin actin-binding repeat-containing protein 2	XIRP2			1	0.43	1	0.40	1	1.00	1	0.53
P01860	Ig gamma-3 chain C region	IGHG3	3	30.71	2	50.00	3	11.89	2	57.38	2	15.46
P61981	14-3-3 protein gamma	YWHAG			1	0.69	1	0.70	1	1.19	1	0.90
P39023	60S ribosomal protein L3	RPL3	1	1.03	1	2.10	2	1.76	2	2.39	2	2.28
P60228	Eukaryotic translation initiation factor 3 subunit E	EIF3E			1	0.23	1	0.36	1	0.28	2	0.45
P19474	E3 ubiquitin-protein ligase TRIM21	TRIM21	4	2.62	4	3.74	3	5.14	4	5.52	5	6.52
Q96P63	Serpin B12	SERPINB12	1	2.06	1	2.16	1	1.83	3	1.83	3	2.30
Q8NBM8	Prenylcysteine oxidase-like	PCYOX1L					1	0.36			1	0.45
P78344	Eukaryotic translation initiation factor 4 gamma 2	EIF4G2	1	0.99	1	1.15	3	1.42	3	1.52	3	1.79
O15381	Nuclear valosin-containing protein-like	NVL	1	0.61	2	0.49	2	0.45	2	0.62	2	0.56
P10599	Thioredoxin	TXN	2	10.39	2	6.45	2	5.11	2	8.03	2	6.38
P23396	40S ribosomal protein S3	RPS3	1	0.53	2	0.81	2	0.93	2	1.61	2	1.17

P07099	Epoxide hydrolase 1	EPHX1			1	0.47	1	0.37	1	0.68	1	0.45
O75400	Pre-mRNA-processing factor 40 homolog A	PRPF40A	1	0.30	1	0.47	1	0.80			1	0.98
Q13200	26S proteasome non-ATPase regulatory subunit 2	PSMD2					1	1.10			2	1.33
Q9NSD9	Phenylalanine--tRNA ligase beta subunit	FARSB	1	0.71	1	0.49	2	0.83	2	1.21	2	1.00
P25311	Zinc-alpha-2-glycoprotein	AZGP1	4	2.20	4	1.00	1	1.31	1	2.02	3	1.60
Q14152	Eukaryotic translation initiation factor 3 subunit A	EIF3A	3	0.56	2	1.27	5	1.39	6	1.29	5	1.68
Q15370	Transcription elongation factor B polypeptide 2	TCEB2			1	0.57	2	1.05	1	1.09	2	1.26
Q6DD88	Atlastin-3	ATL3					2	0.53			2	0.63
P05387	60S acidic ribosomal protein P2	RPLP2			2	4.14	5	5.23	4	6.20	2	6.14
P27635	60S ribosomal protein L10	RPL10					1	0.82	1	1.46	1	0.95
P14618	Pyruvate kinase PKM	PKM	2	1.89	4	2.29	6	3.76	9	6.57	8	4.36
O15372	Eukaryotic translation initiation factor 3 subunit H	EIF3H	1	4.24	1	3.52	1	8.52	1	5.40	1	9.86
P26373	60S ribosomal protein L13	RPL13					1	0.36	1	0.59	1	0.41
P0C0S5	Histone H2A.Z	H2AFZ					2	2.31	2	3.85	2	2.63
Q99623	Prohibitin-2	PHB2	1	0.51	1	1.51	1	2.12	6	7.92	5	2.41
P62269	40S ribosomal protein S18	RPS18					1	1.19	2	1.97	1	1.35
P46060	Ran GTPase-activating protein 1	RANGAP1					1	0.29	2	1.00	2	0.33
P31944	Caspase-14	CASP14	10	11.92	7	7.04	5	6.87	10	10.89	5	7.73
P53999	Activated RNA polymerase II transcriptional coactivator p15	SUB1	1	2.12	1	2.59	1	3.98	1	5.63	1	4.47
Q02413	Desmoglein-1	DSG1	5	1.06	7	1.92	4	0.93	8	1.22	7	1.02
Q96PE2	Rho guanine nucleotide exchange factor 17	ARHGEF17					1	0.59	1	0.35	2	0.64
P0DMV9	Heat shock 70 kDa protein 1B	HSPA1B	3	1.68	3	3.76	5	5.32	6	5.13	6	5.78
Q08188	Protein-glutamine gamma-glutamyltransferase E	TGM3	7	2.48	4	4.74	4	1.88	8	2.58	5	2.04
P20930	Filaggrin	FLG	4	2.51	7	4.51	4	1.83	4	1.70	3	1.99
Q9UHX1	Poly(U)-binding-splicing factor PUF60	PUF60	2	0.81	2	1.01	2	1.45	2	1.49	2	1.56
P28074	Proteasome subunit beta type-5	PSMB5			1	0.87	2	3.19	1	0.54	2	3.42
P62195	26S protease regulatory subunit 8	PSMC5					1	0.26			2	0.28
Q9NRR5	Ubiquilin-4	UBQLN4					1	1.89	1	0.52	1	2.02
O00231	26S proteasome non-ATPase regulatory subunit 11	PSMD11					1	2.98			1	3.15
P04406	Glyceraldehyde-3-phosphate dehydrogenase	GAPDH	7	6.52	3	2.23	4	7.43	7	13.14	6	7.82
Q15006	ER membrane protein complex subunit 2	EMC2					1	0.54			1	0.57
Q9NQ29	Putative RNA-binding protein Luc7-like 1	LUC7L			1	0.37	1	0.42	1	0.70	1	0.44
Q9GZT8	NIF3-like protein 1	NIF3L1			1	0.28	2	0.65	2	0.38	1	0.67
Q96MG8	Protein-L-isoaspartate O-methyltransferase domain-containing protein 1	PCMTD1	1	0.61	1	1.37	2	2.93	2	1.88	1	3.02
O00767	Acyl-CoA desaturase	SCD					1	2.18	1	0.96	1	2.24
Q96HS1	Serine/threonine-protein phosphatase PGAM5, mitochondrial	PGAM5			1	0.73	1	0.66	1	0.65	1	0.68
P62241	40S ribosomal protein S8	RPS8			1	0.43	1	0.83	2	0.99	1	0.85
O75477	Erlin-1	ERLIN1					1	0.94	1	0.39	1	0.95
P52272	Heterogeneous nuclear ribonucleoprotein M	HNRNPM					1	1.78	7	5.04	3	1.79
Q9UL46	Proteasome activator complex subunit 2	PSME2					1	0.78			1	0.78
O00232	26S proteasome non-ATPase regulatory subunit 12	PSMD12					3	1.65			3	1.64
P02545	Prelamin-A/C	LMNA	7	2.44	11	3.47	14	3.98	12	3.69	13	3.93
P35998	26S protease regulatory subunit 7	PSMC2					1	1.02			1	1.00
O75223	Gamma-glutamylcyclotransferase	GGCT	3	2.32	3	3.51	3	2.07	3	1.85	3	2.04
O43242	26S proteasome non-ATPase regulatory subunit 3	PSMD3					5	2.18			6	2.14

Q13347	Eukaryotic translation initiation factor 3 subunit I	EIF3I	1	0.56			2	1.16	1	0.74	2	1.14
Q14498	RNA-binding protein 39	RBM39	1	0.92	1	0.36	1	1.97	1	4.41	1	1.92
P62753	40S ribosomal protein S6	RPS6	2	0.89	2	1.48	2	2.87	2	3.71	2	2.78
O75821	Eukaryotic translation initiation factor 3 subunit G	EIF3G					2	0.95	3	1.66	1	0.91
Q9NV79	Protein-L-isoaspartate O-methyltransferase domain-containing protein 2	PCMTD2	1	1.04	1	1.70	3	2.59	3	1.84	2	2.48
P35613	Basigin	BSG	1	0.64	1	1.08	2	1.52	1	1.40	1	1.45
P04844	Dolichyl-diphosphooligosaccharide--protein glycosyltransferase subunit 2	RPN2					1	1.54	1	0.76	1	1.47
Q9NZT1	Calmodulin-like protein 5	CALML5	1	0.57			1	0.56			1	0.53
P11142	Heat shock cognate 71 kDa protein	HSPA8	4	3.83	4	6.89	8	10.95	5	9.73	7	10.33
P01040	Cystatin-A	CSTA	7	4.16	3	1.60	5	2.55	5	2.42	6	2.40
P31689	DnaJ homolog subfamily A member 1	DNAJA1					1	0.67			1	0.63
O43765	Small glutamine-rich tetratricopeptide repeat-containing protein alpha	SGTA					1	1.80			1	1.69
P46379	Large proline-rich protein BAG6	BAG6					1	2.76			1	2.59
O15269	Serine palmitoyltransferase 1	SPTLC1			3	1.06	3	1.35	3	1.36	3	1.26
Q96MT1	RING finger protein 145	RNF145	1	1.68	4	9.74	7	22.87	7	13.39	7	21.14
P62333	26S protease regulatory subunit 10B	PSMC6					1	0.36			1	0.33
Q9UNM6	26S proteasome non-ATPase regulatory subunit 13	PSMD13					1	1.49			1	1.36
Q8N163	Cell cycle and apoptosis regulator protein 2	CCAR2	2	2.50	1	2.85	1	3.66	3	3.04	2	3.33
P55884	Eukaryotic translation initiation factor 3 subunit B	EIF3B	5	5.82	3	5.77	6	7.46	6	4.83	6	6.76
O15371	Eukaryotic translation initiation factor 3 subunit D	EIF3D	1	4.09			1	0.36	1	0.32	1	0.32
Q13263	Transcription intermediary factor 1-beta	TRIM28	1	0.63			1	1.39	1	1.77	1	1.25
O15294	UDP-N-acetylglucosamine--peptide N-acetylglucosaminyltransferase 110 kDa subunit	OGT			1	0.45	1	0.66	2	0.59	3	0.59
Q08170	Serine/arginine-rich splicing factor 4	SRSF4					1	0.81	1	0.85	1	0.73
Q16850	Lanosterol 14-alpha demethylase	CYP51A1					2	0.73	1	0.36	2	0.66
P63208	S-phase kinase-associated protein 1	SKP1					1	0.45	1	1.04	1	0.41
Q9Y5K5	Ubiquitin carboxyl-terminal hydrolase isozyme L5	UCHL5					1	0.79			1	0.70
Q9Y5Z0	Beta-secretase 2	BACE2					1	3.91			1	3.47
P61626	Lysozyme C	LYZ	1	2.96	1	1.95	1	1.79	1	5.04	1	1.56
Q15149	Plectin	PLEC			2	0.59	1	0.86	5	2.07	4	0.75
P11310	Medium-chain specific acyl-CoA dehydrogenase, mitochondrial	ACADM	1	0.67	1	1.32	1	0.94	1	2.14	1	0.82
Q12907	Vesicular integral-membrane protein VIP36	LMAN2			1	4.94	1	9.84	1	5.32	1	8.54
Q7L0Y3	Mitochondrial ribonuclease P protein 1	TRMT10C					1	1.19	1	1.15	1	1.03
P28066	Proteasome subunit alpha type-5	PSMA5			1	0.91	2	5.37	1	0.64	2	4.65
Q99714	3-hydroxyacyl-CoA dehydrogenase type-2	HSD17B10			1	0.54	1	0.60	1	0.20	1	0.51
Q63HN8	E3 ubiquitin-protein ligase RNF213	RNF213			1		1	0.54			2	0.46
P05023	Sodium/potassium-transporting ATPase subunit alpha-1	ATP1A1			1	0.44	2	0.96	2	0.46	2	0.81
Q13426	DNA repair protein XRCC4	XRCC4	3	1.93	3	2.13	4	3.48	4	3.03	4	2.91
Q9Y262	Eukaryotic translation initiation factor 3 subunit L	EIF3L	3	1.54	4	1.56	5	3.48	5	3.55	6	2.90
Q13501	Sequestosome-1	SQSTM1					2	2.95	2	1.95	3	2.40
Q8NBM4	Ubiquitin-associated domain-containing protein 2	UBAC2			1	2.46	1	5.96	1	3.14	1	4.79
P60709	Actin, cytoplasmic 1	ACTB			2	1.77	5	1.89	6	1.70	5	1.52
P08238	Heat shock protein HSP 90-beta	HSP90AB1	2	1.83	1	2.45	5	5.56	4	8.22	5	4.42
Q15843	NEDD8	NEDD8	1	0.54	1	1.00	1	2.63	1	2.14	1	2.08
Q14165	Malectin	MLEC					1	0.85			1	0.66

Q02543	60S ribosomal protein L18a	RPL18A					1	0.86	1	0.86	1	0.66
P19338	Nucleolin	NCL	2	2.62	3	3.77	5	6.61	5	6.47	3	5.04
P38646	Stress-70 protein, mitochondrial	HSPA9	2	0.51	7	5.01	7	5.33	5	3.46	6	4.03
Q04837	Single-stranded DNA-binding protein, mitochondrial	SSBP1	1	2.85	1	5.56	1	3.79	1	3.80	1	2.84
P51648	Fatty aldehyde dehydrogenase	ALDH3A2					2	1.47	1	0.81	2	1.10
Q13310	Polyadenylate-binding protein 4	PABPC4	1	0.43			1	0.69	1	1.34	2	0.51
P53985	Monocarboxylate transporter 1	SLC16A1					1	0.81			1	0.58
Q9HCY8	Protein S100-A14	S100A14	1	2.40	1	6.10	1	1.61	1	2.71	1	1.15
O14818	Proteasome subunit alpha type-7	PSMA7	1	0.94	1	1.93	3	7.24	1	2.09	4	5.12
Q96SW2	Protein cereblon	CRBN			1	0.82	1	1.20	1	1.36	1	0.85
Q09666	Neuroblast differentiation-associated protein AHNAK	AHNAK	9	1.52	12	3.68	22	5.39	19	4.42	20	3.81
Q15008	26S proteasome non-ATPase regulatory subunit 6	PSMD6					1	0.49			2	0.34
P51114	Fragile X mental retardation syndrome-related protein 1	FXR1	2	0.41	1	0.35	3	1.00	3	0.78	2	0.70
P31025	Lipocalin-1	LCN1			1	1.35	1	1.35	1	2.08	1	0.94
P21333	Filamin-A	FLNA	18	3.40	18	3.16	27	5.92	21	4.20	24	4.11
P10809	60 kDa heat shock protein, mitochondrial	HSPD1	4	4.26	7	5.17	8	6.15	7	6.76	4	4.25
O75165	DnaJ homolog subfamily C member 13	DNAJC13					1	2.94			1	2.03
P55036	26S proteasome non-ATPase regulatory subunit 4	PSMD4					2	2.93			2	1.92
O00264	Membrane-associated progesterone receptor component 1	PGRMC1					1	1.86	1	1.47	1	1.21
P60900	Proteasome subunit alpha type-6	PSMA6					1	3.35			2	2.15
Q14254	Flotillin-2	FLOT2	1	0.64	1	0.60	1	0.81	1	0.81	1	0.52
P27824	Calnexin	CANX	3	0.73	4	4.71	6	11.34	4	6.56	5	7.14
P68871	Hemoglobin subunit beta	HBB	4	2.45	3	1.63	2	2.66	4	2.75	2	1.66
P08195	4F2 cell-surface antigen heavy chain	SLC3A2	4	3.09	6	4.66	7	8.71	6	5.39	6	5.43
Q00839	Heterogeneous nuclear ribonucleoprotein U	HNRNPU			1	0.41	3	1.23	3	2.19	2	0.76
P04843	Dolichyl-diphosphooligosaccharide--protein glycosyltransferase subunit 1	RPN1			1	0.48	2	1.13	1	0.69	1	0.69
P05089	Arginase-1	ARG1	1	3.86	3	1.03	1	3.97	6	3.53	1	2.39
P36578	60S ribosomal protein L4	RPL4	1	4.92	1	8.45	1	18.62	1	26.89	1	10.89
O15427	Monocarboxylate transporter 4	SLC16A3	1	0.46	1	0.60	1	1.50	1	0.78	1	0.88
Q99460	26S proteasome non-ATPase regulatory subunit 1	PSMD1					1	2.54			2	1.47
P52597	Heterogeneous nuclear ribonucleoprotein F	HNRNPF					1	2.09	1	2.46	1	1.21
P09622	Dihydrolipoyl dehydrogenase, mitochondrial	DLD	1	0.62	1	1.20	1	0.93			1	0.53
Q01650	Large neutral amino acids transporter small subunit 1	SLC7A5	2	1.94	3	1.75	4	6.71	4	2.96	4	3.86
P11166	Solute carrier family 2, facilitated glucose transporter member 1	SLC2A1			1	0.34	1	0.49	1	0.16	1	0.28
P05109	Protein S100-A8	S100A8	6	9.69	8	12.37	4	3.19	6	11.46	3	1.82
P07355	Annexin A2	ANXA2	5	2.21	3	3.96	7	3.22	7	2.93	4	1.82
P07339	Cathepsin D	CTSD	2	2.91	1	12.31	1	9.14	4	2.20	1	5.13
P16989	Y-box-binding protein 3	YBX3	1	0.61	1	0.27	1	0.89	1	0.48	1	0.50
P06702	Protein S100-A9	S100A9	8	17.36	8	17.12	5	11.28	8	15.94	4	6.22
Q99436	Proteasome subunit beta type-7	PSMB7			1	0.79	1	4.21	1	0.56	2	2.32
P21796	Voltage-dependent anion-selective channel protein 1	VDAC1	1	1.94	1	1.64	1	4.17	2	4.78	1	2.28
P31327	Carbamoyl-phosphate synthase [ammonia], mitochondrial	CPS1	1	0.87	3	0.62	2	2.03	6	5.68	3	1.11
P05388	60S acidic ribosomal protein P0	RPLP0			1	0.54	2	1.68	2	2.08	1	0.92
Q9UNL2	Translocon-associated protein subunit gamma	SSR3					1	0.36			1	0.19
P49917	DNA ligase 4	LIG4	1	0.65			1	1.13	2	0.51	2	0.60

P56537	Eukaryotic translation initiation factor 6	EIF6					1	0.56	1	0.62	1	0.30
P05187	Alkaline phosphatase, placental type	ALPP	1	1.10	1	2.22	1	1.85	1	1.60	1	0.95
Q13867	Bleomycin hydrolase	BLMH	2	1.15	1	0.81	2	0.74	3	0.87	2	0.38
Q12931	Heat shock protein 75 kDa, mitochondrial	TRAP1	1	1.74			1	7.26			2	3.63
P55072	Transitional endoplasmic reticulum ATPase	VCP			2	0.87	4	2.60	3	0.89	4	1.28
Q07021	Complement component 1 Q subcomponent-binding protein, mitochondrial	C1QBP	3	1.00	2	0.77	3	2.18	3	1.52	3	1.07
P60660	Myosin light polypeptide 6	MYL6	1	1.79	1	8.52	1	16.11	4	38.40	3	7.31
P40939	Trifunctional enzyme subunit alpha, mitochondrial	HADHA	1	0.88	2	1.22	2	0.97	1	1.22	1	0.44
P07900	Heat shock protein HSP 90-alpha	HSP90AA1	1	0.72	2	0.94	2	2.92	2	2.83	3	1.30
P51659	Peroxisomal multifunctional enzyme type 2	HSD17B4	2	0.72	2	1.06	1	0.98	2	0.60	2	0.39
P69905	Hemoglobin subunit alpha	HBA1	2	1.58	2	1.16	2	0.90	3	1.27	1	0.36
Q9HCD6	Protein TANC2	TANC2					1	0.74			2	0.29
P62979	Ubiquitin-40S ribosomal protein S27a	RPS27A	3	3.55	3	5.17	4	68.35	3	11.01	4	26.52
P25705	ATP synthase subunit alpha, mitochondrial	ATP5A1	4	1.15	3	1.49	4	2.15	2	1.69	2	0.82
P04792	Heat shock protein beta-1	HSPB1					1	0.78	4	1.71	2	0.29
P22735	Protein-glutamine gamma-glutamyltransferase K	TGM1	2	1.29	3	1.61	1	1.62	1	1.75	1	0.57
P30044	Peroxiredoxin-5, mitochondrial	PRDX5	1	0.54			1	1.35	1	0.92	1	0.47
P11021	78 kDa glucose-regulated protein	HSPA5	3	0.60	3	0.86	6	4.58	6	1.65	6	1.46
P29508	Serpin B3	SERPINB3	7	2.61	2	1.08	2	2.77	2	0.73	3	0.83
Q02878	60S ribosomal protein L6	RPL6					2	2.21	2	3.99	1	0.51
P61604	10 kDa heat shock protein, mitochondrial	HSPE1	1	0.53	2	0.70	3	0.68			1	0.11
A6NDV4	Transmembrane protein 8B	TMEM8B					1	10.91				
B4DEH9	Acetyl-coenzyme A synthetase, cytoplasmic	ACSS2					1	1.26				
O14975	Very long-chain acyl-CoA synthetase	SLC27A2					1	0.52				
O43615	Mitochondrial import inner membrane translocase subunit TIM44	TIMM44			2	0.32	1	0.25	3	0.71		
O60884	DnaJ homolog subfamily A member 2	DNAJA2					1	0.09				
O75044	SLIT-ROBO Rho GTPase-activating protein 2	SRGAP2					1	0.34				
O75190	DnaJ homolog subfamily B member 6	DNAJB6					1	0.21	1	0.20		
O75390	Citrate synthase, mitochondrial	CS					1	0.95				
O75947	ATP synthase subunit d, mitochondrial	ATP5H					1	0.18				
O95831	Apoptosis-inducing factor 1, mitochondrial	AIFM1	1	0.85	1	1.72	1	0.64	1	1.00		
O96005	Cleft lip and palate transmembrane protein 1	CLPTM1			1	5.92	1	11.20	1	2.31		
P00338	L-lactate dehydrogenase A chain	LDHA					1	0.45	2	0.55		
P00367	Glutamate dehydrogenase 1, mitochondrial	GLUD1			1	0.38	1	0.26	2	0.26		
P02671	Fibrinogen alpha chain	FGA					1	0.35				
P02675	Fibrinogen beta chain	FGB					1	3.38				
P02679	Fibrinogen gamma chain	FGG					1	0.58				
P06748	Nucleophosmin	NPM1					1	0.46	1	0.57		
P07954	Fumarate hydratase, mitochondrial	FH			1	0.39	1	0.33				
P08670	Vimentin	VIM					1	0.49	3	0.71		
P08910	Monoacylglycerol lipase ABHD2	ABHD2					1	0.34				
P10515	Dihydrolipoyllysine-residue acetyltransferase component of pyruvate dehydrogenase complex, mitochondrial	DLAT			1	0.53	1	0.44				
P11532	Dystrophin	DMD					1	0.39	1	0.32		
P13073	Cytochrome c oxidase subunit 4 isoform 1, mitochondrial	COX4I1	1	1.40	1	2.01	1	2.19	1	1.52		
P13804	Electron transfer flavoprotein subunit alpha, mitochondrial	ETFA	1	0.20	1	0.42	1	0.60				
P16435	NADPH--cytochrome P450 reductase	POR					1	0.22				

P20700	Lamin-B1	LMNB1					1	0.71				
P25789	Proteasome subunit alpha type-4	PSMA4					1	1.31				
P30042	ES1 protein homolog, mitochondrial	C21orf33			1	0.27	1	0.19				
P30048	Thioredoxin-dependent peroxide reductase, mitochondrial	PRDX3			1	1.07	1	0.89				
P30084	Enoyl-CoA hydratase, mitochondrial	ECHS1					1	0.61				
P31040	Succinate dehydrogenase [ubiquinone] flavoprotein subunit, mitochondrial	SDHA			1	3.13	1	2.36	1	2.01		
P34897	Serine hydroxymethyltransferase, mitochondrial	SHMT2					1	0.44				
P43121	Cell surface glycoprotein MUC18	MCAM					1	0.95	1	0.68		
P46777	60S ribosomal protein L5	RPL5			1	0.19	1	0.29	1	0.77		
P48594	Serpin B4	SERPINB4			1	2.79	1	3.80	1	1.03		
P49411	Elongation factor Tu, mitochondrial	TUFM	1	3.56			1	3.31				
P55809	Succinyl-CoA:3-ketoacid coenzyme A transferase 1, mitochondrial	OXCT1			1	0.46	1	0.23				
P62266	40S ribosomal protein S23	RPS23					1	0.24	1	0.43		
P62899	60S ribosomal protein L31	RPL31					1	0.17				
P68371	Tubulin beta-4B chain	TUBB4B	1	0.32	2	0.88	2	1.77				
Q01469	Fatty acid-binding protein, epidermal	FABP5			1	0.35	1	0.26				
Q06787	Synaptic functional regulator FMR1	FMR1					1	1.22	1	1.11		
Q06830	Peroxiredoxin-1	PRDX1	1	0.95			1	0.76	1	1.26		
Q07020	60S ribosomal protein L18	RPL18					1	0.24				
Q13835	Plakophilin-1	PKP1			2	1.19	1	0.44				
Q14416	Metabotropic glutamate receptor 2	GRM2					1	0.23				
Q15165	Serum paraoxonase/arylesterase 2	PON2					1	1.33				
Q15392	Delta(24)-sterol reductase	DHCR24					1	0.50				
Q15758	Neutral amino acid transporter B(0)	SLC1A5			1	0.80	1	0.30	1	0.34		
Q5J8M3	ER membrane protein complex subunit 4	EMC4					1	0.55				
Q5T9A4	ATPase family AAA domain-containing protein 3B	ATAD3B			1	0.60	1	1.39	1	2.97		
Q7L014	Probable ATP-dependent RNA helicase DDX46	DDX46					1	0.52	1	0.33		
Q7L5D6	Golgi to ER traffic protein 4 homolog	GET4					1	1.17				
Q7Z7M9	Polypeptide N-acetylgalactosaminyltransferase 5	GALNT5					1	0.68				
Q86WA8	Lon protease homolog 2, peroxisomal	LONP2					1	7.00	1	0.51		
Q8N490	Probable hydrolase PNKD	PNKD					1	0.24				
Q8TCJ2	Dolichyl-diphosphooligosaccharide--protein glycosyltransferase subunit STT3B	STT3B					1	1.08	1	0.59		
Q95604	HLA class I histocompatibility antigen, Cw-17 alpha chain	HLA-C					1	1.21	1	1.49		
Q96A54	Adiponectin receptor protein 1	ADIPOR1					1	1.51				
Q99550	M-phase phosphoprotein 9	MPHOSPH9					1	0.47				
Q99614	Tetratricopeptide repeat protein 1	TTC1					2	0.60				
Q9C0I3	Serine-rich coiled-coil domain-containing protein 1	CCSER1					1	0.31				
Q9NX63	MICOS complex subunit MIC19	CHCHD3					1	0.61				
Q9NYF0	Dapper homolog 1	DACT1					1	0.45				
Q9UBX3	Mitochondrial dicarboxylate carrier	SLC25A10					1	0.21				
Q9UJS0	Calcium-binding mitochondrial carrier protein Aralar2	SLC25A13					1	0.43				
Q9UJZ1	Stomatin-like protein 2, mitochondrial	STOML2	1	0.77	1	1.17	1	1.11	1	1.19		
Q9Y282	Endoplasmic reticulum-Golgi intermediate compartment protein 3	ERGIC3					1	0.35				
A0A024RA52	Proteasome subunit alpha type	PSMA2									1	1.71
A0A075B6X0	Protein TRAJ45 (Fragment)	TRAJ45									1	0.94

A0A0A0MS15	Immunoglobulin heavy variable 3-49	IGHV3-49							1	0.69
A0A0G2JMW3	Cadherin-related family member 5	CDHR5							1	0.38
A0A1B0GTL5	Rab11 family-interacting protein 5	RAB11FIP5							1	
A6NHZ5	Leucine-rich repeat-containing protein 14B	LRRC14B	1							
A6NIE6	Putative RRN3-like protein RRN3P2	RRN3P2	1	1.54						
B5ME19	Eukaryotic translation initiation factor 3 subunit C-like protein	EIF3CL				1	0.87	1	1.00	
B9EGA3	SMARCD2 protein	SMARCD2						1		
F8VWW7	SPRY domain-containing protein 3	SPRYD3			1					
F8W7C6	60S ribosomal protein L10	RPL10				1	1.18			
H0YI64	Endoplasmic reticulum mannosyl-oligosaccharide 1,2-alpha-mannosidase (Fragment)	MAN1B1						1		
H7BZJ3	Protein disulfide-isomerase A3 (Fragment)	PDIA3				1	0.69	1	0.45	
H7C205	Rho GTPase-activating protein 26 (Fragment)	ARHGAP26						1		
K7EL20	Eukaryotic translation initiation factor 3 subunit G (Fragment)	EIF3G				1	2.14	1	2.18	
O00165	HCLS1-associated protein X-1	HAX1				1	1.20			
O00410	Importin-5	IPO5				1	0.61			
O14617	AP-3 complex subunit delta-1	AP3D1						1	0.39	
O15027	Protein transport protein Sec16A	SEC16A				1	0.10			
O43175	D-3-phosphoglycerate dehydrogenase	PHGDH				1	1.79	2	2.04	
O43399	Tumor protein D54	TPD52L2				1	0.63			
O43448	Voltage-gated potassium channel subunit beta-3	KCNAB3						1		
O43513	Mediator of RNA polymerase II transcription subunit 7	MED7			1					
O43707	Alpha-actinin-4	ACTN4	1	0.32						
O43776	Asparagine--tRNA ligase, cytoplasmic	NARS				1	3.27			
O43823	A-kinase anchor protein 8	AKAP8				2	1.37			
O60284	Suppression of tumorigenicity 18 protein	ST18				1	0.88			
O60573	Eukaryotic translation initiation factor 4E type 2	EIF4E2				3	1.16			
O60716	Catenin delta-1	CTNND1				3	1.42	1	0.92	
O60763	General vesicular transport factor p115	USO1						1	0.43	
O60841	Eukaryotic translation initiation factor 5B	EIF5B						2	0.68	
O75342	Arachidonate 12-lipoxygenase, 12R-type	ALOX12B	2	0.61		1	0.55	1	0.54	
O75420	PERQ amino acid-rich with GYF domain-containing protein 1	GIGYF1				4	1.35	1	0.49	
O75874	Isocitrate dehydrogenase [NADP] cytoplasmic	IDH1				1	0.48			
O75955	Flotillin-1	FLOT1				1	0.33			
O76003	Glutaredoxin-3	GLRX3				2	1.03	2	0.34	
O76031	ATP-dependent Clp protease ATP-binding subunit clpX-like, mitochondrial	CLPX				2	1.14			
O76094	Signal recognition particle subunit SRP72	SRP72				1	0.50			
O94973	AP-2 complex subunit alpha-2	AP2A2			1					
O95232	Luc7-like protein 3	LUC7L3				1	0.21			
O95373	Importin-7	IPO7						1	4.05	
O95425	Supervillin	SVIL				1	1.33			
O95573	Long-chain-fatty-acid--CoA ligase 3	ACSL3						1	0.51	
O95628	CCR4-NOT transcription complex subunit 4	CNOT4				2	0.32			
O95684	FGFR1 oncogene partner	FGFR1OP				1	0.54			
P00966	Argininosuccinate synthase	ASS1				2	0.77			
P01031	Complement C5	C5				1	0.36			

P01706	Immunoglobulin lambda variable 2-11	IGLV2-11									1	0.78
P01876	Ig alpha-1 chain C region	IGHA1	2	0.52				3	1.23	2	0.99
P02647	Apolipoprotein A-I	APOA1						1	3.46		
P04040	Catalase	CAT			1	0.59					
P04075	Fructose-bisphosphate aldolase A	ALDOA	1	0.38	2	0.39		1	0.47	1	0.41
P04083	Annexin A1	ANXA1						1	0.25	3	0.69
P04279	Semenogelin-1	SEMG1	2	0.74	2	0.70				2	0.63
P04908	Histone H2A type 1-B/E	HIST1H2AB			2	2.13					
P05141	ADP/ATP translocase 2	SLC25A5	1	0.18	1	0.53				1	0.46
P05198	Eukaryotic translation initiation factor 2 subunit 1	EIF2S1								2	1.16
P05362	Intercellular adhesion molecule 1	ICAM1						1	0.37	1	0.40
P06753	Tropomyosin alpha-3 chain	TPM3			1	1.88					
P07437	Tubulin beta chain	TUBB						4	2.86	5	4.39
P07814	Bifunctional glutamate/proline--tRNA ligase	EPRS						1	0.36		
P07910	Heterogeneous nuclear ribonucleoproteins C1/C2	HNRNPC			1	0.35		1	0.58	1	0.57
P08559	Pyruvate dehydrogenase E1 component subunit alpha, somatic form, mitochondrial	PDHA1						1	0.50		
P08621	U1 small nuclear ribonucleoprotein 70 kDa	SNRNP70						1	0.24		
P08708	40S ribosomal protein S17	RPS17								1	1.05
P09525	Annexin A4	ANXA4			1	0.54					
P0CW18	Serine protease 56	PRSS56						1	0.33	1	0.61
P0DME0	Protein SETSIP	SETSIP						1	0.16		
P11177	Pyruvate dehydrogenase E1 component subunit beta, mitochondrial	PDHB						1	0.87		
P11498	Pyruvate carboxylase, mitochondrial	PC						1	0.44		
P11586	C-1-tetrahydrofolate synthase, cytoplasmic	MTHFD1			1			2	2.19	1	2.15
P11684	Uteroglobin	SCGB1A1						1	0.57		
P12004	Proliferating cell nuclear antigen	PCNA						1	0.88	1	1.15
P12270	Nucleoprotein TPR	TPR						1	0.45		
P12956	X-ray repair cross-complementing protein 6	XRCC6	1	0.20	1		1	1	0.50	1	0.27
P13010	X-ray repair cross-complementing protein 5	XRCC5						1	1.10		
P13639	Elongation factor 2	EEF2			2	0.22		1	0.37		
P13995	Bifunctional methylenetetrahydrofolate dehydrogenase/cyclohydrolase, mitochondrial	MTHFD2						1	0.07		
P14625	Endoplasmin	HSP90B1			1	0.17		1	0.51		
P14735	Insulin-degrading enzyme	IDE			1	0.46					
P15880	40S ribosomal protein S2	RPS2						1	0.31		
P16333	Cytoplasmic protein NCK1	NCK1						1	0.84	1	1.14
P16402	Histone H1.3	HIST1H1D						2	0.38	3	0.53
P16615	Sarcoplasmic/endoplasmic reticulum calcium ATPase 2	ATP2A2								1	0.42
P17661	Desmin	DES								1	0.57
P17812	CTP synthase 1	CTPS1						4	4.43	3	1.96
P17900	Ganglioside GM2 activator	GM2A	1	0.69						1	0.20
P17980	26S protease regulatory subunit 6A	PSMC3								1	0.68
P17987	T-complex protein 1 subunit alpha	TCP1						1	0.83		
P18077	60S ribosomal protein L35a	RPL35A						1	1.40		
P18206	Vinculin	VCL						1	0.47		
P19971	Thymidine phosphorylase	TYMP			1	0.51					
P20042	Eukaryotic translation initiation factor 2 subunit 2	EIF2S2								2	1.70

P20933	N(4)-(beta-N-acetylglucosaminyl)-L-asparaginase	AGA	2	0.36							1	0.24
P22033	Methylmalonyl-CoA mutase, mitochondrial	MUT							1	0.23		
P22061	Protein-L-isoaspartate(D-aspartate) O-methyltransferase	PCMT1							1	0.20	1	0.29
P22234	Multifunctional protein ADE2	PAICS									1	0.74
P22732	Solute carrier family 2, facilitated glucose transporter member 5	SLC2A5							1	0.12		
P23258	Tubulin gamma-1 chain	TUBG1							2	2.07		
P23458	Tyrosine-protein kinase JAK1	JAK1							1	0.67	1	0.40
P23490	Loricrin	LOR	1	0.34	1	0.15						
P24071	Immunoglobulin alpha Fc receptor	FCAR			1	0.84						
P25205	DNA replication licensing factor MCM3	MCM3							2	0.92		
P25788	Proteasome subunit alpha type-3	PSMA3					1	1.96			1	
P28072	Proteasome subunit beta type-6	PSMB6									1	0.34
P28340	DNA polymerase delta catalytic subunit	POLD1							2	1.12	1	0.31
P29401	Transketolase	TKT									1	0.30
P29590	Protein PML	PML							1	1.41		
P30153	Serine/threonine-protein phosphatase 2A 65 kDa regulatory subunit A alpha isoform	PPP2R1A							1	0.54		
P30566	Adenylosuccinate lyase	ADSL							1	0.95		
P31949	Protein S100-A11	S100A11	1	0.19					1	0.42		
P32189	Glycerol kinase	GK							1	0.44		
P33176	Kinesin-1 heavy chain	KIF5B							6	2.02		
P35251	Replication factor C subunit 1	RFC1							1	0.69	1	0.76
P35580	Myosin-10	MYH10							12	2.80	3	0.65
P35659	Protein DEK	DEK									2	1.71
P36776	Lon protease homolog, mitochondrial	LONP1			1	0.28						
P37108	Signal recognition particle 14 kDa protein	SRP14							1	0.04	2	0.91
P39748	Flap endonuclease 1	FEN1							1	1.28		
P42765	3-ketoacyl-CoA thiolase, mitochondrial	ACAA2							1		1	1.11
P43007	Neutral amino acid transporter A	SLC1A4									1	0.23
P45880	Voltage-dependent anion-selective channel protein 2	VDAC2	1	1.04					1	5.19	1	1.92
P47929	Galectin-7	LGALS7			1	0.88			1	0.66	1	0.58
P48643	T-complex protein 1 subunit epsilon	CCT5							1	1.32		
P49327	Fatty acid synthase	FASN							4	1.57	1	0.43
P49458	Signal recognition particle 9 kDa protein	SRP9									1	0.48
P49750	YLP motif-containing protein 1	YLPM1							1	0.49		
P49756	RNA-binding protein 25	RBM25									2	0.41
P49792	E3 SUMO-protein ligase RanBP2	RANBP2							1	0.57		
P50213	Isocitrate dehydrogenase [NAD] subunit alpha, mitochondrial	IDH3A							1	0.81		
P50914	60S ribosomal protein L14	RPL14							1	0.10		
P50990	T-complex protein 1 subunit theta	CCT8							1	0.30		
P50991	T-complex protein 1 subunit delta	CCT4							3	0.83	2	0.87
P51531	Probable global transcription activator SNF2L2	SMARCA2					1					
P51570	Galactokinase	GALK1									1	0.46
P51993	Alpha-(1,3)-fucosyltransferase 6	FUT6					1					
P52701	DNA mismatch repair protein Msh6	MSH6							2	1.17	1	0.43
P53618	Coatomer subunit beta	COPB1									2	0.93
P53621	Coatomer subunit alpha	COPA									1	0.33
P54709	Sodium/potassium-transporting ATPase subunit beta-3	ATP1B3	1	0.22	1	0.50						

P54920	Alpha-soluble NSF attachment protein	NAPA							1	0.32		
P55060	Exportin-2	CSE1L									1	2.21
P56192	Methionine--tRNA ligase, cytoplasmic	MARS							1	0.55	1	0.50
P60174	Triosephosphate isomerase	TPI1	1	0.20					1	0.24		
P61026	Ras-related protein Rab-10	RAB10			1	0.26						
P61289	Proteasome activator complex subunit 3	PSME3							1	0.91		
P61353	60S ribosomal protein L27	RPL27							1	0.63	1	0.45
P62191	26S protease regulatory subunit 4	PSMC1									1	0.14
P62244	40S ribosomal protein S15a	RPS15A							1	0.27		
P62701	40S ribosomal protein S4, X isoform	RPS4X							1	0.49		
P62736	Actin, aortic smooth muscle	ACTA2	4	2.06	1	0.45						
P62750	60S ribosomal protein L23a	RPL23A							1	0.74	1	1.09
P62829	60S ribosomal protein L23	RPL23							1	0.48	1	0.50
P62851	40S ribosomal protein S25	RPS25							1	0.25		
P62857	40S ribosomal protein S28	RPS28									1	0.29
P62861	40S ribosomal protein S30	FAU							1	0.25		
P62913	60S ribosomal protein L11	RPL11							1	0.43	1	0.41
P63173	60S ribosomal protein L38	RPL38									1	0.33
P67809	Nuclease-sensitive element-binding protein 1	YBX1							1	1.16		
P68431	Histone H3.1	HIST1H3A							1	0.75		
P80723	Brain acid soluble protein 1	BASP1			1	0.13			1	0.85		
P83881	60S ribosomal protein L36a	RPL36A							1	0.26	1	0.30
P84098	60S ribosomal protein L19	RPL19							1	1.10	1	0.72
Q00325	Phosphate carrier protein, mitochondrial	SLC25A3			1	0.55					1	0.15
Q00610	Clathrin heavy chain 1	CLTC							2	0.58	1	0.50
Q02388	Collagen alpha-1(VII) chain	COL7A1									1	
Q05639	Elongation factor 1-alpha 2	EEF1A2			1	0.29						
Q05932	Folylpolyglutamate synthase, mitochondrial	FPGS							1	0.30		
Q06710	Paired box protein Pax-8	PAX8									1	3.67
Q07866	Kinesin light chain 1	KLC1							1	0.32		
Q07955	Serine/arginine-rich splicing factor 1	SRSF1			1				1	0.39	2	0.31
Q08211	ATP-dependent RNA helicase A	DHX9					1	0.56	2	1.24	1	
Q08345	Epithelial discoidin domain-containing receptor 1	DDR1					1					
Q08380	Galectin-3-binding protein	LGALS3BP							1	0.20		
Q08752	Peptidyl-prolyl cis-trans isomerase D	PPID							1	0.81		
Q0P6D6	Coiled-coil domain-containing protein 15	CCDC15									1	0.62
Q12772	Sterol regulatory element-binding protein 2	SREBF2									1	0.43
Q12864	Cadherin-17	CDH17									1	
Q12873	Chromodomain-helicase-DNA-binding protein 3	CHD3			1	0.83						
Q12965	Unconventional myosin-Ie	MYO1E							1	0.50		
Q13201	Multimerin-1	MMRN1							1			
Q13426-2	Isoform 2 of DNA repair protein XRCC4	XRCC4							2	0.69		
Q13428	Treacle protein	TCOF1							1	0.51		
Q13510	Acid ceramidase	ASAH1	2	0.53	1	1.10			2	0.99	1	0.64
Q14157	Ubiquitin-associated protein 2-like	UBAP2L							1	0.89		
Q14192	Four and a half LIM domains protein 2	FHL2							2	1.57	1	2.09
Q14331	Protein FRG1	FRG1									1	0.80
Q14527	Helicase-like transcription factor	HLTF							1	0.82		
Q14534	Squalene monooxygenase	SQLE									1	0.68

Q15084	Protein disulfide-isomerase A6	PDIA6							3	0.58		
Q15233	Non-POU domain-containing octamer-binding protein	NONO							1	0.69		
Q15365	Poly(rC)-binding protein 1	PCBP1							3	2.12		
Q15517	Corneodesmosin	CDSN			1	0.45			2	0.68	2	1.25
Q15831	Serine/threonine-protein kinase STK11	STK11									1	
Q16891	MICOS complex subunit MIC60	IMMT							1	0.90		
Q27J81	Inverted formin-2	INF2									1	0.30
Q53GS7	Nucleoporin GLE1	GLE1							1	1.13		
Q53RT3	Retroviral-like aspartic protease 1	ASPRV1							1	0.41		
Q5MNZ9	WD repeat domain phosphoinositide-interacting protein 1	WIPI1							1	0.71		
Q5SZL2	Centrosomal protein of 85 kDa-like	CEP85L							1	0.40		
Q5T3I0	G patch domain-containing protein 4	GPATCH4							1	0.56	1	0.55
Q68CJ9	Cyclic AMP-responsive element-binding protein 3-like protein 3	CREB3L3					1					
Q6NUK1	Calcium-binding mitochondrial carrier protein SCaMC-1	SLC25A24			1	1.88			1	1.25	1	0.98
Q71RC2	La-related protein 4	LARP4							1	0.08		
Q71UM5	40S ribosomal protein S27-like	RPS27L			1	0.87			1	1.97	1	1.66
Q76G19	PDZ domain-containing protein 4	PDZD4							1			
Q7L3B6	Hsp90 co-chaperone Cdc37-like 1	CDC37L1							1			
Q7L5L3	Glycerophosphodiester phosphodiesterase domain-containing protein 3	GDPD3			1	0.41						
Q7RTM1	Otopetrin-1	OTOP1									1	10.68
Q7RTU9	Stereocilin	STRC					1					
Q7Z2K8	G protein-regulated inducer of neurite outgrowth 1	GPRIN1							1	0.43		
Q7Z406	Myosin-14	MYH14			1	0.19						
Q7Z4G4	tRNA (guanine(10)-N2)-methyltransferase homolog	TRMT11									1	3.90
Q7Z4I7	LIM and senescent cell antigen-like-containing domain protein 2	LIMS2							1	0.45		
Q86UE4	Protein LYRIC	MTDH									1	0.25
Q86VP6	Cullin-associated NEDD8-dissociated protein 1	CAND1									2	0.47
Q8IUK5	Plexin domain-containing protein 1	PLXDC1									1	
Q8IW75	Serpin A12	SERPINA12			1	0.70					1	0.24
Q8IWT1-3	Isoform 3 of Sodium channel subunit beta-4	SCN4B							1	0.36		
Q8IWU4	Zinc transporter 8	SLC30A8					1					
Q8IXK2	Polypeptide N-acetylgalactosaminyltransferase 12	GALNT12							1	0.32		
Q8IY18	Structural maintenance of chromosomes protein 5	SMC5							1	1.56		
Q8IY67	Ribonucleoprotein PTB-binding 1	RAVER1							1	1.11	1	0.21
Q8IYB3	Serine/arginine repetitive matrix protein 1	SRRM1									1	0.56
Q8N264	Rho GTPase-activating protein 24	ARHGAP24									1	
Q8N4Q1	Mitochondrial intermembrane space import and assembly protein 40	CHCHD4			1	0.47						
Q8N8S7	Protein enabled homolog	ENAH							1	0.81		
Q8NE71	ATP-binding cassette sub-family F member 1	ABCF1									6	4.01
Q8NGZ4	Olfactory receptor 2G3	OR2G3							1			
Q8TA86	Retinitis pigmentosa 9 protein	RP9							1	0.79		
Q8TE49	OTU domain-containing protein 7A	OTUD7A			1							
Q8WVV4	Protein POF1B	POF1B	1	0.22	1							
Q8WWI1-3	Isoform 3 of LIM domain only protein 7	LMO7							2	1.05		
Q8WY22	BRI3-binding protein	BRI3BP									1	0.21

Q92804	TATA-binding protein-associated factor 2N	TAF15			1	0.95						
Q92833	Protein Jumonji	JARID2							1			
Q92841	Probable ATP-dependent RNA helicase DDX17	DDX17									1	0.57
Q92945	Far upstream element-binding protein 2	KHSRP							6	1.60		
Q92973	Transportin-1	TNPO1							1	0.21	1	0.51
Q96AE4	Far upstream element-binding protein 1	FUBP1							3	1.23	2	0.63
Q96D46	60S ribosomal export protein NMD3	NMD3									1	
Q96EY7	Pentatricopeptide repeat domain-containing protein 3, mitochondrial	PTCD3							1			
Q96F44	E3 ubiquitin-protein ligase TRIM11	TRIM11							1	0.87		
Q96J01	THO complex subunit 3	THOC3							1	0.39		
Q96KP4	Cytosolic non-specific dipeptidase	CNDP2							1	0.70		
Q96PK6	RNA-binding protein 14	RBM14							4	0.74	1	0.40
Q96QA5	Gasdermin-A	GSDMA	1	0.14	2	0.37			1	0.24		
Q96TA2	ATP-dependent zinc metalloprotease YME1L1	YME1L1			1	0.54						
Q99832	T-complex protein 1 subunit eta	CCT7									1	0.68
Q99848	Probable rRNA-processing protein EBP2	EBNA1BP2							1	0.58		
Q9BRZ2	E3 ubiquitin-protein ligase TRIM56	TRIM56							1	0.15		
Q9BVP2	Guanine nucleotide-binding protein-like 3	GNL3									1	0.42
Q9BWF3	RNA-binding protein 4	RBM4							4	0.56		
Q9BYJ1	Hydroperoxide isomerase ALOXE3	ALOXE3			1	1.07					1	0.35
Q9BZF3	Oxysterol-binding protein-related protein 6	OSBPL6			1	0.73						
Q9H0B6	Kinesin light chain 2	KLC2							2	0.76		
Q9H0H5	Rac GTPase-activating protein 1	RACGAP1									1	
Q9H222	ATP-binding cassette sub-family G member 5	ABCG5							1	0.30		
Q9H2R5	Kallikrein-15	KLK15			1	15.69						
Q9H3U1	Protein unc-45 homolog A	UNC45A							1	1.09	1	0.61
Q9H936	Mitochondrial glutamate carrier 1	SLC25A22									1	0.44
Q9H9J2	39S ribosomal protein L44, mitochondrial	MRPL44							1	1.87		
Q9HC84	Mucin-5B	MUC5B							1			
Q9NP64	Nucleolar protein of 40 kDa	ZCCHC17							1	0.70	2	0.53
Q9NQ87	Hairy/enhancer-of-split related with YRPW motif-like protein	HEYL							1	0.45		
Q9NQI0	Probable ATP-dependent RNA helicase DDX4	DDX4							1	0.62	1	0.42
Q9NR30	Nucleolar RNA helicase 2	DDX21							2	0.49	1	0.43
Q9NWX6	Probable tRNA(His) guanylyltransferase	THG1L									1	0.57
Q9NX58	Cell growth-regulating nucleolar protein	LYAR							1	0.54	1	0.64
Q9NXL9	DNA helicase MCM9	MCM9									1	0.86
Q9NYF8	Bcl-2-associated transcription factor 1	BCLAF1							1	0.63		
Q9NZ01	Very-long-chain enoyl-CoA reductase	TECR									1	0.31
Q9NZH6	Interleukin-37	IL37							1	0.18		
Q9P0K7	Ankycorbin	RAI14							1	0.30		
Q9P0U4	CXXC-type zinc finger protein 1	CXXC1							2	0.56		
Q9P2E9	Ribosome-binding protein 1	RRBP1			1	0.63			1	1.38	1	1.13
Q9UBG3	Cornulin	CRNN									1	0.73
Q9UEF7	Klotho	KL							1			
Q9UG63	ATP-binding cassette sub-family F member 2	ABCF2							2	0.78		
Q9UHN1	DNA polymerase subunit gamma-2, mitochondrial	POLG2					1					
Q9UN30	Sex comb on midleg-like protein 1	SCML1									1	0.49
Q9UPN3	Microtubule-actin cross-linking factor 1, isoforms 1/2/3/5	MACF1									1	0.47

Q9UPQ0	LIM and calponin homology domains-containing protein 1	LIMCH1			3	0.77	1	0.31
Q9UPQ9	Trinucleotide repeat-containing gene 6B protein	TNRC6B			3	1.01		
Q9Y263	Phospholipase A-2-activating protein	PLAA					3	0.61
Q9Y285	Phenylalanine--tRNA ligase alpha subunit	FARSA			1	0.43		
Q9Y2K2	Serine/threonine-protein kinase SIK3	SIK3	1					
Q9Y446	Plakophilin-3	PKP3			2	0.86	1	0.46
Q9Y4W6	AFG3-like protein 2	AFG3L2			1	0.51		
Q9Y597	BTB/POZ domain-containing protein KCTD3	KCTD3			1	0.52	1	0.53
Q9Y5M8	Signal recognition particle receptor subunit beta	SRPRB					1	1.31
Q9Y696	Chloride intracellular channel protein 4	CLIC4			1	1.00		